INSTITUTO SUPERIOR DE ENGENHARIA DO PORTO
MESTRADO EM ENGENHARIA MECÂNICA




ROBUST ANALYSIS AND OPTIMIZATION OF A FLATTEN SURFACE TECHNIQUE

EDUARDO FERREIRA DA SILVA MONTEIRO AMARAL
novembro de 2020

POLITÉCNICO
DO PORTO

Instituto Superior de Engenharia do Porto

ROBUST ANALYSIS AND OPTIMIZATION OF A FLATTEN SURFACE TECHNIQUE

Eduardo Ferreira da Silva Monteiro Amaral

1140416

2020

ISEP- School of Engineering, Polytechnic of Porto

Department of Mechanical Engineering

POLITÉCNICO
DO PORTO

POLITÉCNICO
DO PORTO

Instituto Superior de Engenharia do Porto

ROBUST ANALYSIS AND OPTIMIZATION OF A FLATTEN SURFACE TECHNIQUE

Eduardo Ferreira da Silva Monteiro Amaral

1140416

Dissertation presented to ISEP – School of Engineering, Polytechnic of Porto to fulfil the requirements necessary to obtain a Master's degree in Mechanical Engineering, carried out under the guidance of the Professor Francisco José Gomes da Silva and Co-supervision of Professor Arnaldo Manuel Guedes Pinto..

2020

ISEP- School of Engineering, Polytechnic of Porto
Department of Mechanical Engineering

POLITÉCNICO
DO PORTO

POLITÉCNICO
DO PORTO

JURY

President

Manuel Jorge Dores de Castro, PhD
Associate Professor, ISEP - School of Engineering, Polytechnic of Porto

Main Supervisor

Francisco José Gomes da Silva, PhD
Associate Professor, ISEP - School of Engineering, Polytechnic of Porto

Examiner

Abílio Manuel Pinho de Jesus, PhD
Associate Professor, FEUP - Faculty of Engineering of University of Porto

ACKNOWLEDGMENTS

I would like to thank Ing. Gerrit Klaseboer and Dr. ir Redmer van Tijum for giving me the opportunity to work under their advisement in Philips. I have learned a lot from them. I am also thankful for their guidance, patience and straight availability. Further, I want to thank the Metal Forming Research and Development team at Philips, for all their support and help. Finally, I want to express my gratitude to my supervisor at ISEP, Professor Francisco Silva for all the ideas, understanding and full support. I also would like to thank my parents Paula Ferreira da Silva and Mario Amaral, my grandparents, Guido Ferreira da Silva and Patá da Neves, my siblings, Miguel Amaral, Sofia Amaral, Joana Amaral, my girlfriend Ana Lopes and my friends André Silva, Pedro Preto, Vitor Santos for all the support and assistance given throughout my academic career and, especially, in my life. Without them, none of my achievements would be possible.

PALAVRAS CHAVE

Deformacão Plástica, DACE, Optimização Robusta, Metamodelos, Optimização

RESUMO

Atualmente, as empresas têm como principal enfoque o melhoramento da qualidade do produto, a redução do desperdício e do tempo de produção através de processos de optimização. Neste trabalho, foi usada uma técnica, *Waffling process*, com o objetivo de aplainar a superfície do material. Uma vez que o conhecimento científico relacionado com este método é ainda muito limitado, foi necessário realizar um estudo sobre este tema para permitir a elaboração do trabalho. A metodologia utilizada teve como base o Método de Elementos Finitos (MEF), a Análise e *Desing* de Experiências Computacionais (DACE - *Design and Analysis of Computer Experiment*), Optimização Robusta (OR) e um teste prático que, por sua vez, possibilitou a validação da simulação por elementos finitos. A simulação através do MEF permite a compreensão do comportamento de uma estrutura ou de um componente, facilitando a sua otimização antes do seu fabrico, diminuindo os custos associados à sua produção. No entanto, existem algumas desvantagens como, por exemplo, o elevado custo do programa computacional, o tempo despendido para replicar a realidade e a existência de vários fatores que podem originar resultados distintos da realidade. Para ultrapassar estas desvantagens foi utilizada a metodologia OR que toma em consideração a incerteza que existe no mundo real, permitindo melhorar a precisão, predizendo os *inputs/outputs* da simulação. Este método recorre ao uso de *metamodels*, que permitem diminuir o tempo e custo do processamento da simulação, de modo a obter um maior entendimento sobre o processo e, consequentemente, a otimização do mesmo. A escolha do *metamodel* foi determinada com base no valor de predição e no valor do desvio presente em cada simulação. A simulação e os testes práticos apresentam algumas diferenças ao nível do valor de *springback*, que poderá ter sido uma consequência da rigidez da ferramenta de *waffling* utilizada na simulação, uma vez que, a densidade da malha tem um limite máximo de elementos ou, ainda, devido às diferenças causadas pela variação das propriedades do material entre a dobragem, pré-dobragem e *rolling*. Em suma, este trabalho permitiu adquirir um maior conhecimento sobre este processo e uma redução média de 13.3% no ângulo final de dobragem.

KEYWORDS

Metal forming, DACE, Robust Optimization, Metamodels, Optimization

ABSTRACT

In the globalization era, companies are focusing their efforts on product quality improvement, reducing scraps, and decreasing the time of production by process optimization. In this work, a technique to flatten the surface, the waffling process, is developed to support this trend. Since the knowledge regarding this method is still very minimal, investigation and optimization are needed to be develop in this work. The methodology used is based on the FEM (Finite element method), DACE (Design and Analysis of a Computer Experience), the robust strategy and a practical test to validate the FE simulation. The FE simulation is used to replicate the waffling process without extra cost on tooling. However, it has some drawbacks, as it can be computationally costly, time-consuming and the existence of numerous factors that can replicate difference results that might differ from reality. One way to overcome these drawbacks is by using the RO (Robust Optimization) methodology. RO takes into account the uncertainty of the real world, resulting in the improvement of the accuracy, and predicts the input/output of the simulation. This method uses metamodels which lead to a decrease in the time and the cost to get a better understanding, and therefore leading to the optimization process. The best metamodel was chosen based on the one that had higher prediction and less deviation on the simulations, being the Kriging. The simulation and the practical test have some springback deviation, which could be caused by the waffling tool in the simulation being rigid, the mesh having a limited number of elements and the material properties variance on the bending and pre-bending and the rolling. With this methodology, it is possible to gain greater knowledge about this process and optimize it with an average reduction of 13.3% on the output angle of bending.

LISTS OF SYMBOLS, UNITS AND ABBREVIATIONS

List of abbreviations

AISI	American Iron and Steel Institute
ANOVA	Analysis of variance
ANN	Artificial Neural Network
BLUP	Best Linear Unbiased Prediction
CAD	Computer-Aided Design
CAE	Computer-Aided Engineering
CAM	Computer-Aided Manufacturing
DACE	Design and Analysis of Computer Experiment
DOE	Design of Experience
FE	Finite Element
FEA	Finite Element Analysis
FEM	Finite Element Method
DIN	German Institute for Standardisation
LHD	Latin Hypercube Design
LOOCV	Leave-One-Out Cross-Validation
MLE	Maximum Likelihood Estimation
MSE	Mean Square Error
MC	Monte Carlo
NN	Neural Networks
OUU	Optimization under uncertainty
QQ	Quantile-Quantile
RBF	Radial Basis Functions
RSM	Response Surface Method
RO	Robust Optimization
RMSE	Root-Mean Square Error
SNR	Signal-to-Noise Ratio
SO	Simulation Optimization
TM	Taguchi Method
3D	Three Dimensions
2D	Two Dimensions
UTS	Ultimate Tensile Strength

Lists of Units

Degrees	Degrees
KN	Kilonewtons
MPa	Megapascal
μm	Micrometre
mm	Millimetre
N	Newton

List of Symbols

α	Angle/area (pre-bending)
Ani	Anisotropy
%	Area reduction
e	Basic function or a stochastic part
$d\varepsilon$	Coefficient of determination
μ	Coefficient of friction
σ_e	Cross-section area at the fracture
x	Design variable
A_0	Design variable of uncertainty
σ_v	Equality constraints
e_t	Estimation of the error variance
A_r	Force
F / a	Force/area
A_f	Fraction factional design
μ_{fric}	Friction
E	Function values for each individual optimization in terms of mean performance
τ	Function values for each individual optimization in terms of variance
r	Inequality constraints
r_0	Infinitesimal strain
r_{45}	Lankford coefficient
r_{90}	Lankford coefficient average weighted
r_m	Lankford coefficient direction diagonal
ε_w	Lankford coefficient direction parallel
ε_t	Lankford coefficient direction transverse
p	Lower design

D	Material Depth
H	Material Height
t	Material Thickness
z	Matrix containing the correlation between the points
z_p	Mean of the object function
z_x	Noise variables
f	Object function
k_g	Normal distribution that contains the probability of constraints
μ_z	Normal setting
h	Number noise variables
g	Number of design variables
ub	Number of simulations
ib	Number of the design variables
x_c^*	Number of the regression coefficient
μ_f'	Original cross-section area
σ_f'	Parameter of uncertainty
α	Parameters
μ_f	Percentage
$R^2 - \text{Value}$	Prediction of the metamodel
e_{-i}	Prediction error
σ_f	Quadratic loss function
R	Radius (cylindrical)
y	Random error
ε	Regularization constant
$\hat{y}$	Relationship between the known measurement points
$y(x_1^+)$	Response measurements at the highest levels of variance
$y(x_1^-)$	Response measurements at the lowest levels of variance
X	Response of the prediction at one point
β	Shear stress
$L_2 - \text{norm}$	Standard deviation object function
$RMSE - CV$	Standard deviation of the LOOCV
$\hat{y}_0$	Strain
σ^2	Stress
p	Thickness strain
L	Tool dimensions
m	Total elongation
$\mathrm{Z}(x)$	True model

σ_g	Uncertain constraints
μ_g	Uncertain deviation
$R\left(x_i, x_{\cdot}\right)$	Upper design
r_0	Vector of regression coefficients
R	Vector that has the correlation between the points
λ	Vectors standard deviation
R^2	Vectors the uncertain constraints
2^{k-q}	Weighing factor
i	Width strain
j	Yield strength
σ_Y	Yield stress
n	Strain-hardening exponent
E	Young's (E-) Modulus

GLOSSARY OF TERMS

Algorithm	Finite sequence of well-defined, computer-implementable instructions, typically to solve a class of problems or to perform a computation.
FlexMM	A flexible material description enabling to describe complex materials in a user-friendly way developed by Philips® and implemented in Marc.
Marc Mentat®	Nonlinear finite elements analysis software used to simulate behaviour of complex materials.
MATLAB®	MATLAB (an abbreviation of "matrix laboratory") is a proprietary multi-paradigm programming language and numerical computing environment developed by MathWorks.
PreCrystal	Software made by Philips to design processes.
Software	Collection of data or computer instructions that tell the computer how to work. This is in contrast to physical hardware, from which the system is built and actually performs the work.

LIST OF FIGURES

LIST OF TABLES

INDEX

INTRODUCTION

1 INTRODUCTION

1.1 Background

Since the beginning of civilization, metal forming has been used in various ways, and with the development of the society, the increasing need for the usage of such process led to its rapid improvement. Nowadays, sheet metal forming is used to produce countless products for many industries. This process is used mainly in mass production, which is automatized and has several parameters and different approaches. In modern times, the metal forming industry is very competitive. Therefore, the success of a company depends on having an industry with zero failure production and by reducing both the costs and time-to-market. To achieve this ambitious goal, companies are focusing their efforts on product quality improvement, reducing scrap and decreasing the time of production by process optimization.

Metal forming is a complex process with many different parameters. By using the traditional process as a practical experiment of “trial and error”, getting a better optimization is very expensive, time-consuming and with so many variables it can be almost impossible to achieve this goal. With the finite element method (FEM) simulation it can be done more easily without extra cost on tooling. However, it has some drawbacks, as it can be computationally costly, time-consuming and as it tries to replicating the “real world “system it cannot be 100% accurate. One way to overcome these drawbacks is using the robust optimization (RO) methodology. RO considers the uncertainty of the real world, improving the accuracy, and predicts the input/output of the simulation, which leads to a decrease the time and cost to reach process optimization [1].

1.2 Objectives

The aim of this dissertation project is to develop a process to reduce the spread of a metal sheet, producing a flat surface. These defects happen as a result of the previous processes. To accomplish this goal, it was necessary to study the behaviour of the material and then, an optimization strategy was implemented. Summarizing, to accomplish the objective of this work, it was needed to go through a series of steps:

- Modelling a FEM simulation of a Waffling process;
- Analysis of the behaviour of a plastic deformed material;
- Use a Robust optimization strategy;

- Practical test to validate the numerical results;
- Finding optimum parameters and study the effects of the variables on the final angle;
- Creating a process to reduce the spread on the surface of the sheet metal.

1.3 Methodology used

The methodology used is represented in Figure 1. First, it was made the modelling of the waffling process, to replicate the “real world scenario”. This modelling, in the beginning, was made in 2D and then in 3D. With the output of the simulations, it became possible to analyse the behaviour of a plastic deformed sheet metal and the range of the parameters, by changing the Waffling force and by using different pre-bending angles. Then was the preparation of the RO analysis, which consists of the 3D Robust model of the process, a program to do the simulation automatically, a program to get the output of the simulations, and finally making the calculation robust for DACE. After the preparation is done, it was implemented the RO strategy. The RO strategy itself, made it possible to find the optimal parameters and to get a better understanding of the process.

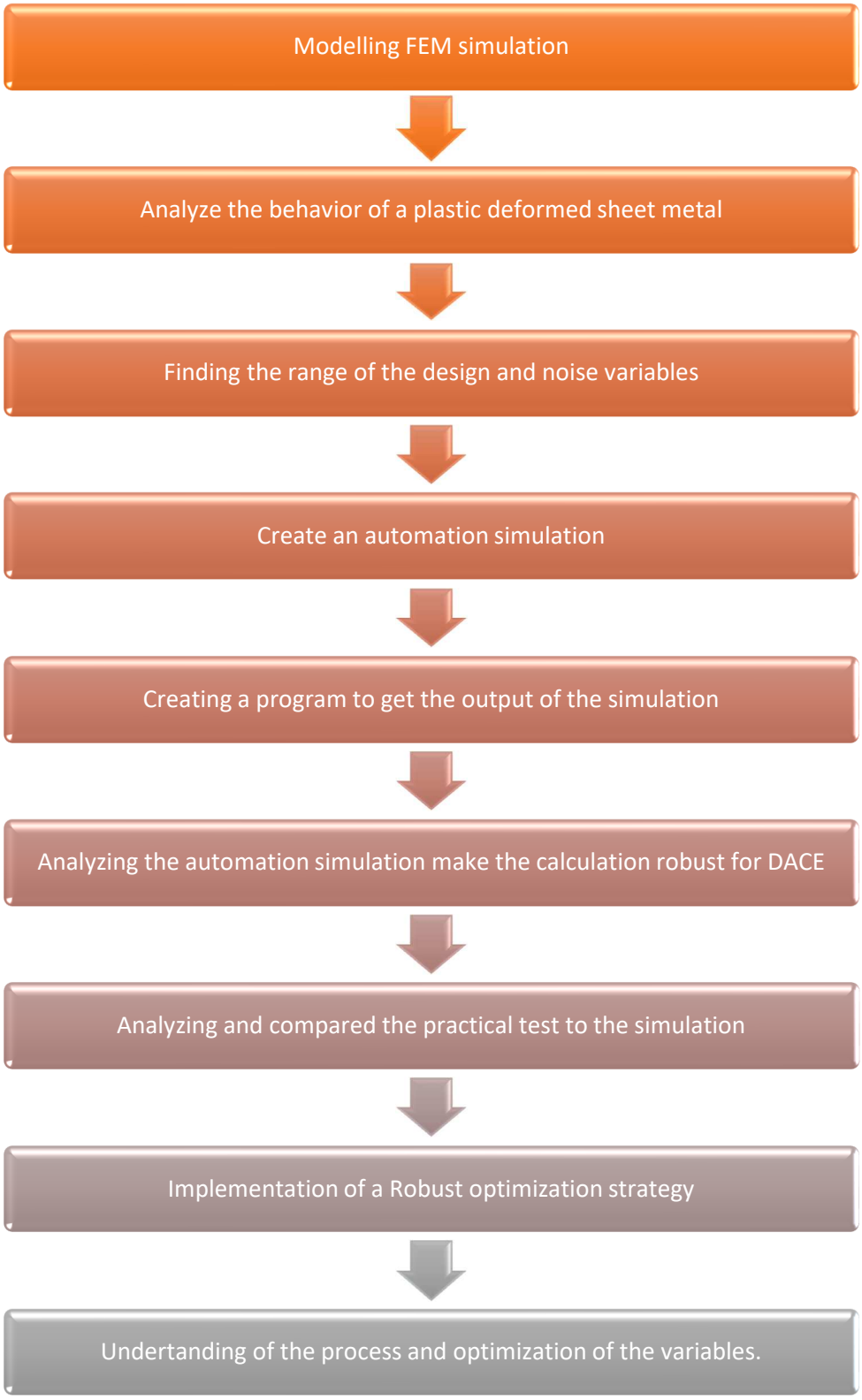

Figure 1 - Methodology used.

1.4 Outline

This thesis is divided in 6 chapters. This present chapter describes the background, the objectives of this project, the methodology used and the company.

Chapter 2 provides a literature review of metal forming, the FE simulations, explains the different variables (noise and design), the different constraints, DOE (Design of Experiments), DACE (Design and Analysis of Computer Experiment), space filling design, the optimization and simulation optimization. It also reviews the Deterministic and Robust optimization. On the Robust optimization subchapter, it is explained the variable-based robust optimization, the Taguchi method, the MC (Monte Carlo), a comparison and explanation of the different metamodels are described and, finally, the screening is reviewed.

Chapter 3 addresses the company characteristics, explains the problem of the spread of an unflatten surface on the sheet metal and the solution to overcome this problem, along with its possible advantages and disadvantages.

Chapter 4 describes the methodology used in this work. In the first place, an explanation of the new model is presented along with the introduction of the robust strategy. Then, the study of the effects of the parameters in the output angle in 2D (Two Dimensions), 3D (Three Dimensions) and the robust 3D and the method applied in practical test and, finally, a more detailed discussion of the steps of the robust strategy.

In Chapter 5, the results are described and, the range chosen for the robust optimization and the effects of the parameters in 2D and 3D, the validation of the numerical results, the metamodels' results on the prediction and deviation, the metamodel optimum value for the design variables, the validation of the optimum and finally a better understanding of the parameters' influence on the flattened surface. Chapter 6 concludes this project with a summary of the most relevant conclusions and recommendations for future work.

1.5 Company

The project presented in this thesis was accomplished at Philips® Consumer Lifestyle B.V., located in Tussendiepen 4 Drachten, The Netherlands, division of Function & Technology Development, Forming, and it was orientated by the Gerrit Klaseboer and Dr. Redmer van Tijum. The internship period had a total duration of 7 months and 13 days (began at 17/02/2020 until 30/09/2020) with 8 hours of work per day during weekdays.

LITERATURE REVIEW

2 LITERATURE REVIEW

2.1 Metal forming processes

Nowadays, technology is the base of our modern lifestyle, in which metal forming technology plays a key role. This process is used by many manufacturers to make various products and semi-finished products, as more than 90% of melted metal is processed by different methods of metal forming. The metal forming has many fields of application such as: products for building construction, automotive sector, household appliances and packaging industries [2-4].

When metal forming was invented, most of the work was done by hand, which required an impressive degree of talent, create an excellent works in silver, bronze, copper, brass, and gold. The early phase of the 80s was marked by the first production of iron sheets with rolling parts [4].

In today's world with the growing of the export volume and complexity of the processes in metal forming generates an early process of globalisation. The metal forming processes are currently used as highly automated mass production processes for manufacturing a wide variety of metal parts that range from car doors to beverage cans, among many other applications. Maximizing product quality and profit (or minimizing costs) are the major goals. It is required to achieve this aim to be competitive in this industry. The developments on the field of design, mechanical engineering, fluid dynamics and hydraulics are being recently influenced by the computer-aided technology CAD (Computer-Aided Design), CAM (Computer-Aided Manufacturing), CAE (Computer-Aided Engineering) and, especially, FEA (Finite Element Analysis), which are some of the most important methods to achieve the goals of each company [2-4].

As explained on DIN 8580 [5], and represented in Figure 2, the manufacturing processes are classified into six main groups:

- Primarily shaping - Production of the initial shape form molten or formless solid;
- Dividing - Local of separation of the material;
- Joining - Assembly of the workpiece;
- Modify the material properties - Changes the material properties to achieve a certain useful property (could be heat treatment processes such as hardening or recrystallization);
- Coating - Application of layers on component;

- Forming technology is defined by the DIN 8580 [5] as “manufacturing through the three-dimensional or plastic modification of a shape while retaining its mass and material cohesion” [4].

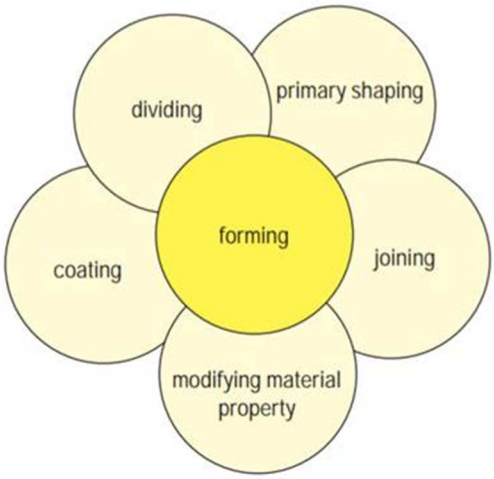

Figure 2 - Overview of production processes [4].

In practical, the forming methods not only include this category discussed above but also subtopics. The most important are:

- Forming under compressive conditions;
- Forming under combined tensile and compressive conditions;
- Forming under tensile conditions;
- Forming by bending;
- Forming under shear conditions.

Figure 3 shows the most important production processes used in the field of forming technology with some examples. The different forming processes corresponding to distinct relative movement between die and workpiece, die geometry and workpiece geometry [4].

The material properties depend on the variance of the temperature. Therefore, the temperature has an important role in the metal forming. There are three ranges of temperature in metal forming: cold working, warm working (above room temperature but below recrystallization temperature) and hot working (higher than recrystallization temperature) [6].

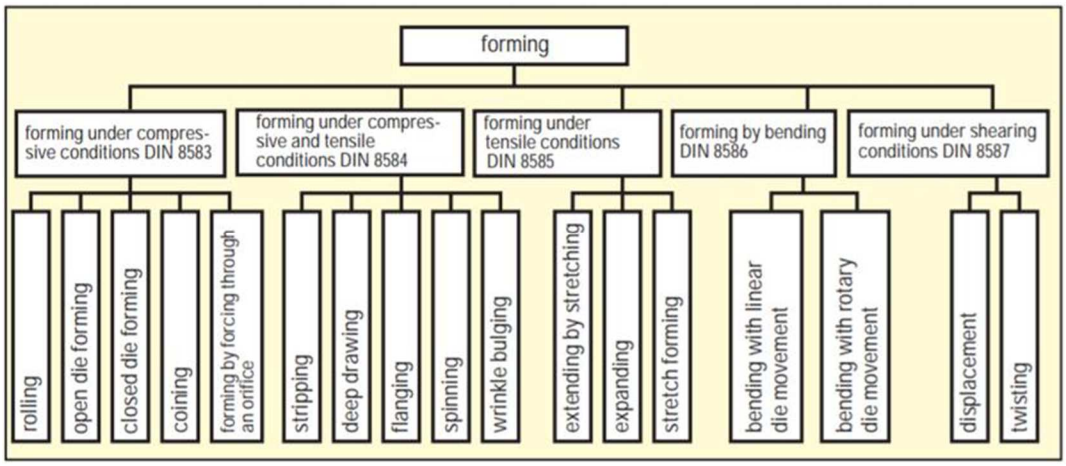

Figure 3 - Classification of production processes used in forming according with DIN 8582 [4].

2.1.1 Plastic deformation – strain

As mentioned before, the metal forming changes the shape of the metal and these changes need to be controlled, and to accomplish this, it is required to know the amount of plastic deformation. It is also possible to determine the forming load and the possibility of defects and failures. The strain is the variable to describe the quantity of shape change [2].

Uniform or homogeneous deformation means that the magnitude of the atrain has the same value for all material points, as it can be seen in Figure 4 and the strain, e , can be defined by the equation (1) [2].

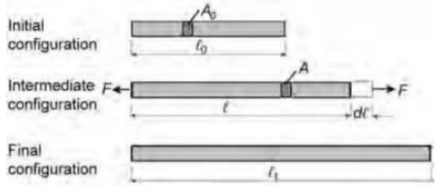

Figure 4 - Uniform deformation of a strip under tensile force [2].

$$e = \frac{l - l_0}{l_0} = \frac{\Delta l}{l_0} \tag{1}$$

here l_0 represents the initial length, the l is the final length and Δl is the difference between the l_0 and l .

For large plastic strain it is used a different equation to measure it. The definition of the inner engineering strain de can be rewritten to different changes of the length dl ,

$$de = \frac{dl}{l_o} \text{ yielding } e = \int_0^e de = \int_{l_o}^{l_1} \frac{dl}{l_0} = \frac{l_1 - l_0}{l_0} \tag{2}$$

So the infinitesimal strain $d\varepsilon$ can be written as the equation (3).

$$d\varepsilon = \frac{dl}{l} \tag{3}$$

The integration over the whole stretching period yields is represented in equation (4). Where the ε is the true strain. For metal forming, as it normally uses a large plastic strain, the engineering strain and the true strain can be related by equation(4).

$$\begin{aligned} \varepsilon &= \int_0^{\varepsilon} d\varepsilon = \int_{l_0}^{l_1} \frac{dl}{l} = \ln\left(\frac{l_1}{l_0}\right) \\ \varepsilon &= \ln\left(\frac{l_1}{l_0}\right) = \ln\left(\frac{l_0 + \Delta l}{l_0}\right) \\ &= \ln\left(1 + \frac{\Delta l}{l_0}\right) \end{aligned} \tag{4}$$

The volume is not changed by the plastic deformation.

2.1.2 Plastic deformation – flow stress, anisotropy.

When the material is deformed, two types of deformation occur, plastic and elastic deformations. The elastic is the beginning phase, where the material will change its geometry as the load is applied, but when the load is removed the material returns to its original shape. The relationship between the load and the amount of deformation in this phase is linear. When the load increases beyond the plastic deformation, the material enters in a plastic phase, in which the material deforms permanently. On this phase, the relationship between the load and deformation is not linear. All this information can be seen in the top of the Figure 5, that represents the stress-strain curve [2].

The stress σ_e is defined by the force F divided by the original cross-section area A_0 as represented in equation (5).

$$\sigma_e = \frac{F}{A_0} \tag{5}$$

The curve of stress-strain is used to determine several basic mechanical properties as:

- Yield strength (y or σ_y) - Indicates the beginning of plastic deformation;
- Ultimate tensile strength (UTS or σ_{UTS}) - The maximum stress in a tensile test;
- Elastic modulus or Young´s modulus (E) - Slope of the elastic part;
- Uniform elongation or elongation break (e_u) - The elongation at the maximum load;

- Total elongation (e_t) - The total elongation of the tensile specimen at fracture, it has e_u and post uniform elongation;
- Area reduction (A_r) - The percentage reduction in the area, it is calculated by the cross-section area at the fracture (A_f) and the initial section area (A_0).

All of these properties are represented in Figure 5.

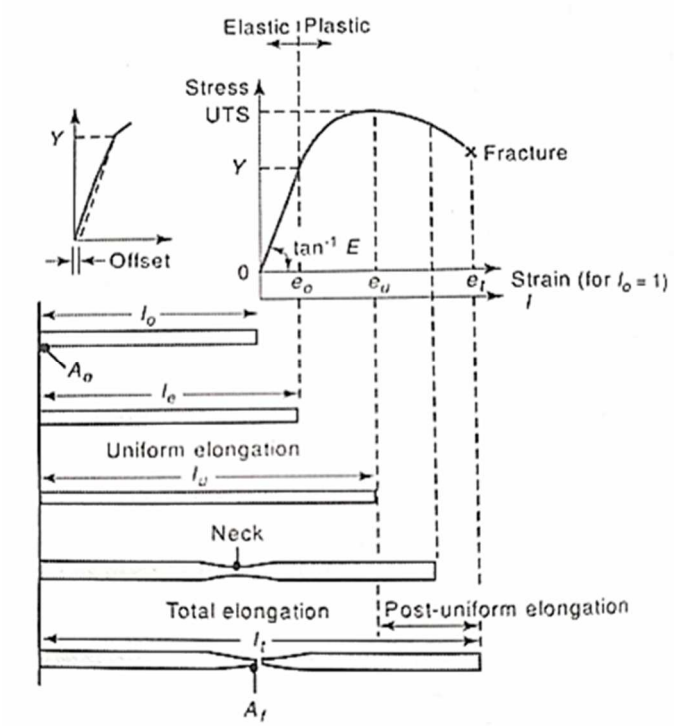

Figure 5 - Stress-strain curve with the ultimate tensile strength [2].

The stress-strain relationship in the elastic region is represented in equation (6).

$$\sigma_e = Ee \tag{6}$$

In the plastic region, the relationship between them is not linear, so it is used the true stress strain definition by using the empirical Hollomon´s stress-strain relationship law, where k represents the strength coefficient and n is the strain-hardening exponent, as represented in equation (8) [2].

$$\sigma = k\varepsilon^n \tag{7}$$

The force can be applied in any direction so the stress needs to be organized by that, being $\sigma_{xx}, \sigma_{yy}, \sigma_{zz}$. They are known as the normal stresses components and are represented in equation (8).

$$\sigma_{xx} = \frac{F_x}{A_{yz}}, \sigma_{yy} = \frac{F_y}{A_{xz}}, \sigma_{zz} = \frac{F_z}{A_{xy}} \tag{8}$$

The A_{yz} is the area normal to the x direction, A_{xz} is the area normal to the y direction and A_{xy} is the area normal to the z direction.

The shear stress (τ) components are on the areas tangent to the force direction and are represented in equation (9).

$$\tau = \frac{F}{A} \tag{9}$$

Both the normal stress and the shear stress are organized by different directions, being τ_{xy}, τ_{yx}, τ_{xz}, τ_{zx}, τ_{yz} and τ_{yz}. The $\tau_{xy} = \tau_{yx}$ because it is a static equilibrium of momentum. The shear stresses are represented in equation (10).

$$\tau_{xy} = \frac{F_y}{A_{yz}}, \tau_{yz} = \frac{F_z}{A_{xz}}, \tau_{zx} = \frac{F_x}{A_{xy}} \tag{10}$$

The normal and shear stresses in an imaginary cube of material can be seen in Figure 6.

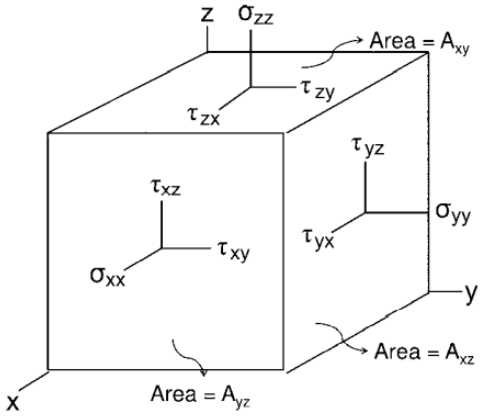

Figure 6 - Stress cube [2] .

The anisotropy is related to the direction of the microstructure. It is divided in two forms (Figure 7):

- Normal anisotropy - Measures the change in the material characteristics that differ through the thickness;
- Planar anisotropy - Measures the change of material characteristics in various directions in plane of the sheet.

The microstructure of the material influences its capability to form into a desirable shape.

The degrees of anisotropy in the plate and through the thickness of the material are determined by the plastic strain ratio (or Lankford coefficient) r represented in equation (11).

$$r = \frac{\varepsilon_w}{\varepsilon_t} \tag{11}$$

The ε_w and ε_t are the width and thickness strain, respectively, as represented in Figure 8. If the ratio is equal to one, it means that it is isotropic (the structure is uniform in all directions). If the value of r is higher, it means that the material is resistant to thinning, so it is more desirable for metal forming. If the material has lower r it has more probability to rupture when deformed.

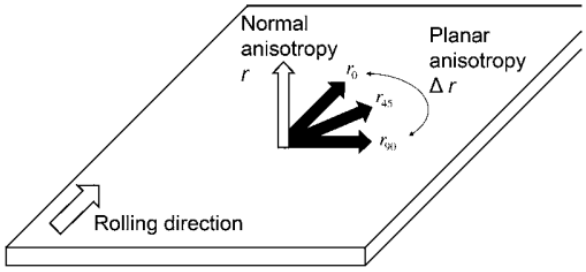

Figure 7 - The normal and planar anisotropy [2].

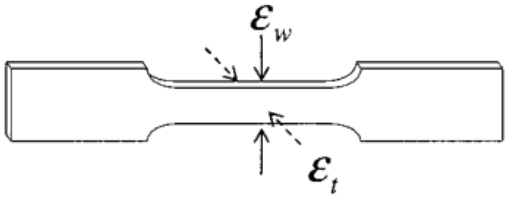

Figure 8 - Representation of the strain in the width and thickness [2].

The plastic strain ratio is usually determined into the rolling direction, normally it has an along direction parallel (r_0), diagonal (r_{45}) and transverse (r_{90}), which can be seen in Figure 7. The average weighted (r_m) of this strain ratio it is normal anisotropy represented in equation (12).

$$r_m = \frac{r_0 + 2r_{45} + r_{90}}{4} \tag{12}$$

2.1.3 Bauschinger effect

The Bauschinger effect refers to a change in material properties by hardening during the reverse load, which is caused by the Geometrically Necessary Dislocations (GNDs) near the passivation layer. This occurs when the material is plastically deformed in one direction of the load and when it is reversed in the direction of the load, the metal is, again, plastically deformed, but in that moment the flow stress has less magnitude than the first direction. This is not what was expected in the isotropic hardening (increasing the yield stress increasing the plastic strain), so it was not possible to predict the true response, but for that anisotropy hardening is used. The result of this effect in a stress-strain graph is represented in Figure 9. The increase in yield stress towards of the applied stress and plastic deformation leads to a decrease in the yield stress in the reverse direction [7-10].

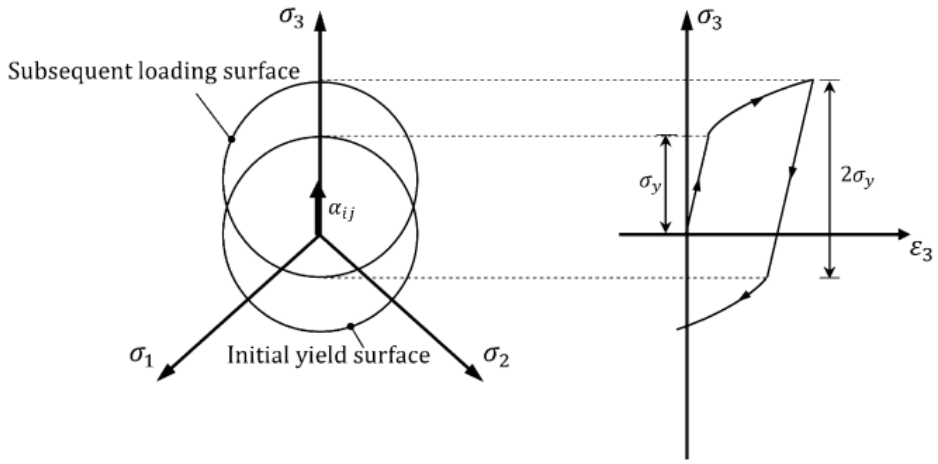

Figure 9 - Representation of the Bauschinger effect in a stress-strain curve and π-plane during uniaxial cyclic loading [9].

2.2 Simulation

As already explained, metal forming is one of the processes that are more used, becoming nowadays a complex, competitive and advanced field. As the technology grows to optimize the process, different innovations and easy methods are being applied. One of the most known methods is the computational simulation. This method replicates the process in a "virtual world", making it easy to change the variables without the cost of tools and material, and therefore making it economically viable. This differs from the traditional model "one shot" and becomes a "sequential" design. With this method it is possible to analyse defects, load profiles, stress-strain curve and many other things. The aim of the simulation is to estimate the true output of the variation of the inputs of the simulation model [6, 11-13].

The expense in this area is related to the computer cost and human resources. The simulation uses the FEA, and the mesh grid over the desired surface. Generally, a more refined mesh leads to better results in terms of the simulation accuracy, but this comes associated with a higher processing time of the simulation. The software for the simulation needs to be provided with the specifications of the process, material, amongst others, to obtain the predictable idea of the process. If the previous parameters are well defined, the simulation results should be very accurate [6, 11, 13].

The simulation could be used to predict and understand the impact of the process parameters. In metal forming, it is commonly used to check the viability of the process design, evaluating the product properties, studying the process insight in order to optimize it and among other applications [11].

The success of the simulation on the process needs [11]:

- The existence of a physical problem properly defined, in which the numerical analysis can be used as a solution;
- The correct analysis of the physical problems, such as simplifications, assumptions, among others;
- The correct spatial discretization such as type, topology and density of elements mesh;
- The correct boundary conditions, for example, friction, heat transfer, and some others;
- The correct use of material laws and parameters, such as flow curve, anisotropy, failure and others;
- A correct selection of numerical parameters (convergence limits, increment sizes, remeshing criterion, among others);
- An economic analysis, being the aware of the computer time, modelling, and others;
- A correct interpretation of the results.

2.2.1 Finite element method

Nowadays the trial-and-error approach in metal forming is not an ideal option and the complex problems in the industry are being solved by numerical simulations. These methods commonly use the FEM and have a wide diversity of engineering application problems [13, 14]. The linear method of FEM has a significant drawback, the limitation of the linear elasticity or, more generally, a linear behavior. To overcome this drawback and, to have a more accurate analysis, the non-linear FEM is often used. The non-linear behavior has two forms [15]:

- Non-linear material - The behavior of a nonlinearity of the elasticity for which the stress is not linearly proportional to the strain;
- Non-linear geometry - The change in geometry of the structure during the analysis, it occurs when the magnitude of the displacement affects the response of the structure.

The FE simulation is a tool to find a numerical solution for complex problems. This simulation tool can be used in heat transfer, stress analysis, among many other fields. The FEM is commonly used in structural mechanics. The concept in the physical interaction of the FEM is the subdivision of the mathematical model into components of simple geometry called FE. Every element has a response expressed in terms of finite number degrees of freedom characterized as the value of an unknown function at a set of nodal points. The output of the response of the mathematical model is an approximation of this model by the connection of the elements [15, 16]. On the representation, in the Figure 10 – (a), shown one structure with the FE model containing multiple hexahedron element as the Figure 10 – (b) with each one having 8 nodal points.

As this is an approximation, the FE simulations are hardly exact. The way to increase the accuracy is by increasing the number of elements, but by increasing the elements it will increase the time of the simulation, so a balance between the accuracy and processing time of the FE simulation must be considered[17, 18].

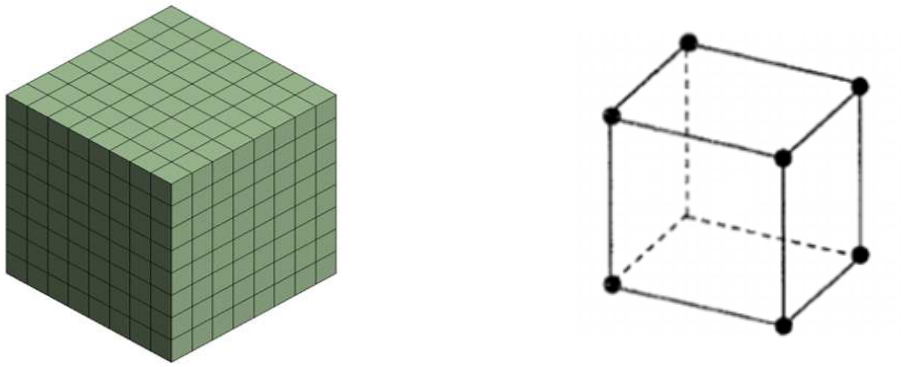

a b

Figure 10 – (a) Structure of the FE model, composed by multiple (b) hexahedron elements.

2.2.2 Black box

The Black-box function is a simulation computer model. How the function works is not going to be discussed here, however, this function is used to replace a set of FEM models and there is only one request that needs to be fulfilled in order to do this: the function needs to be able to process a set of input variables and return one or multiple response values and, as a result, the optimization process becomes suitable for the numerical model. The layout of the black-box optimization is show on Figure 11 [19].

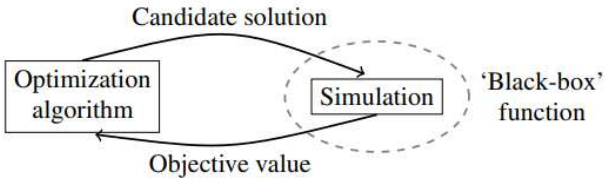

Figure 11 - Layout of black-box optimization problem [19].

2.2.1 Variables

The inputs of the simulation are the variables, such as the load, the tool dimensions, amongst many others. In the manufacturing environment the process is influenced by two types of variables, the controllable, called design, and the noncontrollable, which can be called uncertainty or noise variable [1, 16, 20, 21].

2.2.1.1 Uncertain or noise variable

The uncertainty or numerical noise, as mentioned above, is an uncontrollable variable. This is an unavoidable and inherent characteristic. There are several examples of these inputs on metal forming, such as the different material parameters between different pieces of the same material, the friction coefficient, and others. The repercussions of these variations can be seen on the quality of the response which also varies, contrarily to the deterministic approach. To boost the accuracy, it is crucial and necessary to develop an approach of uncertainty analysis [16, 21-24].

The relationship function f between the design variable x and the parameters p on the output is:

$$f = f(x, p) \tag{13}$$

the parameter of uncertainty is the denoted by z_p, being the perturbation of the parameters,

$$f = f(x, p, z_p) \tag{14}$$

the design variable of uncertainty will often enter the process in terms of a perturbation z_x of the design variable as equation (15) shows [16].

$$f = f(x + z_x, p) \tag{15}$$

2.2.2 Constraints

The constraints represent the border between the acceptable problem and the rejected problem. They can be divided in linear or non-linear constraints and implicit or explicit constraints. The explicit constraints directly depend on the design variable and this does not require the run of FE simulation, as it can be seen in Figure 12. One example of this type of constraints is the volume of the workpiece's dimensions after the process. The implicit constraints indirectly depend on the design variables and need to run the FE simulation as it can be seen in Figure 12, in metal forming this is sometimes related to the final deformation and/or accuracy geometry, many examples of this type of constraint result on the wrinkling or fracture of the product, thus bringing a significant amount of scrap rate and higher deformation [16, 21].

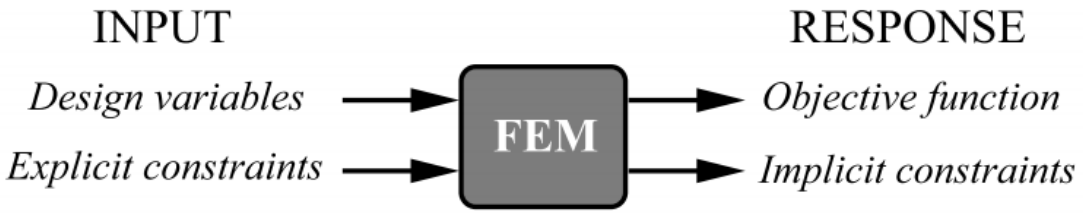

Figure 12 - Input and output with two types of constraints [21].

2.2.3 DOE

The Design of Experiement (DOE) is a process planning design and analysis of the experiment. It is a statistical technique that, by fixing values during the simulation experiment, creates an empirical model to determine the input combination of the system. It is used to design problems with uncertainty [1, 25-27].

The DOE methodology is applied to determine the variables (input factors) and to obtain an empirical model, like the robust system, by reducing both the combination of inputs and resources needed [27, 28]. A general model to DOE is shown in Figure 13 . It has a potential application on manufacturing processes such as [1]:

- Improved process yield and stability;
- Improved profits and return on investment;
- Improved capability of the process;
- Reduced process variability and having consistent performance on production;
- Reduced manufacturing costs;
- Reduced process design and development time;
- Increased understanding of the relationship between key process inputs and output(s);
- Increased business profitability by reducing scrap rate, defect rate, rework, retest, and many more.

This technique is performed by changing the input process or machine variables to analyze and observe the corresponding changes in the output process [1]. Its biggest disadvantage resides in the cost involving the application [27, 28].

Parameters and input variables together are called factors. The output is called response and the number of different variations of the factors are called level in DOE [29].

In some experiments increasing of the DOE points does not increase the accuracy of the experience on a significant level. A way to get a better accuracy is by placing the points at a specific location [16, 23].

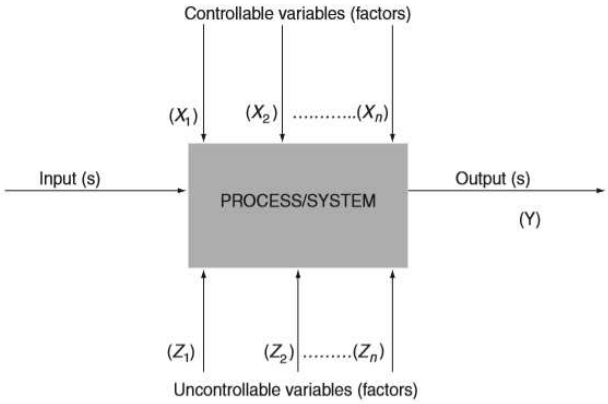

Figure 13 - General model of a process/system [1].

2.2.4 DACE

The DACE is a DOE when the scenario at hands is a simulation where the main objective is to improve the efficiency and effectiveness of the analysis by getting the effect of the input parameters [27, 29, 30]. However, there are some differences between DACE and DOE, as the DACE reproduces the FEM response, it can be used with different approaches and investigates mainly the basic understanding of the system. The computer simulation can have a large number of inputs variables, which make the usage of the DOE not advisable. Another big difference is the complexity of the relationship between the response and the output variables. The DOE only enables the creation of noncomplex formulas, while the DACE can result in a non-relationship. The usage of the classic DOE is not ideal for a computer simulation sample plan, since it can lead to low efficiency in predicting the output in comparison to DACE. The application of DACE differs from the classic one, because the computer environment lacks on random variations, conditions for which the DOE was developed [27, 29].

One of the criteria for applying the DACE is the need for space-filling. The other is the prevention of the two-level of a non-important factor to be united, which is called the small discrepancy design [27].

Some literature considers DACE to be a part of DOE [27].

The DACE approach can be used to build metamodels, facilitating the reduction of many material resources, the develop time of enterprising products, and by also improving the quality of the product development process [27].

2.2.5 Space-filing design

The optimal design is selected by the input that will produce a computer output, which then needs to achieve a specific goal. Some optimal design uses the response of the sample only in the extreme points of the design space (full factorial design or fractional factorial design). This is done by minimizing the variation of prediction. A drawback is that it does not specify well the model, and if the response is nonlinear it is not appropriate to use this approach due to the poor approximation. The approach well suited for this problem is the space filing design. With this technique it is possible to explore the nature of the response surface by obtaining the observation through the range of the design space and not only in the extreme points [31, 32]. The commonly known space filing is the stratified random sample, the Latin Hypercube sample and Monte Carlo sampling. They are used in different approaches, the Monte Carlo sampling is used when the metamodel already exists, while the Latin Hypercube sample is used to get the points for the metamodel [31-33].

The stratified random sample uses a set of N points created by dividing the experimental region into n layers, spread evenly throughout the experimental region, and randomly choosing a single point for each. By varying the size and position of the layers, along with

having sampling with different distribution in the layer it allows a significant flexibility in selecting the design. The disadvantage is due to the difficulty to guarantee the project properties of the design. To solve this problem, a sample of the Latin Hypercube can be used [32].

The Latin Hypercube samples are called LHD (Latin Hypercube Design). In many cases this is the best space filing design [34, 35] . It uses an array of n (this n is the amount of design variables which are divided into subintervals) and columns of m (m is the amount of design variables). This is made by assigning to each column a random permutation of $\{1,\ldots,n\}$, independent of the other column. Each line (row) of the output array defines the design point for the n-run experiment, either at a fixed point in each subinterval, being in the end point or midpoint or random point within the subinterval. The generation of this interval is made by a lattice square which is created from a set of orthogonal Latin squares. By using this, a point appears only in each row and column of the matrix, as it can be seen in Figure 14. This technique selects each sample by ensuring that the points are (marginally) spread evenly over the values of each input variable [29, 31, 32, 35, 36]. The input value can be sampled by any distribution, uniform, Gaussian or others and it is used on robust optimizations. The advantage is when one of the parameters does not have much influence on the process and can be neglected, meaning that the LHD will collapse. This happens due to the space filing the remaining parameters get more density [33, 35-38].

The MC analysis is analyzed in chapter 2.4.3.

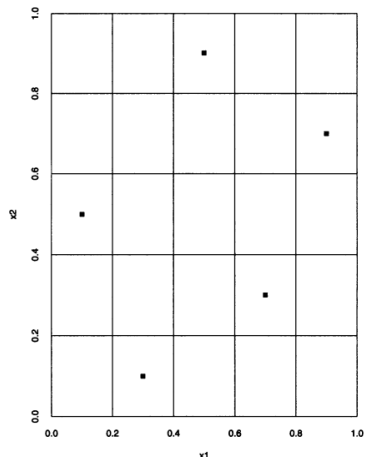

Figure 14 - Space filing Latin Hypercube Design [32].

2.2.6 Optimization

The basic idea of mathematical optimization is to study the problems and minimize or maximize a certain function by systematically choosing the values of certain variables [16, 21].

The optimization coupling with the FE simulation has many industrial applications. This approach uses the FE simulation as the process design and, this technique is more efficient than the conventional (trial-and-error approach) [16].

The optimization occurs by minimizing the object function f, by finding the optimization value of the design variables x. A few types of restrictions and constraints can be presented as equality constraints h, inequality constraints g or box constraints. The box constraints or sometimes denoted as bonds, define the variation by an ub (upper design variable) and ib (lower design variable). The optimization problem can be described by the following formulation [16, 21].

$$\begin{aligned} &\min f(x) \\ &s.t.\ h(x) = 0 \\ &\quad g(x) \le 0 \\ &\quad ib \le x \le ub \end{aligned} \tag{16}$$

The result of this optimization is the optimum value x_c^* as shown on Figure 15.

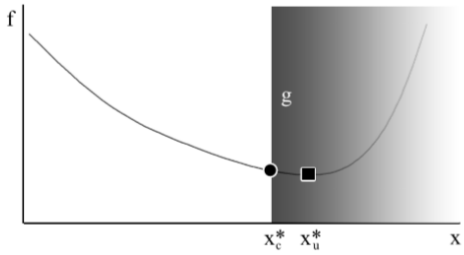

Figure 15 - Mathematical optimisation [21].

2.2.7 Simulation Optimization

The SO (Simulation Optimization) is classified into two models: the model-base, where the simulation running time is reasonable, while the other is a metamodel-base. In this last one the simulation is applied to more complex systems, particularly when uncertain and when more time-consuming and higher computer cost problems [30, 39].

The metamodel-base is the most interesting model of the two, as said above. It can be used by considering the uncertainty and increases the complexity to resemble the “real world”. This type of SO uses a metamodel combined with RO [30, 40].

This technique aims to find the optimum value model for the simulation output while reducing the resources. The challenge of increasing the simulations’ accuracy by taking into account uncertainty is overcome by the robust optimization and SO that allows the possibility of defining the optimal set point for input while keeping the output more similar to the ideal point [25, 30, 40, 41].

In order to optimize, this simulation technique strategy can be split into two parts, the first being the simulation modelling and the second one being the SO, as it can be seen in Figure 16 [30, 39].

The SO approach depends on the problem that needs to be optimized [25, 30].

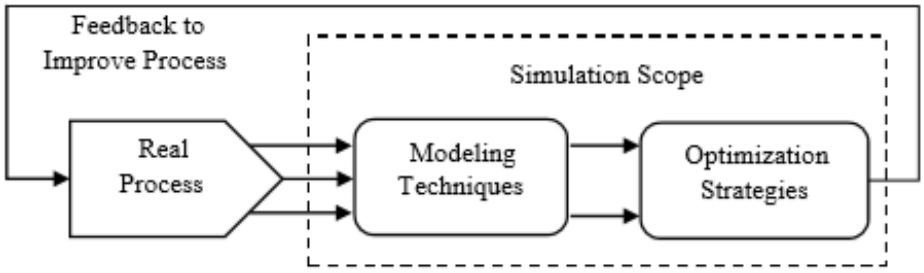

Figure 16 - An overview of simulation scope [30].

2.3 Deterministic optimization

Deterministic optimization has been successfully applied to a variety of design problems in structures on different industries such as automotive, aerospace transportation, and many more [42].

This approach has a considerable drawback, the variables are considered all known, so the inputs are only controllable variables. As explained before, neglecting the uncertainty does not replicate the "real world" scenario. The accuracy of the optimization depends on the inputs since in this approach these are only design variables. Subsequently, the output of the optimization will be less accurate. For several design problems, the uncertainty needs to be analyzed in order to get better accuracy and the most reliable approach is in fact the robust optimization [16, 21, 22, 29, 43].

2.4 Robust optimization

The Robust optimization (RO) finds the optimal combination of the design variables, taking into account the uncertainty of the system. This approach manages the uncertainty of the "real world" in a probability way. The first developer of RO was Taguchi. This approach focuses on optimizing the design that minimalizes the sensitivity of the uncertainty, being the main goal an optimum design with the lowest possible variance of the object function Adequate sample size and implementation of post-process have a higher impact on finding a global robust optimization [1, 44].

The principle of robust design optimization is shown in Figure 17, being f the variable of the response. This variable is quantified and minimized by selecting variable settings $x_2 + z_2$, instead of $x_1 + z_1$, leading to a narrower response distribution, and therefore creating a more robust design [16, 21].

The work by RO is made by DOE, to get the output data by experiments. A metamodel can be used in order to achieve an optimal design variables solution, and also to validate a statistical approach [26, 28, 38].

The RO formulation is given by [16]:

$$\begin{aligned} &\min \sigma_f(x) \\ &s.t.\ \ g(x) \le 0 \\ &\quad ib \le x \le ub \end{aligned} \tag{17}$$

In this way the response distribution is minimized [16].

One of the main disadvantages resides in the prediction of the variance, which may contain a large local error due to this type of optimization being determined by successive approximation models [44]. Another disadvantage that needs to be taken into consideration is the high computational cost [43].

The RO has a different numerical approach to SO, such as the Taguchi method, Monte Carlo Analysis and metamodel [37].

There are many possible combinations to achieve the RO, one of them is by using the Kriging metamodel, the Pareto-optimal solution [26], the other one is by applying Taguchi robust terminology and finally the crossed array design. Some of the statistical techniques are replaced by DACE and Kriging [24, 33], or by Latin hypercube sampling and Kriging [43], amongst others.

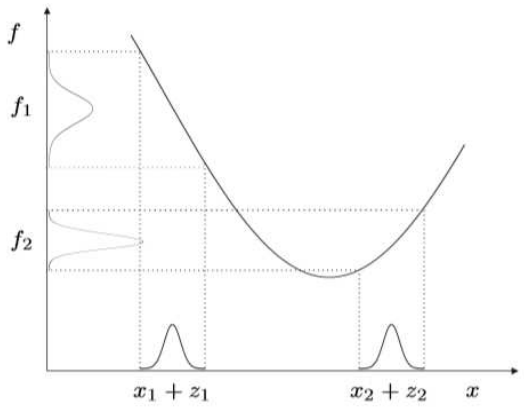

Figure 17 - Principle of robust Design Optimization [21].

2.4.1 Variance-based robust optimization

The Optimization Under Uncertainty (OUU) works by optimizing the process, reducing the impact of the uncertainty to an acceptable level. The reliability of this approach is formulated by moment matching constraints formulation expressed on the equation (18).

$$\mu_g(x) + k_g \sigma_g(x) \le 0 \tag{18}$$

The σ_g and μ_g are vectors that signify the uncertain constraints and standard deviation, respectively. The k_g is a normal distribution that contains the probability of

constraints. This way the k_g = 3, which means 3 σ_g represents the chance of 99.73 % that $g(x) \leq 0$, if the constraints have a normal distribution.

The robust process has a higher potential to result in a better process accuracy because the process has limited response variation and it is simple to satisfy all the uncertain constraints, than having a process that has a significant response variation. There are different types of optimization formulas, one of them being the *multi-objective type* or *weighted sum formulation,* whose aim (19) is to minimize the mean performance and the response variation, simultaneously.

$$\alpha \frac{\mu_f(x)}{\mu'_f} + (1-\alpha) \frac{\sigma_f(x)}{\sigma'_f} \tag{19}$$

The μ'_f and σ'_f are the function values for each individual optimization in terms of mean performance and variance, respectively. The α is the weighing factor, and it depends on the importance of minimizing the mean-variance.

The equation (19) can be written in a form comparable to the equation (18) although it only considers the mean μ_f and standard deviation σ_f. The optimization occurs by reducing the single optimization as it sets α as a constant before the optimization. As it is a robust it takes into consideration the noise variables z. The noise variable has an normal distribution with the mean value μ_z and a corresponding variance σ_z^2 so $z \sim N(\mu_z, \sigma_z^2)$. The robust optimization formula is shown in the equation (20).

$$\begin{aligned} &\min_x \ \mu_f(x) + \alpha \sigma_f(x) \\ &s.t. \ \ \mu_g(x) + k_g \sigma_g(x) \leq 0 \\ &\qquad ib \leq x \leq ub \\ &\text{where } z \sim N(\mu_z, \sigma_z^2) \end{aligned} \tag{20}$$

2.4.2 Taguchi Method

The Taguchi Method (TM) is a technique whose objective is to optimize the product development, through an approach that leads to the creation of a robust product with higher quality. The objective of the TM is to minimize the variation in the response by identifying a proper set of design variables. It can be used on technical feasibility and manufacturing [16, 26, 34, 45].

This approach uses DOE base on orthogonal arrays to evaluate the response of mean and variance. There are two arrays, the inner array consists of the design variance, and the crossed array which consists on the noise variable. The optimization is achieved by a factor level of combinations, which contains both the control factor (inner array) and the noise factor that are tested against multiple combinations. This can be referred to a

"quasi-repetition", this way the behaviour of each factor level can be tested in the influence of the noise factor [16, 24, 40, 45, 46].

The analysis of the experiments on this DOE is performed by calculating a signal-to-noise ratio (SNR), this preforming criteria taking into account the process mean and variance by the ratio between the power of the signal and the power of the noise. In order to find the optimal design variation, it can maximize the SNR followed by a "pick-the-winner approach"[16, 45, 46].

This method is usually used on DOE because it requires a small number of tests, and it could be used on practical experiments, as well as in simulations [45].

The TM is easy to understand and does not require higher knowledge of statistics, and at the same time it is capable of reducing the computer time [16, 45-47]. But there is a downside to this method, there is a limitation on simple optimization problems with a low number of parameters. Another disadvantage resides in the fact that the SNR combines the mean and variance, and can be confused on the response, resulting in the incapability of not being able to distinguish which of the parameters are affecting the mean and which ones are affecting the variance. At last, it must be considered as another downside the impossibility to take into account the interaction effects between the design variables [16, 45].

2.4.3 Monte Carlo

The Monte Carlo (MC) analysis can be used to analyze, solve and optimize many mathematical or physics problems, by generating a large number of statistical random samples to simulate stochastic events. It can be applied to a normal distribution, to exponential distribution, to Weibull distribution, and many others. It takes into account the uncertainty in the inputs and does not need to know the parameters distribution type and probability parameters [16, 22, 29, 30, 48]. In other words, the MC method is a computer-based simulation or method that can calculate the mean and variance of the distribution's response. The accuracy highly depends on the number of samples, as it is needed a large number of responses, and to improve the robustness of the new product, it is required an adjustment on the precision value of random design variables on Monte Carlo [16, 48]. It is possible to improve time calculation in MC with a response surface [29].

There are many advantages to this technique, as an instance, it can avoid increasing costs, due to duplicate experiments and excessive design precision, it is easy to understand and does not require higher knowledge of statistics [16, 48]. As for the disadvantages, the computer expenses are increased by a combination directly related to the number of simulations, and consequently, a limited number of MC will be generally evaluated. Nowadays, however, there are already better techniques that have higher efficiency than the MC Analysis, as some examples, the adapted MC, multilevel

Monte Carlo, descriptive simulation, importance sampling. Another approach results from combining the Monte Carlo Analysis with a metamodel [16, 49].

2.4.4 Metamodels

A metamodel approximates the input/output function that is defined by the simulation model, in the equation (21) shows the objective of the metamodel $\hat{y}$ on accurately approximate a true model y and the ε is the random error. It is an interpolation obtained from an experimental plan that simulates the physical behaviour of a product using virtual prototyping, like several runs of computer experiments, which culminates on the reduction of the development time of the said product. This metamodel optimization approach is interconnected with the simulation by guiding a DOE [16, 27, 29, 30, 50-52].

$$y=\hat{y}+\varepsilon \tag{21}$$

The aim is to create an empirical model emulating the behaviour of the original code, and due to this, a much larger number of experiments can be done in a short time. Another advantage is that it has a deterministic structure, and therefore it is preferred, compared to the iteration optimization [16, 27, 34].

It is majorly used on complex simulations under uncertainty and higher running costs as it takes into account the design and noise variables. Its performance strongly depends on the chosen building block for the algorithm. To estimate and validate the uncertainty of the radial function metamodel it is applied the LOOCV (Leave-One-Out Cross-Validation) measurement [16, 37].

There are two models on the metamodel-base: the determinist and the stochastic model. The big difference between them is that the determinist model response lacks random error, contrarily to the response on the stochastic or random model, which usually follows some probability distribution, that may vary around the space and takes into account the random errors [30].

The metamodel methodology is divided into two categories, the non-adapted metamodel and the adapted metamodel. The first one is the traditional method, using data sample strategies to uniform the input parameters space to improve the quality of the metamodel. On the other hand, on the adapted metamodel the data sample is sequential, so on the first step the initial sample data builds an initial metamodel, this step locates the input parameters to collect the next sample. In the second step, the new sample is used to update the metamodel, then this new data has a new input location and is updated to the next step. This process is iterative and only stops until the model satisfies the request that was initially made [53].

The most used metamodels are the Response surface methodology, Kriging (Gaussian process), and neural networks [16, 25, 30, 50, 51].

2.4.4.1 Dual response surface method

The Dual response surface methodology is one of the most commonly used approaches in robust optimization. It is obtained with the DOE to get the response information. This approach uses the design of points, which combines the control and uncertainty variables and uses a combined array design. This results in two responses separately, one for the mean and other for the variance [16, 54, 55]. The dual response surface can be fitted within two metamodels, for the multiple design variable setting. The output of the metamodel provides an understanding of the change in mean and variance as a function in the design variable [16, 55, 56]. One advantage is that it allows for metamodel improvement by sequentially adding DOE, it has iterations effects and the mean and variance are not confounded. But the disadvantage is that many of the response evaluations are required for noise and design variance [16].

This technique has different optimization approaches [46].

2.4.4.2 Single response surface method

The Single response surface method is used by a DOE in combination with design noise variables in space that determines the relationship between the variables and the response. For this approach, only a single metamodel is fitted, and to obtain an estimative of the mean and variance of the response, an MC Analysis that runs with the metamodel can be resorted.

This technique has many approaches with various DOE and metamodels (Kriging, RSM (Response Surface Method) and NN (Neural Networks)).

The advantages are the same as the dual response surface method [16].

2.4.4.3 Response Surface Method or Polynomial Regression

The Response Surface Method (RSM) is a linear-regression metamodel that consists of a sequence of local first-order and second-order polynomials that is useful for developing and optimizing a process [25, 29, 30, 33, 47, 51, 57].

The metamodel algoristhm of RSM involves iterative improvement of the objective and constraints function employing locally supported nonlinear approximation and due to this, it employs a sequence of local experience analysis and can be combined with various optimizations methods for single or multiple responses [25, 30, 34, 57].

The RSM is a metamodel implemented through the response measurements or observations y providing a random error term ε. The equation (21) can now be represented as equation (22) [16, 29].

$$y=X\beta+\varepsilon \tag{22}$$

Where X is a matrix containing the levels of independent variables, the β is a vector of regression coefficients and ε , as already explained, it is the vector of random error terms. Matrix X can have a non-linear terms with respect to the variables. The order of these terms is the order of the polynomial model. The metamodel is represented in equation (23) [16].

$$\hat{y}=\mathrm{X}\beta \tag{23}$$

The unknown regression of coefficients β are defined by minimizing the error sum of squares at the points, also said as quadratic loss function or $L_2-\mathrm{norm}$ as represented in equation (24) [16].

$$\varepsilon^T\varepsilon=\left(y-\mathrm{X}\beta\right)^T\left(y-\mathrm{X}\beta\right) \tag{24}$$

As the goal is to determine β it was rewritten the equation (24) and setting the result to zero yields the finest estimation of β, representing this in equation (25) [16].

$$\hat{\beta}=\left(\mathrm{X}^T\mathrm{X}\right)^{-1}\mathrm{X}^T y \tag{25}$$

Where $\hat{\beta}$ is the estimation of β. The response prediction $\hat{y}_0$ at an point x_0 is represented in equation(26) [16].

$$\hat{y}_0=x_0^T\hat{\beta} \tag{26}.$$

The variance at this localization is represented by the equation(27) [16].

$$\mathrm{Var}\left(\hat{y}_0\right)=\sigma^2 x_0^T\left(\mathrm{X}^T\mathrm{X}\right)^{-1}x_0 \tag{27}$$

Where σ^2 is the unbiased estimation of the error variance and it is represented in the equation (28) [16].

$$\begin{aligned}\hat{\sigma}^2&=\frac{\varepsilon^T\varepsilon}{n-p}\\&=\frac{\sum_{i=1}^{n}\varepsilon_i^2}{n-p}\\&=\frac{\sum_{i=1}^{n}\left(\hat{y}_i-y_i\right)^2}{n-p}\end{aligned} \tag{28}$$

Where n is the number of response measurement and p is the number of the regression coefficient. For a linear metamodel, coefficients $p=m+1$ where the m equals the number of the design variables. The prediction uncertainty of the metamodel is given by the square root of the variance, as represented in equation(27) [16].

This polynomial regression metamodel can be used as two main consecutive steps, first it is done the screening and then the optimization. In the first step, the levels of interest

of input factors can be identified and in the second step, the reduced interval of input factor can be studied [25, 30].

One of the aims of RSM is to explore the relationship between design variables and single or multi-response, analyzing and finding the best operating conditions of the process by setting a factorial or independent variable, which are then characterized by the equations model suitable to be used for optimization and implementing robust against uncertainty [23, 25, 30]. This RSM approach is an alternative to replace a complex model by an approximate one based on results calculation at some points on the design space [30, 57]. One of the main objectives for this method is to be able to do a polynomial approximation for a true response function, based on Taylor series expansion around a set point [30].

The validation is applied so that it can analyze the accuracy of this method and for the RSM model the validation is based on (ANOVA) and a residual plot [51].

When using this approach, the input of the irrelevant effects should not be eliminated in a local first-order polynomial because this input could be significant in the next local area [25]. It can be used to analyze the springback [57].

The advantages of this model are that it is easy to establish, it has a better performance on low order non-linear response function, it can get a more distinct and sensitive analysis and it is also less complex and cheaper to work with [23, 30, 47, 56].

The disadvantages of this technique reside on the problems that come from using this approach on constraints, the achievement of a computationally costly database, less efficiency on problems with highly non-linear and irregular performance, amongst some others [23, 25, 56].

2.4.4.4 Kriging

The RO can be developed using a Kriging or Gaussian process. This statistical model obtains a design formula that can be expressed in a mathematical way, managing to simplify optimization, which uses an interpolation method and mathematical relationship between the uncertainty and design variation [16, 26, 42, 44, 58]. This model is fitted to the data collected on global experience areas, more than in small locals (the small locals usually use low-order polynomials) [16, 26, 33, 44]. The statistics for simulation experience points are determined by using MC based on the Kriging model of response [42, 44].

As the response should interpolate through the response value at the points, the remaining random error $\mathcal{E}$ is represented in equation(21). This metamodel uses a defined base function or regression part represented in equation (29). The random error $\mathcal{E}$ will be replaced by a basis functions or a stochastic part $\mathrm{Z}(x)$ to evaluate the exact predictions at the points [16].

$$y = \mathrm{X}\beta + \mathrm{Z}(x) \tag{29}$$

Where $\mathrm{Z}(x)$ is a Gaussian stochastic process with a mean zero. The process variance σ_z^2 and spatial covariance function is represented in equation (30) [16].

$$\mathrm{cov}\left(\mathrm{Z}(x_i), \mathrm{Z}(x_j)\right) = \sigma_z^2 R\left(x_i, x_j\right) \tag{30}$$

Where $R\left(x_i, x_j\right)$ is the relationship between the known measurement points x_i and x_j, R is the correlation function that determines the shape of the metamodel between measurement points and is, this case the Gaussian exponential correlation function, represented in equation (31) [16].

$$R\left(\theta, x_i, x_j\right) = \exp^{-\theta\left(x_i - x_j\right)^2} \tag{31}$$

For the m design variables presented, the correlation function depends on the m one-dimensional correlation functions as represented in equation(32)[16].

$$R\left(\theta, x_i, x_j\right) = \prod_{l=1}^{m} \exp^{-\theta\left(x_{il} - x_{jl}\right)^2} \tag{32}$$

Being the entries of the vector $\theta = \{\theta_1, \theta_2, ..., \theta_m\}^T$ and the distance between the known measurement points x_i and x_j it can be determined the structure of $R\left(\theta, x_i, x_j\right)$. This metamodel is introduced to minimize the mean square error between the prediction $\hat{y}(x)$ and the true value, although it is still unknown the response function $y(x)$. This is represented in equation (33) [16].

$$\begin{aligned} &\min\ E\left(\hat{y}(x) - y(x)\right)^2 \\ &\text{s.t.}\quad E\left(\hat{y}(x) - y(x)\right)^2 = 0 \end{aligned} \tag{33}$$

As already explained, it will minimize the mean square error subjective to the constraint, certifying that there is no systematic error between the metamodel and the true function. The BLUP (Best Linear Unbiased Prediction) $\hat{y}(x)$ at a point x_0 is represented in equation(34).

$$\hat{y}_0 = x_0^T \beta + r_0^T R^{-1}\left(y - \mathrm{X}\beta\right) \tag{34}$$

Where X is the design matrix containing the respective points. r_0 is the vector that has the correlation between the points $\left(x_0, y_0\right)$ and the known measurement $\left(x_i, x_j\right)$. R is the matrix containing the correlation between the points given by equation (31).

The calculation of the MSE (Mean Square Error) can be done at a location x_0 by the equation(35).

$$\mathrm{MSE}\left(y_0\right) = \sigma_z^2 \left(1 - \begin{bmatrix} x_0^T r_0^T \end{bmatrix} \begin{bmatrix} 0 & \mathrm{X}^T \\ \mathrm{X} & \mathrm{R}^{-1} \end{bmatrix} \begin{bmatrix} x_0 \\ r_0 \end{bmatrix}\right) \tag{35}$$

The unknown parameter β, σ_z^2 and θ can be estimated by the MLE (Maximum Likelihood Estimation). The MLE function is equal to minimizing the error sum of squares when the error can be accepted as a Gaussian noise. This optimization is solved by applying the DACE MATLAB toolbox [16].

The regression in Kriging is done to improve the ability of the prediction. This is made by applying a regularization constant λ to the leading diagonal of the correlation matrix R as $R + \lambda \mathrm{I}$. This allows the metamodel to regress the data and approximate the noise functions. Without the regression constant, every single point has an exact correlation with itself, making the metamodel pass through the points. The regression constant λ is optimized along with the other unknown parameters in the MLE, delivering the regression Kriging prediction given by the equation (36).

$$\hat{y}_0 = x_0^T \beta + r_0^T \left(R + \lambda \mathrm{I}\right)^{-1} \left(y - \mathrm{X}\beta\right) \tag{36}$$

There are many advantages to this process, such as flexibility due to a wide range of correlation functions, reducing the computer time on achieving the statistic of a real model, accounting and quantifying the intrinsic random noise, it can be applied to problems with up to 20 parameters, a more accurate approximation over a wide range of samples, size and design [24, 25, 33, 34, 37, 40, 50, 56].

The disadvantage of Kriging is that it is more complex than a low-order polynomial (RSM), it has limited parameters, as the increasing on the limitations leads to an increase in the running time, and it has a poor accuracy of prediction in cases of extrapolation sample data [30, 33].

The accuracy of this metamodel can be analyzed by cross-validation, prediction error and MSE [22, 51, 56].

This metamodel approach is considered to be more reliable and flexible than the Response surface method, it presents more accurate predictions of a highly nonlinear function, the behavior of Kriging is appropriate to carry out an effective and efficient robust optimization where there is uncertainty. It can be applied to a real-world data, and while compared to NN and RBF (Radial Basis Functions) it can quantify variations [22, 24, 30, 33, 34, 37, 42, 43, 59].

2.4.4.5 Neural Network

The ANN (Artificial Neural Network) is a metamodel used for extracting the effectiveness of the input variables on the objectives and to aim the desired function. It can recognize the complex relationship between input and output data set and then predict new results based on experience [60-65].

The most used NN is the feed-forward, multilayer perception trained by back-propagation algorithms base on the gradient descent method. This algorithm can give an approximation to any continuous function and has a reduced duration. To develop

the most proper ANN, it was used several neurons in the hidden layer and layers with different transfer functions to estimate the optimal system. Different variations of the network structure were used until convergence was accomplished as can be seen in Figure 18 [61, 65].

This metamodel approach is electable, capable of capturing the nonlinear relationship and interaction of the process parameters [62].

To evaluate the analysis of this metamodel it resorted to the MSE, the RMSE (Root-Mean Square Error), and the coefficient of determination R^2, which are statistical verifications [60, 61].

The benefits of this approach are in the capability of getting a higher accuracy and flexibility, it makes it possible to solve more complex engineering systems, and where it is difficult to introduce a mathematical model [60-62, 66].

The disadvantage is that the training process can be time consuming, the software can limit the number of parameters, and the influence of training can lead to a lack of robustness [67].

The NN could be used to solve a wide variety of problems on metal forming [60, 61, 63, 64, 66].

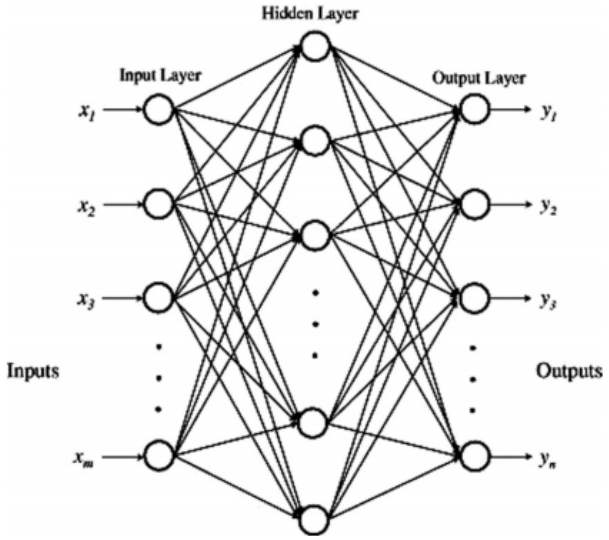

Figure 18 - Multilayers perception for NN [65].

2.4.4.6 Conclusion of the metamodels

In the Table 1 is the summary of the advantages and disadvantages of the metamodel described above.

Table 1 - Summary of the advantages and disadvantages of the metamodel.

Metamodels	Advantages	Disadvantage
RSM	• It is easy to establish; • It has a better performance on low order non-linear response function; • It can get a more distinct and sensitive analysis; • It is less complex and cheaper to work with [23, 30, 47, 56].	• The achievement of a computationally costly database; • Less efficiency on problems with highly non-linear and irregular performance, amongst some others [23, 25, 56]
Kriging	• It has flexibility due to a wide range of correlation functions; • It reduces the computer time on achieving the statistic of a real model; • It accounts and quantifies the intrinsic random noise; • It can be applied to problems with up to 20 parameters; • It has a more accurate approximation over a wide range of samples, size and design [24, 25, 33, 34, 37, 40, 50, 56].	• It is more complex than a low-order polynomial (RSM); • It has a poor accuracy of prediction in cases of extrapolation sample data [30, 33].
ANN	• It has the capability of getting a higher accuracy and flexibility; • It makes it possible to solve more complex engineering systems; • It can solve problems when it is difficult to introduce a mathematical model [60-62, 66].	• The metamodel can be time consuming; • The software can limit the number of parameters; • The influence of training can lead to a lack of robustness [67].

2.4.5 Screenings

Most simulations models have many variables, and some of them have little to no effect on the objective function. Screening is used to determine the variables that have the greatest impact on the output while eliminating the unimportant ones. This has an impact on reducing the size, therefore improving the analysis of the important inputs, and as a consequence, it increases the efficiency of the RO [1, 16, 25, 30, 38, 51, 60, 68, 69].

It is important to select the data through DOE, so in the case of the screening, the input can be reduced using the factorial DOE [16, 23]. The factorial DOE is attached to two levels to each of the k design and noise, k being the sum of the number of design and noise variables [16]. The first stage of screening consists of knowing how many simulations are needed, and for that, the fractional design is applied. This can be achieved by fractional factorial design, saving on the number of simulations. A fraction factional design is 2^{k-q} (q – positive integer). A frequently used DOE on screening is the III fraction factional design as it gives an independent estimation of the linear effects. This approach is 2^{k-p}_{III} as can be seen in Figure 19 - (b). An example of fraction factorial design is represented in Figure 20 .The linear effect is used on screening neglecting iteration on nonlinear effects, because at this stage the efficiency is more important than accuracy [1, 30, 51, 52, 60, 68, 69].

The second stage objective is to reduce the size of the optimization problem, by selecting the most important input. After applying the resolution III and finishing the FE simulation, the linear effects can be analyzed by applying the statistical techniques, such as ANOVA (Analysis of Variance) [16, 38, 51, 69].

The DOE is applied to a dimensional space of single $i+j$, in which i and j are the number of design and noise variables respectively. This provides an efficient way to obtain Analysis of variance, main effect plots and Pareto plot. These are employed to estimate the importance of the input. Thereafter, only the most important variables are taken into consideration for the optimization problem [38, 51, 68].

The Pareto plots illustrate the *main effect* on different variables in the response, the expression for a two-level fractional factorial design is shown in equation (37).

$$main\ effect(x_1) = \frac{\sum y(x_1^+) - \sum y(x_1^-)}{\frac{2}{n}} \tag{37}$$

Where n represents the number of simulations, $y(x_1^+)$ and $y(x_1^-)$ are the response measurements at the highest and lowest levels of variance. The percentual accumulation effect is plotted, which can help in determining how many variables are used on the optimization problem.

The *error effect* can be calculated by:

$$error\ effect = \frac{\sqrt{nSSE}}{\frac{2}{n}} \tag{38}$$

where the SSE is the error sum of squares,

$$SSE = \sum_{i=1}^{n} (y_i - \hat{y}_i)^2 \tag{39}$$

and y_i is the response measurement, while $\hat{y}_i$ is the metamodel prediction of measurement i of the linear RSM model.

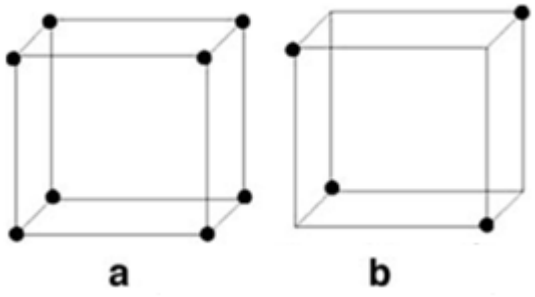

Figure 19 - (a) 2^3 full factorial design, (b) 2^{k-p}_{III} fraction factorial design [51].

Specification	k	q	n
2^{3-1}_{III}	3	1	4
2^{4-1}_{III}	4	1	8
2^{5-2}_{III}	5	2	8
2^{6-3}_{III}	6	3	8
2^{7-4}_{III}	7	4	8
2^{8-4}_{III}	8	4	16
2^{9-5}_{III}	9	5	16
2^{10-6}_{III}	10	6	16

Figure 20 - Fraction factorial design [12].

COMPANY CHARACTERIZATION AND PREVIEW OF SOLUTIONS

3 COMPANY CHARACTERIZATION AND PREVIEW OF SOLUTIONS

3.1 Company characterization

It was in 1891 that Gerard Philips and his father, Frederik Philips, founded what was going to become one of the greatest companies of todays' modern world, Philips. Philips had its first base in Eindhoven, where it started to produce in 1892 carbon-filament lamps and some other electronics. From being a small company, Philips grew over the years to become a very well-known company all over the world. It was in 1998 that the Dutch Monarchy recognised the company, awarding it the royal honorary title for its national importance, but mostly for being one of the leading companies' in its field of expertise. Along the years the focus of the company had been changing from the electronics field to the health technology [70].

Philips is organized into three main divisions:

- Philips Consumer Lifestyle (formerly Philips Consumer Electronics and Philips Domestic Appliances and Personal Care), it was founded in 2008 from the combination of Philips Consumer Electronics and Philips Domestic Appliances and Personal Car;
- Personal Health (formerly Philips Medical Systems);
- Signify N.V. (known as Philips Lighting prior to 2018).

Nowadays, with so many fields of research, Philips maintains a set of honourable, but still necessary goals, some of them being:

- Connecting products and services supporting the health and well-being of people;
- Integrating modalities and clinical informatics to deliver definitive diagnosis;
- Real-time guidance and smart devices for minimally invasive interventions;
- Connecting therapeutic products and services for chronic care patients;
- Connecting patients and providers for more effective, coordinated, personalized care;
- Managing population health, leveraging real-time patient data and clinical analytics.

Going forward, Philips aims to bring many more technology capable of helping and improving the many people's lives around the globe [70].

3.2 Problem characterization

There are many relevant factors nowadays that need to be taken into consideration for companies to be competitive in the industrial environment. Some things, such as zero failure production might help the company to reduce the costs of the production and therefore bringing its level of competition on the market to a higher one.

In this work the material has a spread due to some previous processes, among these a metal forming one. This last process might bring a problem to the production, as it originates a wave or a concave geometry on the material. This leads to a series of events that may cause irregularity, inconsistency, and due to this a scrap, being this one of the most significant problems for the company's production, leaving a negative impact, and as a consequence downgrading the company's competitives. A solution for this problem at hand is to flatten the material, which will lead to the reduction of the spread. As a result, companies are obligated to focus their efforts on product quality improvement, by reducing the occurrence of this kind of problems, which will lead them to flourish in the world's most competitive markets.

3.3 Analysis of possible solutions

3.3.1 Parallel-Roll Straightening

Parallel Roll straightening is a cold-finishing mill process by which bars and structural shapes are provided with adequate straightness for most applications, it can be seen in Figure 21. For bars and shapes on which close tolerances must be maintained, roll straightening can be followed by press straightening [71]. The disadvantage is that it cannot be used on separated pieces, therefore this solution was not used.

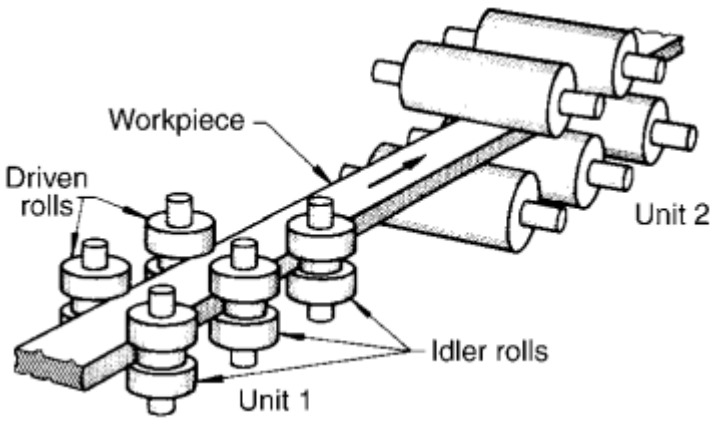

Figure 21 - Roll straightener for straightening a rectangular-section bar [71].

3.3.2 Moving-Insert Straightening

The moving-insert Straightening is used for linear, flat, or irregularly shaped parts, this can be seen in Figure 22. Moving-inserts straightening is formed due to a reciprocal stroke transmitted to the tooling insert by rotary-cam action. The amplitude of the movement is progressively reduced during the cycle until it approaches a straight line. The degree and the bending movement and the number of the bending cycles are adjustable, and varying insert spacing is available. The advantages of this process are that it has both the ability to straighten flat or irregularly shapes parts, with or without projections, bends, and others, and to produce straightness or single curves, the tolerance is 0.03 mm, there are only needed minimal skill requirements to impose on the operator. The downside of it is similar to the disadvantages presented in Parallel Roll, and so this solution was not used as well because in the present study it is used separated pieces [71].

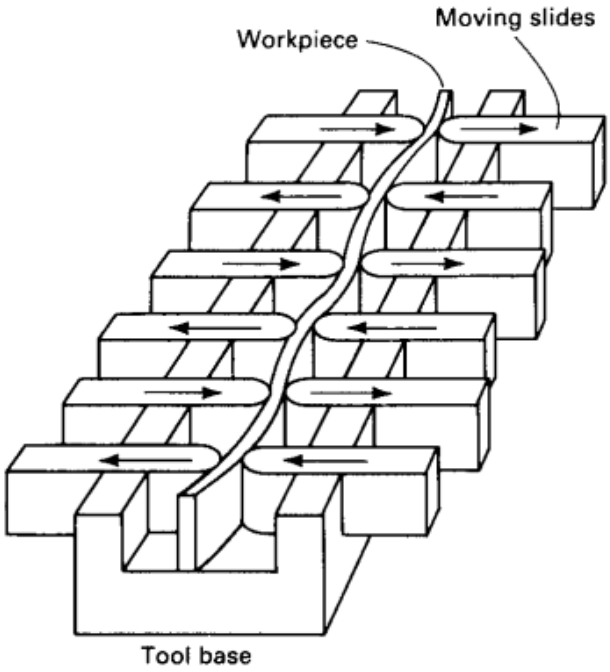

Figure 22 – The representation of the process moving-insert Straightening [71].

3.3.3 Thermal forming of Sheet and Plate

Thermal forming of sheet and plate is a process that deforms without the application of external mechanical force. Its fundamental principle is based on expanding when heated and contracting when cooled down. If the expansion is limited in two dimensions, compressive stresses build up and result in localized plastic deformation when the temperature is sufficiently high (no melting is allowed).

It is used to do the straightening of structures. More recently, it has been revealed that it can also be achieved using a laser beam and plasma technology for heating.

The laser is used for rapidly heating metallic materials provided by the energy of the beam, it can be transferred to the material by “coupling” rather than being deflected away. Coupling is usually accomplished by using a spray coating of graphite on the workpiece surface to promote heat absorption. The energy transferred by laser systems into the workpiece material is rather low ($<10\%$), although it requires higher safety precautions.

The plasma arc system does not need an electric connection to the workpiece, and they are normally safer than laser. The energy transfer is usually $<85\%$ [71].

The amount of deformation achieved with each thermal scan is limited. Thus, multiple repeated scans are required to develop significant amounts of bending or to achieve a change in shape [71-73].

Bending toward the heat source is a term used to describe a metal sheet-bending process in which there is a concave hinge on the bending straight surface. During this process, heating and cooling are combined, as can be seen in Figure 23 [71].

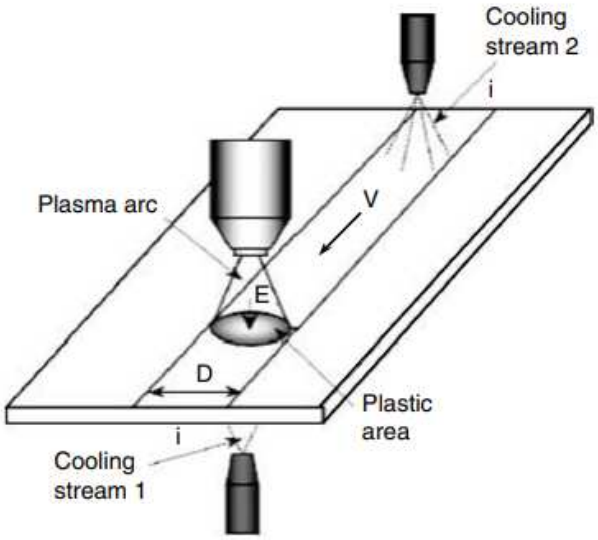

Figure 23 - Method of bending towards the heat source [71].

The material in zone $S1$ expands because of bending heat and $S2$ restrains the stiffness, it inhibits free expansion within $S2$ as can be seen in Figure 24.

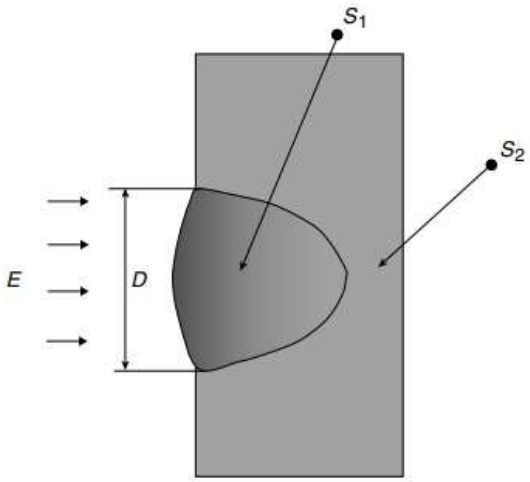

Figure 24 - Heating phase of the plate bending towards the heat source.

Stresses in the $S1$ zone are compressive because the expansion of these areas is restrained by the surrounding metal that is at a lower temperature. The compression stress will reach the yield level of the material at that temperature, and plastic deformation will originate in the $S1$ zone.

Because $S2$ is an elastic state, the two workpieces become bent away from the heat source by an angle α_1.

As the metal in the heated and cooled zones tries to shrink, tensile stresses are induced in zone S1. These manifests itself by a bend toward the heat source at an angle α_2.

As a result of these two processes (the heating and cooling), a permanent deformation appears as an angle $\alpha_3 = \alpha_1 + \alpha_2$, as it can be seen in Figure 25 [71].

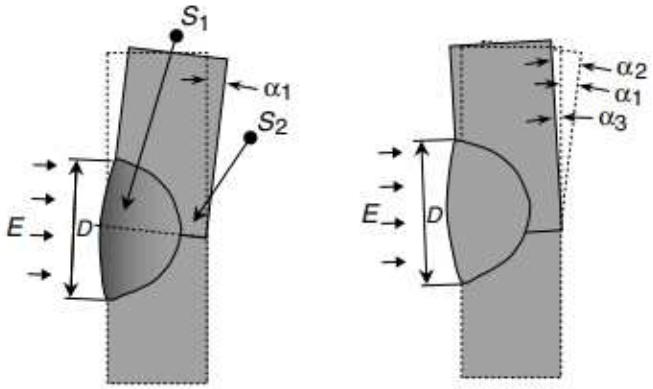

Figure 25 - Deformation of metal sheet during heating and cooling processes [71].

Bending away from the heat source is a term used to describe a metal sheet bending process in which there is a concave hinge. The heating and cooling processes are very similar to the one shown in Figure 26, the difference being that the energy beam is wider compared to the sheet thickness, and the total thickness is heated thoroughly. The

cooling stream can be under the plate or not used at all. The metal near the heat source is heated at a higher temperature than the metal away from the heat source. The hotter metal expands, and the sheet bends away from the plasma. Additionally, the total thickness of the sheet is heated. A relatively plastic strain is produced by the terminal cycle and after cooling [71].

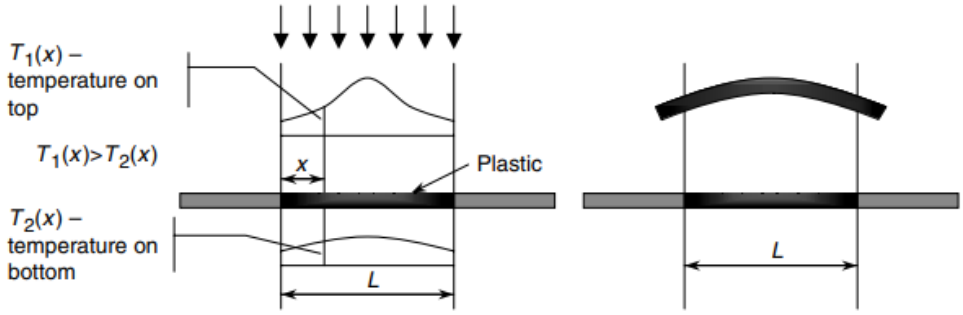

Figure 26 - Deformation of plate bent away from the heat source [71].

The disadvantage settles in the fact that the mechanical properties will change and such forming approaches are best suited for making parts in small quantities, because it requires repeated scans [71-73]. Based on this the Thermal forming of Sheet and Plate technique was not used.

3.3.4 Waffling

Waffling technique is a generic name applied when a bent or out of plane punched part needs to be flattened, although it is still not very acknowledgeable in literature. In the literature, the standard texture is a pyramid-like shape, as shown in Figure 27 the objective is to reduce the residual stresses of the previous process. The waffling process has the same movement as the press, playing a compressive load [12]. In the Figure 28 is the representation of the prototype of waffling tool for the steam iron

In the past, there were already some experiences in Philips with the waffling applied on both sides, but the scratches were in the two surfaces. The higher elongation of parts and higher loads were a drawback that was solved by the one side waffling.

However, single side waffling can only be successful if the following conditions are met:

- Correct tool geometry;
- Stable press;
- Adjustable waffling blocks.

The chosen method was therefore the one side waffling because it has many advantages, such as having only scratches in one surface, can be introduced in the press and is able to flatten the material in a mass-production.

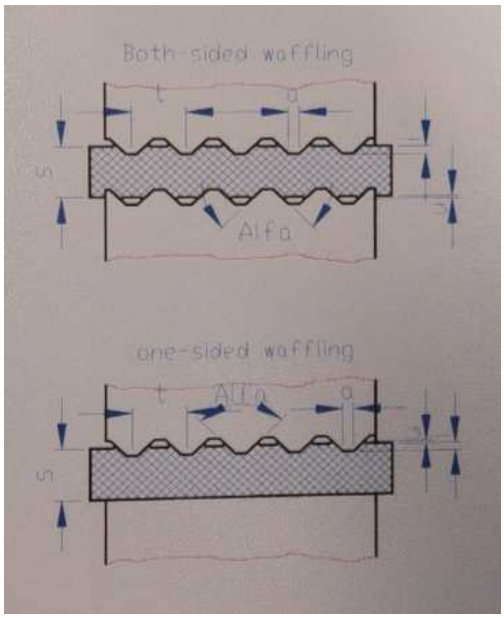

Figure 27 - Standard texture of waffling [12].

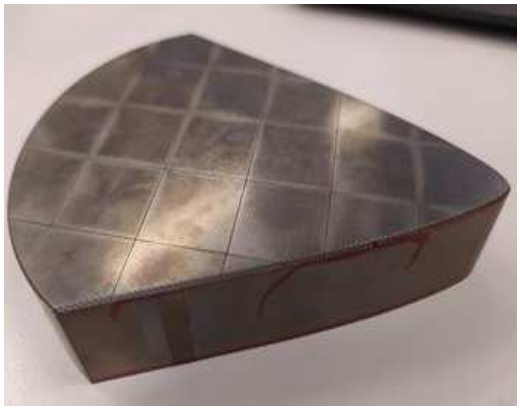

Figure 28 - Waffling prototype for the steam iron.

METHODOLOGY

4 METHODOLOGY

The material analysed is stainless steel AISI 420 with a thickness of 0.3 mm. The mechanical properties of the AISI 420 are in a database made by Philips and some of them are represented in Table 2 .

Table 2 - Mechanical properties of the AISI 420.

Material type	Yield strength	Tensile strength	Young's (E) Modulus	Elongation
AISI 420	250-300 [27]	655 MPa	190-230 [Gpa]	>25 %

The methodology aim is to gather knowledge of the effects made by the process parameters, since this process is almost unknown by the literature. After that, it is intended to introduce the RO strategy.

The RO strategy can be seen in Figure 29. For this technique, the noise and design variables are under consideration.

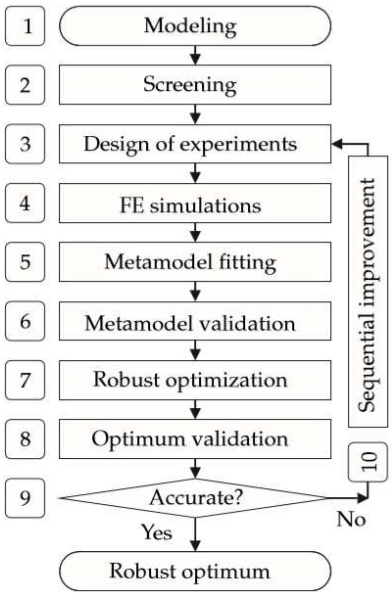

Figure 29 - Flowchart of the robust optimization [16].

Step 1 is modelling, being the creation of a model of a waffling process. As it is an RO, it takes into consideration the uncertainty of the system, so it was added more noise variables with a larger variation. The noise variable (z) could be the design variable uncertainty (z_x) or the parameter of uncertainty (z_p). The normal distribution is

described by both the noise variable and mean value μ_z and as for the variance is σ_z,i.e., $z \square N(\mu_z, \sigma_z^2)$. The parameter (p) is a set of certain fixed values before the optimization.

Step 2 is screening, this step was already introduced in chapter 2.4.5, it reduces the number of variables and the variation of these variables by finding its effects on the response. Only the relatively large influence parameters will be used for further steps in the strategy, where it will be used in the resolution III fraction factorial design, and a metamodel, an RSM, is fitted. The resolution III and the RSM are used because in this stage the focus is on efficiency, as in a time-consuming FE simulation this is more important than accuracy. From the RSM model the Parrett plot and Main effect plot are obtained and this can determine the most important variables and their variations

Step 3 is DOE. The DOE combined with the noise and design variable is the basis of a metamodel. The type of DOE is the space-filling because it is a computer simulation, and the space filling is LHD. Together with the LHD the FFD (Full Factorial Design) is used. This FFD puts the DOE on all the corners of the design domain. This step aims to do a minimal number of initial simulations and at the same time, it tries to grant a proper initial base for the metamodel. If the initial metamodel is not accurate, the DOE scheme can be improved in a later stage of the strategy.

Step 4 includes the FE simulation, in this step, the simulation runs with the specific DOE.

Step 5 comprehends the metamodel fitting. In this, getting the correct metamodel is a very difficult task because the response is still unknown. It was already mentioned before the advantage of the metamodels, but due to their complex behaviour and the lack of knowledge of this process, the metamodels that fitted were RSM and Kriging.

On step 6 there is the metamodel validation, and for this, the LOOCV was implemented over the ANOVA. The reasoning for this choice is due to the fact that the ANOVA has a major drawback, if the metamodel interpolates through the response, it cannot be used due to the remaining fitting error being zero in the DoE point, and as the main objective is to use Kriging, the ANOVA cannot be executed. The R^2 is normally used to analyse the significance of the metamodel and the range goes from 0 up to 1, being 1 the perfect fit of the response measurement. The LOOCV evaluates the performance of the metamodel, as it uses the prediction error (e_{-i}) by the equation (40), and uses the prediction $R^2 - \mathrm{Value}$, i.e., R^2_{pred}, the best response is the one that has the highest $R^2_{pred} - Value$ [16].

$$e_{-i} = y(x_i) - \hat{y}_{-i}(x_i) \tag{40}$$

In Step 7 have RO. This step is solved by equation (20), which in turn can be resolved by the metamodel. In order to solve this equation, it need to get the prediction of the mean response and the standard deviation as the function of the design variable. For the RSM,

this can be obtained analytically, but for the Kriging this is not possible and as a result, an MCA function was needed. This function is an evaluation and it runs on the metamodel in each evaluation of the optimization algorithm, and this way the MCA is very efficient. The prediction of the mean and standard deviation are used by a gradient-based optimization in order to solve the equation (20). The DOE points have the algorithm to minimize the risk of the optimization process being a local optimization [16].

Step 8 is optimization validation. This is needed to check the influence of the left out parameters. This is accomplished by performing new FE simulations to obtain the accuracy and reliable solution of the metamodel prediction.

In step 9 it is determined if the accuracy gutted is good or not. When it is accurate enough the RO is over, otherwise, it goes to step 10 where there is a sequential improvement.

In all of this process, it is only taken into consideration a numerical validation between the metamodel and the FE simulation, as the practical test is still unknown.

4.1 Creation of the model

To overcome the spread created by the previous process it was used, as already mentioned the Waffling technique. To study how to solve the problem by the waffling technique it was made a model that first replicates the spread by the pre-bending the material and then it is used the force by waffling tool. The traditional tool for the waffling is a punch with multiple topped off pyramids in the contact surface, as can be seen in Figure 30. To make the numerical model similar to the ones on the “real world” and to also make it faster to analyse, it was chosen to model only a block as shown in Figure 31. This choice was made based on the fact that the behaviour of one block is equal to the others. So first, one basic model is created, and some variations are started. This variation is used to study this waffling technique and the behaviour of the material applied.

Figure 30 - Waffling tool with the geometry square.

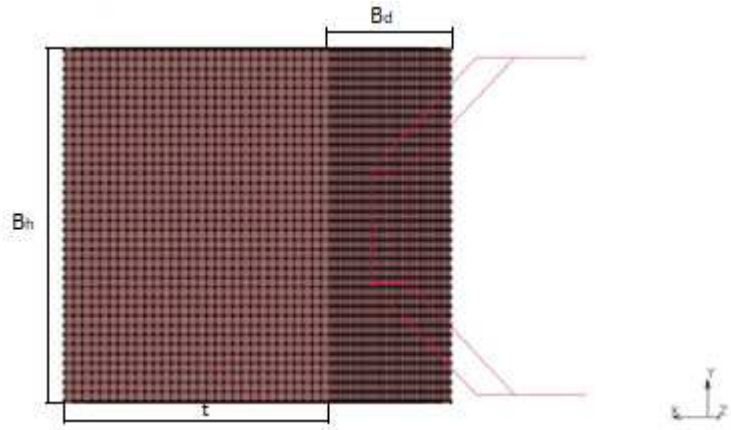

Figure 31 - Waffling square model of the stainless steel material, with the tool in red lines coming from the right.

The initial study of this project uses the variables as, force and pre-bending (method to replicate the bending stress in the block). This analysis was performed first in 2D and then in 3D, for these two the only noise taking into consideration was the bending angle. The final analysis was also done in 3D but as a Robust strategy, as it has more noise and design variables and variations.

The model created was produced initially by modelling the process steps with an user friendly pre-processor software for FEM made by Philips, called PreCrystal. Then, an interface is used between a commercial FEM pre-processor Marc Mentat® and PreCrystal software, and finally it was calculated using the MSC.Marc solver software.

First, the project is created in PreCrystal, in which the material is defined, the plate itself, the forming steps, ridges and if it is 3D.

For the material, it was taken into consideration the properties of the material AISI 420 by FlexMM database, made by Philips® .

In PreCrystal's project options, on the one named "plates" it was chosen the name, the origins (0,0), the dimensions, the number of elements in the width and height, this is represented in the Figure 32 by the numbers 1 to 5. When the analysis is in 3D, it also need the number of elements in the zz direction, which are called divisions, which are represented in Figure 32 by the number 6. These divisions change depending on the simulations, as it can be seen in Figure 32. As for the dimensions for this project, when made in 2D the dimensions would be 0.375×0.3 mm and as for the 3D the dimensions would be $0.375 \times 0.375 \times 0.3$ mm. The type of the simulation was plane strain because of the thick body, the height is almost the same measure as the thickness.

In the "step and rigids", the name of the step is defined and how many rigids (tools) will be needed. In the step, there are movements and rigids. In the movements, the actions of the tools are created. For the rigids the tools dimensions and their geometries are created.

One example of a project in PreCrystal is shown in Figure 32.

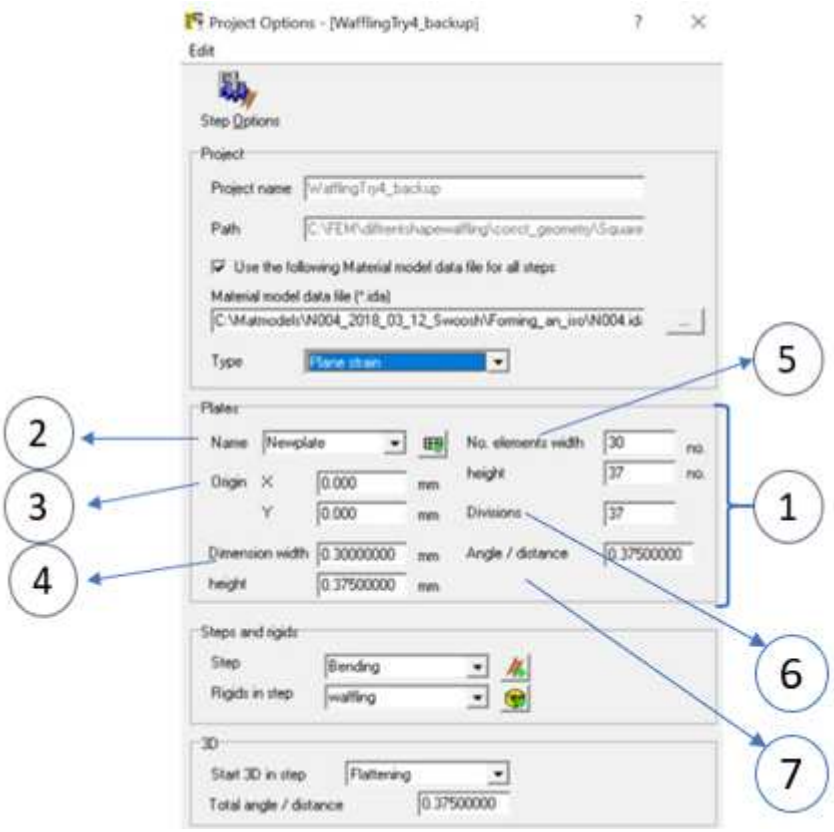

Figure 32 - Project in PreCrystal.

In this project there are 3 steps, the Bending, the Flattening and the Opening. In these steps, the only rigids that change are the upwall and backwall (in fact these represent symmetry boundary conditions) but only in length of the Bending to have better rotation. The movements on the other hand are all different.

For the Bending:

1) Moment - It rotates the upwall and downwall with the same angle and opposite rotation direction, the waffling tool geometry and block tool are fixed. The material can move freely on the upwall and downwall. This is done to create a curvature in the material producing stress from an ideal moment load case;
2) Back-moment - it is similar to the Moment, as it rotates the upwall and downwall with the same angle but with the opposite rotation's direction. This step is used to model a material so that it can be pressed flat, originating the same stress;
3) Movement – the waffling and block touch the material. This is a step needed to prepare the material for the next step.

For the Flattening:

4) Waffling – the tool applies a force in order to flatten the surface by introducing stress that creat plastic deformation.

For the Opening:

5) Opening – it makes the upwall and downwall, waffling and the block free of the material so it can be properly analyzed and study the springback.

All this information can be seen in Figure 33.

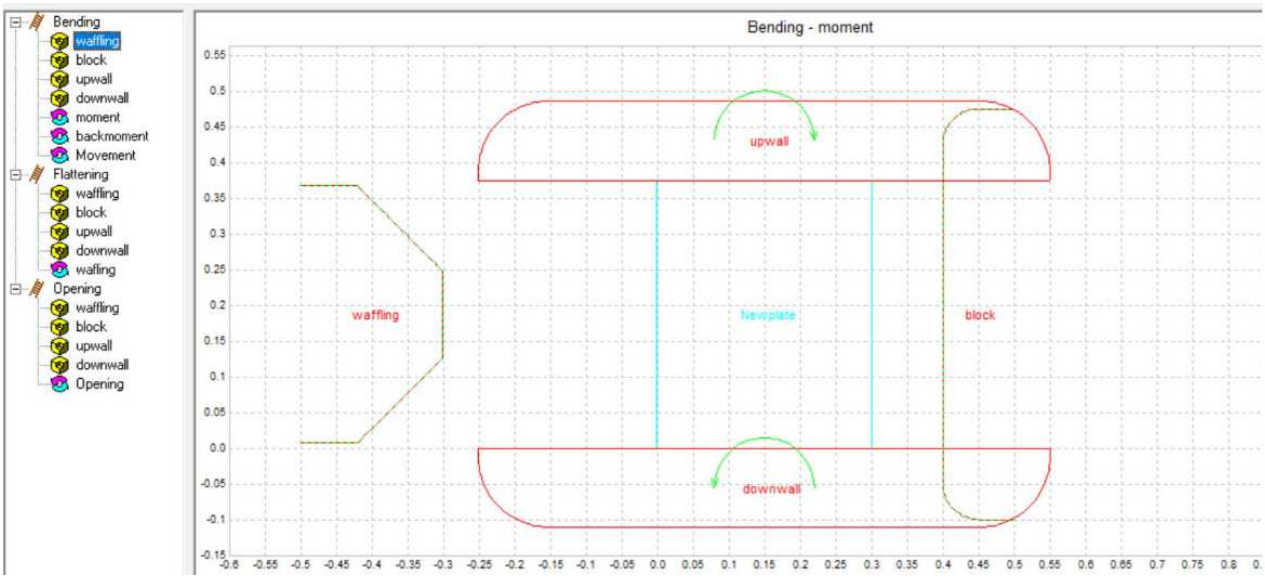

Figure 33 - Model in PreCrystal.

The interface between PreCrystal and Marc Mentat® converts the data of the model in PreCrystal.

The Marc Mentat® needs to be prepared if it is a 3D simulation. It needs to define the boundaries in the z direction and adjust the geometries in the Flattening step (so during the waffling process). The Bending step does not need an adjustment because it is done in 2D and in the Opening step it is only needed to free the material as it can be seen in Figure 34.

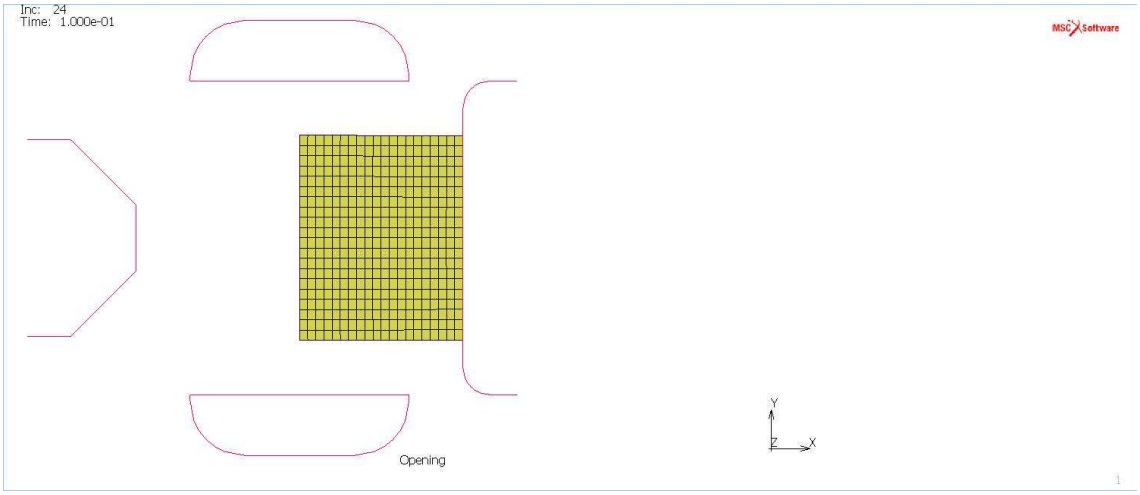

Figure 34 - Opening step.

For the Flattening step, the boundary conditions added in Marc Mentat will produce a replication. These conditions confine the material movements in the z direction because in the “real world” it has another material next to it. The boundaries are made by creating two surfaces that work like two walls, the left wall and the right wall, being the displacement zero, as can be seen in Figure 35.

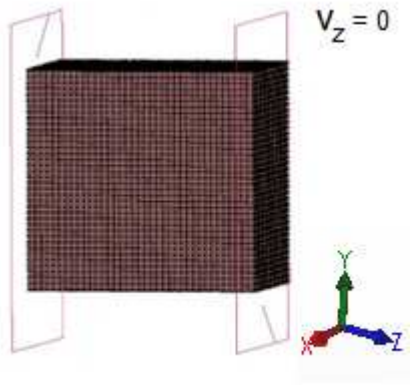

Figure 35 - Model of the boundary wall.

As this technique is still not very known in the literature, the influence on changing the geometry of the tool is still unknown as well, so it will be necessary to create new geometries and new dimensions of the tool. The study on the geometry was always performed in 3D. The geometries that were then chosen to be analysed were the standard (square), the conical and the cylindrical, all of them can be seen in Figure 36 and there technical draw are in Appendix 8.1.1, 8.1.2 and 8.1.3 . For the 2D simulations, the variation of the square tool dimensions was made manually. For the cylindrical and conical geometries, the SolidWorks® software was used to create the geometry and then it was converted to Marc Mentat® by Parasolid as can be seen in Figure 36. For robust analysis the geometry, their variation in dimensions and the distance between the contact areas is study. This last one is changed by the dimension of the plate in height, depth.

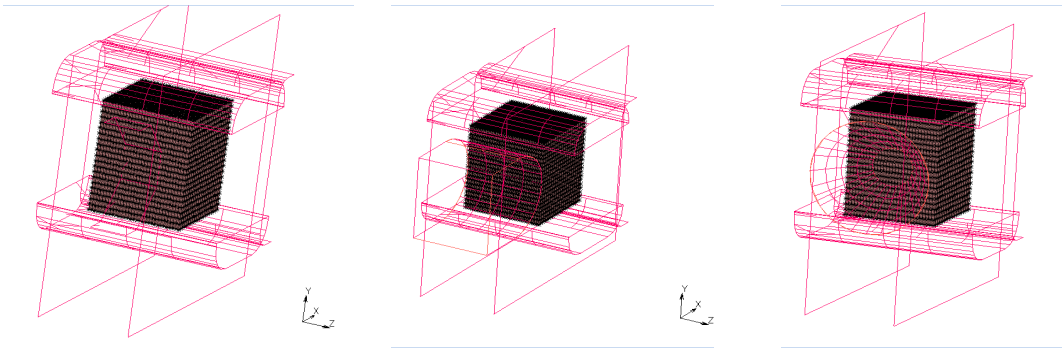

(a) (b) (c)

Figure 36 - (a) Square geometry, (b) Cylindrical geometry and (c) Conical geometry.

In a more advanced phase of the project, it was introduced the automation, which will then be explained in another chapter.

For the RO analysis the constraints needed to be chosen from two big groups, the explicit and the implicit. In these groups there are the different types of constraints, as they can be presented as equality constraints (h), inequality constraints (g) or box constraints. For the explicit constraints they depend directly on the variables, in the project it will be considered in the dimensions of the block, maximum and minimal will be introduce, the design variables and noise variables. For the block analysed the restriction was used the thickness (t), depth (B_d) and height (B_h) as it can be seen in Figure 31. The implicit constraints indirectly depend on the variables and they need to run the simulation because it restricts the feasible or infeasible output for the process that is going to be used. For this process, as the objective is to have a flatten surface, the explicit constraints will be related to having a lower elongation, taking into scrap rate. For the elongation, it will be used the absolute value between the difference between the thickness before and after the process.

4.2 Analysis of the behaviour of a plastic deformed sheet metal and define the noise and design variable.

Multiple simulations are performed to analyse the behaviour of the material after being plastically deformed and the possible variables that could influence the result, taking into consideration the main goal.

In this simulation's experiments, the force of the tool and the angle of the pre-bending are the modifiable variables.

The Design variable here analysed is the force. The variation of the force was initially based on the information retrieved from one book [12], which also shows the pressure. For the 2D simulation, it will be analysed in plane strain and the force will be presented in N/mm, and as for the 3D it will be presented in N. To save some time, in the beginning, the simulations were made 2D, to understand the behaviour and the range of the parameters that will be used, and later they were done in 3D. For the Noise variable, the bending and back-bending angle were the only things taken into consideration. In this variable, it was studied the difference in the behaviour of a plastically deformed material, and for that, the angles used were 0.4, 0.8, 1.6, 2.4 degrees.

To have a robust optimization, it is needed to consider other noise variables, such as the thickness, friction, flow stress, young modulus, and hardness. These new variables will be added in the automation simulations.

4.2.1 Analyses of the results from 2D simulations

In this analysis it was studied the impact of the bending angle and the waffling load in the metal sheet. To perform this investigation, it was used a 2D simulation with a block, whose dimensions were 0.3 mm of thickness and 0.375 mm of height. On this analysis the behaviour of the bending angle and force are studied, with the variation that is shown in Table 3 used the angle AC and the GE and the distance of BF and HD, as Figure 37 shows, in this figure the waffling is played in AG, the wall is in the CE, the thickness is in the x direction and the pre-bending is made by rotating the AC and GE.

Table 3 - Variation of the variables for the 2D simulation square tool

Variables	Variation
Bending Angle (degrees)	*0.4; 0.8; 1.6; 2.4*
Force (N/mm)	*0; 23; 26; 30; 50; 70; 90; 110; 140; 210*

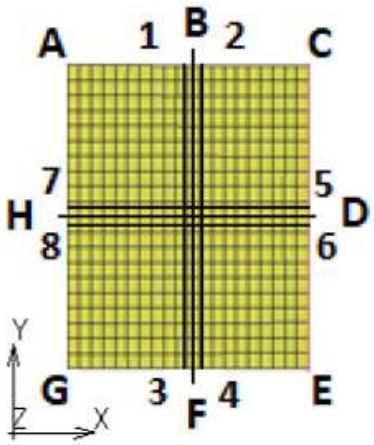

Figure 37 - The block for 2D.

Excel® was the chosen software to get the angle of AC after the all process. First, the distance between A and C in the x -direction and in the y -direction are calculated. Then the angle (α_{AC}) is calculated by the inverse sin as can be seen in Figure 38. The GE angle (α_{GE}) was determined in the same way, although on this was considered the GE on the x-direction and in the y -direction.

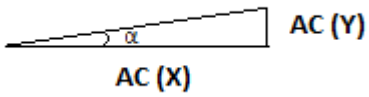

Figure 38 – Angle α_{AC}.

For the distance BF, as the material is bent, it is difficult to find a node that is in the middle to determine the exact location of B and F. To overcome this problem, the distance is measured between the nodal on the right and on the left as it can be seen in

Figure 37 for the numbers 1, 2, 3 and 4. Afterward, as the distance in the x -direction is already known, being the middle of the distance AC (x -direction), the F distance in the y -direction and the B distance in the y -direction can be calculated using the interpolation equation (41) and equation (42), respectively.

$$F(YY)=3(YY)+\frac{F(XX)-3(XX)}{4(XX)-3(XX)}\times(4(YY)-3(YY)) \quad (41)$$

$$B(YY)=1(YY)+\frac{B(XX)-1(XX)}{2(XX)-1(XX)}\times(2(YY)-1(YY)) \quad (42)$$

In the end, it can get the distance between BF (y-direction).

To determine the HD distance, a very similar method can be used, considering points 5, 6, 7 and 8. H and D in the y direction are determined by measuring the middle of the AG and CE in the y-direction. Then, to calculate D and H, this time on the x-direction, it use the equation (43) and equation (44), respectively.

$$D(XX)=5(XX)+\frac{D(YY)-5(YY)}{6(YY)-5(YY)}\times(6(XX)-5(XX)) \quad (43)$$

$$H(XX)=7(XX)+\frac{H(YY)-7(YY)}{8(YY)-7(YY)}\times(8(XX)-7(XX)) \quad (44)$$

Then, the difference between H and D in the x -direction calculates the distance HD in the x -direction.

4.2.2 Analysing the results from normal 3D simulations

The response of the 3D simulation will be studied, taking into view what kind of influence the input (variables) have on the response. This response is analysed by how curved the bent material is, so to perform this, the angle and the delta thickness (difference of the new thickness to the original thickness) will be the output of the simulation.

The 3D simulation with the variables and variation is shown in Table 4. To analyse the effects of the bending, the bending will be generated by rotation of the surface that contains the line AB and CD. The waffling will be played in the surface that contains the line EH and it is represented with an arrow, which is shown in Figure 39 - (a). The output is studied by calculating the angles AB and CD to analyse the y -direction (for the robust analysis it is called angle left right), and the angles EF and GH to analyse the z -direction (for the robust analysis it is called angle front back) as it is shown in Figure 39 - (a). The representation of the block bended is shown in Figure 39 – (b).

Table 4 - Variation of the variables for the 3D simulation square tool.

Variables	Variation
Bending Angle (degrees)	*0.4; 0.8; 1.6; 2.4*
Force (N)	*0; 7; 20; 30; 40; 45; 50; 55; 60*

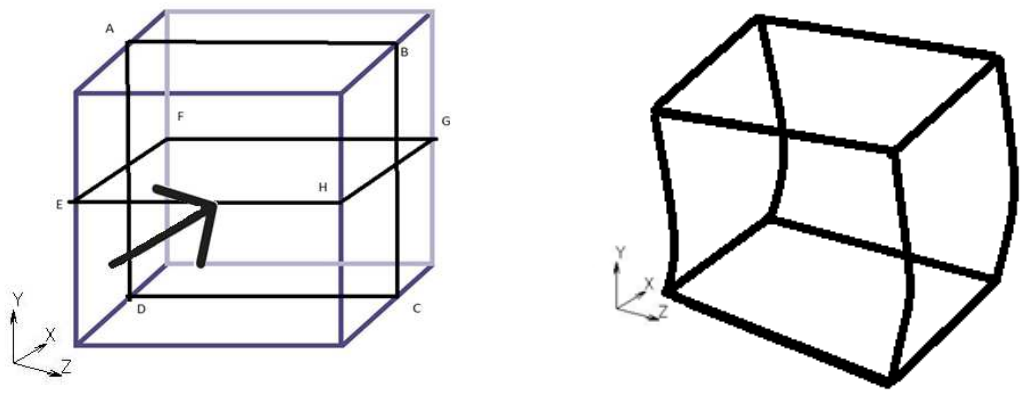

a B

Figure 39 – (a) Analyse of the angle and thickness in the block and (b) block deformed by pre-bending.

Measuring the angle in 3D can be done in a similar way to the one used in the 2D. The angle of AB is calculated by getting the distance between AB in the y and x direction and then by calculating the angle , α_{AB} ,by the $\sin^{-1}(AB(X)/AB(Y))$, as it can be represented in Figure 40. For CD , α_{CD}, the process is the same, $\sin^{-1}(CD(X)/CD(Y))$. To calculate the angle of EF α_{EF} , and GH , α_{GH} , although identical to the way that AB and CD were calculated, in the EF and the GH the distance is in the x and z direction and the angle is $\sin^{-1}(EF(X)/EF(Z))$ and $\sin^{-1}(GH(X)/GH(Z))$, respectively.

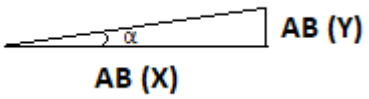

Figure 40 - Angle α_{AB} in a 3D simulation.

4.3 Preparation of 3D simulations in a RO model

2D and 3D simulations provide the knowledge to understand the behaviour of the material without plastic deformation and with plastic deformation and the impact of the waffling load. Based on this result, a range of waffling loads is used between 20 and 45 N. To understand more about the behaviour of the material without plastic deformation,

the range to be studied for the bending angle is between 0 and 2.4 degrees for the robust 3D simulation.

4.3.1 The automation simulation programs

The automation simulation program allows us to use an Excel® input sheet and change the variations, making it automatically. The average time of the simulation is 3 hours.

The Excel® structure for changing the parameters and made the automatically the simulation of the square and conical is shown in Figure 41, the column 1 contains the number of simulations, column 2 the number of the processor (determines in which automatic "batch file" it will come), the columns 3, 4, 7, 8, 9, 10 the noise variables and the columns 5, 6, 11, 13 and 14 are the design variables. The information on the noise variables variation is based on the Philips database. Column 5 the material height and column 6 the material depth, this represent the analysed block dimension, therefore, the distance between the contact area could be determined. The column 10 Angle/area (degrees/mm^2), in which the "Angle" means the angle of the bending and back-bending and as for the "Area", it represents the area of the 2D simulation, as the bending action is done in 2D. The noise variables variation can be seen in Table 5, the column 11 Force/area, in which the "Force" represents the waffling force and the "Area" represents the area of contact of the tool. The Force/area demonstrates the pressure that the tool gives to the material. For the square and the conical, the column 13 and the 14 are the same. It is made in two columns because in future investigation different geometries can be used.

The Excel® structure for the cylindrical is shown in Figure 42, and the only difference between this and the square and conical is on the column 11 and 13. Here the area of the tool cannot be used, so the alternative is to use the length instead. So, on column 11 it is the Force/length (N/mm), being the "force" the load of the tool and the "length" is the length of the tool in the z direction. On column 13 the tool radius (mm) is shown for the cylindrical. All this is shown in Figure 42.

The design variable changes with the geometry and it can be seen in Table 6, Table 7 and Table 8.

For the square and conical geometries, the values used for the Force/area are the same, being the force 20 N, 33 N and 45 N, and the area 0.046 mm^2, so the results are 500 MPa, 825 MPa and 1100 MPa. The values used for Force/length on the cylindrical geometry were for the force 20 N and length 0.25 mm, 0.3 mm and 0.375 mm so the Force/length was 53.3 N/mm, 66 N/mm and 80 N/mm. For the angle/area, the values were the same for all geometries and the angle of the bending was between 0 and 2.4 degrees, and the area was 0.1406 mm^2.

1 nr.	2 batchnr.	Parameters											
		3 Friction	4 Material Thickness	5 Material Height	6 Material Depth	7 Yield Stress	8 Young's (E) Modulus	9 Anisotropy	10 Angle/area	11 Force/area	12 Rotation of the tool	13 Tool width or Radius	14 Tool depth
1	1	0,15	0,3	0,375	0,375	250	210000	1,4	4,266666667	825	0	0,2	0,2
2	1	0,1	0,3	0,375	0,375	250	210000	1,4	4,266666667	825	0	0,2	0,2
3	1	0,11	0,3	0,375	0,375	250	210000	1,4	4,266666667	825	0	0,2	0,2
4	1	0,12	0,3	0,375	0,375	250	210000	1,4	4,266666667	825	0	0,2	0,2
5	1	0,13	0,3	0,375	0,375	250	210000	1,4	4,266666667	825	0	0,2	0,2
6	1	0,14	0,3	0,375	0,375	250	210000	1,4	4,266666667	825	0	0,2	0,2
7	1	0,16	0,3	0,375	0,375	250	210000	1,4	4,266666667	825	0	0,2	0,2
8	1	0,17	0,3	0,375	0,375	250	210000	1,4	4,266666667	825	0	0,2	0,2
9	1	0,18	0,3	0,375	0,375	250	210000	1,4	4,266666667	825	0	0,2	0,2
10	1	0,19	0,3	0,375	0,375	250	210000	1,4	4,266666667	825	0	0,2	0,2
11	1	0,2	0,3	0,375	0,375	250	210000	1,4	4,266666667	825	0	0,2	0,2
12	1	0,15	0,29	0,375	0,375	250	210000	1,4	4,266666667	825	0	0,2	0,2
13	1	0,15	0,292	0,375	0,375	250	210000	1,4	4,266666667	825	0	0,2	0,2
14	1	0,15	0,294	0,375	0,375	250	210000	1,4	4,266666667	825	0	0,2	0,2
15	1	0,15	0,296	0,375	0,375	250	210000	1,4	4,266666667	825	0	0,2	0,2
16	1	0,15	0,298	0,375	0,375	250	210000	1,4	4,266666667	825	0	0,2	0,2
17	1	0,15	0,3	0,375	0,375	250	210000	1,4	4,266666667	825	0	0,2	0,2
18	1	0,15	0,302	0,375	0,375	250	210000	1,4	4,266666667	825	0	0,2	0,2
19	1	0,15	0,304	0,375	0,375	250	210000	1,4	4,266666667	825	0	0,2	0,2

Figure 41 - Excel® structure for the square and conical.

1 nr.	2 batchnr.	Parameters											
		3 Friction	4 Material Thickness	5 Material Height	6 Material Depth	7 Yield Stress	8 Young's (E) Modulus	9 Anisotropy	10 Angle/area	11 Force/length	12 Rotation of the tool	13 Tool Radius	14 Tool length
1	1	0,15	0,3	0,375	0,375	250	210000	1,4	4,266666667	66	0	0,5	0,25
2	1	0,1	0,3	0,375	0,375	250	210000	1,4	4,266666667	66	0	0,5	0,25
3	1	0,11	0,3	0,375	0,375	250	210000	1,4	4,266666667	66	0	0,5	0,25
4	1	0,12	0,3	0,375	0,375	250	210000	1,4	4,266666667	66	0	0,5	0,25
5	1	0,13	0,3	0,375	0,375	250	210000	1,4	4,266666667	66	0	0,5	0,25
6	1	0,14	0,3	0,375	0,375	250	210000	1,4	4,266666667	66	0	0,5	0,25
7	1	0,16	0,3	0,375	0,375	250	210000	1,4	4,266666667	66	0	0,5	0,25
8	1	0,17	0,3	0,375	0,375	250	210000	1,4	4,266666667	66	0	0,5	0,25
9	1	0,18	0,3	0,375	0,375	250	210000	1,4	4,266666667	66	0	0,5	0,25
10	1	0,19	0,3	0,375	0,375	250	210000	1,4	4,266666667	66	0	0,5	0,25
11	1	0,2	0,3	0,375	0,375	250	210000	1,4	4,266666667	66	0	0,5	0,25
12	1	0,15	0,29	0,375	0,375	250	210000	1,4	4,266666667	66	0	0,5	0,25
13	1	0,15	0,292	0,375	0,375	250	210000	1,4	4,266666667	66	0	0,5	0,25
14	1	0,15	0,294	0,375	0,375	250	210000	1,4	4,266666667	66	0	0,5	0,25
15	1	0,15	0,296	0,375	0,375	250	210000	1,4	4,266666667	66	0	0,5	0,25
16	1	0,15	0,298	0,375	0,375	250	210000	1,4	4,266666667	66	0	0,5	0,25
17	1	0,15	0,3	0,375	0,375	250	210000	1,4	4,266666667	66	0	0,5	0,25
18	1	0,15	0,302	0,375	0,375	250	210000	1,4	4,266666667	66	0	0,5	0,25
19	1	0,15	0,304	0,375	0,375	250	210000	1,4	4,266666667	66	0	0,5	0,25

Figure 42 - Excel® structure for the cylindrical.

Table 5 - Variation of the noise variable.

Noise Variable	Mean value μ_z	Standard deviation σ_z	Lower setting $(\mu_z - 3\sigma_z)$	Upper setting $(\mu_z + 3\sigma_z)$
Bending Angle/length (degrees/mm)	4.26	-	0	6.4
Material Thickness (mm)	0.3	0.01	0.27	0.33
Friction	0.1	-	-	0.2
Yield Strength (MPa)	250	16.67	200	300
Young Modulus (GPa)	210	6.67	190	230
Anisotropy	1.4	-	1.2	1.6

Table 6 - Square design variables.

Square	Normal setting	Lower setting	Upper setting
Force/area (MPa)	825	550	1100
Rotation angle of the tool (Degrees)	0	-45	45

Square	Normal setting	Lower setting	Upper setting
Length of the Square (mm)	0.2	0.12	0.3
Material height (mm)	0.375	0.35	0.4
Material depth (mm)	0.375	0.35	0.4

Table 7 - Conical design variables.

Conical	Normal setting	Lower setting	Upper setting
Force/area (MPa)	825	500	1100
Radius of the cylindrical (mm)	0.1	0.0677	0.15
Material height (mm)	0.375	0.35	0.4
Material depth (mm)	0.375	0.35	0.4

Table 8 - Cylindrical design variables.

Cylindrical	Normal setting	Lower setting	Upper setting
Force/length (N/mm)	66	53.3	80
Rotation angle of the tool (Degrees)	45	0	90
Radius of the conical waffling (mm)	0.5	0.185	1
Material height (mm)	0.375	0.35	0.4
Cylindrical	**Normal setting**	**Lower setting**	**Upper setting**
Material depth (mm)	0.375	0.35	0.4

4.3.2 The program to calculate the angle and thickness

As the material is plastically deformation it leads to curvature and because of the waffling it changes the thickness. This curvature can be measured by taking the angles of the surfaces of the material.

The calculation of the angle and thickness program works by primarily getting the corners data of the output of the simulation. The analysis of all the simulations are automatically and gathers the information in the Excel®.

For the angle, the program uses the data to create the normal vector of the surface, and then it compares the angles of the different surfaces by the equation.

$$\cos\theta = \frac{|n_1 \times n_2|}{\|n_1\| \|n_2\|} \tag{45}$$

Where n_1 and n_2 are the normal vectors of the 2 planes that are taking into consideration, as for example the left and right, front and back or top and bottom or as it shows in Figure 43, Figure 44 and Figure 45. The thickness is measured by the distance between the points of the surface on the top and on the bottom.

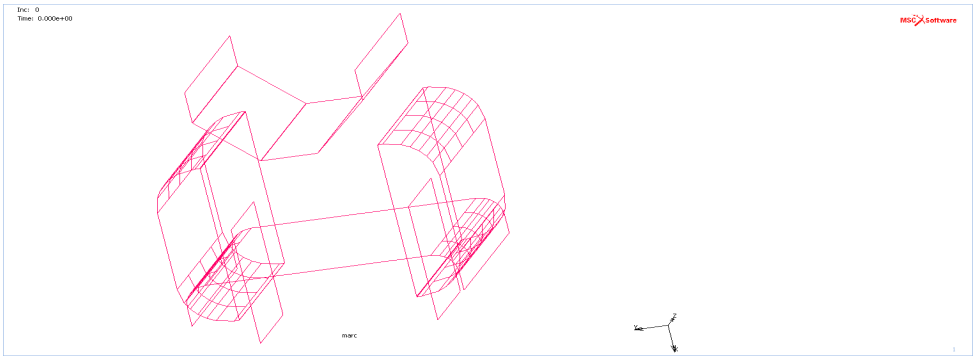

Figure 43 – Surface right and left.

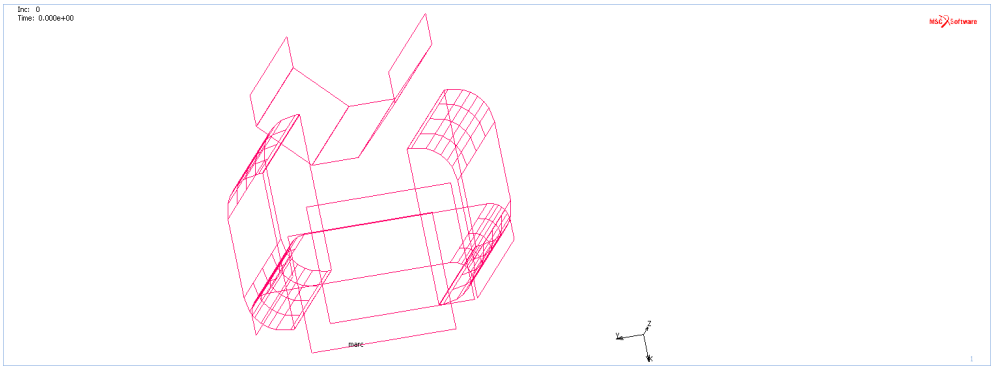

Figure 44 - Surface front and back.

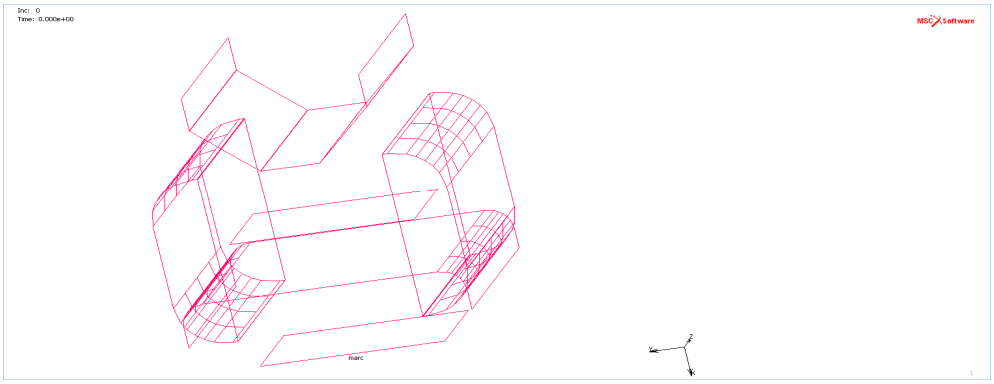

Figure 45 - Surface top and bottom.

4.3.3 Make the calculation robust for DACE

After knowing the data of the 2D and 3D simulations and having a program to get the output, it is needed to assess if the calculation is ready for the Robust strategy for that was used an mesh convergent study.

This analysis is made in 10 steps, this approach works by 10 different variations of every single design and noise variables. By using this, it is possible to study the sensitivity of the calculation and look for continuity in the response. This is done by looking at "jumps" in the outcome of the different experiments.

4.4 Practical test

The practical test was made with the objective of validating the FE simulation. The FE simulation, as already explained, use a block to analyse, but being the practical test impossible to analyse as one block, a plate was used. For the practical test, the material properties and dimensions are shown in Table 9, the variation of the parameter with the respective number of experiment is in Table 10. In Table 10, the output angle of the simulation was converted to the dimensions of the plate in the practical test, then this dimension was converted to the radius and then to the height of the material.

Table 9 - Material properties.

Material type	Thickness	Width	Height	Yield strength	Tensile strength	Elongation
AISI 420	0.3 mm	15 mm	60 mm	300 Mpa	655 MPa	>25 %

Table 10 - Parameters of the practical test.

Number of experiences	Angle of the material (degrees)	Radius of the material (mm)	Height (mm)	Pressure (MPa)
1	0	-	0	60
2	50	34.4	12.3	60
3	59	29.1	14.1	60
4	67	25.7	15.7	60
5	0	-	0	80
6	50	34.4	12.3	80
7	59	29.1	14.1	80
8	67	25.7	15.7	80
9	0	-	0	500
10	50	34.4	12.3	500
11	59	29.1	14.1	500

Number of experiences	Angle of the material (degrees)	Radius of the material (mm)	Height (mm)	Pressure (MPa)
12	67	25.7	15.7	500
13	0	-	0	750
14	50	34.4	12.3	750
15	59	29.1	14.1	750
16	67	25.7	15.7	750

The Variation of the force occurred by converting the pressure of the waffling force to the block. The waffling force used ranges of the dimensions of 0.2×0.2 , so it differs from the one that were used in the practical test, so a difference was made new FE simulation.

To obtain the force of the practical test, it was calculated first the force of the waffling is calculated by the equation (46). Then, the force applied by the waffling is divided by the total area of the block ((0.375×0.375) mm), as it can be seen by using the equation (47). The pressure on the block is the same as the pressure on the plate, and by multiplying it by the contact area of the plate (60×15) mm, it is obtain the force that will be used on the press by using the equation (48). The pressure on the block and the force of the press can be seen in Table 11. As the pressure of the waffling used in the practical test has a different area (0.2), to convert in the pressure of the simulation it needed to use the equation (49), admitting that the contact area was (0.12^2). On the Table 11 it is represented the pressures, being pressure the uses in the simulation, the average tool pressure is the pressure on the block (for 60 and 80 as they are based as the pressure of the block on the literature information [71]) the total force is the result of the equation (48) and finally the pressure of the simulation is as the names suggest the pressure used in the FE simulation.

Table 11 - Conversion pressure of the block to force applied in the practical test.

Pressure (MPa)	Average Tool pressure (MPa)	Total Force (kN) Sample of 15mm x 60mm	Pressure of the simulation (MPa)
-	60	54	585.93
-	80	72	781.25
500	142	128	1138

Pressure (MPa)	Average Tool pressure (MPa)	Total Force (kN) Sample of 15mm x 60mm	Pressure of the simulation (MPa)
750	213	192	2083

$$P_{waffling} = \frac{F_{waffling}}{A_{contact}} \qquad (46)$$
$$F_{waffling} = P_{waffling} \times A_{contact}$$

$$P_{Block} = \frac{F_{waffling}}{A_{block}} \qquad (47)$$

$$F_{press} = P_{block} \times A_{contac\ are} \qquad (48)$$

$$P_{waffling\ simulation} = \frac{F_{waffling}}{A_{contact}} \qquad (49)$$

Although it is advised to perform the test three times with the same settings, due to the lack of time, this was not possible. Besides that, by performing the test only one time it gives an understanding that permits to be created a comparison between the FE simulation and the "real world". Furthermore, the variations in the angle presented in Table 12 (the angle used on the simulation converted to the practical test) were causing some issues, as the height that it produced was not compatible with the 3D laser scanner (automatically measuring system, the NanoFocus), but the main reason for the occurrence of these issues is that, to produce the required angle in rolling, it is very difficult and time consuming to define the springback. This was made by the roll and with four different angles that can be seen in Figure 46.

Table 12 - Characteristic of the waffling in the practical test.

Waffling tool	Geometry of the contact	Dimensions of the block
Practical test	Square	0.12×0.12

Figure 46 - Pre-bended sample.

The practical test was performed by using the waffling tool that was already produced on Philips as it can be seen in Figure 47. This waffling uses the square geometry, and its dimensions are presented in Table 12. To analyze the effect of the waffling it was performed on a plate with the dimensions $15 \times 60\ mm^2$. The total contact area between the waffling tool and the plate is the total surface of the last one. As said above, the initial idea was to compare the simulations with the practical test by converting the angle in the block to the angle of the plate, this conversion is possible by using equation (50).

$$angle\ of\ \ the\ plate = \frac{plate\ length}{block\ length} \times angle\ of\ \ the\ block \tag{50}$$

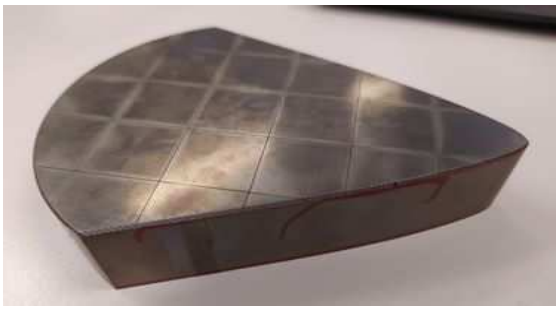

Figure 47 - Waffling tool.

The equation (51) was supposed to be used, which would result in the conversion of the pre-bending of the simulation to the radii that should be used in the practical test. This equation uses the perimeter of the circle compared with the angle used, and its length is half of the plate (30 mm).

$$\begin{aligned} \frac{\text{angle of pre-bending}}{360} \times 2\pi \times radii &= length \\ radii &= \frac{180 \times length}{\text{angle of pre-bending} \times \pi} \end{aligned} \tag{51}$$

As this was impossible to use the angles of the simulation, it was opted for an inverse engineering of what was supposed to be done. So, the angle of the practical test is the angle introduced in the simulation. This angle is used to study the difference between the numerical result and the practical test. Equation (52) makes a comparison between the height of the plate and the radii to the *cos* of the angle, as can be seen in Figure 48. The height of the material is measured after the pre-bending, and then it is converted by equalizing equation (51) and equation (52), which then gives the origin to the equation (53).

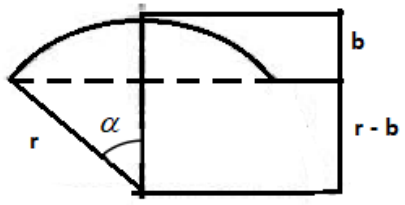

Figure 48 - Obtaining the angle of the plate.

$$\cos\alpha = \frac{R-b}{R}$$
$$\cos\alpha - 1 = \frac{b}{R} \quad (52)$$
$$R = \frac{-b}{\cos\alpha - 1}$$

$$\frac{a\times 180}{\pi\times\alpha} = \frac{-b}{\cos\alpha - 1}$$
$$\frac{-b\times\pi}{a\times 180} = \frac{\cos\alpha - 1}{\alpha} \quad (53)$$

With this in mind, several simulations were produced to get the same pre-bending angle as the practical test, by only using (in the model) the pre-bending and opening action.

The practical test consists out of the following steps:

1. The material was cut off in strips of 15 mm width of the wideband, as it can be seen in Figure 46. A line was drawn so that the strips can be cut in 60 mm length as can be seen Figure 49. These lines are necessary because if the material is curved, the length cannot be measured any more.
2. The different radii were created by the rollers presented in Figure 50. The material is rolled in one stage through the rollers.
3. The strips were cut by a guillotine, to get the 60 mm in length direction, represented in Figure 51.
4. To measure the height, as can be seen in Figure 53, it taster measurement is needed (taster), shown in Figure 52, and the laser measuring machine in Figure 54. This was performed by using these two methods since some curvatures are

too large to measure with the laser measuring machine. The focus of the laser measurement on the different heights is out of range.

5. The plate and the waffling tool (represented in Figure 47) are introduced into the press, as can be seen in Figure 55, and afterwards the defined load is applied by the press
6. Measuring the curvature with the laser measuring after the press has goes in the same way as has been explained above. Also, the marks of the tool on the sample are analyzed under the microscope.

Figure 49 - Strips of 15mm width

Figure 50 - Rolling process of the sheet metal.

Figure 51 - Guillotine tool.

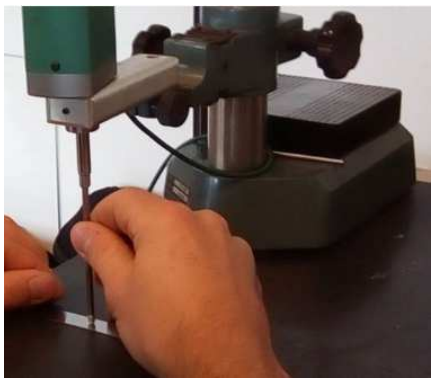

Figure 52 – The taster measuring the height.

Figure 53 - Measure dimension.

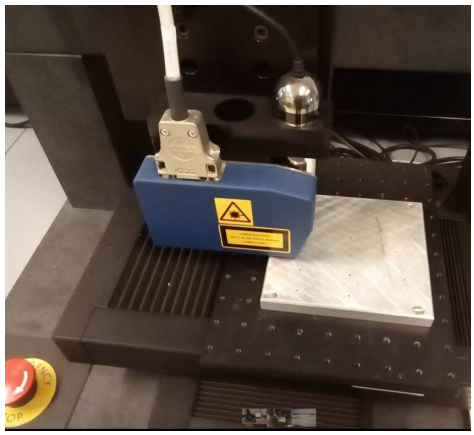

Figure 54 - Laser measuring in more detail.

Figure 55 - Hydraulic press with the waffling tool and plate.

The variation of the variables on the experience is shown in Table 13. To compare the practical test and the FE simulations, some simulations were made without applying force to get the same angle as the one in the practical test. The conversion of the angles in the simulation is accomplished by dividing the average angle for every level of pre-bending and divide by the difference of the length ($60 / 0.375$ mm). This can be seen in Table 14. The simulation used the average of the noise variables, for the exception of angle/area. The parameters used in the simulation and the meaning of each number is represented are shown in the appendix 8.2.1

Table 13 - Variation of the variables on the practical test.

Sample number	Height before the test (mm)	Applied Force (kN)	Comments
1.1	0.50	54	Already some curvature on roll
1.2	0.60	72	Already some curvature on roll
1.3	0.60	128	Already some curvature on roll
1.4	0.65	192	Already some curvature on roll
2.1	1.12	54	Failed (sample was upside down)
2.2	1.10	72	-
2.3	1.12	128	-
2.4	1.14	54	Repetition of sample 2.1
3.1	3.25	54	-
3.2	2.70	72	-
3.3	3.09	128	-
3.4	3.25	192	-
4.1	5.44	54	-
4.2	5.40	72	-
4.3	5.70	128	-
4.4	5.82	192	-

Table 14 – Simulation for compaction between the practical and theoretical work.

Average angle of the practical test (degrees)	Angle of the simulation (degrees)	True value of the angle of the simulation (degrees)
2.246	0.0140	0.0135
4.281	0.0268	0.02476
11.780	0.0736	0.0721
21.609	0.1351	0.1381

4.5 Screening

After having made the responses of the calculation robust (meaning a smooth response without jumping steps in the response), the second step of the robust strategy is introduced, the screening, which was previously explained. The main goal is to eliminate the variables that have a lower influence on the response. By performing the resolution III a Plackett-Burman design $[-1;1]$ was made by the function in MATLAB® $fracfact$. For the square and the conical geometries, the simulation has 10 parameters, the respective index is represented in Table 15 and the Plackett-Burman table is in Table 16. The 13 and 14 are the same for both geometries because it is a square and a cone (contact area is a circle). The resolution III is in this case performs $2^{10-6}=16$ simulations with the table $[-1;1]$ shown in Table 16. In the cylindrical geometry, the only change is the 11 - force/length, 13 - tool radius and 14 - tool length, so the resolution III is $2^{11-7}=16$ simulations, and the table of Plackett-Burman are shown on Appendix 8.3. Then the value of -1 was converted to the minimal value of that parameter and the value 1 to the higher value. The result of the conversion to the variables values are represented in Table 17 for the square and the other geometries in in Appendix 8.3. Later, this table is introduced in the Excel® of the automation program. After running the 16 simulations the program is capable to originate an output to calculate the angle and thickness, and then a MATLAB® program was applied. This program uses the input of the DOE that is represented in Table 17 and Appendix 8.3, with the variables and the response of the simulations. A linear model is used to perform the ANOVA, which then will originate the ANOVA table, the Pareto plots (where it is possible to visualize the main effect) and the Main effect plots. The Pareto principle will be used to determine the more important variables. There will be analysed 2 outputs, the angle of the left-right and front-back.

Table 15 - Parameters and respective indexes of Table 16 and Table 17.

Parameter	Number
Friction	3
Material Thickness	4
Material Height	5
Material Depth	6
Yield stress	7
Young's (E-)Modulus	8
Anisotropies	9
Angle/area	10
Force/area	11
Tool Radius or tool depth	13
Tool depth	14

Table 16 - Plackett-Burman with 10 parameters for the square and conical.

3	4	5	6	7	8	9	10	11	13 and 14
-1	-1	-1	-1	-1	-1	-1	-1	1	1
-1	-1	-1	1	-1	1	1	1	-1	1
-1	-1	1	-1	1	1	1	-1	-1	1
-1	-1	1	1	1	-1	-1	1	1	1
-1	1	-1	-1	1	1	-1	1	-1	-1
-1	1	-1	1	1	-1	1	-1	1	-1
-1	1	1	-1	-1	-1	1	1	1	-1
-1	1	1	1	-1	1	-1	-1	-1	-1
1	-1	-1	-1	1	-1	1	1	-1	-1
1	-1	-1	1	1	1	-1	-1	1	-1
1	-1	1	-1	-1	1	-1	1	1	-1
1	-1	1	1	-1	-1	1	-1	-1	-1
1	1	-1	-1	-1	1	1	-1	1	1
1	1	-1	1	-1	-1	-1	1	-1	1
1	1	1	-1	1	-1	-1	-1	-1	1
1	1	1	1	1	1	1	1	1	1

Table 17 - Parameters and their variation for square screening.

3 $[\mu]$	4 $[mm]$	5 $[mm]$	6 $[mm]$	7 $[MPa]$	8 $[MPa]$	9	10 [Degrees]	11 $[MPa]$	13 and 14 $[mm]$
0,1	0,27	0,35	0,35	200	190000	1,2	0	1125	0,3
0,1	0,27	0,35	0,4	200	230000	1,6	6,4	500	0,3
0,1	0,27	0,4	0,35	300	230000	1,6	0	500	0,3
0,1	0,27	0,4	0,4	300	190000	1,2	6,4	1125	0,3
0,1	0,33	0,35	0,35	300	230000	1,2	6,4	500	0,1
0,1	0,33	0,35	0,4	300	190000	1,6	0	1125	0,1
0,1	0,33	0,4	0,35	200	190000	1,6	6,4	1125	0,1
0,1	0,33	0,4	0,4	200	230000	1,2	0	500	0,1
0,2	0,27	0,35	0,35	300	190000	1,6	6,4	500	0,1
0,2	0,27	0,35	0,4	300	230000	1,2	0	1125	0,1
0,2	0,27	0,4	0,35	200	230000	1,2	6,4	1125	0,1
0,2	0,27	0,4	0,4	200	190000	1,6	0	500	0,1
0,2	0,33	0,35	0,35	200	230000	1,6	0	1125	0,3
0,2	0,33	0,35	0,4	200	190000	1,2	6,4	500	0,3
0,2	0,33	0,4	0,35	300	190000	1,2	0	500	0,3
0,2	0,33	0,4	0,4	300	230000	1,6	6,4	1125	0,3

Later on, was made a screening to see the impact of the different geometry. The geometry that could be used to compare that is the square and conical because it uses the same contact area. In the parameter geometry in this screening is used the -1 equals the square and the 1 the conical, the rest of the parameters are equal to the square and conical screening. As in this case, the parameter used are 11 so the resolution III is $2^{11-7} = 16$ simulations the rest of the procedure are equal to the conical.

4.6 The design of experience

As the waffling tool already exists and taking into consideration the short amount of time, the analysis will be done with the geometry of the waffling tool used on the practical test, as already shown in Figure 47 . The different waffling geometries will not be considered further on.

The third step of the robust optimization is the design of experience. In this step, it is only going to be analyzing the 6 parameters chosen by the screening. Here, the accuracy of the analysis needs to be higher, because the metamodel will be fitted accordingly. The prediction of the metamodel will be variating, depending on which DOE approach will be used. To get a higher linear prediction, was used a FFD (full factorial design), for the non-linear prediction was used an LHD.

The number of FFD increases with the number of parameters. The LHD plus the FFD will place DOE points in all corners of the design, in the interior and also on the boundaries of the design space. The objective is to perform a minimal number of simulations and at the same time having a suitable fitting of the metamodel. The number of FFD used was 64 (2^6) simulations and as for the LHD, it starts with 32 simulations. The number necessary for DOE points cannot be known before the method is implemented and it is must consider that it also variates depending on the problem at hand. The DOE can be enhanced in later stages.

MATLAB® is used to produce the FFD and the LHD. For the FFD the function $fullfact$ is used and then it converted the $[1, 2]$ to the variables, being the 1 the minimal value of the variable and 2 the maximum value of the variable. On the other hand, for the LHD an $lhsaugment$ function was put into work. The result that it got was 96 DOE points.

4.7 The FE simulation and implementation of the metamodel

Following the DOE setting specifications, the FE simulation is the fourth step of robust optimization. After that simulation, a program gets the output (angle). By having a DOE and its output, a metamodel can be implemented, which is the fifth step of the robust strategy. There are various types of metamodels, but they cannot be acknowledged beforehand because the response function is still unknown. The metamodel that has the

best fitting for replicating the simulation response will be the one used. In literature, several authors stated that Kriging is the best metamodel to use in this situation, as it is more reliable and flexible than the RSM, it has more accurate predictions of a highly nonlinear function, the behavior is appropriate to carry out an efficient robust optimization where there is uncertainty [22, 24, 30, 33, 34, 37, 42, 43, 59]. While others suggest RSM is the most appropriate metamodel because it has several advantages, it can locally support nonlinear approximation that employs a sequence of local experience analysis, this model is easy to establish, it has a better performance on low order non-linear response function, it can get a more distinct and sensitive analysis, and it is also less complex and cheaper to work with [23, 30, 47, 56].

In this case, it will use different types of metamodels because of the unknown factor on the response behavior and in the design space, and also the metamodel could be accurate in different types of response functions, the groups of the metamodels implemented are kriging and RSM. For Kriging, the models that were implemented are using constant (zero-order trend function), linear (first-order trend function) and quadratic (second-order trend function and second regression order). All of these previous models are polynomial trend functions combined with gaussian exponential functions. For RSM the ones implemented are the polynomial models, linear, linear with interaction, elliptic and full quadratic models. With this model's variety, it is possible to achieve an accurate behavior on the function's response.

4.8 Metamodel validation

To be appropriate the metamodel needs to have the same or a very similar behavior as the function's response, this is the sixth step of the robust strategy. To analyze this, ANOVA for RSM is used. It can be estimated how well the metamodel predicts the simulation. It also uses the coefficient of determination R^2, that ranges between 0 and 1, being 0, the different prediction, and 1 the equal prediction (perfectly fitted), of the simulation. The ANOVA is based on a random error term ε, this is fitted after introducing the metamodel to the response. This technique could not be used on Kriging because it cannot be used on a metamodel that interpolates the response, as the fitting error is zero in DOE points. To overcome this, the LOOCV was utilized on the 2 metamodels. This method uses a "one leaves out" measurement point x_{-i} and implements a metamodel in the remaining response measurement. The difference between the real value $y(x_i)$ and the predicted value $\hat{y}_{-i}(x_i)$, is the prediction error e_{-i} and is represented in equation (40) [16].

In Figure 56 is shown the information of the metamodel validation; it can be seen as a cross validation plot (the red line is the prediction of the function's response made by the metamodel and the blue circles are the true values), the range of values that cover zero (the 95% confidence intervals presented in green cover zero and the red ones do not include this value, therefore signalling a significant difference) the error correlation

or error prediction, the distribution of the standard residuals, the normal probability plot (PP plot) (this graph shows how the response function is close to a normal distribution), the error distribution plot (this histogram shows the error distribution of the residuals). The information that will be analysed in more detail is the $R^2_{Prediction}$, $R^2_{Predictionadj.}$ and the $RMSE - CV$. This $RMSE - CV$ represents the standard deviation of the residuals of the cross-validation, and the best values are the ones that are the closest to zero. The $R^2_{Prediction}$, is the coefficient of determination for the prediction of the response. $R^2_{Predictionadj.}$ is used to see to adjust the $R^2_{Prediction}$ by the inclusion of different variables in the model, since it us known that $R^2_{Prediction}$ increases with the number of variables in the model.

In Figure 57 an example can be seen of a Kriging metamodel analyzed by LOOCV, as the ANOVA cannot be used as a method, as already previously discussed. It is basically the same things like the analysis of RSM. The graph has a cross validation plot, standard cross validation plot, a QQ plot (it is a quantile-quantile plot, used to compare the probabilistic distribution of the true response and the metamodel response) and the error distribution plot. For the numerical, it has the same thing as the $R^2_{Prediction}$, $R^2_{Predictionadj.}$ and the $RMSE - CV$, it will be analysed as the RSM.

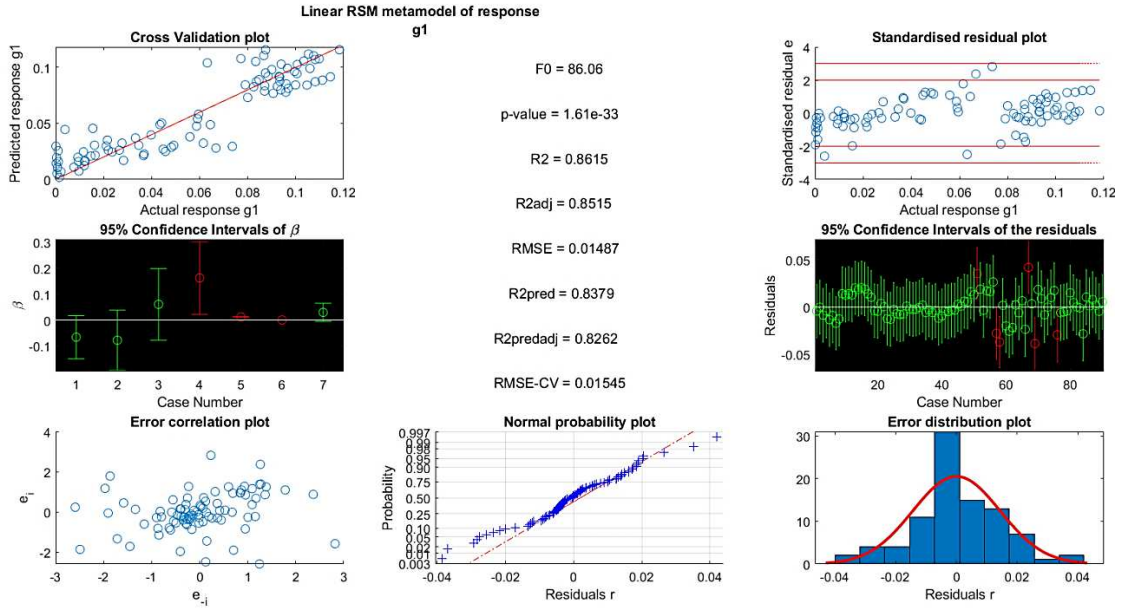

Figure 56 - Example of RSM validation.

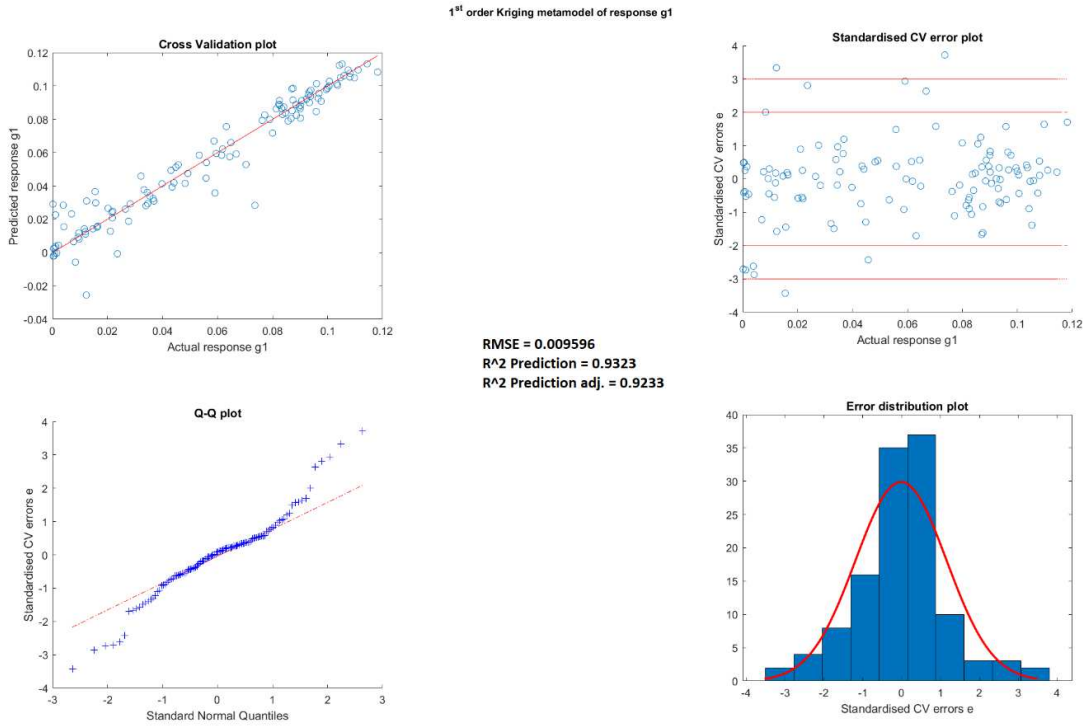

Figure 57 - Example of kriging validation.

4.9 Metamodel-based robust optimization

The step 7 of the robust strategy is an optimization, where the design variables value are found which have less sensitivity to the noise variables and taking into consideration the constraints. To perform this, a metamodel is needed and an optimization algorithm to solve equation (20). For this project it is written into equation (54). The RO minimizes the response function, finding the optimum value of the design variables. In the equation (54) the The function f_f is divided in mean μ_f and standard deviation σ_f. The implicit constraints are: final front back angle $\mu_{front\ back\ angle}$ will have an up and down value of the 0.022 and -0.022 degrees, respectively, and the thickness $\mu_{thickness}$ the up and down value are 0.31 and 0.29 mm, this range of values were chosen to be the acceptable values. The design variable taken into account in this equation is $f\ /\ a$, this being the force/area in MPa, D being the dimensions in mm, B_n being the height of the block in mm and B_n being the depth of the block in mm, for the noise t being the thickness and $\alpha\ /\ a$ the pre-bending angle.

This optimization uses an gradient based algorithm, this MATLAB algorithm is $f\ \mathrm{min}\ con$. The prediction of the response mean and standard deviation are analysed. This is done through the validation of the metamodel by the $R^2_{\mathrm{Pr}ediction}$ and $RMSE - CV$. After this prediction has been done, the result is used by the gradient

basic optimization algorithm for solving the equation (54). This algorithm minimalizes the risk of the overall optimization technique from being trapped in a local optimum.

$$
\begin{aligned}
&\min_{x} \ \mu_f \pm 3\sigma_f \\
&s.t. \quad -0.022 \le \mu_{front\ back\ angle} - 3\sigma_{front\ back\ angle} \\
&\qquad \mu_{front\ back\ angle} + 3\sigma_{front\ back\ angle} \le 0.022 \\
&\qquad 0.29 \le \mu_{thickness} - 3\sigma_{thickness} \\
&\qquad \mu_{thickness} + 3\sigma_{thickness} \le 0.31 \\
&\qquad 0.1 \le D \ge 0.28 \\
&\qquad 500 \le f / a \le 750 \\
&\qquad 0.35 \le \mathrm{B}_h \le 0.4 \\
&\qquad 0.35 \le \mathrm{B}_d \le 0.4 \\
&\text{where} \qquad \mathrm{t} \ \square \ N(0.3, 0.01^2) \\
&\qquad 0 \le \alpha / a \le 6.4
\end{aligned}
\tag{54}
$$

In Figure 58- (a) and Figure 58- (b) represents an example of the MATLAB® program output on the optimum value, in 3D and in 2D respectively.

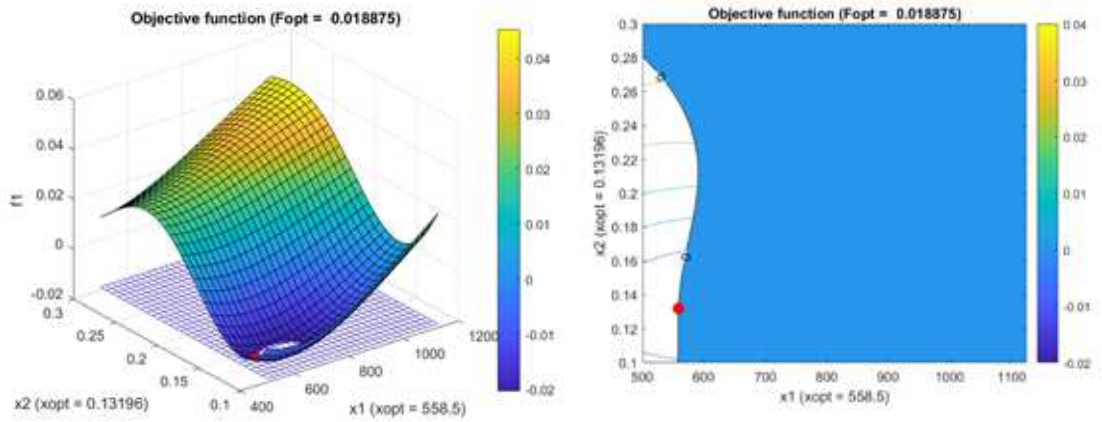

a b

Figure 58 – (a) Representation of an optimum in 3D and (b) representation of the optimal in 2D.

4.10 Validation of the robust optimization

The step 8 of the robust strategy is the validation of the robust optimization. In the step 3 the minimal number of DOE was chosen as increasing this would increase computing cost. The solution used is only a representation of the approximate problem, so the optimization is an estimation of the response function with the number of DOE chosen.

The accuracy of the optimal and of course the metamodel prediction needs to be accurate, but as this is correlated with the number of DOE point chosen, it needs to be asked “Is the model accurately enough?”. This question is the step 9 of robust optimization. If the answer is “yes”, the robust optimization has ended, and it has a Robust optimum. If the answer is “no” it needs to go to step 10. This validation is done by performing multiple FE simulation around the optimum. These simulations are limited due to the time to run the simulation and the coarse estimation of the metamodel that creates a poor prediction accuracy and robust optimization.

4.11 Sequential improvement

The sequential improvement is the step 10 of the robust strategy performed if the model is not accurate. It could be because the metamodel prediction response function is different than the true response function or that the DOE points are not enough to replicate the true response function. The second one happens when the prediction of the optimal changes by using the method to validate the optimum. The sequential improvement is done by going back to the step 3 and crating more DOE points. This creation of DOE can take into consideration the optimization or creating random DOE points, these two use the LHD.

Results

5 RESULTS

5.1 Results of the project

5.1.1 2D result

The 2D simulations are performed to get a basic understanding of the parameters with an easy and quick approach. It was performed 4 different bending angles as 0.4, 0.8, 1.6 and 2.4 degrees. In Figure 59 the 0 N load represents the springback of the bending angle without the waffling method. The legend sum in Figure 59 represents the sum of the angle AC (α_{AC}) and the angle GE (α_{GE}).

In Figure 59 in the line represented by 0.4 degrees, the block is not plastically deformed in the bending and back bending. This effect has an opposite behaviour when comparing to the other, being the response angle minimal with low force, increasing it with the increase of the waffling load.

In Figure 59 the 0.8, 1.6 and 2.4 degrees, increasing of the waffling force decreases the output angle .

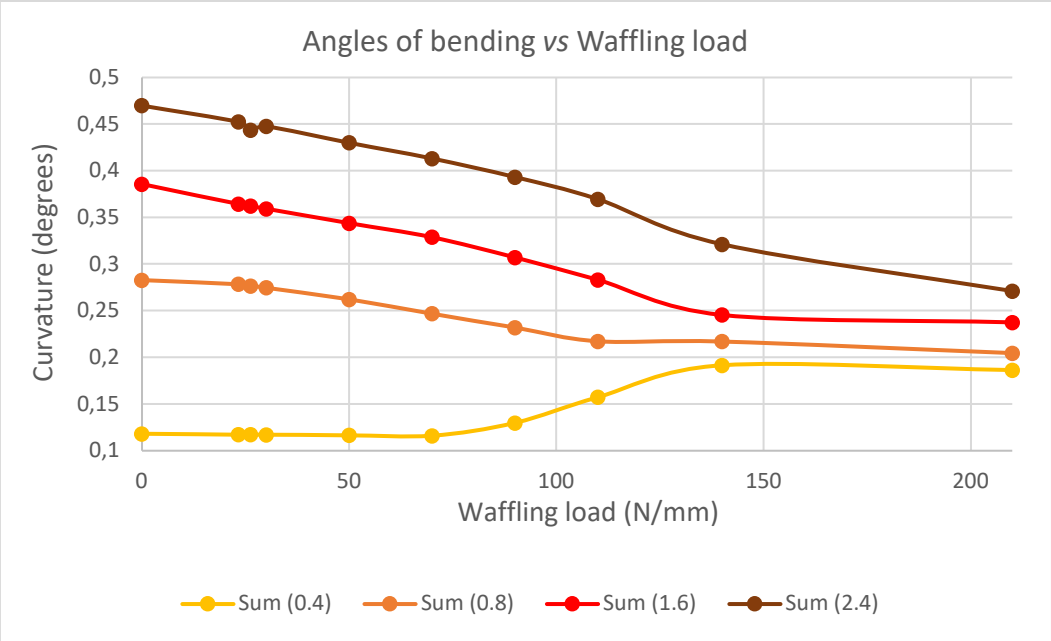

Figure 59 - Angle of bending *vs* waffling load on 2D simulation.

In all the figures, where the material is initially plastic deformed, show that after a certain load (140 N/mm) the difference that increasing the waffling force makes is

irrelevant. This is due to the fact that the contact area after that force starts to have more plastic deformation, when compared to all of the material. This can be seen in Figure 60 - (a) and is analysed in Figure 61. The outcome of these figures shows the delta (is the difference between the final dimensions after the process of waffling and the virgin block dimensions), the delta DH is having a much higher difference than the BF delta, the BF and HD distances are represented in Figure 60 - (b).

In conclusion the optimal parameters of the waffling load are between the 110 N/mm and 140 N/mm. In this range, the stresses caused by the bending and back bending are overruled in a way that: the difference between the plastic deformation on the contact area and the rest of the block is minimal, and the minor effect on flattening the surface of a higher waffling load will not decrease the output angle.

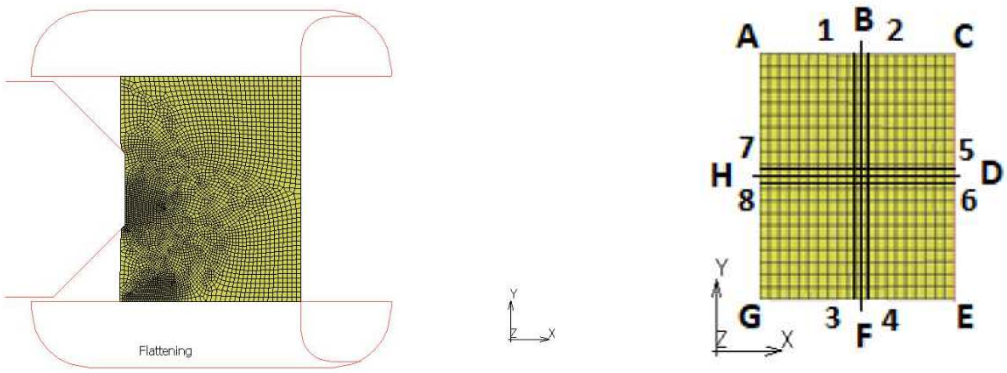

Figure 60 – (a) Represents the block with plastic deformation in the contact area and (b) represents the distance BF and HD.

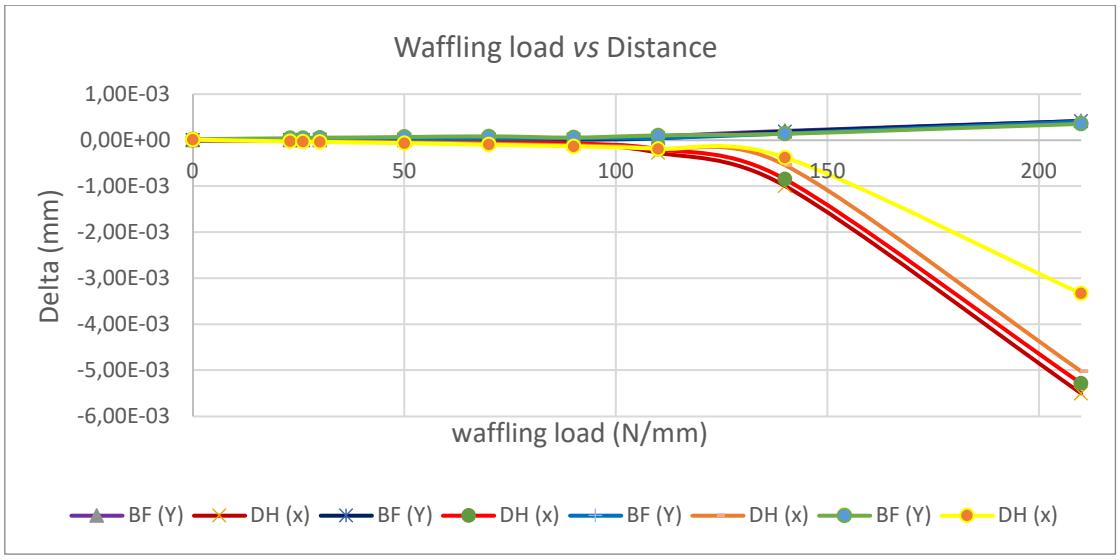

Figure 61 - Distance *vs* waffling force on 2D simulation.

5.1.2 3D results

To determine the range for the 3D waffling load, firstly it is needed to determine the load that had the best result in 2D (110 N/mm and 140 N/mm) and then convert it. This was made by multiplying the length (z-direction) of the waffling tool (0.12 mm). The result is 13.2 N and 16.8 N. Therefore, the first simulation is made with 0 N, 10 N and 20 N. By performing these simulations, it is possible to acknowledge that the best result is given by the load of 20 N. As this is the highest value, more simulations were performed (30 N, 40 N, 45 N, 50 N, 55 N, 60 N). The pre-bending angle, is kept the same as in the 2D, being the range the same as used previously as well.

In the in Figure 62, Figure 63, Figure 64 and Figure 65 the legend represents sum and the different bending angles (pre-bending angle). The mean of the sum is the summation, if it is in the y-direction is AB and CD (could be the distance or the angle) and if it is in the $_z$-direction is the EF and GH (could be the distance or the angle).

The distance in Figure 62 and Figure 63 is the difference between the deformed material and the virgin material.

The distance in y-direction (further expressed by left right) shows that the value that represents the minimal distance (the perfect condition) has a different behavior with different bending angles. The value of the force where the delta is 0 for the 0.8 degrees is between the 20 N and the 30 N. For the 1.6 degrees is 30 N, for the 2.4 degrees is 40 N but the 0.4 degrees is in 10 N and 50 N as it can be seen in Figure 62.

The distance in the z - direction (further express by front back) shows that the higher the angle of bending, the less sensitivity it will have to the waffling force. For the 0.8 and 1.2 degrees the increase of the waffling load for a value higher than the 40 N, results on a bigger increase on the distance. This behavior is also found in values higher than 20 N for the 0.4 degrees. On the other hand, for the 2.4 degrees the increase of the waffling load does not have a major impact. This can be seen in Figure 63.

The study of the waffling load effects and the angle of bending on the result angle in the x -direction, or further expressed by left right angle, is at Figure 64. It can be seen that the 0.8, 1.2 and 2.4 degrees, when increasing the waffling load, have a similar response (the curves are almost parallel to each other), which is the decreasing of the angle. For the 0.4 degrees the curve decreases from 0 N to 40 N and then it increases to 60 N.

The angle of bending on the angle in z -direction, or further expressed by front back angle, and by analysing Figure 65, it can be seen that the response is similar to the distance in the z-direction, when increasing the angle of bending the angle of the final material has less sensitivity. For the pre-bending angle 0.8 and 1.4 degrees, after 40 N the impact on the output angle is highly increased. For the 0.4 degrees this happens after 20 N. For the 2.4 degrees the waffling has a very low sensitivity.

In conclusion, the best range of waffling load to analyse the 3D robust simulation is between 20 and 45 N.

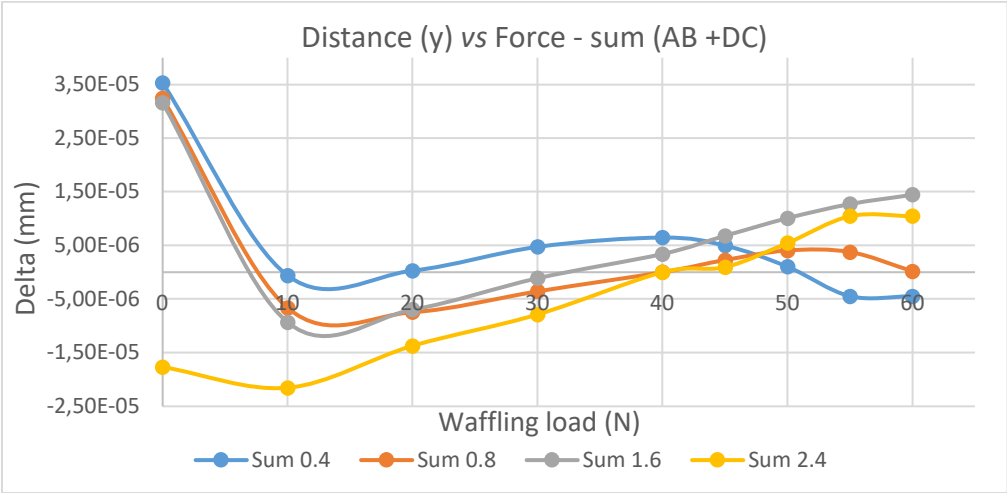

Figure 62 - Distance (x) *vs* waffling force on 3D simulation.

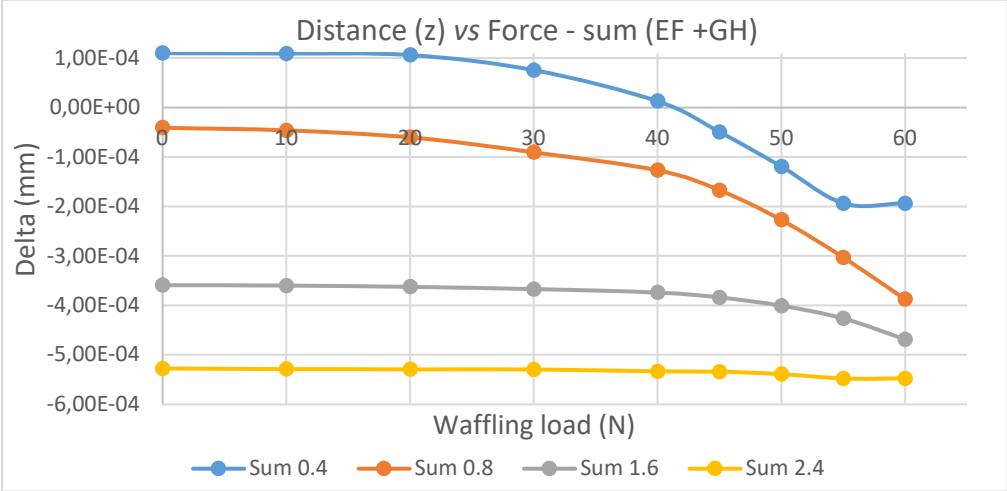

Figure 63 - Distance (z) *vs* waffling force on 3D simulation.

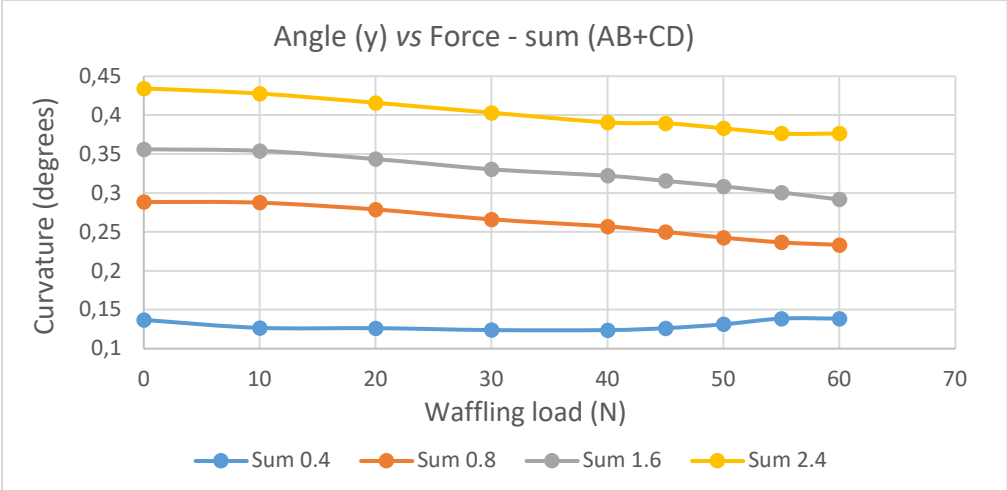

Figure 64 - Angle (x) *vs* waffling force on 3D simulation.

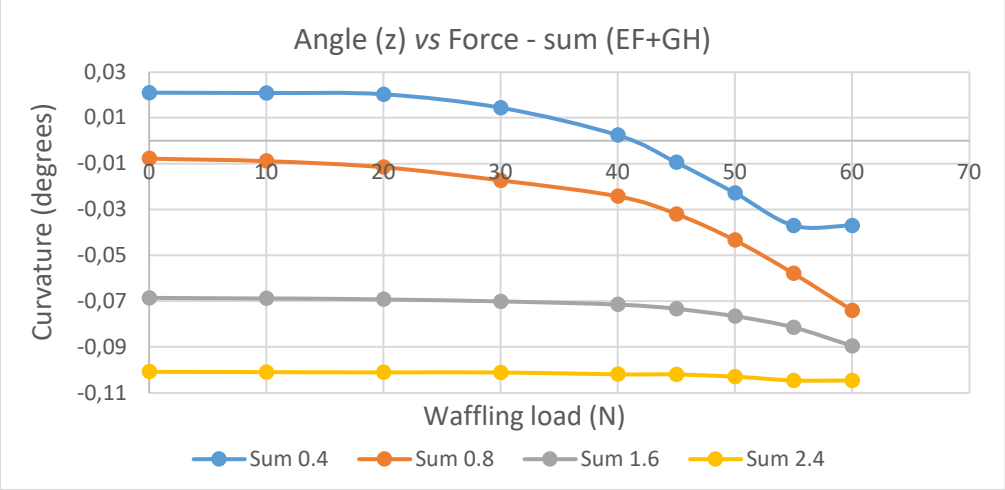

Figure 65 - Angle (z) *vs* waffling force on 3D simulation.

5.1.3 The robust 3D simulation for the square geometry

In the square tool the material has some variations in the parameters with the same behaviours for angle left right and front back as it can be seen in Figure 66 and Figure 67, respectively. The mean of the number is presented in Table 18. The noise parameters are friction (3), material thickness (4), Yield stress (7), Young's Modulus (8) and the Anisotropy (9). There are similarities between the response seen in left right and front back like the friction (3), and Anisotropies (9), when the angle increases these parameters increase as well. On the Young's Modulus (8), the opposite occurs as increasing these parameters results on the decrease of the angle. The noise variables that have different behaviours between the left right and front back are the Yield stress (7) and the Angle/area (10). By increasing the Yield stress (7), for left right angle results in increasing angle, but on the front back it has the opposite behaviour. The Angle/area (10) is the parameter that introduces the stress before the waffling method, so there is a starting range that is not plastic deformed or has very little plastic deformation. In the front back angle, for the simulation's number between 78 and 82, the results are going down and after the 82 it goes up until the higher value of Angle/area (10) is achieved due to the plastic deformation phenomenon. This phenomenon is only found on left right angle for the simulation 78 and 79 and goes up in the 79 to the higher value of Angle/area (10).

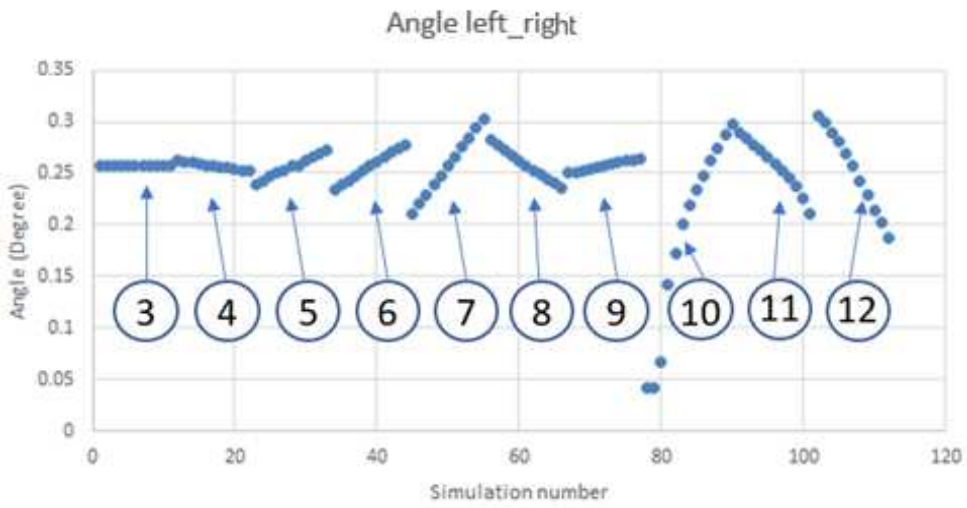

Figure 66 - Left right angle for the square tool.

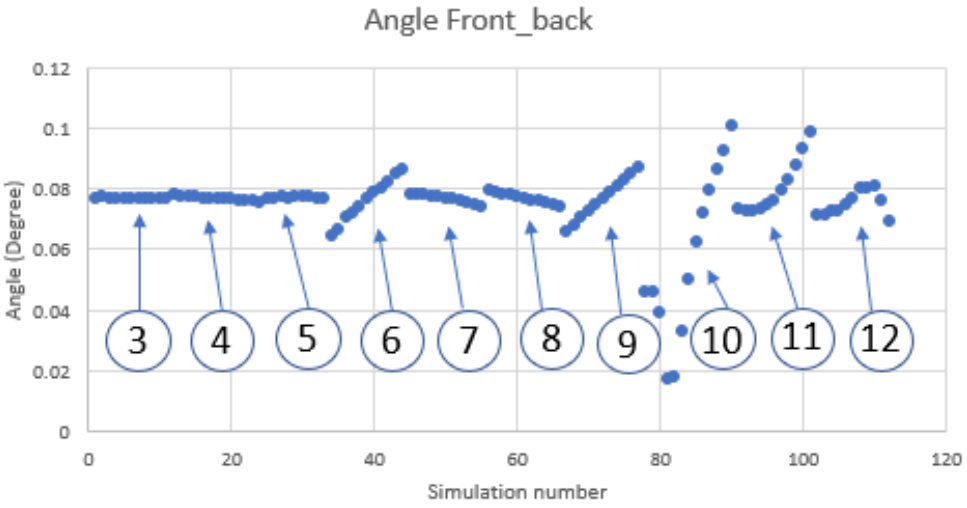

Figure 67 – Front back angle for the square tool.

Table 18 – Parameters and respective indexes in Figure 66 and Figure 67.

Parameter	Number
Friction	3
Material Thickness	4
Material Height	5
Material Depth	6
Yield stress	7
Young's (E-)Modulus	8
Anisotropies	9
Angle/area	10
Force/area	11
Tool dimensions (length)	12

For optimization and to get a flat surface in a robust system, it is necessary to understand the influence of the noise, as these are the variables that cannot be controlled. To reach this goal, it is needed to understand the variables that can be controlled. The design variables are the material height (5), material depth (6), Force/area (11) and Tool dimension (12). Increasing the material height (5) and material depth (6) for the left right it increases the output angle as it can be seen in Figure 68 and Figure 70. The values of the parameters are shown in Table 19 and Table 20, respectively. By increasing the material height (5) it decreases the front back angle but for (6) for the left right it increases as it is demonstrated in Figure 69 and Figure 71, and the values of the parameters are shown Table 19 and Table 20, respectively.

Table 19 – Material height value for the respective simulation number in Figure 68 and Figure 69.

Simulation Number	5 Material height [$m\ m$]
23	0.35
24	0.355
25	0.36
26	0.365
27	0.37
28	0.375
29	0.38
30	0.385
31	0.39
32	0.395
33	0.4

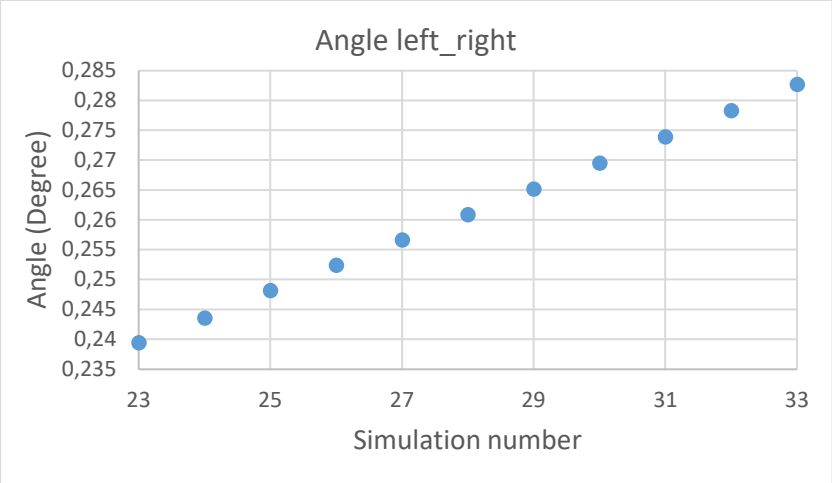

Figure 68 - The effect of material height on the left right angle for the square tool.

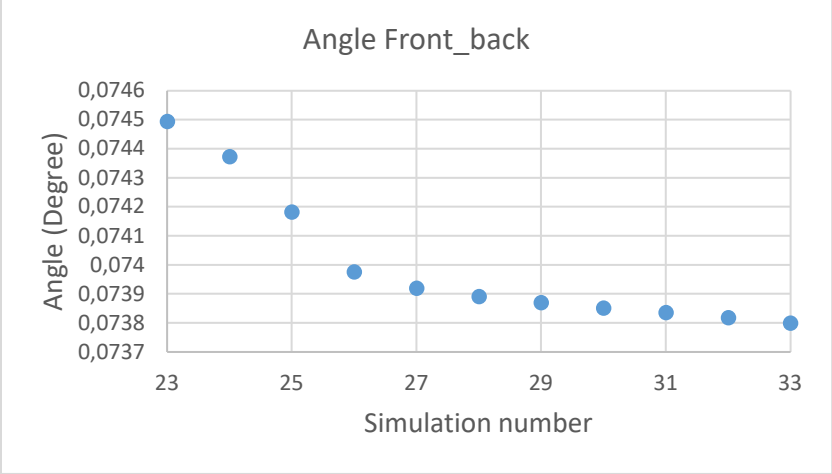

Figure 69 - The effect of material height on the front back angle for the square tool

Table 20 – Material depth value for the respective simulations number in Figure 70 and Figure 71.

Simulation Number	6 Material depth $[mm]$
34	0.35
35	0.355
36	0.36
37	0.365
38	0.37
39	0.375
40	0.38
41	0.385
42	0.39
43	0.395
44	0.4

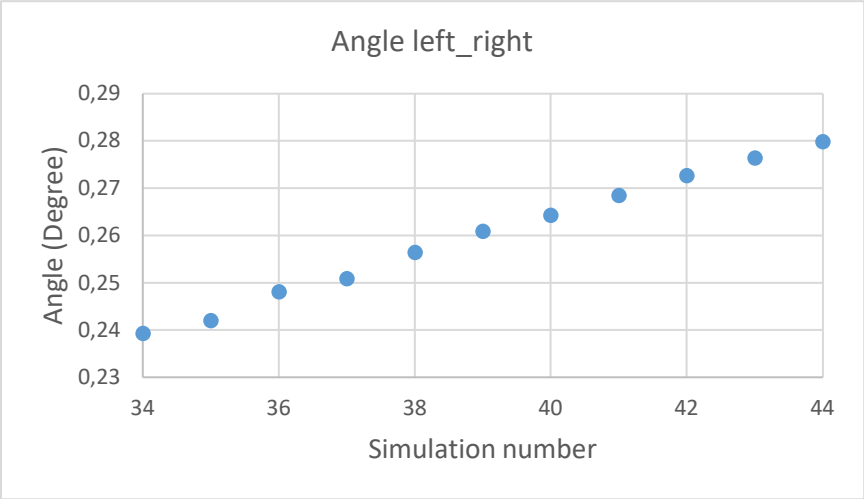

Figure 70 - The effect of material depth on the left right angle for the square tool.

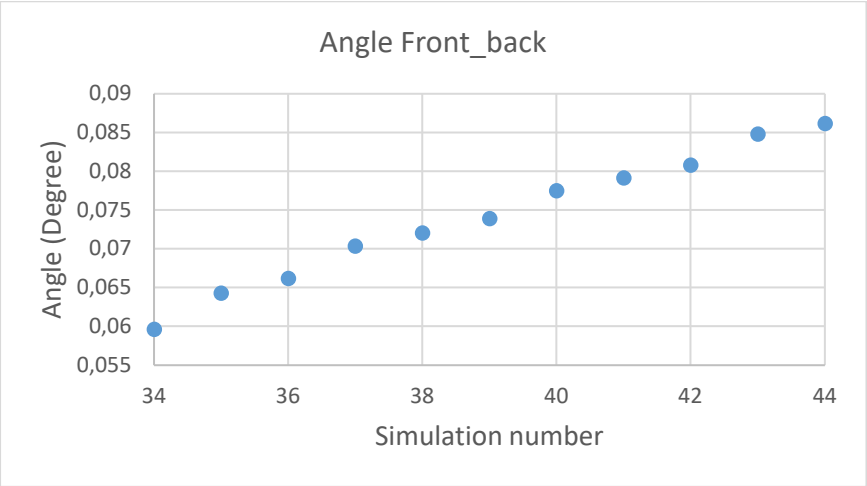

Figure 71 - The effect of material depth on the front back angle for the square tool.

For the Force/area (11) the effect can be seen on the angle left right and front back in Figure 72 and Figure 73, respectively and the value of the parameters in Table 21. For the angle left right increasing the force/area (11) leads to the decrease of the angle but, the opposite occurs in the front back, the angle increases when increasing the Force/area (11). This phenomenon is similar to the noise variable, Yield stress (7) but in the opposite direction. For the Tool dimensions (12) the effect on the angle left right and front back can be seen in Figure 74 and Figure 75, respectively, and the value of the parameters in the Table 22. Increasing this parameter decreases the left right angle. But the influence of this parameter on the output, results in an increase of the front back angle between 102 (0.1 mm of tool width and depth) and 110 (0.26 mm of tool width and depth) and then it drops.

Table 21 – Force/area value for the respective simulations number in Figure 72 and Figure 73.

Simulation Number	11 Force/area $[N/mm^2]$
91	500
92	562.5
93	625
94	687.5
95	750
96	812.5
97	875
98	937.5
99	1000
100	1062.5
101	1125

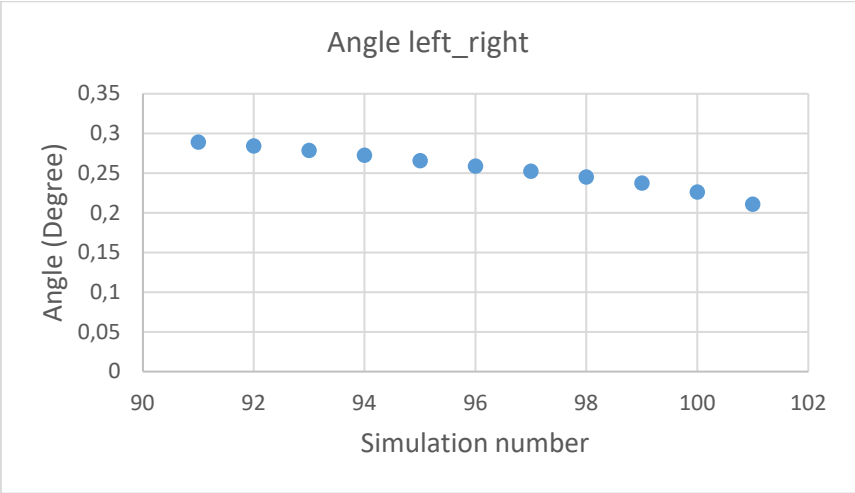

Figure 72 – The effect of force/area on the left right angle for the square tool.

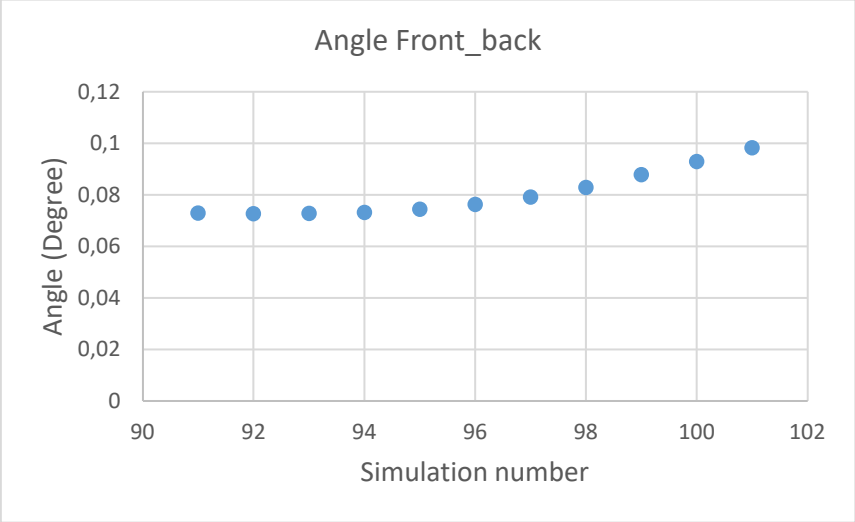

Figure 73 - The effect of force/area on the front back angle for the square tool.

Table 22 – Tool with and depth value for the respective simulations number in Figure 74 and Figure 75.

Simulation Number	12 Tool dimensions	
	Tool Width [$m\ m$]	Tool depth [$m\ m$]
102	0.1	0.1
103	0.12	0.12
104	0.14	0.14
105	0.16	0.16
106	0.18	0.18
107	0.2	0.2
108	0.22	0.22
109	0.24	0.24
110	0.26	0.26

Simulation Number	13 Tool Width [$m\ m$]	14 tool depth [$m\ m$]
111	0.28	0.28
112	0.3	0.3

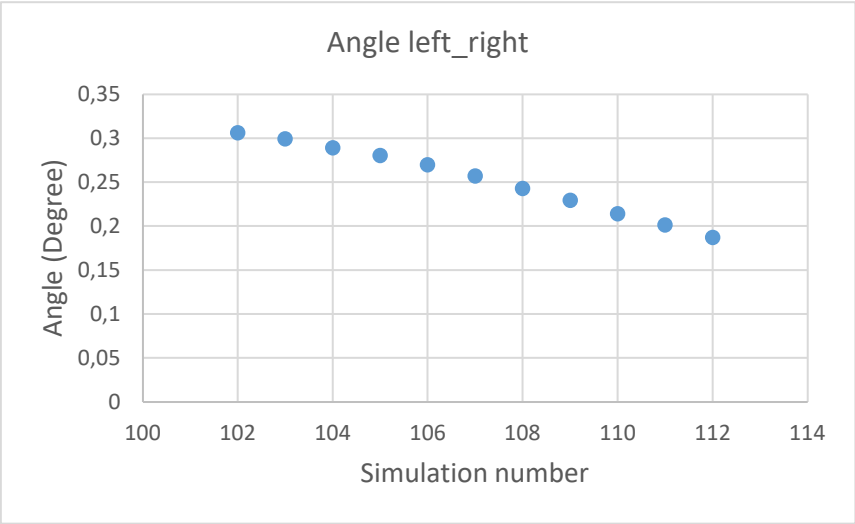

Figure 74 – The effect of dimensions on the left right angle for the square tool.

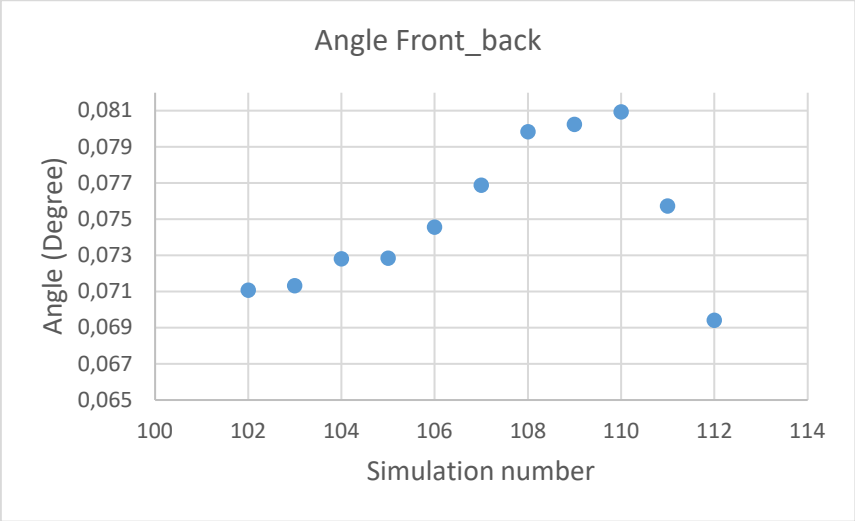

Figure 75 - The effect of dimensions on the front back angle for the square tool.

5.1.4 The robust 3D simulation for the conical geometry

For the conical geometry, the parameters 3, 4 and 7 to 9 are noise variables and their response of them are similar to the square, as it can be compared the Figure 66 and Figure 67 with Figure 76 and Figure 77. The meaning of the numbers of Figure 76 and Figure 77 is represented in Table 23. The noise variables that increase the left right and front back angle are the friction (3) and the Anisotropies (9). The parameters that decrease both angles are material thickness (4) and Young's Modulus (8). The behaviour of the Yield stress (7) and the Angle/area (10) in left right and the front back are the

reverse. Angle/area (10) it has a different output, the angle front back between the simulations 78 to 82 decreases and after those it starts to increase.

Table 23 - Parameters and respective indexes in Figure 76 and Figure 77.

Parameter	Number
Friction	3
Material Thickness	4
Material Height	5
Material Depth	6
Yield stress	7
Young's (E-)Modulus	8
Anisotropies	9
Angle/area	10
Force/area	11
Tool dimensions (radius)	12

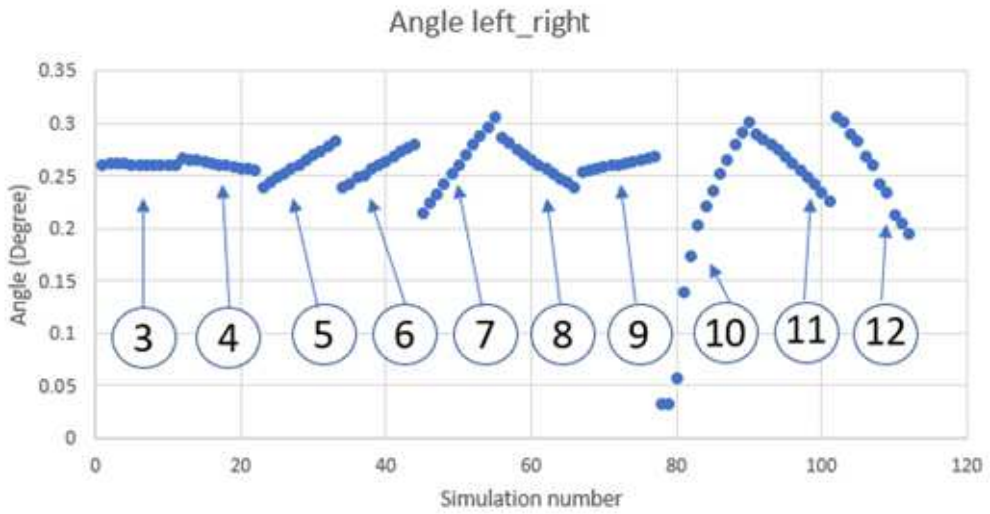

Figure 76 - Left right angle for the conical tool.

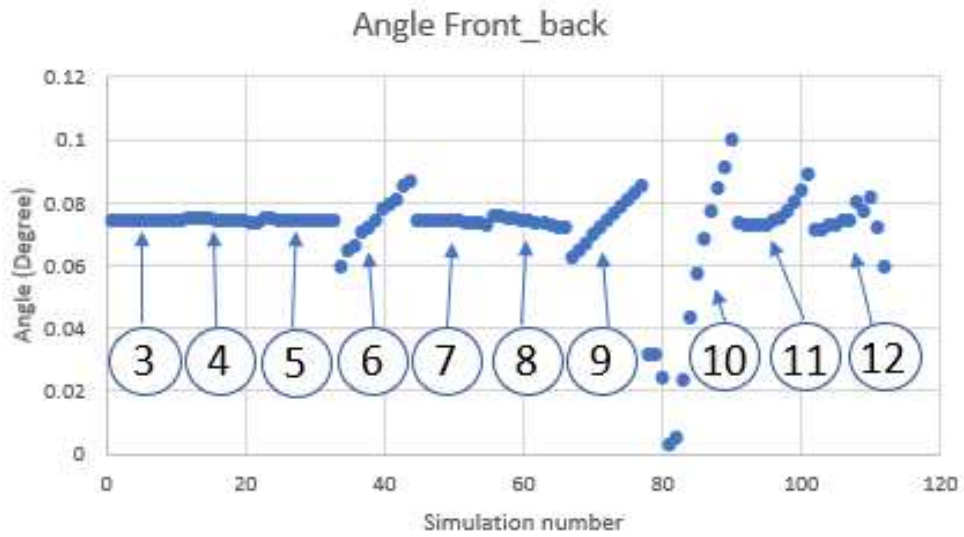

Figure 77 - Front back angle for the conical tool.

The design variables are the material height (5), the material depth (6), the Force/area (11) and the Tool dimension (12). In Table 24,Table 25, Table 26 and Table 28 is represented the index of the number of simulations and their parameter values are represented in Figure 78 and Figure 79, Figure 80 and 80, Figure 82 and Figure 83 and finally Figure 84 and Figure 85, respectively. The increasing on the material height (5) and material depth (6) results on the increase of the left right angle as it can be shown in Figure 78 and Figure 80. The material height (5), due to the "jumps", it was not possible to get the response behaviour for the front back angle as represented in Figure 79. Increasing the material depth (6) results on the increase of the angle, as shown in Figure 81.

Table 24 – Material height value for the respective simulations number in Figure 78 and Figure 79.

Simulation Number	**5 Material height** $[mm]$
23	0.35
24	0.355
25	0.36
26	0.365
27	0.37
28	0.375
29	0.38
30	0.385
31	0.39
32	0.395
33	0.4

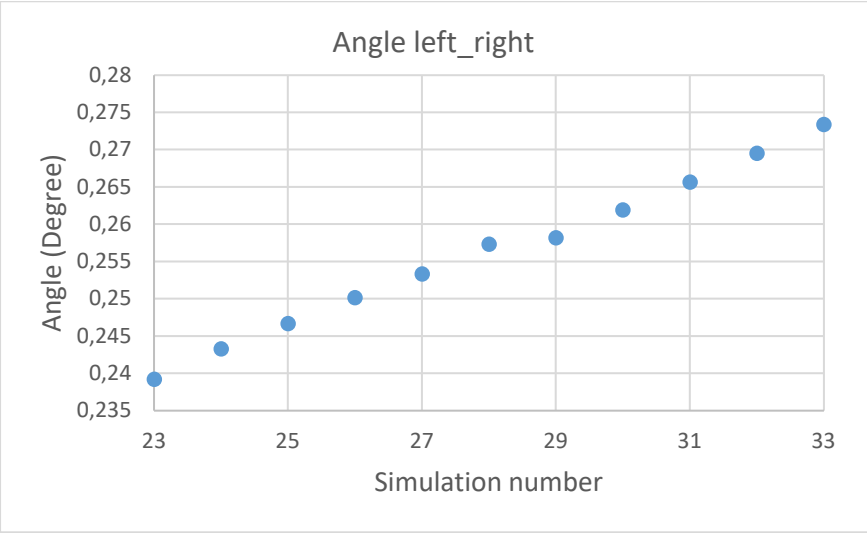

Figure 78 – The effect of material height on the left right angle for the conical tool.

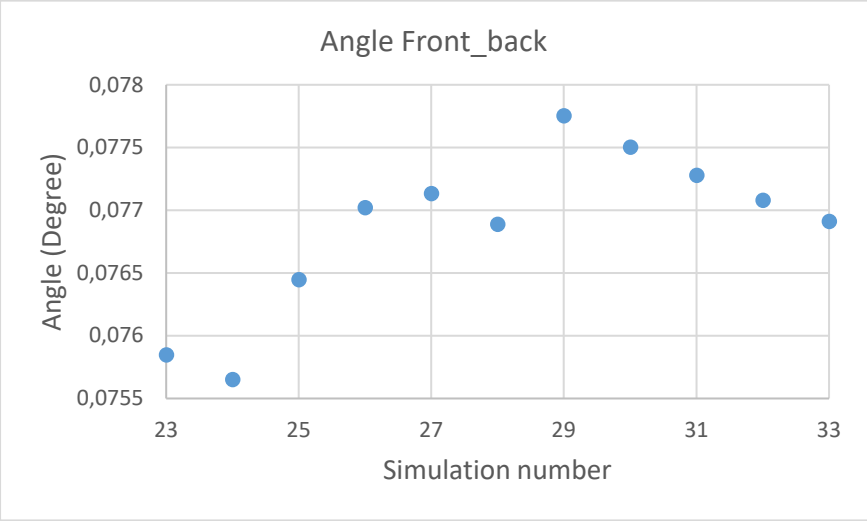

Figure 79 - The effect of material height on the front back angle for the conical tool.

Table 25 – Material depth value for the respective simulations number in Figure 80 and Figure 81.

Simulation Number	6 Material depth [mm]
34	0.35
35	0.355
36	0.36
37	0.365
38	0.37
39	0.375
40	0.38
41	0.385
42	0.39

Simulation Number	6 Material depth [$m\ m$]
43	0.395
44	0.4

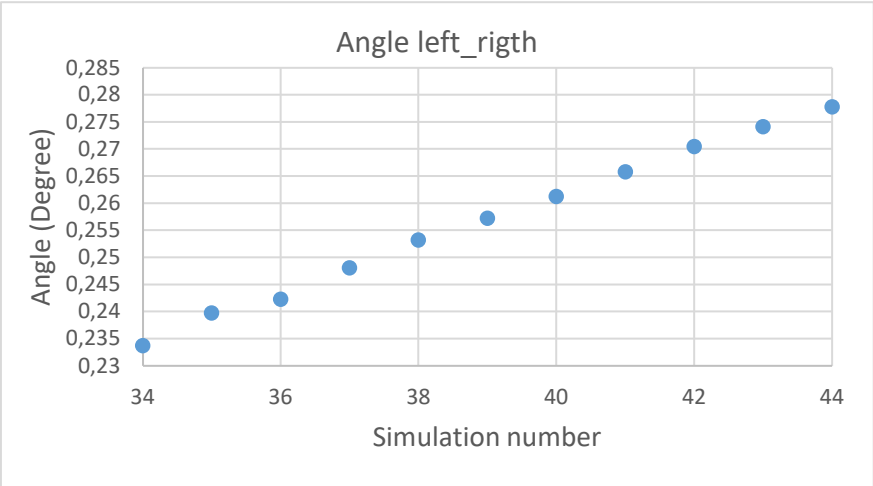

Figure 80 - The effect of material depth on the left right angle for the conical tool.

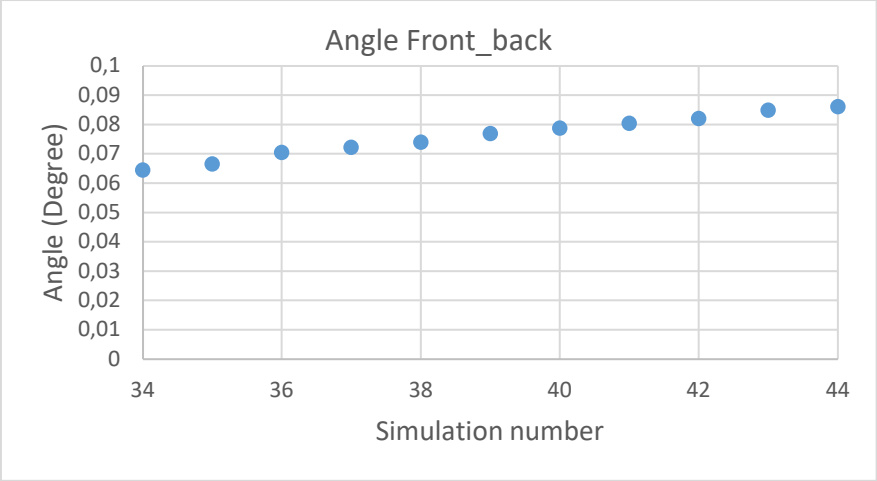

Figure 81 - The effect of material depth on the front back angle for the conical tool.

The Force/area parameter decreases the left right angle, as Figure 82 shows, but the front back angle increases as can be seen in Figure 83. Increasing the tool dimension (radius) (12) decreases the left right angle as shown in Figure 84. As already discussed above, the conical and the square geometries have similar behaviours, and the front back is no exception as it increases until the simulation number 110 (tool radius of 0.1467 mm) and then decreases as shown in Figure 85.

Table 26 - Force/are value for the respective simulations number Figure 82 and Figure 83.

Simulation Number	11 Force/area $[N/mm^2]$
91	500
92	562.5
93	625
94	687.5
95	750
96	812.5
97	875
98	937.5
99	1000
100	1062.5
101	1125

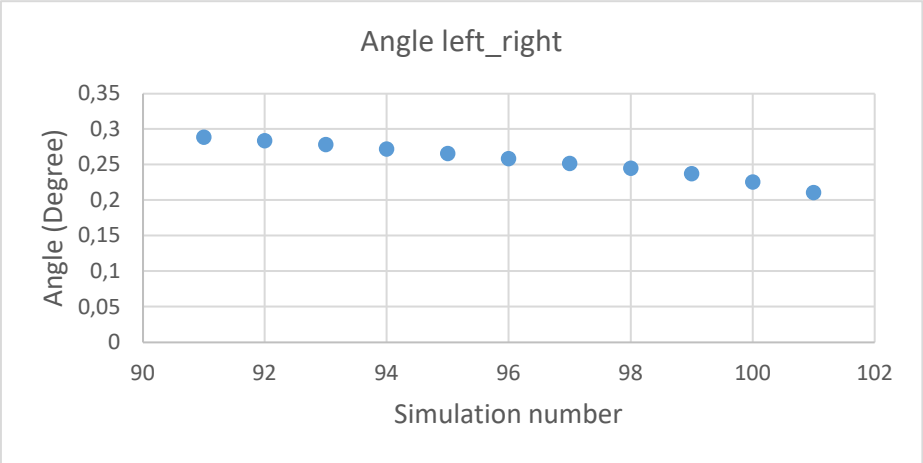

Figure 82 - The effect of force/area on the left right angle for the conical tool.

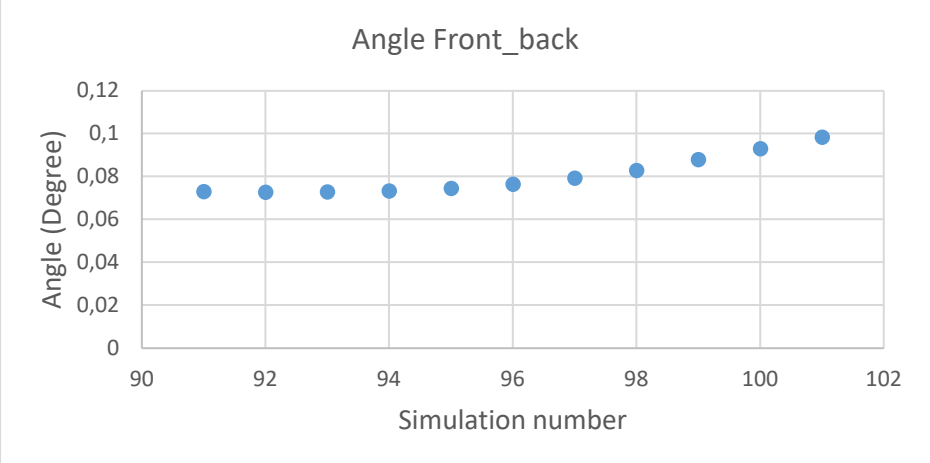

Figure 83 - The effect of force/area on the front back angle for the conical tool.

Table 27 – Tool Dimensions (radii) value for the respective simulations number in Figure 84 and Figure 85 .

Simulation Number	12 Tool Dimensions (Radius) [$m\ m$]
102	0.0564
103	0.0677
104	0.079
105	0.0903
106	0.1016
107	0.1128
108	0.1241
109	0.1354
110	0.1467
111	0.158
112	0.1693

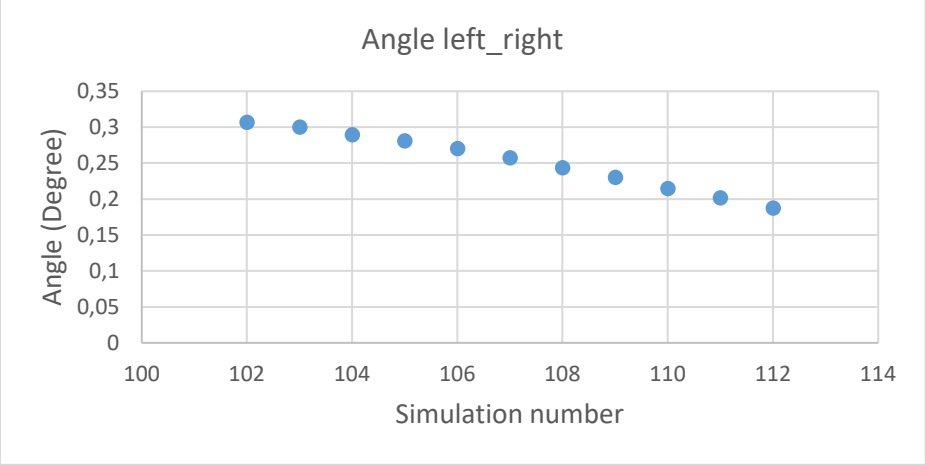

Figure 84 - The effect of tool dimensions on the left right for the conical tool.

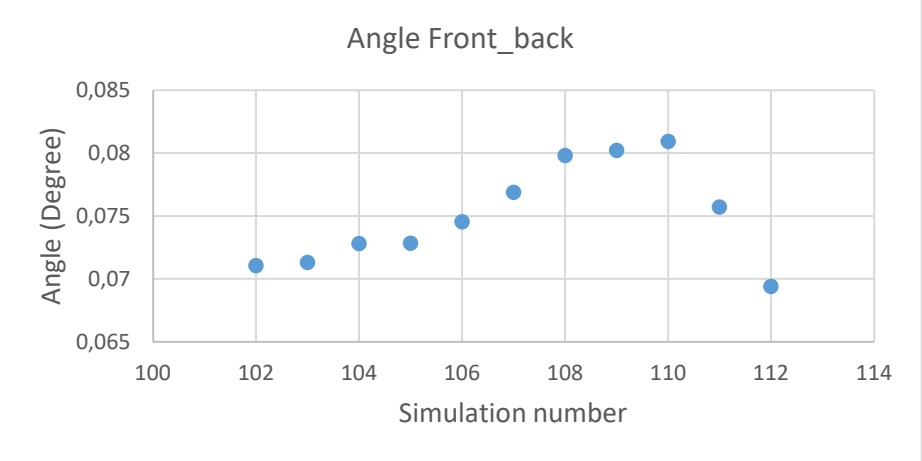

Figure 85 - The effect of tool dimensions on the front back for the conical tool.

5.1.5 The robust 3D simulation for the cylindrical geometry

The cylindrical geometry has an identical behaviour as the conical and square geometries, as shown in comparison with the Figure 66, Figure 67 to Figure 76, Figure 77 to Figure 86, Figure 87. The meaning of the numbers of Figure 86 and Figure 87 is represented in Table 28

Table 28 - Parameters and respective indexes in Figure 86 and Figure 87.

Parameter	Number
Friction	3
Material Thickness	4
Material Height	5
Material Depth	6
Yield stress	7
Young's (E-)Modulus	8
Anisotropies	9
Angle/area	10
Force/area	11
Tool Radius	12
Tool length	13

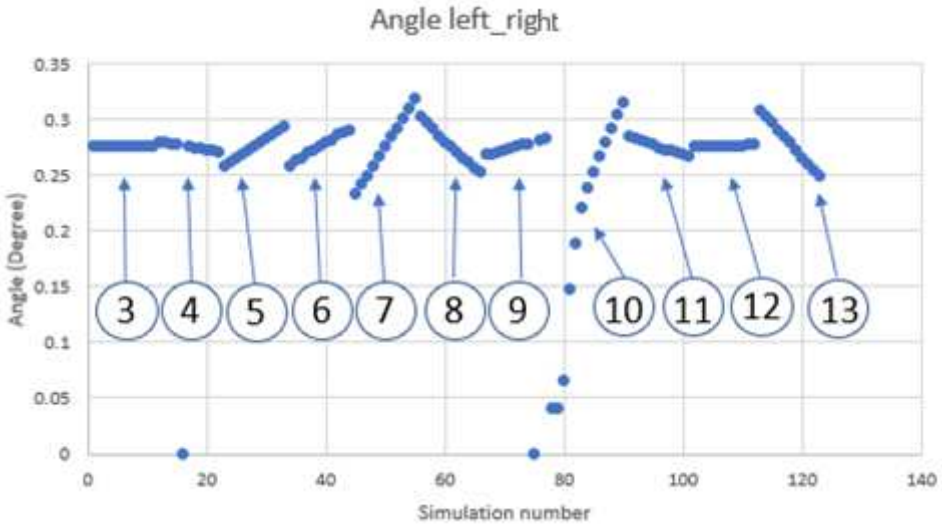

Figure 86 - Left right angle for the cylindrical tool.

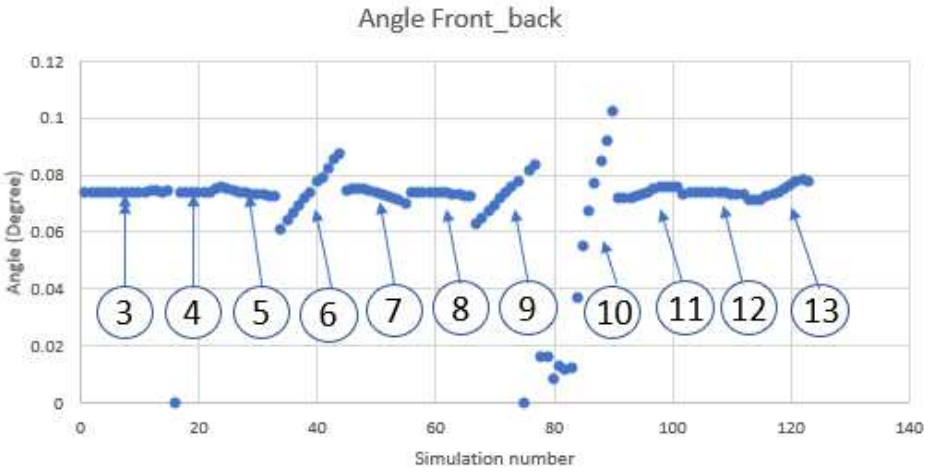

Figure 87 - Front back angle for the cylindrical tool.

The noise variables have similar behaviour as well. These variables are not controllable, so the focus will be on the variables that can be controlled: the material height (5), material depth (6) the force/area (11), the Tool radius (12) and tool depth (13). The variable values, according to simulations number, are in Table 28, Table 29, Table 30, Table 31, Table 32 and Table 33.

The result is not as smooth as the conical and the square geometries, having more "jumps" on the Force/area (11), the tool radius (12) and tool depth (13).

The material height (5) and material depth (6) increases the left right angle, as it can be seen in Figure 88 and Figure 90. For the front back angle the material height (5) and material depth (6) have reverse behaviours on the output angle, increasing the material height (5) decreases the front back angle as the other parameter increases, this is seen on Figure 89 and Figure 91.

Table 29 – Material height values for the respective simulations number in Figure 88 and Figure 89.

Simulation Number	**5 Material height** $[mm]$
23	0.35
24	0.355
25	0.36
26	0.365
27	0.37
28	0.375
29	0.38
30	0.385
31	0.39
32	0.395
33	0.4

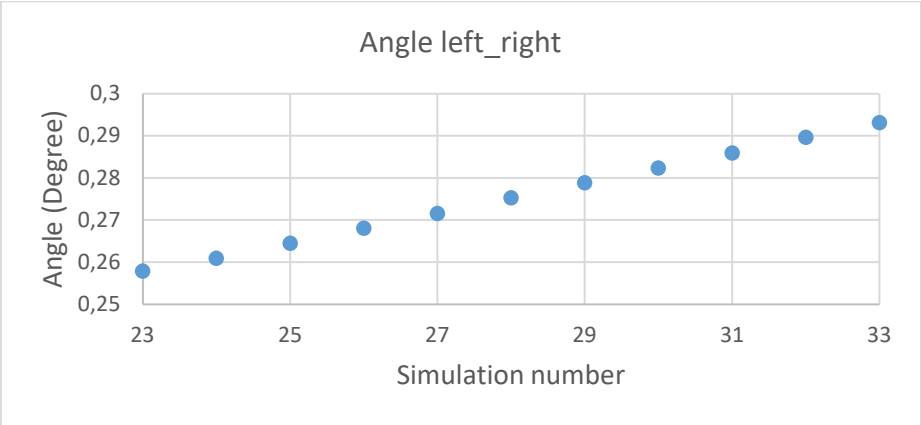

Figure 88 - The effect of material height on left right angle for the cylindrical tool.

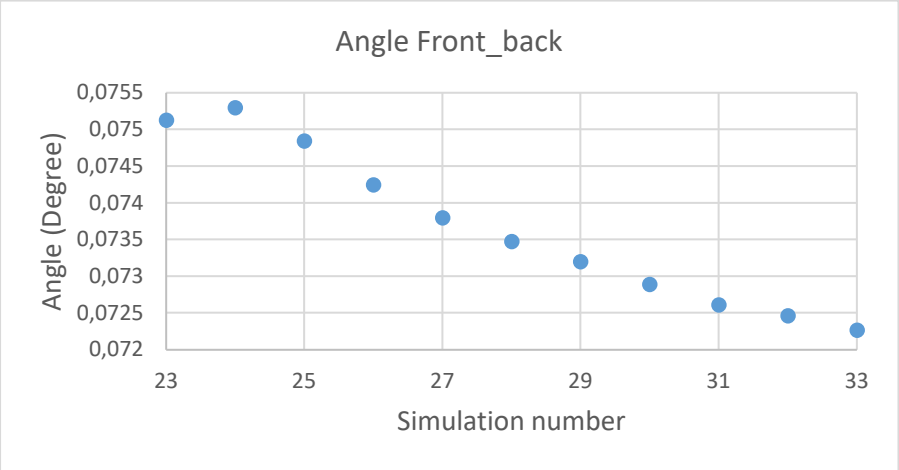

Figure 89 - The effect of material height on left right angle for the cylindrical tool.

Table 30 – Material depth values for the respective simulations number in Figure 90 and Figure 91.

Simulation Number	6 Material depth [mm]
34	0.35
35	0.355
36	0.36
37	0.365
38	0.37
39	0.375
40	0.38
41	0.385
42	0.39
43	0.395
44	0.4

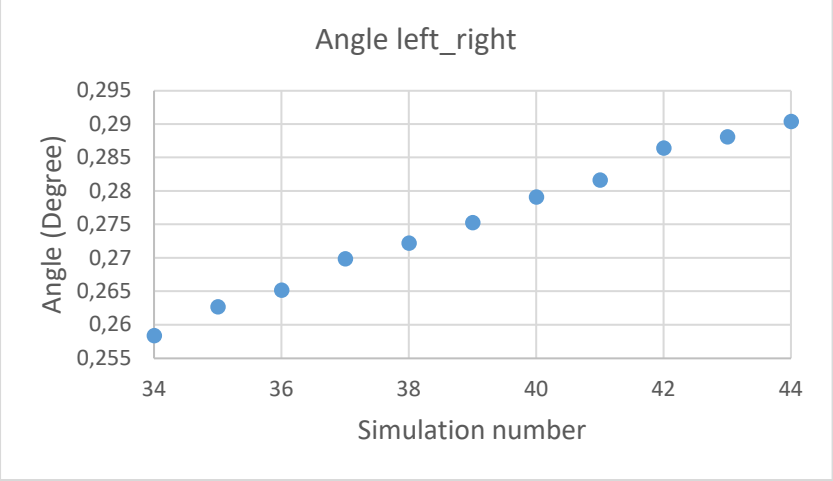

Figure 90 - The effect of material depth on left right angle for the cylindrical tool.

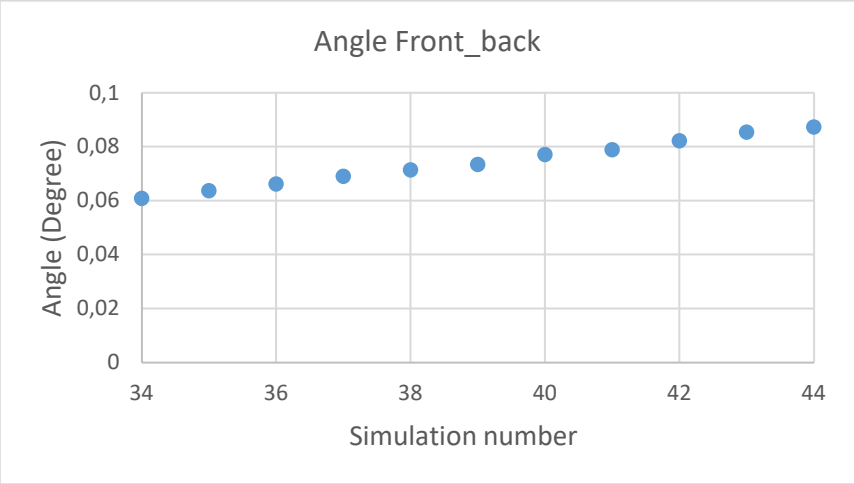

Figure 91 - The effect of material depth on front back angle for the cylindrical tool.

The Force/area (11) influences the left right angle by decreasing it when its value increases almost with a linear response as it can be seen in Figure 92. On the contrary, the front back angle increases when increasing the Force/area (11) and does not have a linear response as it can be seen in Figure 93. When the Tool radius (12) increases, the left right angle increases as can be seen in Figure 94, and as for the behaviour of the front back angle, it increases until simulation 109 and then drops, but has some jumps in the response angle. This response has some jumps as can be seen in Figure 93, Figure 94 and Figure 95. The tool radius and length has an almost no effect on the front back angle, as Figure 95 and Figure 97 shows. The tool length (13) influences the left right angle by decreasing it when its value increases in an almost linear response as shown in Figure 96. On the opposite, the front back angle increases when increasing the tool length (13) and does not have a linear response as can be seen in Figure 97. The meaning of the numbers of the Figure 92 and Figure 93 is represented in the Table 31, for the Figure 94 and Figure 95 is represented in Table 32, for the Figure 96 and Figure 97 is represented in Table 33.

Table 31 - Force/are values for the respective simulations number in Figure 92 and Figure 93.

Simulation Number	11 Force/length $[N/mm^2]$
91	53.33
92	55.997
93	58.664
94	61.331
95	63.998
96	66.665
97	69.332
98	71.999
99	74.666
100	77.333
101	80

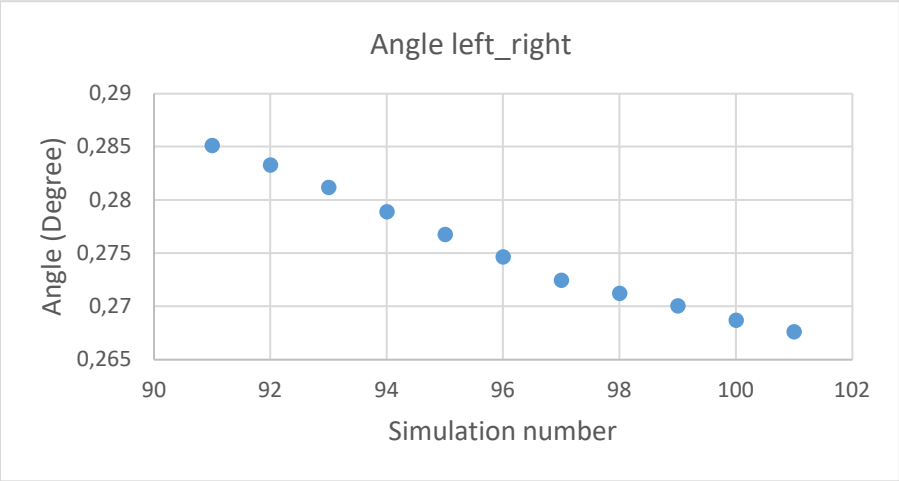

Figure 92 - The effect of force/area on left right angle for the cylindrical tool.

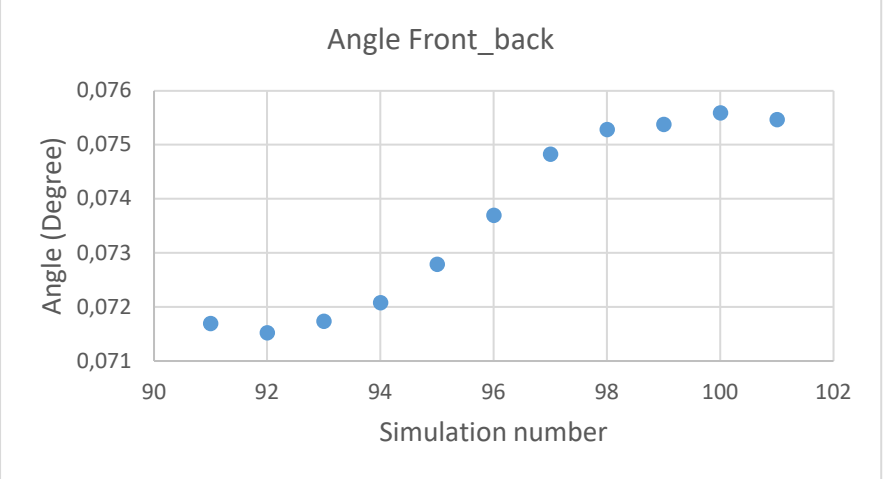

Figure 93 - The effect of force/area on front back angle for the cylindrical tool.

Table 32 – Tool radius values for the respective simulations number in Figure 93 and Figure 94.

Simulation Number	12 Tool Radius [mm]
102	0.185
103	0.2665
104	0.348
105	0.4295
106	0.511
107	0.5925
108	0.674
109	0.7555
110	0.837
111	0.9185
112	1

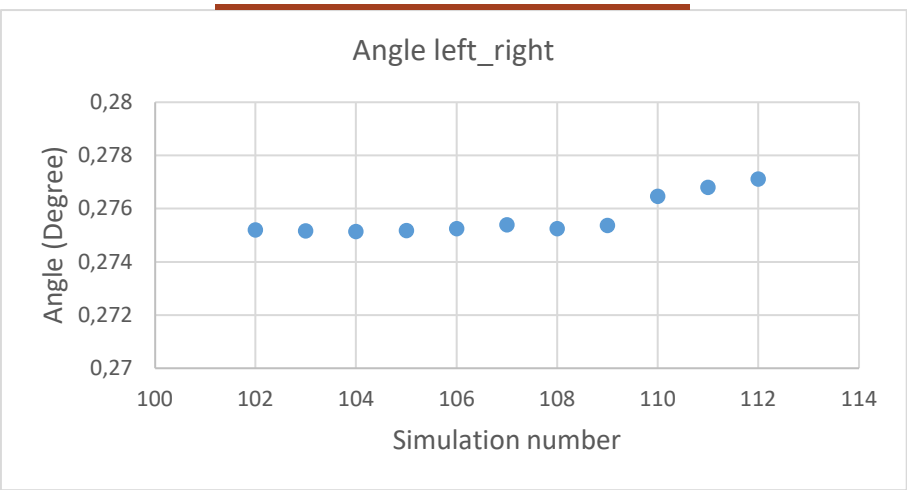

Figure 94 - The effect of tool radius on left right angle for the cylindrical tool.

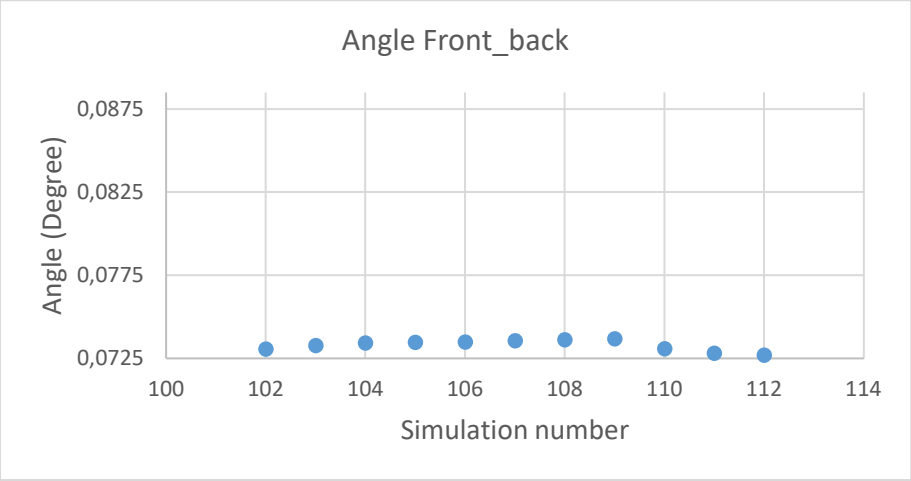

Figure 95 - The effect of tool radius on front back angle for the cylindrical tool.

Table 33 – Tool length values for the respective simulations number in the Figure 96 and Figure 97.

Simulation Number	13 tool length [$m\ m$]
113	0.1
114	0.1275
115	0.155
116	0.1825
117	0.21
118	0.2375
119	0.265
120	0.2925
121	0.32
122	0.3475
123	0.375

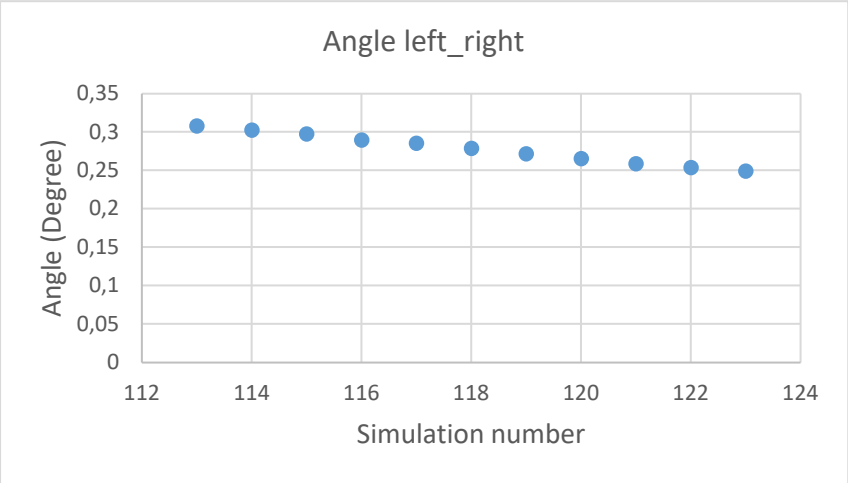

Figure 96 - The effect of tool length on left right angle for the cylindrical tool.

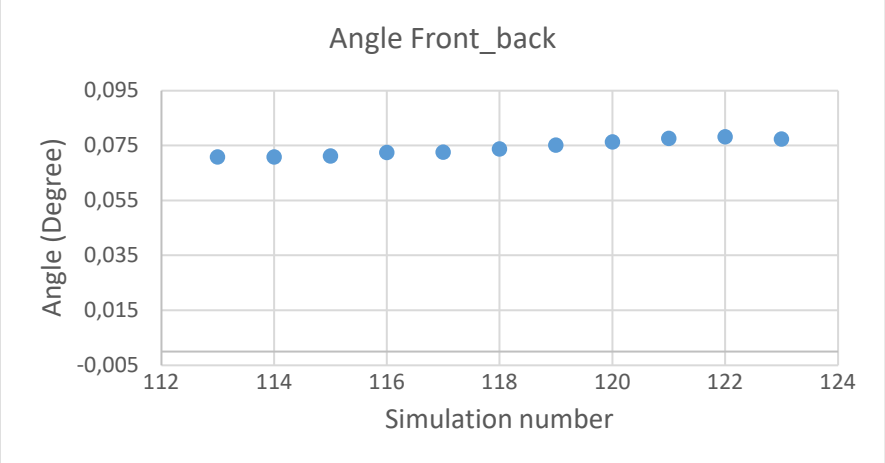

Figure 97 - The effect of tool length on front back angle for the cylindrical tool.

5.1.6 The robust calculation ready to DACE

The first mesh used was 20x20x20 elements on this mesh was made a study to see if the calculation is robust for DACE. For this study was used the 10 step method, that analysed the output of the simulation on variating the same variables 10 times between the range chosen. This variables show some “jumps” in the calculations as can be seen some examples in Figure 75 (square), Figure 85 (conical). The jump in the calculations can be due to not being refined enough (the calculation makes an average of the distance between the nodes), or it might be due to the line of the nodes being in contact to the tool, and in this case, if the geometry changes the same node might not be in contact. To reduce and in some cases eliminate these jumps, a new refined geometry mesh is analysed.

The new mesh has a square geometry, and the number of elements is 37x37x30. With this taken into account, the output of the simulation can be seen in Figure 98 (square), Figure 99 (conical). By analysing this data, it is possible to see the reduction of the “jumps”, although the cylindrical still maintains some of these “jumps”. Remeshing the mesh again will double the simulation time, and as the number of “jumps” has decreased, the relationship between the mesh density and computer cost needed to be taken into consideration. This improvement shows that with the refined elements the FEM calculation is much more suitable for the DACE analysis.

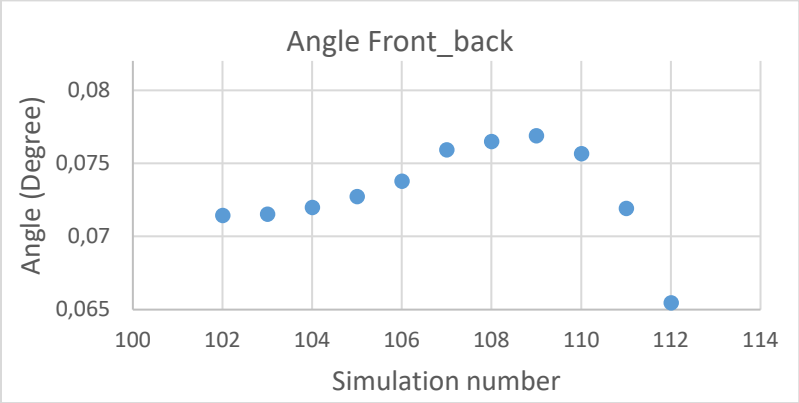

Figure 98 - The effect of tool dimensions on front back angle for the square tool with the refine mesh.

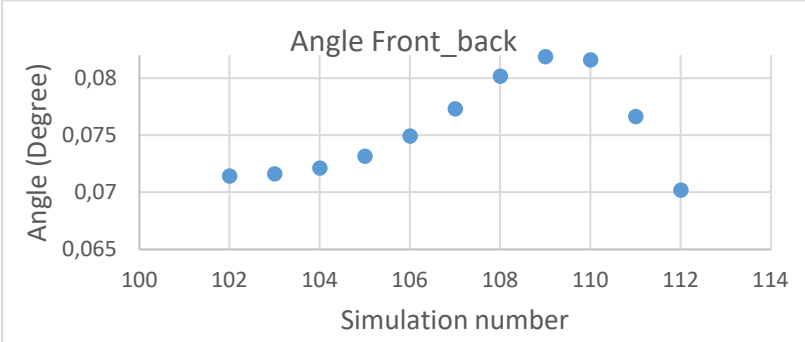

Figure 99 - The effect of tool dimensions on front back angle for the conical tool with the refine mesh.

5.2 Practical test *vs* simulation

Results of the practical tests are shown in Table 34 and in Figure 100. This shows the effect of the pre-bending and the waffling technique. As the results show in Table 34 by sampling number 1.1 to 1.4, it is possible acknowledge that when the material has no plastic deformation the increasing of waffling load will increase the outcome angle, this validates the knowledge by the previous simulations. This table also shows the higher the plastic deformation as the samples 4.1 to 4.4 the higher the waffling load effects the output angle. In Figure 101, Figure 102, Figure 103 and Figure 104. It is possible to see the impact ("indents") of the waffling on the surface. This means that here it actually happens what is expected, increasing the waffling load will result in higher plastic deformation on the contact area, creating bigger indents.

Table 34 - Result of the practical test.

Sample number	Pre-bending [mm]	After waffling measured contact probe [mm]	After waffling measured by Laser [mm]	Pre-bending [$Degrees$]	After waffling measured by Taster [$Degrees$]	After waffling measured by laser [$Degrees$]
1.1	0.5	0.62	0.438	1.9082	2.3672	1.6742
1.2	0.6	0.87	0.672	2.2952	3.3213	2.5653
1.3	0.6	1.18	1.018	2.2952	4.5095	3.8884
1.4	0.65	1.53	1.393	2.4842	5.8506	5.3285
2.2	1.1	0.98	0.823	0.98	3.7444	3.1503
2.3	1.12	1.28	1.110	1.28	4.8965	4.2394
2.4	1.14	0.94	0.849	0.94	3.5914	3.2403
3.1	3.25	1.82	1.650	1.82	6.9577	6.3096
3.2	2.7	1.86	1.644	1.86	7.1107	6.2826
3.3	3.09	1.75	1.640	1.75	6.6877	6.2736
3.4	3.25	1.87	1.793	1.87	7.1557	6.8587
4.1	5.44	2.32	2.174	2.32	8.8839	8.3168
4.2	5.4	2.16	1.988	2.16	8.2628	7.6058
4.3	5.7	2.21	2.032	2.21	8.4608	7.7768
4.4	5.82	2.05	1.935	2.05	7.8398	7.3987

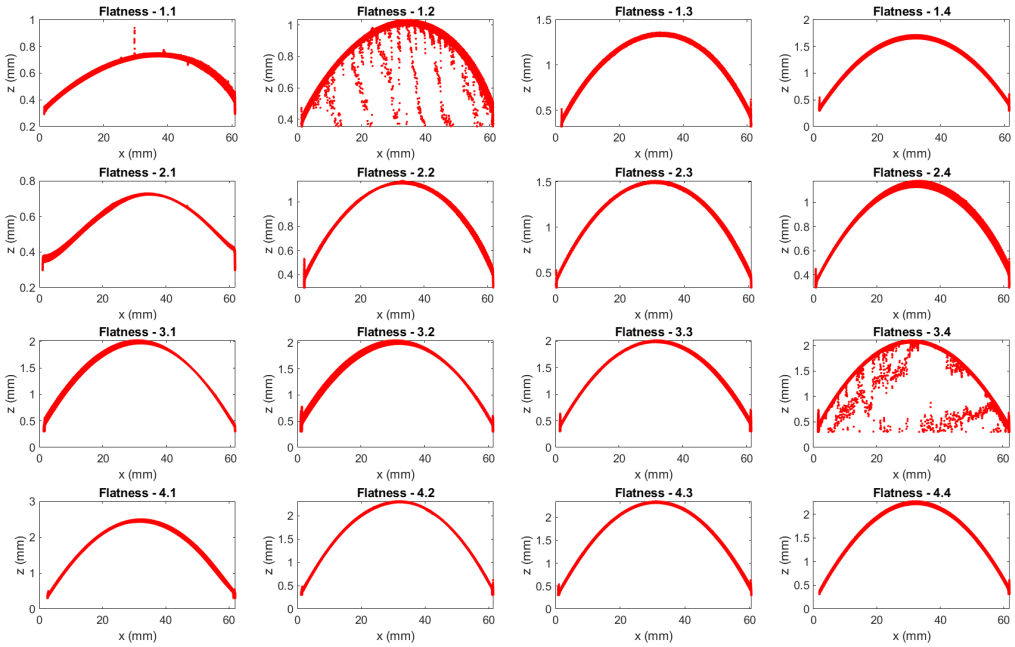

Figure 100 - Height profile measurement after waffling test by automatic 3D Keyence measurement.

Figure 101 - Microscopic view of sample number 1.1.

Figure 102 - Microscopic view of sample number 1.2..

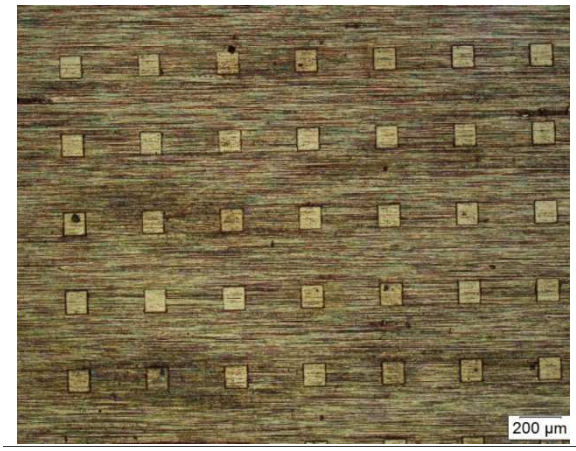

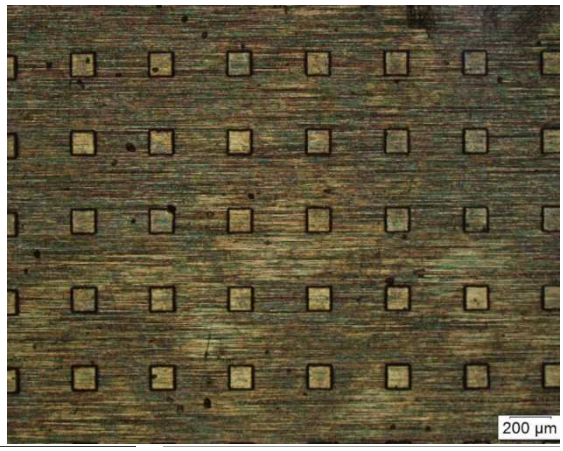

Figure 103 - Microscopic view of sample number 1.3.

Figure 104 - Microscopic view of sample number 1.4.

The comparison between the practical test and the FE simulation is shown in Figure 105, Figure 106, Figure 107 and Figure 108.

These figures show the difference between the results of the simulation and the practical test. The output angle of the simulation is inferior than the practical test, so the springback is lower in the numerical than in the practical test. The deviation between the springback of the numerical model and the practical experiment can be caused by many different reasons: inadequate properties of the model, different behaviour of the material, deviations in the nominal geometry, boundary conditions in the model, or mesh sensitivity [16, 74-76]. In this case the material properties used data based on Philips's database, so this should not be a problem, but the Bauschinger effect is not in the model. It is difficult to control the distributed pressure and the friction and they can be different. Other difficulty resides on the change of material properties like Young's modulus [16, 74]. The difference on the results can also be because of the neglecting of the effect on tool deformation [16, 74]. In the model, the waffling tool is rigid and cannot deform. Other factors that may have some influence are the mesh, because of the limited number of elements, the Bauschinger effect (reverse load on the material) and the difference changes of the material properties on bending and pre-bending and the rolling process.

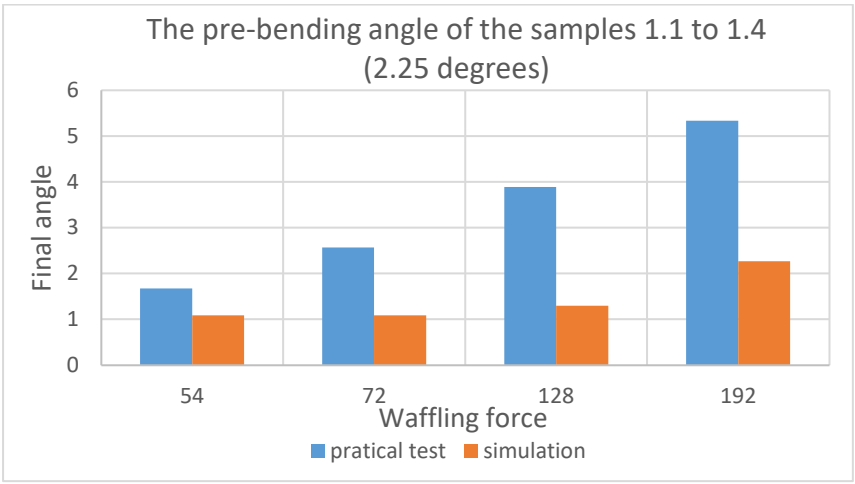

Figure 105 - The comparison between the practical test with the FE simulation for the pre-bending angle of the samples 1.1 to 1.4.

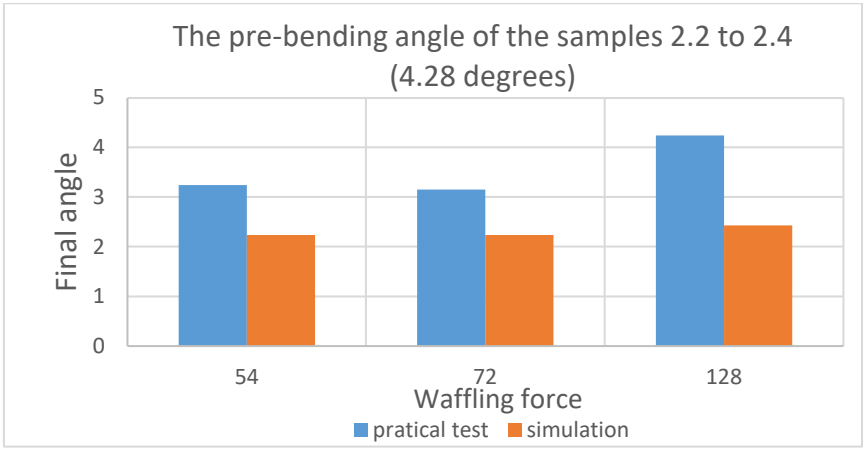

Figure 106 - The comparison between the practical test with the FE simulation for the pre-bending angle of the samples 2.2 to 2.4.

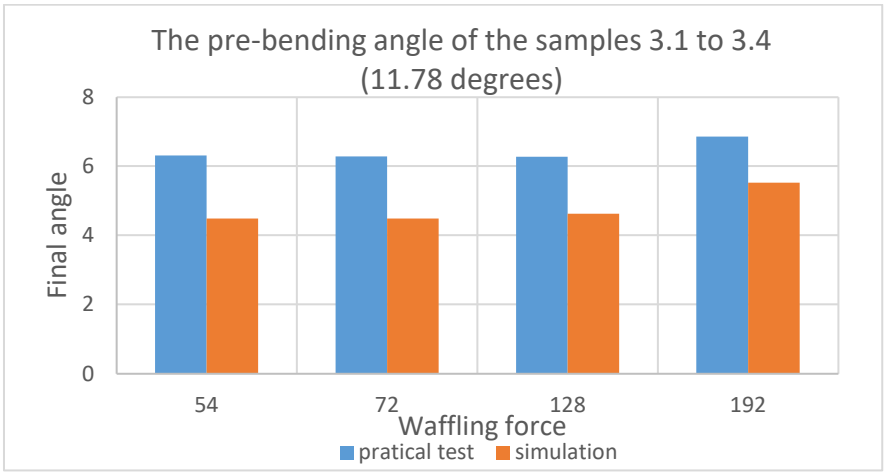

Figure 107 - The comparison between the practical test with the FE simulation for the pre-bending angle of the samples 3.1 to 3.4.

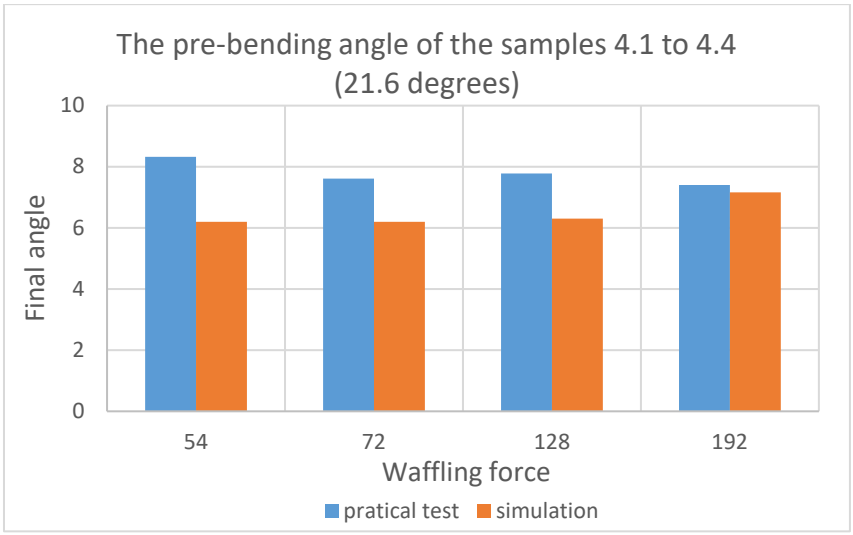

Figure 108 - The comparison between the practical test with the FE simulation for the pre-bending angle of the samples 3.1 to 3.4.

5.3 The Screening

The screening shows the effects that the inputs have on the output by the main effect, as it takes into consideration the noise and the design variables. The Table 35 is show the parameters and their representations in the Pareto Plots figures.

Table 35 - Representation of the parameters in the Pareto Plots.

Parameter	Representation
Friction	μ_{fric}
Material Thickness	t
Material Height	H
Material Depth	D
Yield stress	σ_y
Young's (E-)Modulus	E
Anisotropy	Ani
Angle/area (pre-bending)	α
Force/area	F / a
Tool dimensions (Square)	L
Tool dimensions (conical)	R
Radius (cylindrical)	R
Length (cylindrical)	L
Geometry	GE

5.3.1 The Screening on the square geometry.

The effect of the variables on the left right and the front back angles can be seen in the Pareto plot in Figure 109 and Figure 110. It is possible to see that the inputs have a higher influence on the left right angle than on the front back one, where the input with higher effect in this case is the pre-bending. As the aim of this technique is to find the variables that are critical to the response and the most important angle to analyse is the left right one, the inputs are chosen by the pareto principle for the mentioned angle. The noise variables chosen are the angle/area and the thickness, since these are the ones behind the 80 % line. For the design variables the material height, material depth and tool dimensions are chosen for the same reason as the noise variables, but here it also chosen the force/area, since it is one of the design variables that can be easily changed (in the press), and it can be insignificant in this ANOVA analysis because it could be not linear.

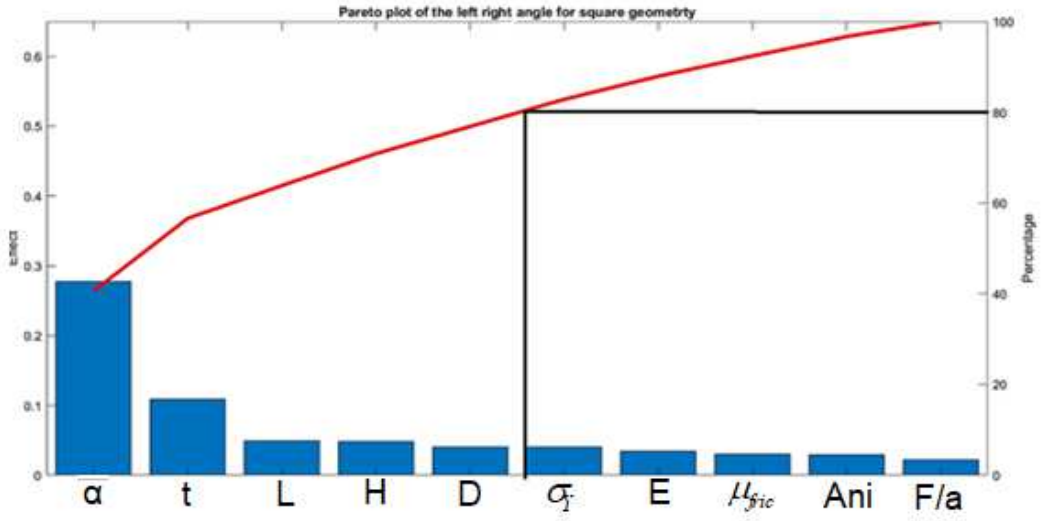

Figure 109 - Pareto plot of the left right angle for the square.

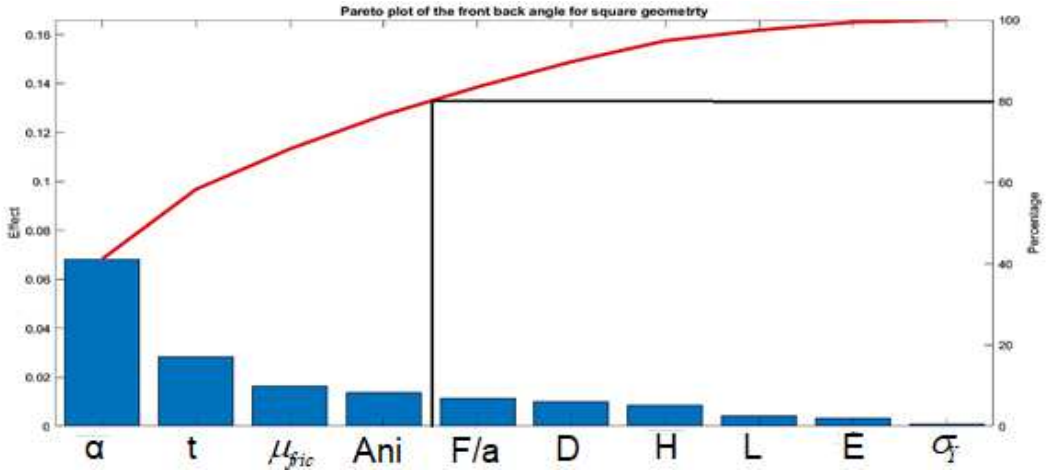

Figure 110 - Pareto plot of the front back angle for the square.

In Figure 111 and Figure 112 it is shown how the variables impact the main effects of the left right and the front back angle. This way the variables that are studied can have either a positive effect or a negative effect, being the ones with a positive effect presenting a positive slope and the ones with a negative effect exhibiting a negative slope.. The focus is on the variables chosen before: the thickness $X2$, the material height $X3$, and material depth $X4$, angle/area $X8$, the force/area $X9$ and the dimensions $X10$. By analysing the Figure 111 it is possible to acknowledge that the thickness, the force/area and the dimensions, when they increase it decreases the angle, but the material height, material depth and angle/area increase the angle. Figure 112 shows that the only input that reduces the angle on this analysis is the thickness, the others increase, so the force/are and the dimensions have the opposite behaviour as the left right angle.

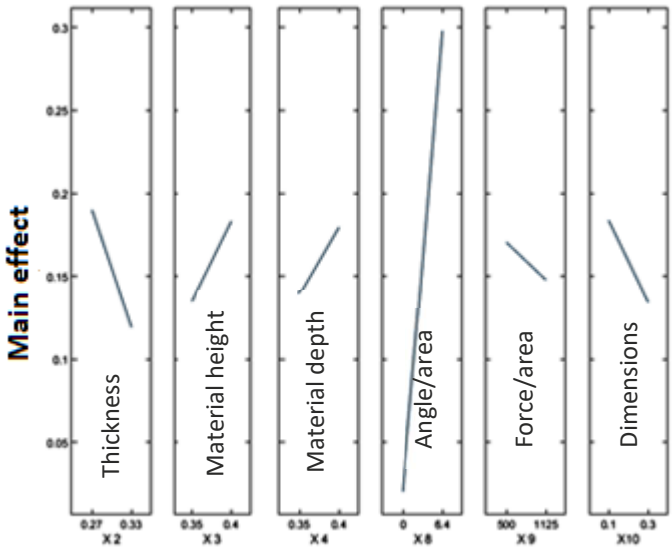

Figure 111 - Main effects of the variables on the left right angle for square.

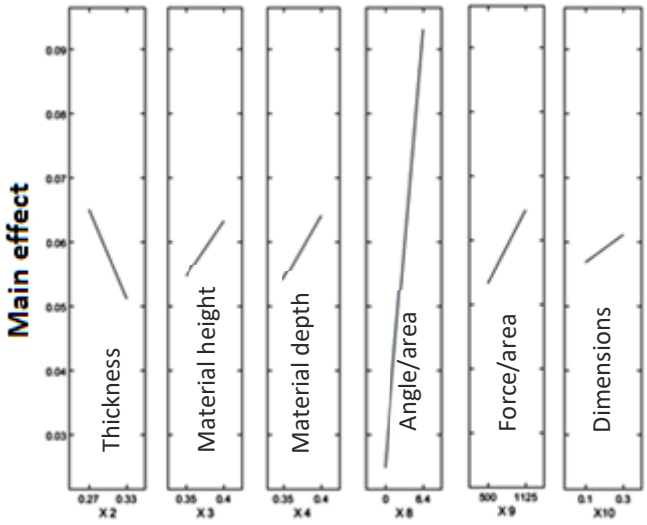

Figure 112 - Main effects of the variables on the front back angle for square.

5.3.2 The Screening on the conical geometry

The screening for the conical geometry is analysed by the effect it has on the variables on the left right and the front back angle by the Pareto plot in Figure 113 and Figure 114. The result of the Pareto plot shows the inputs that have a higher influence on the left right angle than on the front back, which in this case is the pre-bending, very similar to the square geometry. As the objective of this technique is to find the variables that are critical to the response, and the most important angle to analyse is the left right, the inputs are chosen by the pareto principle. The noise variables chosen are the angle/area since these are behind the 80 % line. For the design variables the material depth and the tool dimensions are chosen, for the same reason as the noise variable, but the

force/area is also chosen since it is one of the design variables that can be easily changed and in the front back angle is the second one with the highest effect.

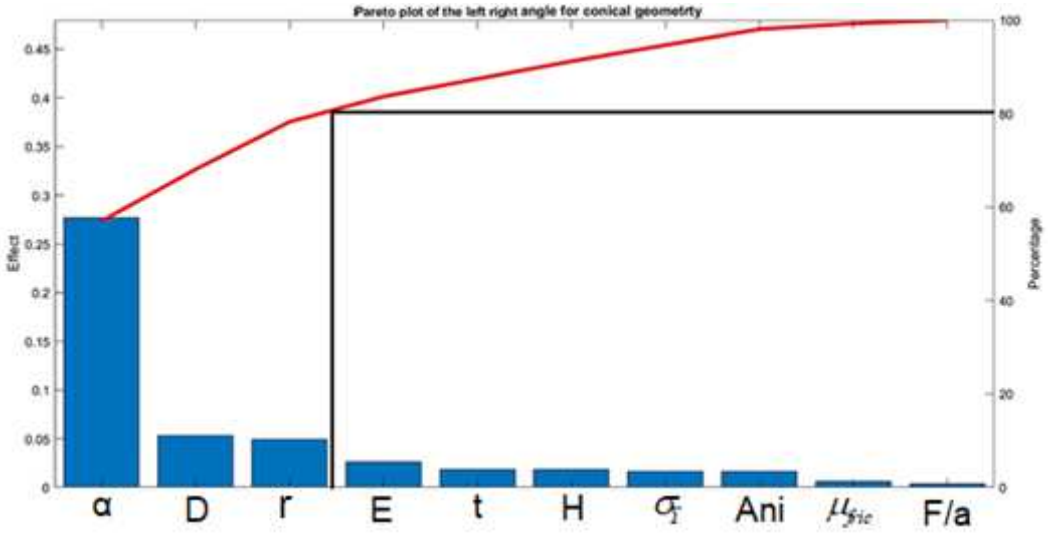

Figure 113 - Pareto plot of the left right angle for the conical.

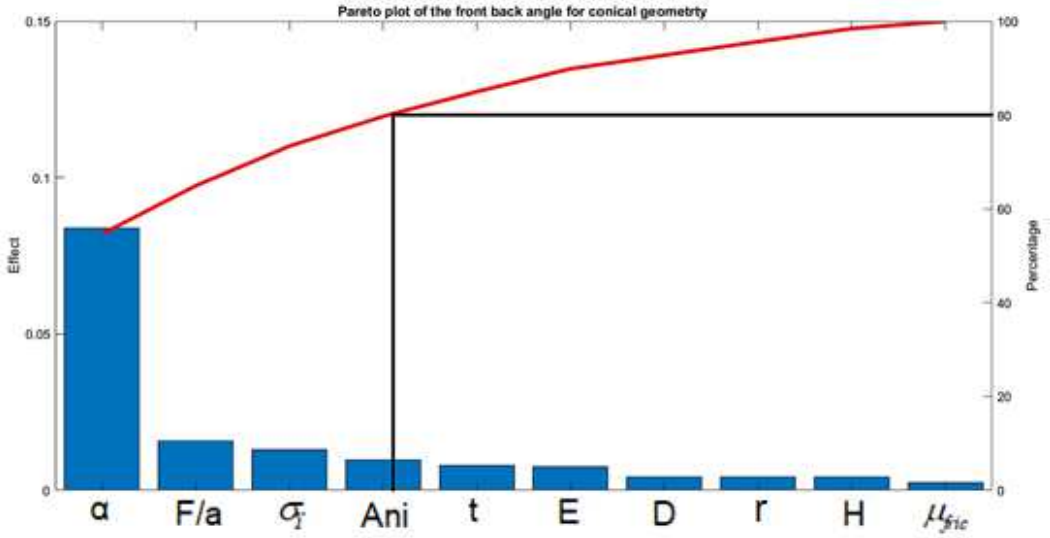

Figure 114 - Pareto plot of the front back angle for the conical.

As it has already been done in the square geometry, here it will also be analysed the effect that the variables have, or in other words, if they increase or decrease the angle. Figure 115 and Figure 116 show the positive or negative effects on the left right and the front back angle. The focus will only be on the variables chosen to be critical: being the material depth $X\,4$, angle/area $X\,8$, the force/area $X\,9$ and the dimensions $X10$. By analysing Figure 115 it is seen that the only parameter that increases the left right angle is the angle/area. Figure 116 show that all the inputs increase the front back angle.

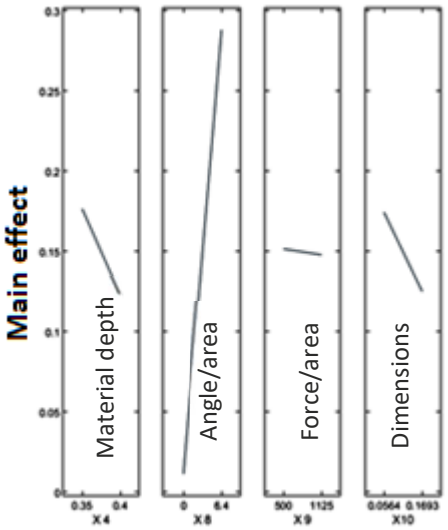

Figure 115 - Main effects of the variables on the left right angle for conical.

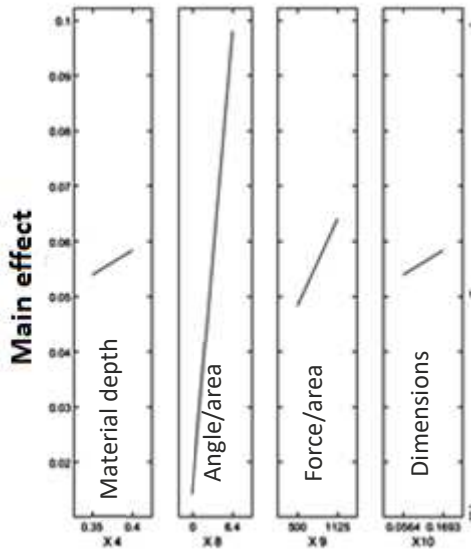

Figure 116 - Main effects of the variables on the front back angle for conical.

5.3.3 The Screening on the cylindrical

The screening in the cylindrical geometry is analysed, as already discussed in the square and conical geometries. The effect the variables have in the left right and the front back angle is presented by the Pareto plot in Figure 117 and Figure 118. The inputs have higher influence on the left right angle than on the front back. The input with the highest effect is the pre-bending, in a very similar way to the geometries discussed above. As the aim of this technique is, once again, to find the variables that are critical to the response and the most important angle to analyse is the left right, the inputs are chosen by the pareto principle. The noise variables chosen were the angle/area, Young's (E) Modulus, and Yield stress because these are the one below the 80 % line. For the design variables the material depth and the length of the tool are chosen based on the same

reasons as the noise variables, but the force/area is also chosen taking into account the same reasons presented on the square geometry and since in the front back angle this parameter is below the 80% line. The Anisotropy is taken into consideration because it is capable of doubling the number of FE simulations and since the influence of the inputs, as already mentioned, is very low in the front back angle and the angle that it is more important is the left right.

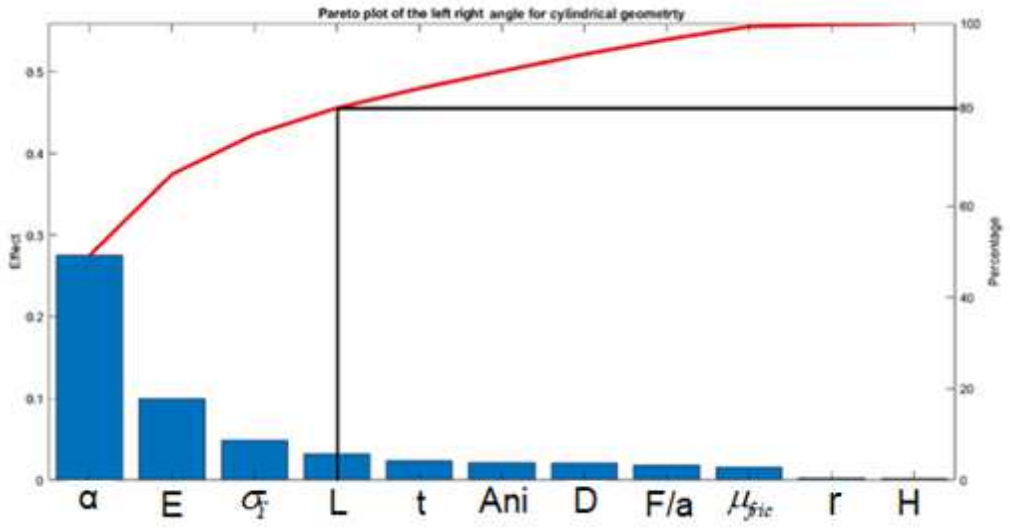

Figure 117 - Pareto plot of the left right angle for the cylindrical.

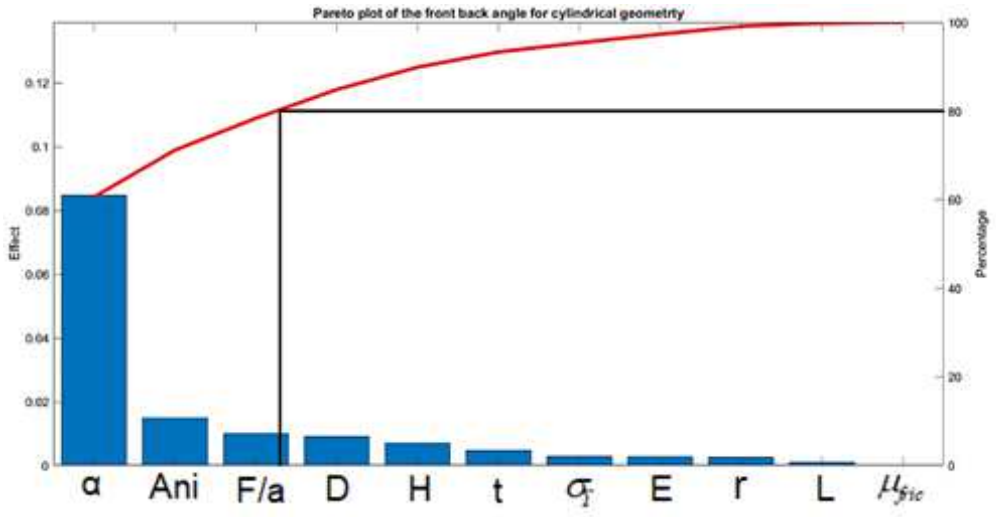

Figure 118 - Pareto plot of the front back angle for the cylindrical.

The effect of the variables on increasing or decreasing the left right and the front back angle is analysed by the main effect represented in Figure 115 and Figure 116 respectively. It will only be focused on the variables chosen to be critical: being Yield stress $X\,5$, Young's (E-) Modulus $X\,6$, angle/area $X\,8$, the force/length $X\,9$ and the tool length $X11$. By analysing Figure 119 it can be seen that the parameters that cause the decrease of the angle are Young's (E-) Modulus and length. The other parameters are the ones responsible for increasing the left right angle. In Figure 120 the length has

a different behaviour, so the only parameter that decreases the front back angle is the Young's (E-)Modulus.

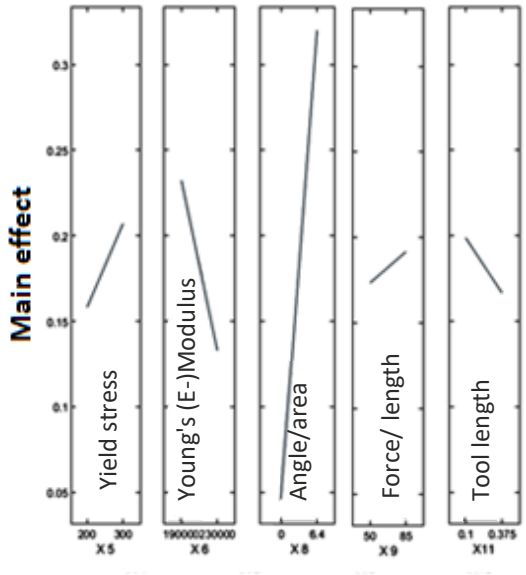

Figure 119 - Main effects of the variables on the left right angle for cylindrical.

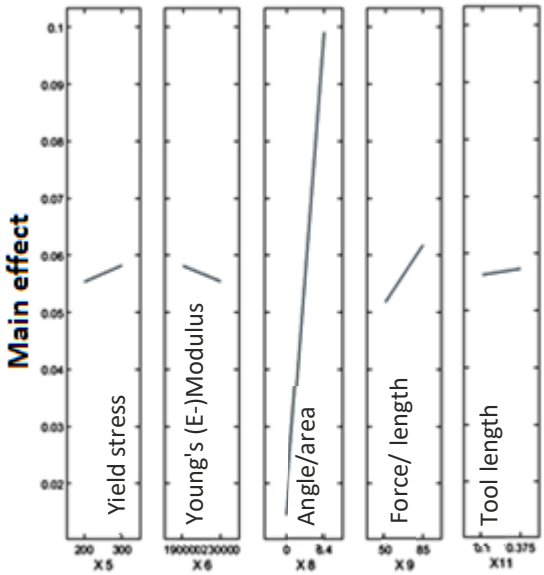

Figure 120 - Main effects of the variables on the front back angle for cylindrical.

5.3.4 The Screening on the square and conical geometry

The screening that was created is used to analyse the impact of the different geometries, for this analysis was only possible to use the conical and square geometry as they have the same contact area.

The effect that the variables have in the left right and the front back angle is presented by the Pareto plot in Figure 121 and Figure 122. The inputs have higher influence on the

left right angle than on the front back. The input with the highest effect is the pre-bending, in a very similar way to the others' analysis of screening. As the objective of this method is, once again, to find the variables that are critical to the response, and the most important angle to analyse is the left right one, the inputs are chosen by the pareto principle. The noise variable chosen is the angle/area, because this is the one below the 80 % line. For the design variables the geometry (GE) material height and the length of the tool are chosen based on the same reasons as the noise variable. This concludes that the geometry is an important parameter to be analysed.

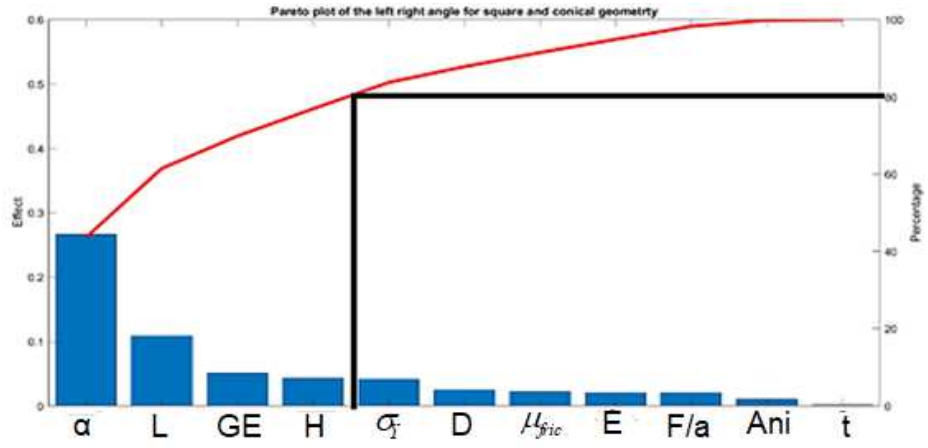

Figure 121 - Pareto plot of the left right angle for the different geometries.

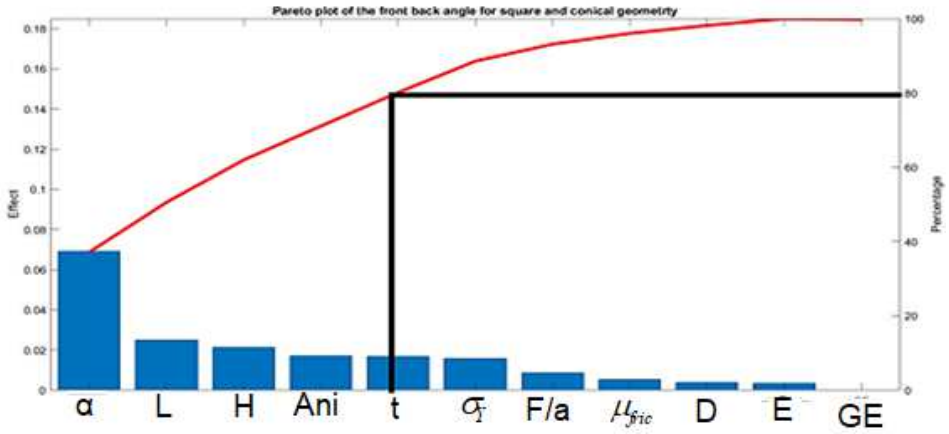

Figure 122 - Pareto plot of the front back angle for the different geometries.

The effect of the variables on increasing or decreasing the left right and the front back angle is analysed by the main effect represented in Figure 123 and Figure 124, respectively. The analysis will only be focused on the variables chosen to be critical these being: different geometries $X1$, material height $X4$, angle/area $X9$, the tool length or radius (depending if it is square or conical, but both have the same contact area) $X11$.

For the different geometries the (-1) represents the square while (1) represents the conical. The square geometry has an inferior left right angle when compared to the conical, so the square creates a higher reduction of the angle, as it can be seen in Figure

123. For the front back angle, changing the geometry has almost no effect, as can be seen in Figure 124. Following these conclusions, the square geometry will be the only one used for the rest of the analysis.

For the material height and angle/area when both are increased, it leads to an increasing of the left right angle and front back angle, as it can be seen in Figure 123 and Figure 124 respectively. For the dimensions of the tool (length or radius) the behaviour is more complex than the others. The -1 and 1 are, respectively the minimal area and maximal area, and these are the same for the different geometries but, as they have different slopes (positive and negative), the mean response creates this complexity, as can be seen in Figure 123 and Figure 124.

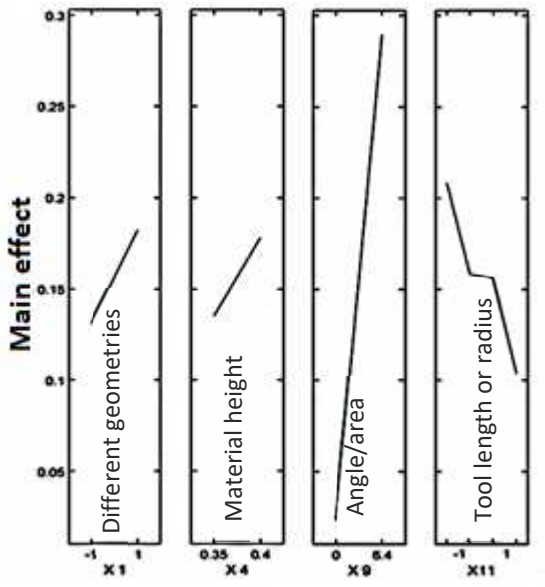

Figure 123 - Main effects of the variables on the left right angle for analysing the geometry.

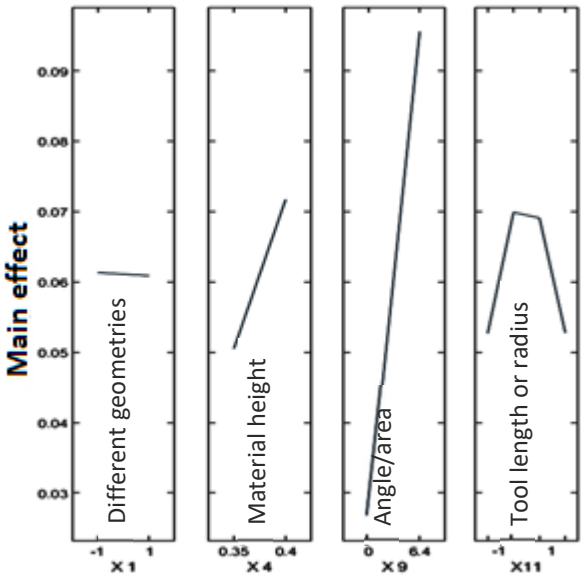

Figure 124 - Main effects of the variables on the front back angle for analysing the geometry.

5.4 Metamodel result

5.4.1 Metamodel validation

The metamodel results contain the validation of the metamodel and the fitted metamodel. In this case, the model used was 64 FFD and 32 LHD. The validation can be seen in Table 36, Table 37 and Table 38, where it is possible to see that in all of them, the differences between the $R^2_{Prediction}$ and $R^2_{Predictionadj.}$ are small. This was expected, as it was made a screening to take only into consideration the parameters that are important. The $RMSE-CV$ has a low value, which means that the difference between the true value and the predicted one is small. Other conclusions that can be drawn from this experience is that the Kriging metamodels have better results than the RSM, and as a consequence, the ones that will be used are the Kriging zero order trend function to left right and the front back angle. The left right angle has a better prediction than the front back angle and the thickness. As the left right angle is more important for this analysis the $R^2_{Prediction}$ of 0.99 and $RMSE-CV$ of 0.01327 are good values. Information about the metamodel validation of Table 36, Table 37 and Table 38 is shown in Appendix 8.4, 8.5 and 8.6.

Table 36- Metamodel validation for FFD plus 32 LHD for the left right angle.

Metamodels	$R^2_{Prediction}$	$R^2_{Predictionadj.}$	$RMSE-CV$
RSM linear	0.8339	0.8219	0.05481
RSM INTERACTION	0.9279	0.9056	0.03612
RSM ELIPTIC	0.8662	0.8454	0.0492
RSM Quadratic	0.9606	0.9435	0.02668
Metamodels	$R^2_{Prediction}$	$R^2_{Predictionadj.}$	$RMSE-CV$
Kriging 0	**0.9903**	**0.9893**	**0.01327**
Kriging 1	0.9863	0.9838	0.01573
Kriging 2	0.9862	0.9772	0.01582
Kriging 2R	0.9852	0.9756	0.01637

Table 37 - Metamodel validation for FFD plus 32 LHD for the front back angle.

Metamodels	$R^2_{Prediction}$	$R^2_{Predictionadj.}$	$RMSE-CV$
RSM linear	0.8379	0.8379	0.01545
RSM INTERACTION	0.925	0.9081	0.01051
RSM ELIPTIC	0.8117	0.7824	0.01665
RSM Quadratic	0.8969	0.8549	0.0122
Kriging 0	**0.9576**	**0.9535**	**0.0079**
Kriging 1	0.9274	0.9138	0.01035
Kriging 2	0.9153	0.86	0.01117

Metamodels	$R^2_{Prediction}$	$R^2_{Predictionadj.}$	$RMSE-CV$
Kriging 2R	0.9129	0.8565	0.01133

Table 38 - Metamodel validation for FFD plus 32 LHD for the thickness.

Metamodels	$R^2_{Prediction}$	$R^2_{Predictionadj.}$	$RMSE-CV$
RSM linear	-0.08697	-0.1655	0.008219
RSM INTERACTION	-0.2892	-0.6873	0.00895
RSM ELIPTIC	0.9524	0.9449	0.001721
RSM Quadratic	0.9505	0.9289	0.001755
Kriging 0	-0.01706	-0.1175	0.007951
Kriging 1	-0.08253	-0.2846	0.008203
Kriging 2	0.9501	0.9178	0.001761
Kriging 2R	**0.9531**	**0.9227**	**0.001707**

To see what the effects of increasing the DOE could randomly do on the accuracy of the prediction it was added 32 LHD, making the model with 64 FFD and 64 LHD. The analysis was made based on a comparison between Table 36, Table 37 and Table 38 with Table 39,

Table 40 and Table 41. The results of $R^2_{Prediction}$ and the $RMSE-CV$ are better for the left right angle, which varies from 0.9903 and 0.01327, respectively to 0.9929 0.0122. For ther front back angle they vary from 0.9576 and 0.0079 to 0.9698 and 0.006409 and as for the thickness they vary from 0.9531 and 0.001707 to 0.9974 and 0.00047 . So it is concluded that this doesn't increase the prediction of the metamodel for both the left right and front back angle by a large margin, although it is considerable in the thickness. The information about metamodel validation of Table 39,

Table 40 and Table 41 are shown on Appendix 8.7, 8.8 and 8.9.

Table 39- Metamodel validation for FFD plus 64 LHD for the left right angle.

Metamodels	$R^2_{Prediction}$	$R^2_{Predictionadj.}$	$RMSE-CV$
RSM linear	0.7964	0.7856	0.05636
RSM INTERACTION	0.8551	0.824	0.04755
RSM ELIPTIC	0.8678	0.853	0.04542
RSM Quadratic	0.9483	0.9331	0.0284
Kriging 0	0.9919	0.9913	0.0122
Kriging 1	0.9901	0.9887	0.01246
Kriging 2	**0.9928**	**0.9899**	**0.01057**
Kriging 2R	0.9897	0.9855	0.01266

Table 40 - Metamodel validation for FFD plus 64 LHD for the front back angle.

Metamodels	$R^2_{Prediction}$	$R^2_{Predictionadj.}$	$RMSE - CV$
RSM linear	0.8362	0.8275	0.01493
RSM INTERACTION	0.9039	0.8834	0.01143
RSM ELIPTIC	0.853	0.816	0.001498
RSM Quadratic	0.9041	0.876	0.01142
Kriging 0	**0.9698**	**0.9698**	**0.006409**
Kriging 1	0.9323	0.9233	0.009596
Kriging 2	0.927	0.8966	0.009968
Kriging 2R	0.9222	0.8898	0.01029

Table 41 - Metamodel validation for FFD plus 64 LHD for the thickness.

Metamodels	$R^2_{Prediction}$	$R^2_{Predictionadj.}$	$RMSE - CV$
RSM linear	-0.09319	-0.1512	0.00968
RSM INTERACTION	-0.3519	-0.6416	0.01077
RSM ELIPTIC	0.9678	0.9642	0.001662
RSM Quadratic	0.9661	0.9561	0.001706
Kriging 0	0.9973	0.9971	0.00048
Kriging 1	0.9972	0.9968	0.00049
Kriging 2	0.9952	0.9932	0.00064
Kriging 2R	**0.9974**	**0.9963**	**0.00047**

5.4.2 Metamodel optimum

The metamodel optimum of the FFD with the 32 LHD and the FFD with the 64 LHD are shown in Figure 125 and Figure 126 respectively. The area that is in blue represents the failure zone (constraint $g > 0$), which means that this zone has many deformations (the absolute value of the difference between the normal thickness and the thickness after the process is higher than 0.01 mm) and the front back angle is higher than 0 degrees. The line that divides the blue and the white area represents the 0 degrees in the left right angle and the thickness varies from 0.301 mm to 0.299 mm. The area in white represents the zone that is feasible to the process. The colour scale on this image shows the range of the output angle (left right angle).

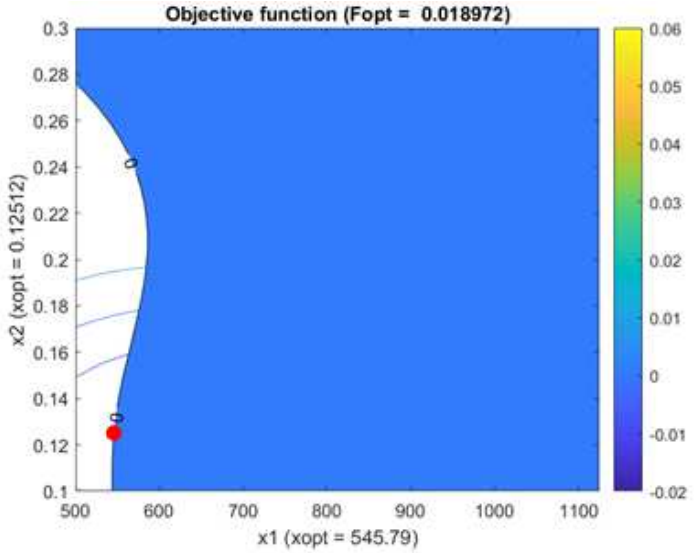

Figure 125 - Metamodel optimal of the FFD with the 32 LHD of the force/are and tool dimensions.

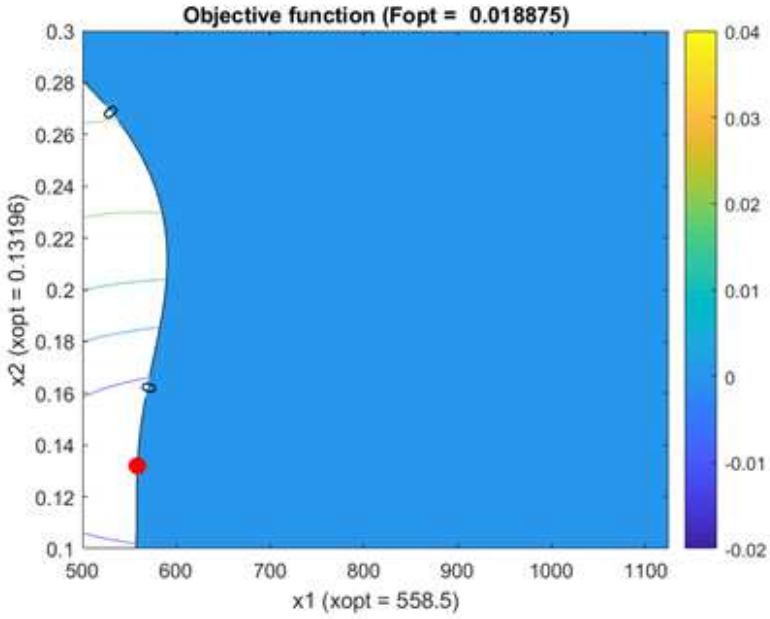

Figure 126 - Metamodel optimal of the FFD with the 64 LHD of the force/are and tool dimensions.

The optimal point is the one that has less sensitivity for the noise variables and the response angle is zero. It can be seen in $X1$, $X2$, $X4$ and $X5$ the design variables, these being the force/area, the dimensions (length), the material height, and material depth respectively. The optimization of 32 LHD to 64 LHD does not have a big impact on the prediction, but in the optimal result it changes to 0.125 mm of length, 645.79 MPa, 0.385 mm in material height and 0.383 mm of material depth to 0.132 mm, 558.5 MPa, 0.385 mm in material height and 0.376 mm of material depth as it can be seen by comparing the Figure 125 and Figure 127 to Figure 126 and Figure 128.

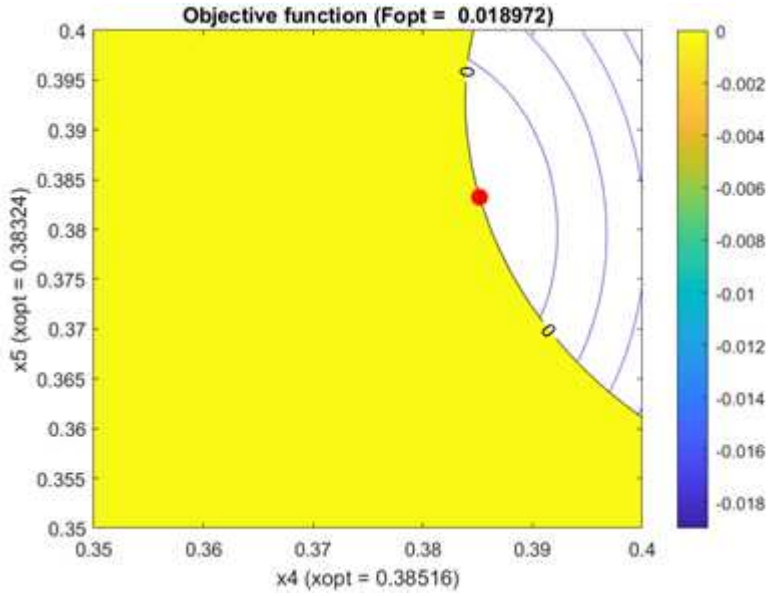

Figure 127 - Metamodel optimal of the FFD with the 32 LHD of the dimension of the block.

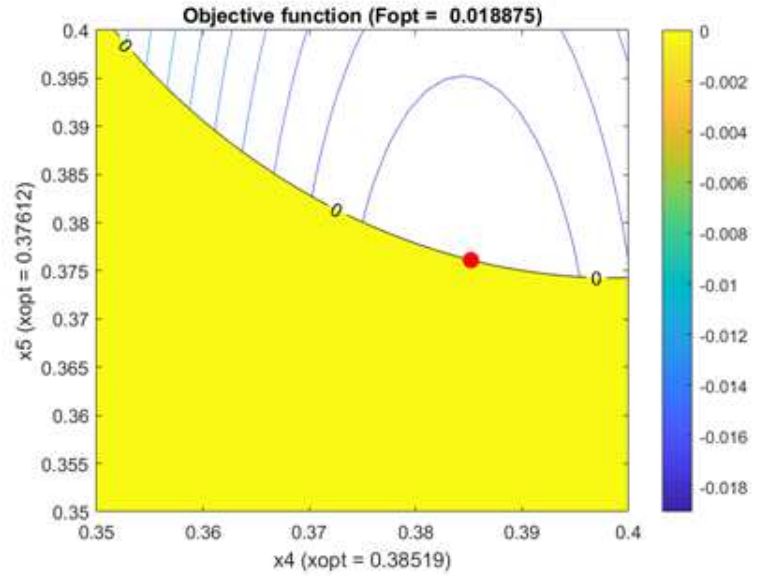

Figure 128 - Metamodel optimal of the FFD with the 64 LHD of the dimension of the block.

5.4.3 The validation of the robust optimum

To validate this optimum there are made 32 LHD around the optimum, the range of the force/area and dimension are chosen by getting the difference (deviation σ_z) of the 32 LHD and the 64 LHD, the normal setting (μ_z) being the average of this 2 value and the upper and lower setting by the equation (55) and (56). So the range of the force/area is 514.015 MPa to 552.145 MPa, the dimensions of the waffling tool is 0.108 mm to 0.149 mm, height of the block 0.38490mm to 0.38545 mm and for the depth of the block 0.3583 mm to 0.401 mm.

$$(\mu_z + 3\sigma_z) \tag{55}$$

$$(\mu_z - 3\sigma_z) \quad (56)$$

The validation of the optimum confirm that the value is between the two optimal response as it can be seen in the Figure 129 and Figure 130 with the $X1$, $X2$, $X4$ and $X5$ optimum being the 521.6 MPa, 0.1276 mm, 0.3771 mm and 0.38491 mm. The $R^2_{Prediction}$ and $RMSE-CV$ are represented in Table 37,Table 38 and Table 39, the representation of each information of the metamodel validation are showing in Appendix 8.10, 8.11 and 8.12. The increasing number of DOE taking into consideration the optimum it increases the prediction for the left right angle to 0.9953, for the front back angle to 0.9715 and for the thickness of to 0.9995 and the $RMSE-CV$ decrease to 0.0091 for the left right angle, 0.00651 for the front back angle and for the thickness 0.002145. With this value it is possible to conclude that, by using the localized DOE, it increases the prediction and at the same time it is able to decrease the deviation, although not by a bigger margin. So, with this number of DOE (160 simulations) it is possible to have an accurately analysis for the optimum and for studying the behaviour of the parameter.

Table 42- Robust optimum validation for left right angle.

Metamodels	$R^2_{Prediction}$	$R^2_{Predictionadj.}$	$RMSE-CV$
RSM linear	0.8193	0.8118	0.05587
RSM INTERACTION	0.8895	0.8784	0.04252
RSM ELIPTIC	0.8947	0.8856	0.04265
RSM Quadratic	0.9635	0.9555	0.02511
Kriging 0	0.9799	0.9788	0.01864
Kriging 1	0.9898	0.9888	0.01326
Kriging 2	0.9925	0.9903	0.01135
Kriging 2R	**0.9953**	**0.9938**	**0.00905**

Table 43 - Robust optimum validation for front back angle.

Metamodels	$R^2_{Prediction}$	$R^2_{Predictionadj.}$	$RMSE-CV$
RSM linear	0.8797	0.8747	0.0133
RSM INTERACTION	0.9315	0.9204	0.0101
RSM ELIPTIC	0.8764	0.8657	0.01356
RSM Quadratic	0.9334	0.9189	0.00995
Kriging 0	0.9507	0.948	0.00856
Kriging 1	0.9423	0.9364	0.00926
Kriging 2	0.9571	0.9442	0.007985
Kriging 2R	**0.9715**	**0.9629**	**0.00651**

Table 44 - Robust optimum validation for thickness.

Metamodels	$R^2_{Prediction}$	$R^2_{Predictionadj.}$	$RMSE - CV$
RSM linear	-0.0485	-0.09187	0.00984
RSM INTERACTION	0.9315	0.9204	0.0101
RSM ELIPTIC	0.9656	0.9626	0.001783
RSM Quadratic	0.964	0.9561	0.001824
Kriging 0	0.996	0.9958	0.000608
Kriging 1	0.9958	0.9954	0.00062
Kriging 2	**0.9995**	**0.9994**	**0.002145**
Kriging 2R	0.9992	0.999	0.002632

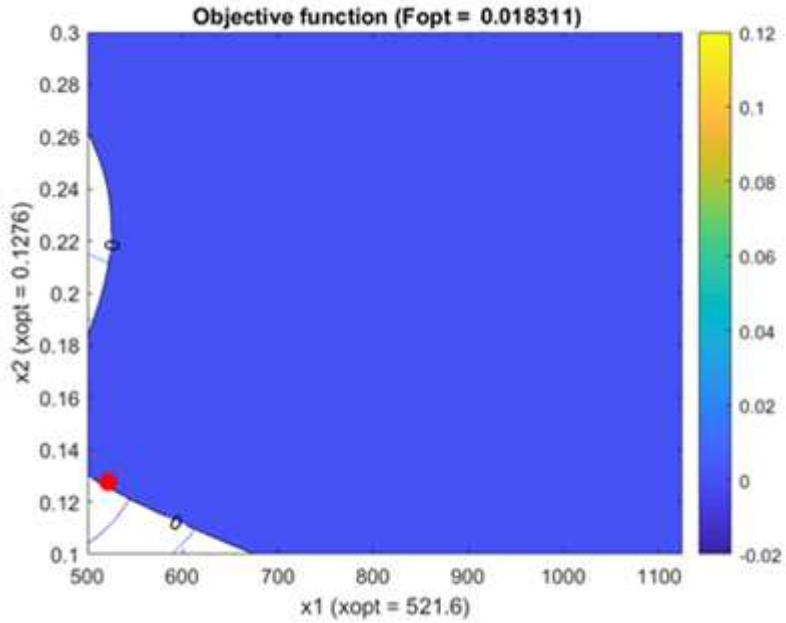

Figure 129 - Metamodel optimal of the FFD with the 64 LHD plus the 32 LHD with the force/are and dimensions.

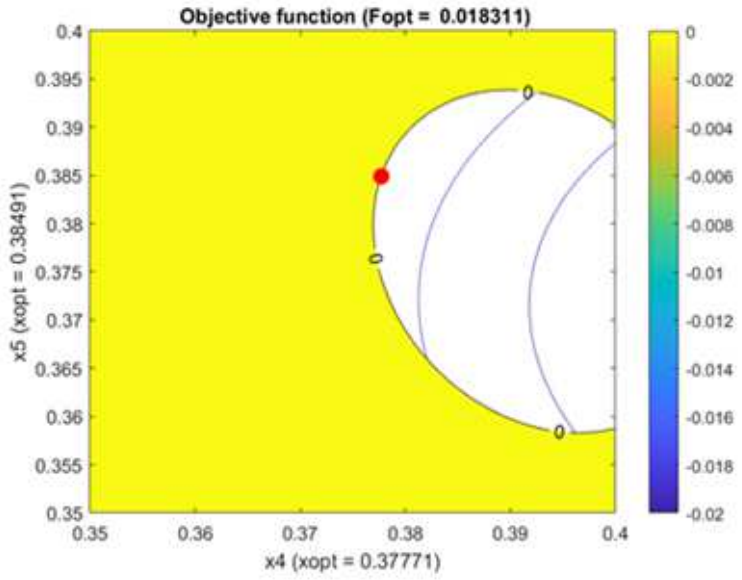

Figure 130 - Metamodel optimal of the FFD with the 64 LHD plus the 32 LHD with the dimension of the block.

With this optimum value of the design variables, it was made 12 simulations with different ranges pre-bending angles, with the waffling method and without the waffling method. The results are represented in Figure 131, which shows an average reduction on the final angle of 13.3 %.

When the angle of the simulation is 0.5 degrees, shows that by using the waffling load in small values of pre-bending it will lead to an increase in the angle, in this case it increases almost 140 %, as the angle without the waffling is almost zero.

The values of reduction increase until the angle of the simulation is 2 degrees (15.8 % of reduction) and then decreases until the angle of the simulation is 6 degrees (12,5 % of reduction).

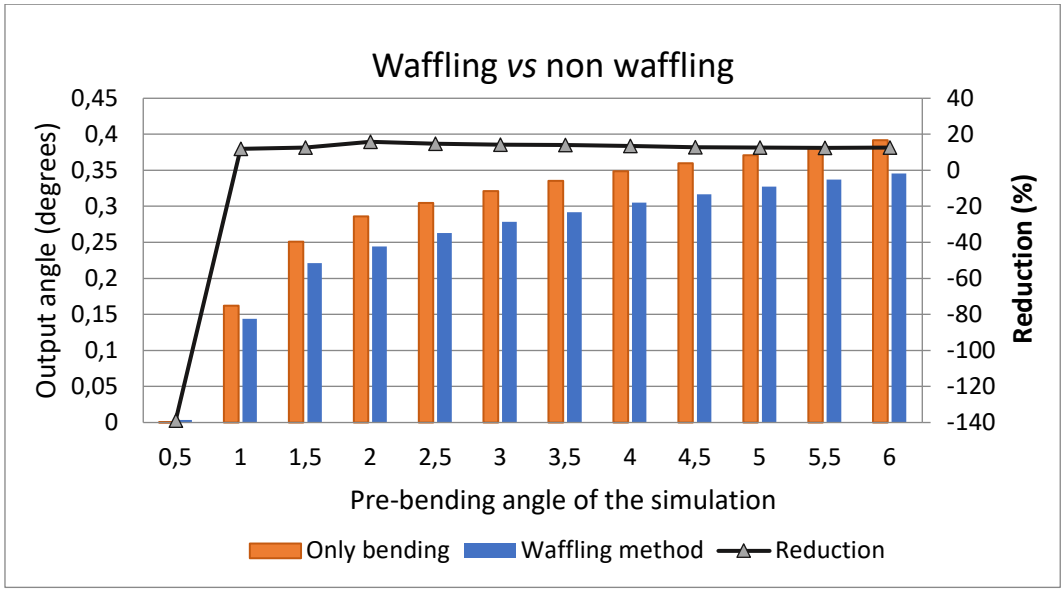

Figure 131 - Waffling optimum *vs* non waffling.

5.4.4 The difference on increasing the number of DOE and a better understanding of the process parameters

The impact of increasing the number of DOE points was already debated about in the previous chapters, but to have a better understanding of this impact it is possible to see the difference in Figure 132 to Figure 142, being the (a) the one with 64 FFD and 32LHD and the (b) the one that has the 64 FFD plus the 64LHD plus 32 LHD, taking into consideration the optimum. One of the biggest differences is the chosen metamodel, the (a) has the zero-order kriging and the (b) has the second order Kriging. In Figure 132 there is a bigger difference on the concave, the (a) has a deeper concave than the (b). In Figure 134, Figure 135 and Figure 141 when comparing the (a) with the (b), the first one has a more complex shape with a deeper concave. In Figure 138 and Figure 142 the complex shape with the deeper concave in (a) changes to an almost linear response. In Figure 133 and Figure 139 the typical concave shape in (a) changes to a more complex concave with waves. Finally, in Figure 136 the difference between the (a) and the (b) is that in (b) it can be seen a more flattened geometry.

To have a better understanding of the flatten technique, the metamodel with the higher prediction value, was used to replicate the response function of the important parameters. By using this, it is possible to study the behaviour of the parameters and what kind of influence they have on the final angle. The focus on this analysis is to see the influence of the design variables and the noise variables between them. The noise variable that will be more interesting to analyse is the angle/area, being this the variable that has more influence in the process, which was determined by the screening technique. On Figure 132 (b), Figure 133 (b), Figure 134 (b), Figure 135 (b), Figure 136 (b), Figure 137 (b), Figure 138 (b), Figure 139 (b), Figure 140 (b), Figure 141 (b) and Figure 142 (b) all the parameters that were not used in the image, their value was the average value.

The behaviour of the dimensions with the design variables tool dimensions are shown on Figure 132 (b), Figure 133 (b), Figure 134 (b) and Figure 135 (b). The dimensions of the tool ($x1$) with the thickness ($x3$) have an impact on the output angle. The dimensions ($x1$) make a parabola curve, and when this increases it decreases the output angle. For the thickness it has an almost linear response, as increasing this parameter will increase the output angle, as can be seen in Figure 132 (b).

The dimensions of the tool ($x1$) with the pre-bending angle or angle/area ($x6$) has a behaviour on the response angle very similar to a parabolic curve with waves, when the pre-bending angle ($x6$) increases, the output angle increases in a complex concave, and as for the dimensions of the tool ($x1$), when the angle of the pre-bending is small, it increases the response angle, but when the angle of the pre-bending is higher, the increase of the dimensions leads to a decrease on the angle, as it is shown on Figure 133 (b).

The dimensions of the tool ($x1$) with the depth dimensions of block ($x5$) and the height dimensions of block ($x4$), have basically the same behaviour so their analysis will be made together, and they will have an impact on the response angle, as the noise variable

creates a linear curve that does not have a vast impact and it is linear, the dimensions of the tool ($x1$), when increasing the dimensions of the tool, it decreases the response angle as it can be seen in Figure 134 (b) and Figure 135 (b).

The tool dimensions ($x1$) and the force/area ($x2$), have an impact on the response of the complex geometry, when increasing both the tool dimensions ($x1$) and the force/area ($x2$), they end up decreasing the output angle, as it can be seen in Figure 136 (b).

The force/area ($x2$) with the thickness ($x3$) and height of the block ($x4$) have a similar response, turning into a rhombus geometry. By increasing the force/area ($x2$) it will decrease the response angle. On the other hand, increasing the thickness ($x3$) or the height of the block ($x4$) will increase the response angle in an almost linear function as it can be seen in Figure 138 (b) and Figure 141 (b).

For the force/area ($x2$) with the pre-bending angle or angle/area ($x6$), it is a very similar situation as to when the design variable is the tool dimension, as both have a response similar to a parabolic curve with waves, although the major difference is that it has less waves. In this case when increasing the pre-bending angle ($x6$), it leads to an increase of the output angle in a complex concave, and for the force/area ($x2$), when the angle of pre-bending is small, it increases the response angle, but when the angle of pre-bending is higher the increase on the dimensions decreases the angle as it can be seen in Figure 139 (b) and Figure 142 (b).

For the force/area ($x2$) and height of the depth ($x5$) the response is similar to a rhombus geometry, but when the block is in depth ($x5$), the response is a concave. In the last case, increasing it will decrease the output angle. The force/area ($x2$) has an almost linear response and when increasing it will decrease the response angle as it can be seen in Figure 141 (b).

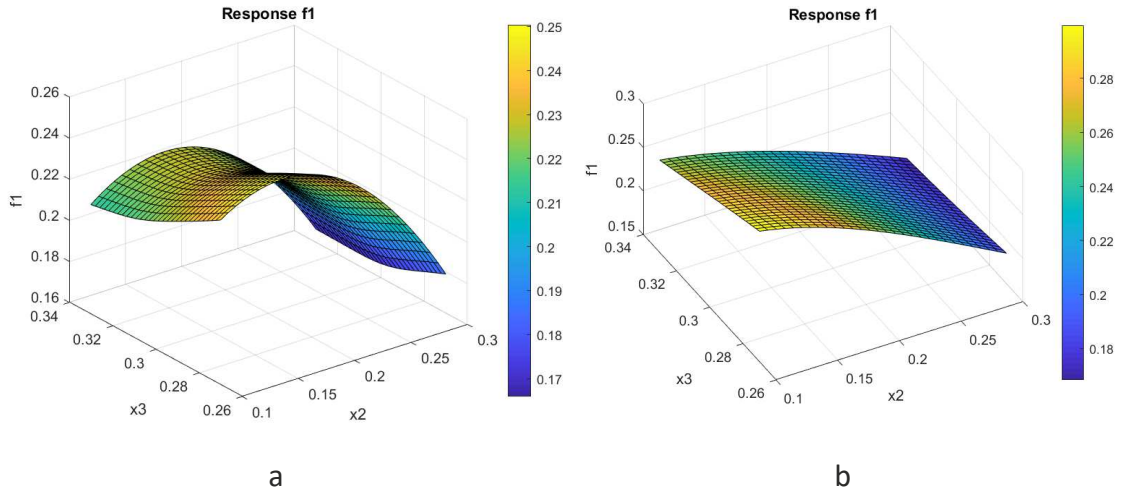

a b

Figure 132 - Metamodel response of thickness and dimensions relatively to the left right angle with (a) being the 32 and (b) the validation of the optimum.

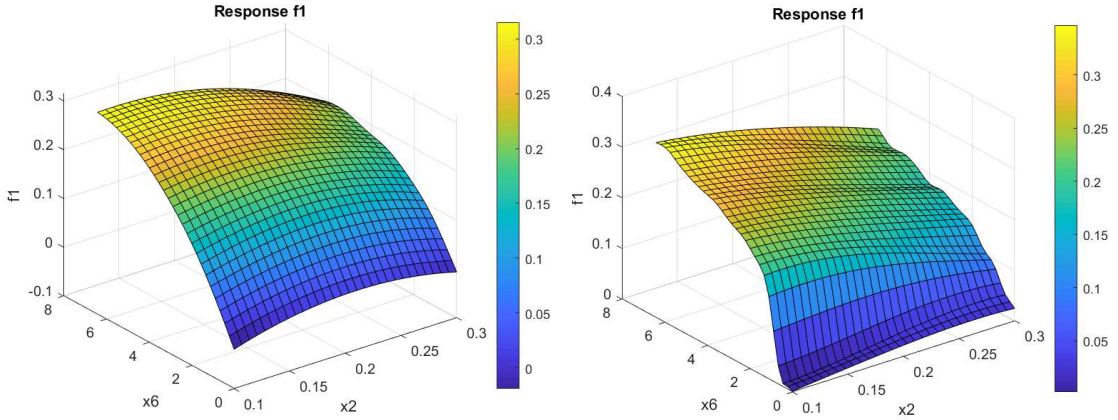

a b

Figure 133 - Metamodel response of angle/area and dimensions relatively to the left right angle, with (a) being the 32 LHD and (b) the validation of the optimum.

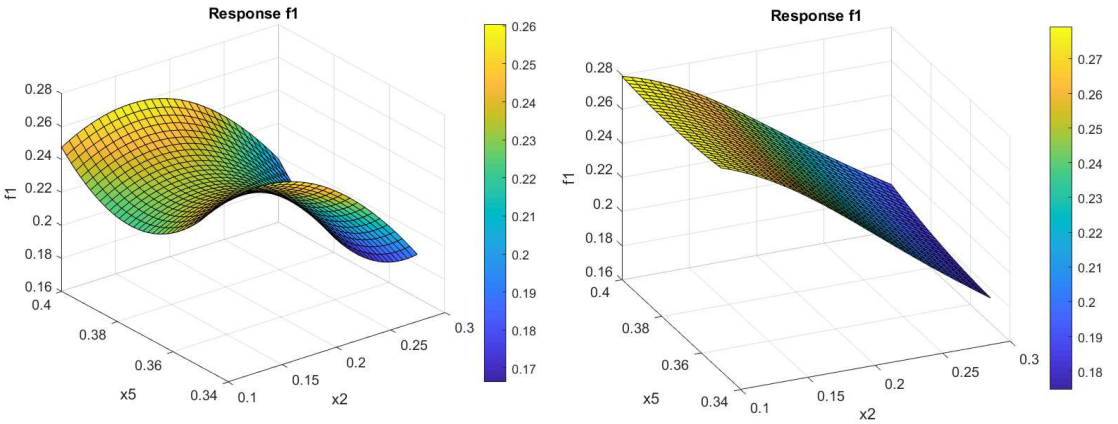

a b

Figure 134 - Metamodel response of depth of the block and dimensions relatively to the left right angle, with (a) being the 32 LHD and (b) the validation of the optimum.

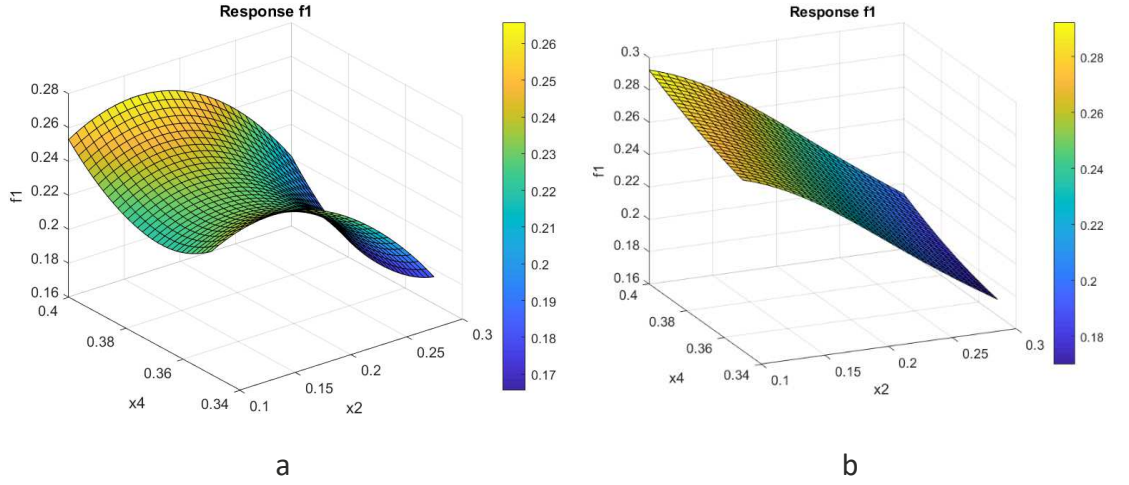

a b

Figure 135 - Metamodel response of height of the block and dimensions relatively to the left right angle, with (a) being the 32 LHD and (b) the validation of the optimum.

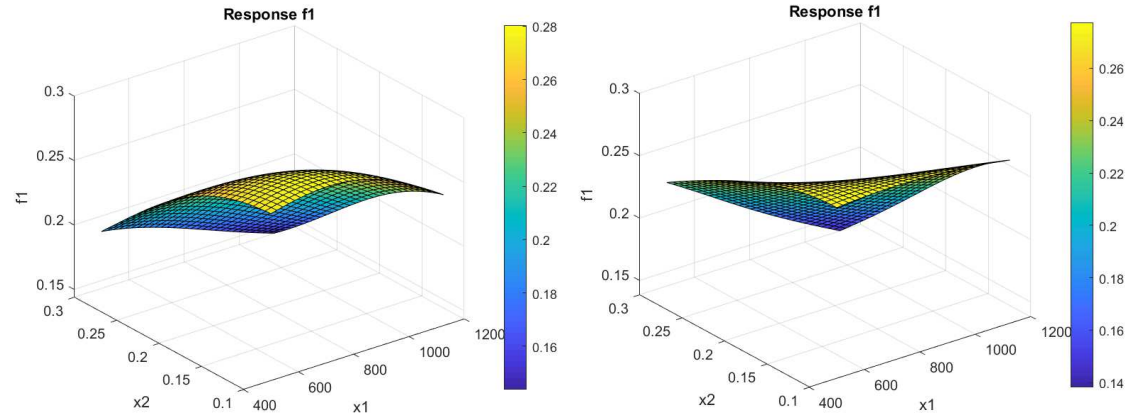

a b

Figure 136 - Metamodel response of force/area and dimensions relatively to the left right angle , with (a) being the 32 LHD and (b) the validation of the optimum.

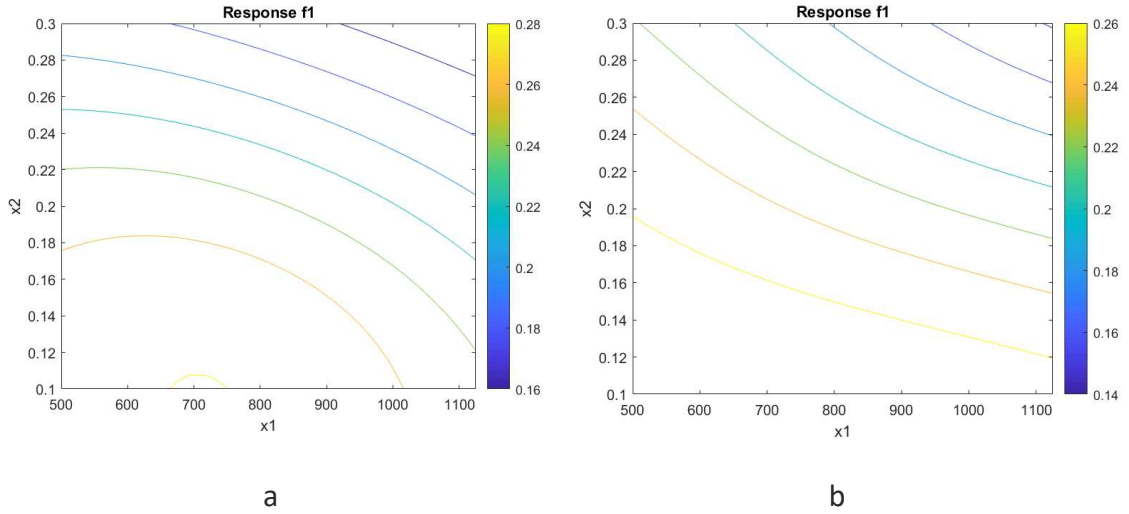

a b

Figure 137 - Metamodel response of force/area and dimensions relatively to the left right angle in 2D, with (a) being the 32 LHD and (b) the validation of the optimum.

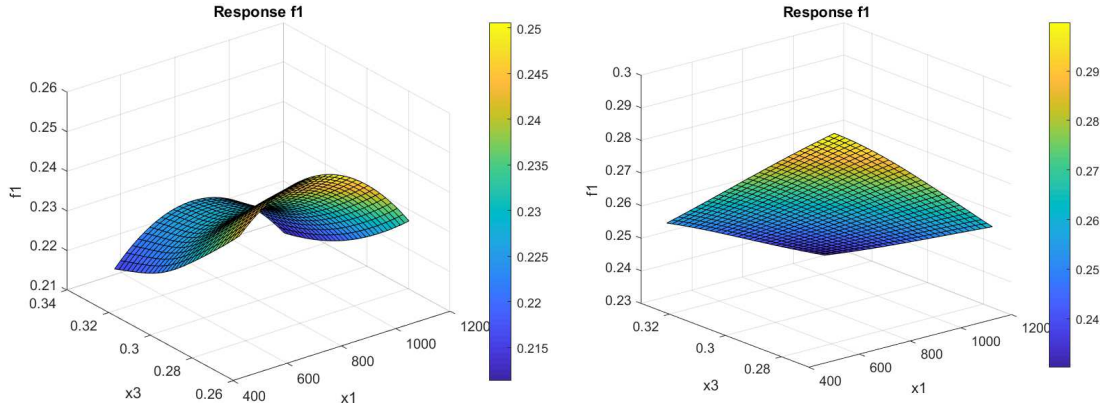

a b

Figure 138 Metamodel response of force/area and thickness relatively to the left right angle, with (a) being the 32 LHD and (b) the validation of the optimum.

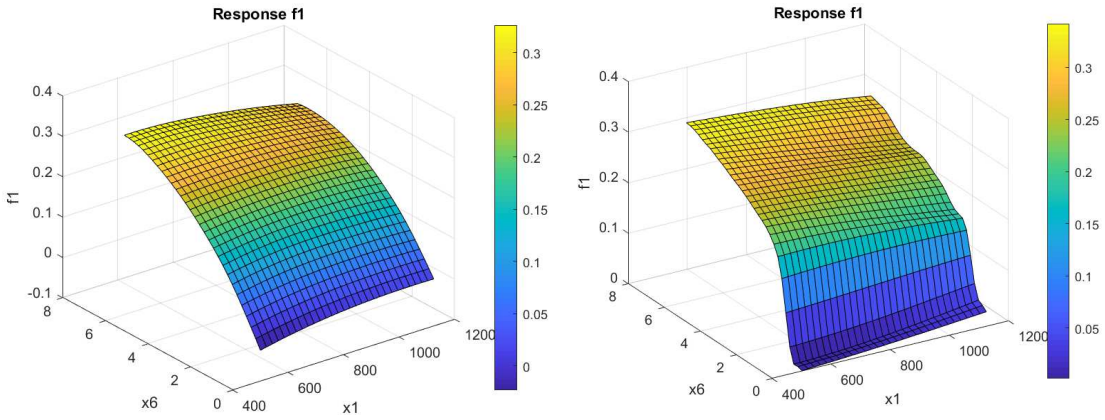

a b

Figure 139 - Metamodel response of force/area and angle/area relatively to the left right angle, with (a) being the 32 LHD and (b) the validation of the optimum.

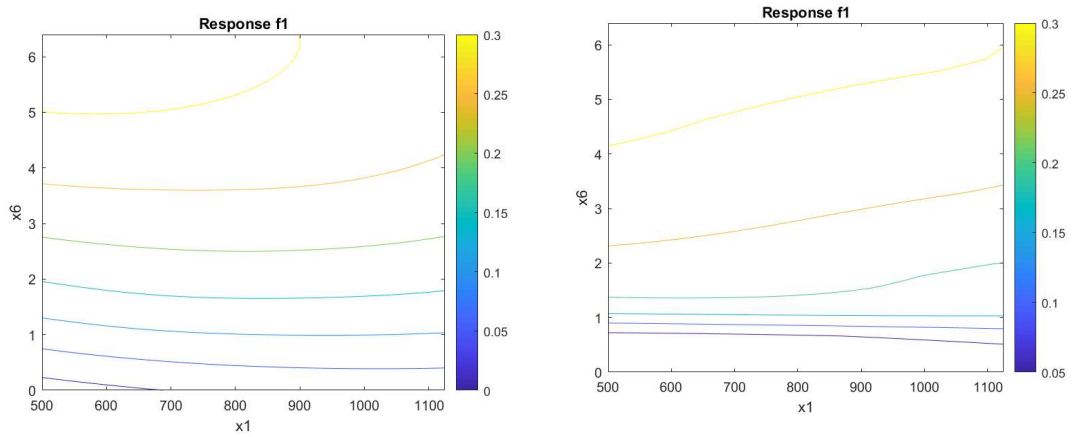

a b

Figure 140 - Metamodel response of force/area and angle /area relatively to the left right angle in 2D, with (a) being the 32 LHD and (b) the validation of the optimum.

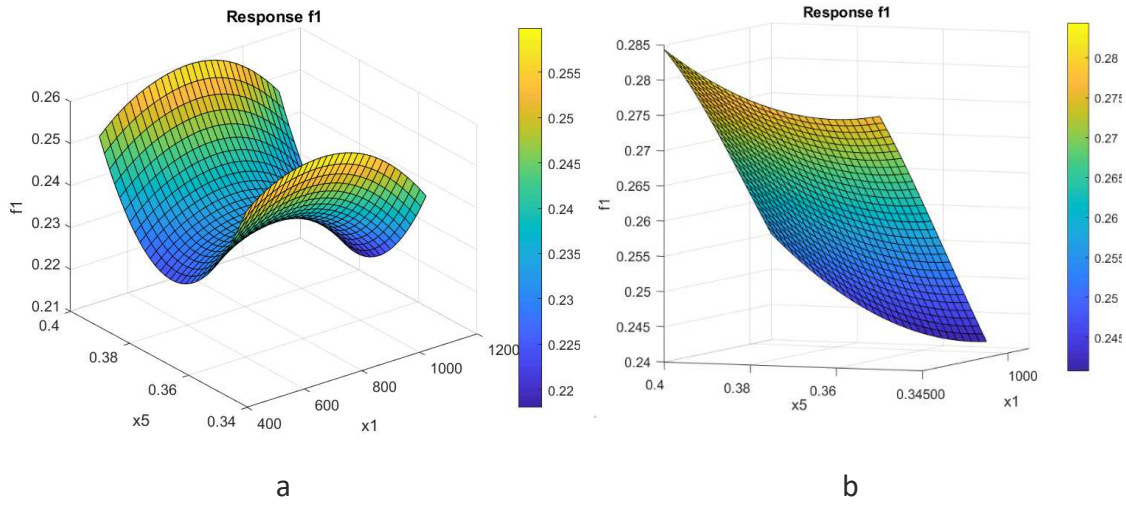

a b

Figure 141 - Metamodel response of force/area and depth of the block relatively to the left right angle, with (a) being the 32 LHD and (b) the validation of the optimum.

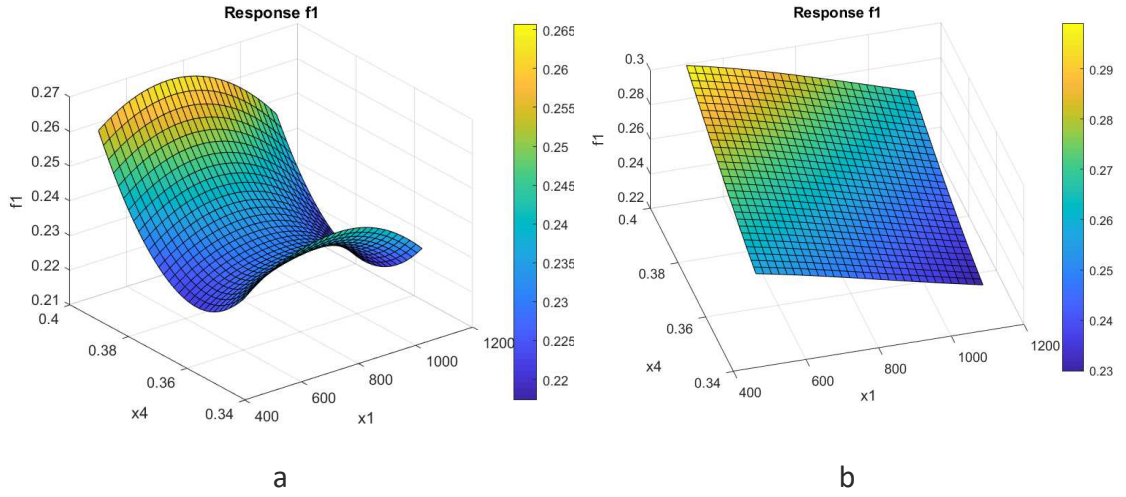

a b

Figure 142 - Metamodel response of force/area and height of the block relatively to the left right angle, with (a) being the 32 LHD and (b) the validation of the optimum.

CONCLUSIONS

6 CONCLUSION AND FUTURE WORKS

6.1 Conclusion

In this work it was studied a new method to flatten the surface and reduce the spread by implementing a robust strategy, making it easier to analyse and optimize this process. Therefore, in terms of conclusion to this investigation:

- A new FE model was developed;
- The initial study of the parameters' effects on a non-robust simulation was performed and new range of parameters' values as bending and waffling force were chosen. These new parameters so that they can be utilized in future work, that will allow to proceed this investigation.
- The effect of the noise variables on the pre-bending show the difference between the non-plastic deformed material and the plastic deformed one, as they have an opposite behaviour. It was shown that when applying the waffling load, it generates a reduction on the angle when the material is plastic deformed, while in the material that is not plastic deformed this angle increases, when under these same previous circumstances. All this behaviour is validated by the practical experiment, despite the fact that in the practical test the samples have already some curvature originated by the rolls of steel sheet;
- The best range of values for the waffling load, with the objective to do an analysis of a simulation in 3D robust, is between 20 and 45 N;
- The difference between the FE simulation and the practical test, can be explained by the fact that the waffling tool is a-rigid and cannot deform. As this is not the one and only explanation, it is needed to consider other factors that may have some influence on this difference. Some of these factors are the mesh, as it only allows a limited number of elements, the Bauschinger effect (reverse load on the material) and the change in material properties on the pre-bending compared to rolling;
- The screening was able to identify the important variables that were then considered in the waffling with the square geometry. These variables are the thickness, material height, material depth, pre-bending, force/area and dimensions (length of the square). The variable that has higher effect is pre-bending, as was expected;
- The metamodel that has the higher accuracy is the Kriging, as it is the one with higher prediction and a smaller deviation in the value. The differences between $R^2_{Prediction}$ and $R^2_{Predictionadj.}$ are small, which means that the variables that were chosen do in fact have an influence on the process, as anticipated by the screening technique;
- The increase in the number of LHD in DOE points without any location results on an increase in prediction, as well as it leads to a decrease in the deviation, even though it

is not by a higher margin. The same results happen when increasing the number of LHD DOE into the optimal location;

- RO optimization is able to predict which of the values of the design variables have less sensitivity to the noise variables, while taking into consideration the constraints. The optimum originated by RO, in order to be utilized in the future, needs further practical tests and some changes in the FE model to be as close as possible to the "real world";
- With the waffling was produced an average reduction on the final angle of 13.3 %.
- A better knowledge about the influence of parameters in flattening the surface can be achieved by visualizing the response of the surface in the metamodel response.

6.2 Future work

The present work is the beginning of a new study to reduce the spread and flatten the surface, using a robust strategy. To continue this development's needs:

- More practical tests need to be performed;
- Approximate the numerical result to the result of the practical test. Revise the model to be more similar as the practical experiments by studying the material behaviour, FEM model, measuring stresses and investigate the bending;
- Make an analysed on the different waffling geometry ;
- Make the programs for the RO more user friendly;
- Test the optimum value of the revised RO;
- Redefine the bending angle range.

REFERENCES AND OTHER SOURCES OF INFORMATION

7 REFERENCES AND OTHER SOURCES OF INFORMATION

Uncategorized References

[1] J. Antony, *Design of Experiments for Engineers and Scientists*. Elsevier, 2003, p. 190.

[2] E. T. Taylan Altan, *Sheet Metal Forming Fundamentals*. ASM International, 2012.

[3] V. N. DANCHENKO, *METAL FORMING*. Porogi, 2007.

[4] S. GmbH, *Metal Forming Handbook*. Springer, Berlin, Heidelberg, 1998.

[5] *DIN 8580, 2003 Edition, MANUFACTURING PROCESSES - TERMS AND DEFINITIONS, DIVISION,* DIN.

[6] M. Saad, S. Akhtar, M. Srivastava, and J. Chaurasia, "Role of Simulation in Metal Forming Processes," *Materials Today: Proceedings,* vol. 5, no. 9, Part 3, pp. 19576-19585, 2018.

[7] J.-L. Strudel, "CHAPTER 25 - MECHANICAL PROPERTIES OF MULTIPHASE ALLOYS," in *Physical Metallurgy (Fourth Edition)*, R. W. Cahn and P. Haasen†, Eds. Oxford: North-Holland, 1996, pp. 2105-2206.

[8] M. E. Kassner, "Chapter 2 - Five-Power-Law Creep," in *Fundamentals of Creep in Metals and Alloys (Third Edition)*, M. E. Kassner, Ed. Boston: Butterworth-Heinemann, 2015, pp. 7-102.

[9] G. Z. Voyiadjis and M. Yaghoobi, "Chapter 2 - Nonlocal continuum plasticity," in *Size Effects in Plasticity*, G. Z. Voyiadjis and M. Yaghoobi, Eds.: Academic Press, 2019, pp. 81-190.

[10] Z. Zhuang, Z. Liu, and Y. Cui, "Chapter 4 - Dislocation-Based Single-Crystal Plasticity Model," in *Dislocation Mechanism-Based Crystal Plasticity*, Z. Zhuang, Z. Liu, and Y. Cui, Eds.: Academic Press, 2019, pp. 91-119.

[11] A. E. Tekkaya, "Simulation of Metal Forming Processes," in *Formability of Metallic Materials: Plastic Anisotropy, Formability Testing, Forming Limits*, D. Banabic, H. J. Bunge, K. Pöhlandt, A. E. Tekkaya, and D. Banabic, Eds. Berlin, Heidelberg: Springer Berlin Heidelberg, 2000, pp. 251-302.

[12] V.-F. P. u. Fertigungsverfahre, *Roughened planishing tools*. Production Equipment - VDI guidelines: VDI 3382, 1972, p. 6.

[13] O. C. Zienkiewicz, R. L. Taylor, and J. Z. Zhu, "Chapter 1 - The Standard Discrete System and Origins of the Finite Element Method," in *The Finite Element Method: its Basis and Fundamentals (Seventh Edition)*, O. C. Zienkiewicz, R. L. Taylor, and J. Z. Zhu, Eds. Oxford: Butterworth-Heinemann, 2013, pp. 1-20.

[14] D. Marinkovic and M. Zehn, "Survey of Finite Element Method-Based Real-Time Simulations," *Applied Sciences,* vol. 9, p. 2775, 07/10 2019.

[15] R. L. T. a. D. F. O. C. Zienkiewicz, *The Finite Element Method for Solid and Structural Mechanics*. Butterworth-Heinemann, 2013.

[16] J. H. Wiebenga, "Robust design and optimization of forming processes," Ph.D., University of Twente, 2014.

[17] Y. Liu, *Effects of Mesh Density on Finite Element Analysis*. 2013.

[18] S. Uzuner, E. Zurnacı, M. Rodriguez, and S. Küçük, *Investigation of the Effect of Mesh Density and Element Type on Behavior of Biphasic Soft Tissues in Finite Element Analysis*. 2018.

[19] Y. Tenne, "Machine–Learning in Optimization of Expensive Black–Box Functions," *International Journal of Applied Mathematics and Computer Science,* vol. 27, 03/01 2017.

[20] J. Lehman, T. Santner, and W. Notz, "Designing Computer Experiments to Determine Robust Control Variables," *Statistica Sinica,* vol. 14, pp. 571-590, 04/01 2004.

[21] M. H. A. Bonte, "Optimization strategies for metal forming processes," Ph.D., University Twente 2007.

[22] C. Huang, B. Radi, and A. E. Hami, "Uncertainty analysis of deep drawing using surrogate model based probabilistic method," *The International Journal of Advanced Manufacturing Technology,* vol. 86, no. 9, pp. 3229-3240, 2016/10/01 2016.

[23] A. Maia, E. Ferreira, M. C. Oliveira, L. F. Menezes, and A. Andrade-Campos, "3 - Numerical optimization strategies for springback compensation in sheet metal forming," in *Computational Methods and Production Engineering*, J. Paulo Davim, Ed.: Woodhead Publishing, 2017, pp. 51-82.

[24] A. Parnianifard, A. S. Azfanizam, M. K. A. Ariffin, and M. I. S. Ismail, "Crossing weighted uncertainty scenarios assisted distribution-free metamodel-based robust simulation optimization," *Engineering with Computers,* vol. 36, no. 1, pp. 139-150, 2020/01/01 2020.

[25] J. Kleijnen, "Simulation Optimization Through Regression or Kriging Metamodels," 2020, pp. 115-135.

[26] W. Zhang and W. Xu, "Simulation-based robust optimization for the schedule of single-direction bus transit route: The design of experiment," *Transportation Research Part E: Logistics and Transportation Review,* vol. 106, pp. 203-230, 2017/10/01/ 2017.

[27] S. B. Baco, P. C. Oprime, L. Campanini, and G. M. D. Ganga, "DESIGN OF EXPERIMENTS USED IN COMPUTER TRIALS: A SUPPORTIVE METHOD FOR PRODUCT DEVELOPMENT %J Pesquisa Operacional," vol. 39, pp. 295-316, 2019.

[28] J. Kamenik *et al.*, "Robust Turbine Blade Optimization in the Face of Real Geometric Variations," *Journal of Propulsion and Power,* vol. 34, pp. 1-15, 09/30 2018.

[29] M. Arnér, "Design and Analysis of Computer Experiments," 2014, pp. 155-176.

[30] A. Parnianifard, A. s. Azfanizam, M. k. a. Mohd ariffin, M. I. S. Ismail, and N. Ale Ebrahim, "Recent developments in metamodel based robust black-box simulation optimization: An overview," *Decision Science Letters,* vol. 8, 05/23 2018.

[31] D. R. C. a. N. REID, *The Theory of the Design of Experiments*. Chapman and Hall/CRC, 2000.

[32] T. J. Santner, Williams, B. J., & Notz, W. I, "Space-Filling Designs for Computer Experiments " in *The Design and Analysis of Computer Experiments*: Springer, New York, NY, 2003, pp. 121-161.

[33] G. Dellino, J. Kleijnen, and C. Meloni, "Robust Optimization in Simulation: Taguchi and Krige Combined," *Informs Journal on Computing,* vol. 24, p. 2012, 08/01 2012.

[34] S. Aydin Cem, S. Ozgurler, B. Durmusoglu Mehmet, and M. Ozgurler, "Response surface approach to robust design of assembly cells through simulation," *Assembly Automation,* vol. 38, no. 4, pp. 450-464, 2018.

[35] W. Shen, D. Lin, and C.-J. Chang, "Design and Analysis of Computer Experiment via Dimensional Analysis," *Quality Engineering,* vol. 30, 04/19 2017.

[36] A. Parnianifard and A. s. Azfanizam, "Metamodel-based robust simulation-optimization assisted optimal design of multiloop integer and fractional-order PID controller," *International Journal of Numerical Modelling: Electronic Networks, Devices and Fields,* 08/01 2019.

[37] J. Havinga, T. Van den Boogaard, and Klaseboer, "Sequential improvement for robust optimization using an uncertainty measure for radial basis functions," *Structural and Multidisciplinary Optimization,* vol. 55, pp. 1345–1363, 04/01 2017.

[38] J. Wiebenga, T. Van den Boogaard, and G. Klaseboer, "Sequential robust optimization of a V-bending process using numerical simulations," *Structural and Multidisciplinary Optimization,* vol. 46, 07/01 2012.

[39] F. Viana, T. Simpson, V. Balabanov, and V. Toropov, "Metamodeling in Multidisciplinary Design Optimization: How Far Have We Really Come?," *AIAA Journal,* vol. 52, 03/31 2014.

[40] M. J. Azizi, F. Seifi, and S. Moghadam, "A robust simulation optimization algorithm using kriging and particle swarm optimization: Application to surgery room optimization," *Communications in Statistics - Simulation and Computation,* pp. 1-17, 2019.

[41] J. Kleijnen, "Design and Analysis of Simulation Experiments: Tutorial," 2017, pp. 135-158.

[42] G. Sun, X. Song, S. Baek, and Q. Li, "Robust optimization of foam-filled thin-walled structure based on sequential Kriging metamodel," *Structural and Multidisciplinary Optimization,* vol. 49, 06/01 2014.

[43] V. Penadés Plà, T. García-Segura, and V. Yepes, "Robust Design Optimization for Low-Cost Concrete Box-Girder Bridge," vol. 2020, p. 398, 03/11 2020.

[44] G.-J. Park and K.-H. Lee, "A Global Robust Optimization Using the Kriging Based Approximation Model," *Transactions of the Korean Society of Mechanical Engineers A,* vol. 29, pp. 1243-1252, 09/01 2005.

[45] S. Kemmler, A. Fuchs, T. Leopold, and B. Bertsche, *Comparison of Taguchi Method and Robust Design Optimization (RDO)*. 2015.

[46] A. Parnianifard, A. s. Azfanizam, M. k. a. Mohd ariffin, and M. I. S. Ismail, "Robust Product Design: A Modern View of Quality Engineering in Manufacturing Systems," *Preprints,* p. 3220, 07/26 2018.

[47] G. Dellino, J. P. C. Kleijnen, and C. Meloni, "Robust optimization in simulation: Taguchi and Response Surface Methodology," *International Journal of Production Economics,* vol. 125, no. 1, pp. 52-59, 2010/05/01/ 2010.

[48] J. Che, J. Wang, and K. Li, "A Monte Carlo Based Robustness Optimization Method in New Product Design Process: A Case Study," *American Journal of Industrial and Business Management,* vol. 04, pp. 360-369, 01/01 2014.

[49] A. Barel and S. Vandewalle, "Robust Optimization of PDEs with Random Coefficients Using a Multilevel Monte Carlo Method," *SIAM/ASA Journal on Uncertainty Quantification,* vol. 7, 11/07 2017.

[50] N. Razaaly, G. Gori, O. Le Maître, G. Iaccarino, and P. M. Congedo, *Robust optimization of turbine cascades for Organic Rankine Cycles operating with siloxane MDM*. 2019.

[51] M. H. A. Bonte, T. Van den Boogaard, and J. Huetink, "An optimisation strategy for industrial metal forming processes : MModelling, screening and solving of optimisation problems in metal forming," *Structural and Multidisciplinary Optimization,* vol. 35, 06/01 2008.

[52] C. M. M. Anderson-Cook, Douglas C.; Myers, Raymond H, *Response Surface Methodology*, Fourth ed. (Process and Product Optimization Using Designed Experiments). John Wiley & Sons, Inc., Hoboken, New Jersey, 2016.

[53] Q. Yang and D. Xue, "Comparative study on influencing factors in adaptive metamodeling," *Engineering with Computers,* vol. 31, pp. 561-577, 07/01 2014.

[54] A. Parnianifard, A. s. Azfanizam, M. k. a. Mohd ariffin, and M. I. S. Ismail, "An overview on robust design hybrid metamodeling: Advanced methodology in process optimization under uncertainty," *International Journal of Industrial Engineering Computations,* vol. 9, 01/01 2018.

[55] İ. Yanıkoğlu, D. den Hertog, and J. Kleijnen, "Robust Dual-Response Optimization (Selected as the Best Paper in IISE Transactions: Operations Engineering & Analytics for 2017)," *IIE Transactions,* vol. 48, pp. 298-312, 10/11 2016.

[56] K. Elsayed and C. Lacor, "Robust parameter design optimization using Kriging, RBF and RBFNN with gradient-based and evolutionary optimization techniques," *Applied Mathematics and Computation,* vol. 236, pp. 325-344, 2014/06/01/ 2014.

[57] H. Naceur, Y. Q. Guo, and S. Ben-Elechi, "Response surface methodology for design of sheet forming parameters to control springback effects," *Computers & Structures,* vol. 84, no. 26, pp. 1651-1663, 2006/10/01/ 2006.

[58] J. Kleijnen, "Simulation-optimization via Kriging and bootstrapping: a survey," *Journal of Simulation,* vol. 8, 11/30 2014.

[59] J. Kleijnen and W. Beers, "Statistical Tests for Cross-Validation of Kriging Models," *SSRN Electronic Journal,* 01/01 2019.

[60] V. Alimirzaloo, F. R. Biglari, M. H. Sadeghi, P. M. Keshtiban, and H. R. Sehat, "A novel method for preform die design in forging process of an airfoil blade based on Lagrange interpolation and meta-heuristic algorithm," *The International Journal of Advanced Manufacturing Technology,* vol. 102, no. 9, pp. 4031-4045, 2019/06/01 2019.

[61] S. Bingöl, T. Altinbalik, and H. Kılıçgedik, *Artificial neural network modeling for the application of lateral extrusion process*. 2015.

[62] F. Djavanroodi, A. Pirgholi, and S. Derakhshani, "FEM and ANN analysis in fine-blanking process," *Materials and Manufacturing Processes,* vol. 25, pp. 864-872, 09/02 2010.

[63] S. Salunkhe, D. Rajamani, B. Esakki, and U. Chandrasekhar, "Prediction of life of piercing punches using artificial neural network and adaptive neuro fuzzy

inference systems," *International Journal of Materials Engineering Innovation,* vol. 10, 02/07 2019.

[64] S. Salunkhe, V. Naranje, and T. Dharma, "Prediction of Life of Compound Die Punch Using Machine Learning," pp. 646-649, 03/02 2020.

[65] A. Alaswad, K. Y. Benyounis, and A. G. Olabi, "Optimization Techniques in Material Processing," in *Reference Module in Materials Science and Materials Engineering*: Elsevier, 2016.

[66] N. Mekras, "Using artificial neural networks to model aluminium based sheet forming processes and tools details," *Journal of Physics: Conference Series,* vol. 896, p. 012090, 2017/09 2017.

[67] P. Tappenden, J. Chilcott, S. Eggington, J. Oakley, and C. McCabe, "Methods for expected value of information analysis in complex health economic models: Developments on the health economics of interferon-β and glatiramer acetate for multiple sclerosis," *Health technology assessment (Winchester, England),* vol. 8, pp. iii, 1-78, 07/01 2004.

[68] J. Hernandez-Vazquez, I. Garitaonandia, M. H. Fernandes, J. Munoa, and L. Lacalle, "A Consistent Procedure Using Response Surface Methodology to Identify Stiffness Properties of Connections in Machine Tools," *Materials,* vol. 11, p. 1220, 07/16 2018.

[69] M. Bonte, T. Van den Boogaard, and E. Veldman, "Modelling, screening, and solving of optimisation problems: Application to industrial metal forming processes," vol. 907, 04/07 2007.

[70] Philips. *Company*.

[71] "Straightening of Bars, Shapes, and Long Parts," vol. 14B, Metalworking: Sheet Forming: ASM International, 2006, p. 0. [Online]. Available: https://doi.org/10.31399/asm.hb.v14b.a0005136.

[72] S. Garg, R. Kant, S. Joshi, and U. Dixit, *A Study on Straightening of Bent Aluminium 5052 Sheets Using Laser Line Heating*. 2016.

[73] T. Ueda, E. Sentoku, Y. Wakimura, and A. Hosokawa, "Flattening of sheet metal by laser forming," *Optics and Lasers in Engineering,* vol. 47, pp. 1097–1102, 11/01 2009.

[74] P.-A. Eggertsen and K. Mattiasson, "Experiences from experimental and numerical springback studies of a semi-industrial forming tool," *International Journal of Material Forming,* vol. 5, 12/01 2011.

[75] V. Gautam, P. Sharma, and D. Ravi Kumar, "Experimental and Numerical Studies on Spring back in U-Bending of 3-Ply Cladded Sheet Metal," *Materials Today: Proceedings,* vol. 5, no. 2, Part 1, pp. 4421-4430, 2018/01/01/ 2018.

[76] M. S. Gupta and D. R. Reddy, "Design and analysis of aircraft sheet metal for spring back effect," *Materials Today: Proceedings,* vol. 4, no. 8, pp. 8287-8295, 2017/01/01/ 2017.

APPENDIX

8 APPENDIX

8.1 Appendix 1- Waffling geometry.

8.1.1 Appendix 1.1- Square or standard

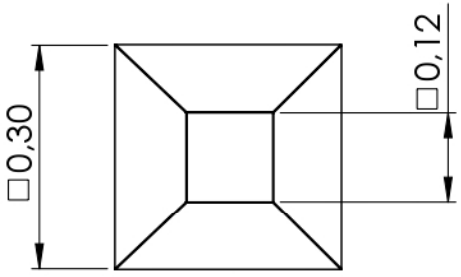

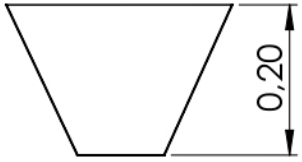

Ra 1,6

ISO 2768
ISO 1302

	Name	Date						
Crea.	Eduardo A.	27/03/2020	PHILIPS isep Instituto Superior de Engenharia do Porto				Quantity	
Verif.	Eduardo A.	27/03/2020					Mass	
Aprov.	Gerrit K.	28/03/2020	ISO 2768	mK	Scale- 100:1	A4	Treatment	None
Name	Square part of the waffling						Material	AISI 420
							Drawing	3

1/1

8.1.2 Appendix 1.2 - Conical

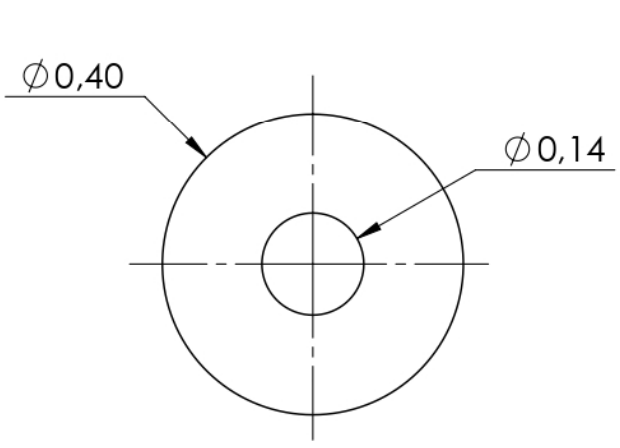

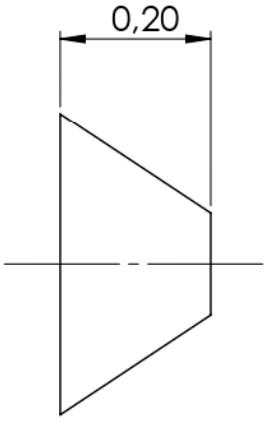

Ra 1,6

ISO 2768
ISO 1302

	Name	Date							
Crea.	Eduardo A.	23/03/2020	PHILIPS isep Instituto Superior de Engenharia do Porto					Quantity	
Verif.	Eduardo A.	23/03/2020						Mass	
Aprov.	Gerrit K.	24/03/2020	ISO 2768	mK	Scale- 100:1		A4	Treatment	None
Name	Conical part of the waffling							Material	AISI 420
								Drawing	1

1/1

8.1.3 Appendix 1.3 - Cylindrical

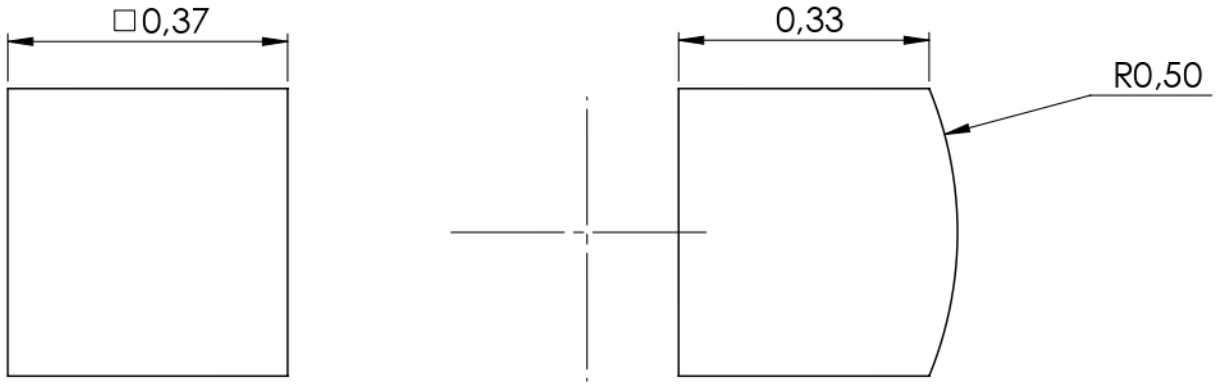

Ra 1,6

ISO 2768
ISO 1302

	Name	Date							
Crea.	Eduardo A.	26/03/2020	PHILIPS isep Instituto Superior de Engenharia do Porto					Quantity	
Verif.	Eduardo A.	26/03/2020						Mass	
Aprov.	Gerrit K.	27/03/2020	ISO 2768	mK	Scale- 100:1		A4	Treatment	None
Name	Cylindrical part of the waffling							Material	AISI 420
								Drawing	2

1/1

8.2 Appendix 2- Practical test

8.2.1 Appendix 2.1 - Parameters of the simulation

Table 45 - Representation of the numbers and their parameters.

Number	Parameter
3	Friction
4	Material thickness
5	Material height
6	Material depth
7	Yield stress
8	Young's modulus
9	Anisotropy
10	Bending angle
11	Force/area
13	Tool width
14	Radius or tool depth

Table 46 - parameter of the simulation to replicate the practical test

3 μ	**4** $[mm]$	**5** $[mm]$	**6** $[mm]$	**7** $[MPa$	**8** $[MPa]$	**9**	**10** [Degrees]	**11** $[MPa]$	**13 and 14** $[mm]$
0.15	0.3	0.35	0.35	250	210000	1.4	0.58	585.93	0,12
0.15	0.3	0.35	0.35	250	210000	1.4	0.58	781.25	0,12
0.15	0.3	0.35	0.35	250	210000	1.4	0.58	1138	0,12
0.15	0.3	0.35	0.35	250	210000	1.4	0.58	2083	0,12
0.15	0.3	0.35	0.35	250	210000	1.4	0.63	585.93	0,12
0.15	0.3	0.35	0.35	250	210000	1.4	0.63	781.25	0,12
0.15	0.3	0.35	0.35	250	210000	1.4	0.63	1138	0,12
0.15	0.3	0.35	0.35	250	210000	1.4	0.63	2083	0,12
0.15	0.3	0.35	0.35	250	210000	1.4	0.73	585.93	0,12
0.15	0.3	0.35	0.35	250	210000	1.4	0.73	781.25	0,12
0.15	0.3	0.35	0.35	250	210000	1.4	0.73	1138	0,12
0.15	0.3	0.35	0.35	250	210000	1.4	0.73	2083	0,12
0.15	0.3	0.35	0.35	250	210000	1.4	0.805	585.93	0,12
0.15	0.3	0.35	0.35	250	210000	1.4	0.805	781.25	0,12
0.15	0.3	0.35	0.35	250	210000	1.4	0.805	1138	0,12
0.15	0.3	0.35	0.35	250	210000	1.4	0.805	2083	0,12

8.3 Appendix 3- Screening

Table 47 - Plackett-Burman with 11 parameters for the cylindrical.

3	4	5	6	7	8	9	10	11	13	14
-1	-1	-1	-1	-1	-1	-1	-1	1	1	1
-1	-1	-1	1	-1	1	1	1	-1	1	1
-1	-1	1	-1	1	1	1	-1	-1	1	-1
-1	-1	1	1	1	-1	-1	1	1	1	-1
-1	1	-1	-1	1	1	-1	1	-1	-1	1
-1	1	-1	1	1	-1	1	-1	1	-1	1
-1	1	1	-1	-1	-1	1	1	1	-1	-1
-1	1	1	1	-1	1	-1	-1	-1	-1	-1
1	-1	-1	-1	1	-1	1	1	-1	-1	-1
1	-1	-1	1	1	1	-1	-1	1	-1	-1
1	-1	1	-1	-1	1	-1	1	1	-1	1
1	-1	1	1	-1	-1	1	-1	-1	-1	1
1	1	-1	-1	-1	1	1	-1	1	1	-1
1	1	-1	1	-1	-1	-1	1	-1	1	-1
1	1	1	-1	1	-1	-1	-1	-1	1	1
1	1	1	1	1	1	1	1	1	1	1

Table 48 - Parameters and their variation for conical screening.

3	4	5	6	7	8	9	10	11	13 and 14
μ	$[mm]$	$[mm]$	$[mm]$	$[MPa]$	$[MPa]$		[Degrees]	$[MPa]$	$[mm]$
0,1	0,27	0,35	0,35	200	190000	1,2	0	1125	0,1693
0,1	0,27	0,35	0,4	200	230000	1,6	6,4	500	0,1693
0,1	0,27	0,4	0,35	300	230000	1,6	0	500	0,1693
0,1	0,27	0,4	0,4	300	190000	1,2	6,4	1125	0,1693
0,1	0,33	0,35	0,35	300	230000	1,2	6,4	500	0,0564
0,1	0,33	0,35	0,4	300	190000	1,6	0	1125	0,0564
0,1	0,33	0,4	0,35	200	190000	1,6	6,4	1125	0,0564
0,1	0,33	0,4	0,4	200	230000	1,2	0	500	0,0564
0,2	0,27	0,35	0,35	300	190000	1,6	6,4	500	0,0564
0,2	0,27	0,35	0,4	300	230000	1,2	0	1125	0,0564
0,2	0,27	0,4	0,35	200	230000	1,2	6,4	1125	0,0564
0,2	0,27	0,4	0,4	200	190000	1,6	0	500	0,0564
0,2	0,33	0,35	0,35	200	230000	1,6	0	1125	0,1693
0,2	0,33	0,35	0,4	200	190000	1,2	6,4	500	0,1693
0,2	0,33	0,4	0,35	300	190000	1,2	0	500	0,1693
0,2	0,33	0,4	0,4	300	230000	1,6	6,4	1125	0,1693

Table 49 - Parameters and their variation for cylindrical screening.

3	4	5	6	7	8	9	10	11	13	14
μ	$[mm]$	$[mm]$	$[mm]$	$[MPa]$	$[MPa]$		[Degrees]	$[MPa]$	$[mm]$	$[mm]$
0,1	0,27	0,35	0,35	200	190000	1,2	0	80	1	0,375
0,1	0,27	0,35	0,4	200	230000	1,6	6,4	53,33	1	0,375
0,1	0,27	0,4	0,35	300	230000	1,6	0	53,33	1	0,1
0,1	0,27	0,4	0,4	300	190000	1,2	6,4	80	1	0,1
0,1	0,33	0,35	0,35	300	230000	1,2	6,4	53,33	0,185	0,375
0,1	0,33	0,35	0,4	300	190000	1,6	0	80	0,185	0,375
0,1	0,33	0,4	0,35	200	190000	1,6	6,4	80	0,185	0,1
0,1	0,33	0,4	0,4	200	230000	1,2	0	53,33	0,185	0,1
0,2	0,27	0,35	0,35	300	190000	1,6	6,4	53,33	0,185	0,1
0,2	0,27	0,35	0,4	300	230000	1,2	0	80	0,185	0,1
0,2	0,27	0,4	0,35	200	230000	1,2	6,4	80	0,185	0,375
0,2	0,27	0,4	0,4	200	190000	1,6	0	53,33	0,185	0,375
0,2	0,33	0,35	0,35	200	230000	1,6	0	80	1	0,1
0,2	0,33	0,35	0,4	200	190000	1,2	6,4	53,33	1	0,1
0,2	0,33	0,4	0,35	300	190000	1,2	0	53,33	1	0,375
0,2	0,33	0,4	0,4	300	230000	1,6	6,4	80	1	0,375

8.4 Appendix 4- Metamodels validation for the FFD plus the 32 LHD for the left right angle.

8.4.1 Appendix 4.1- RSM model

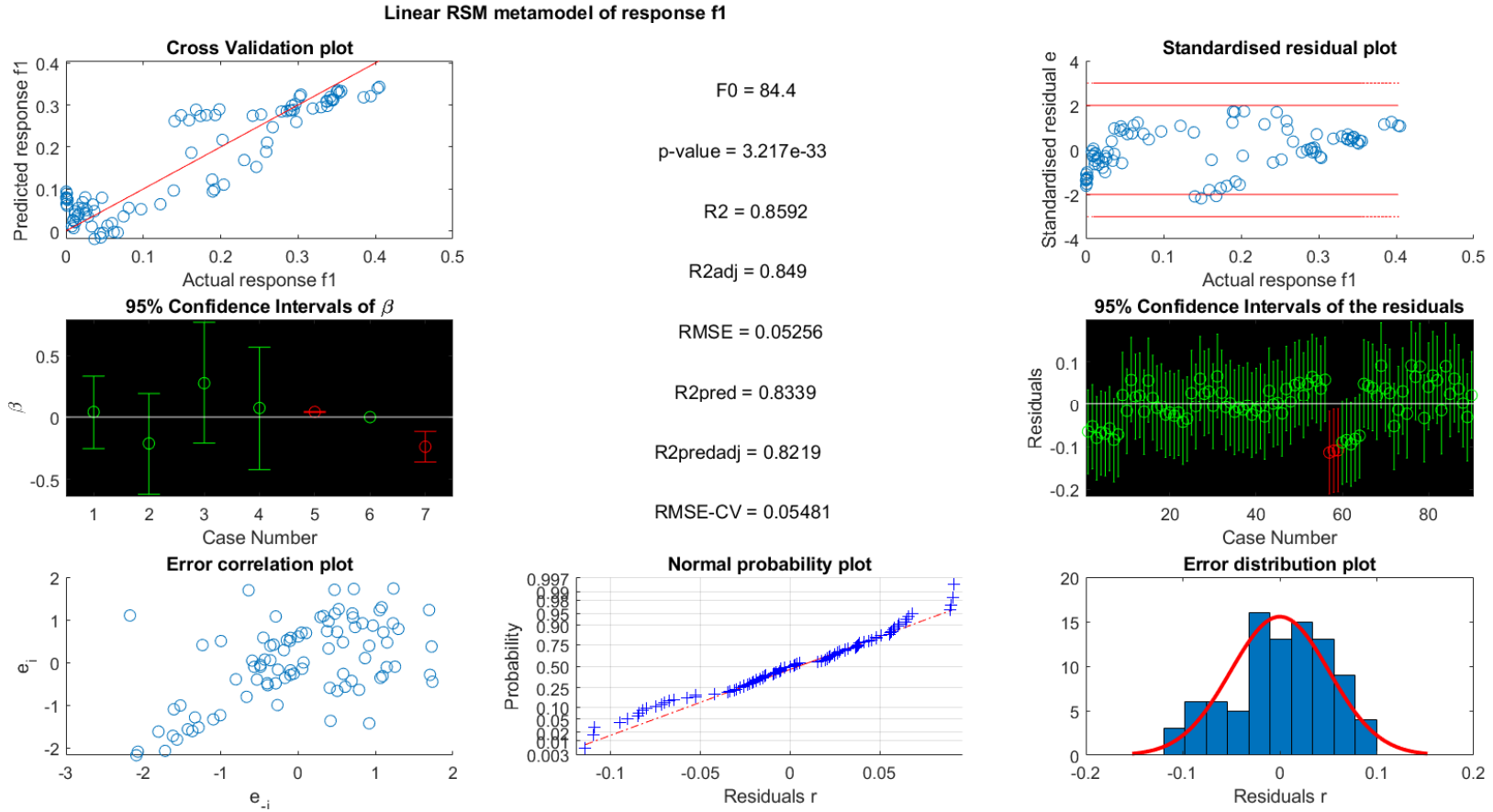

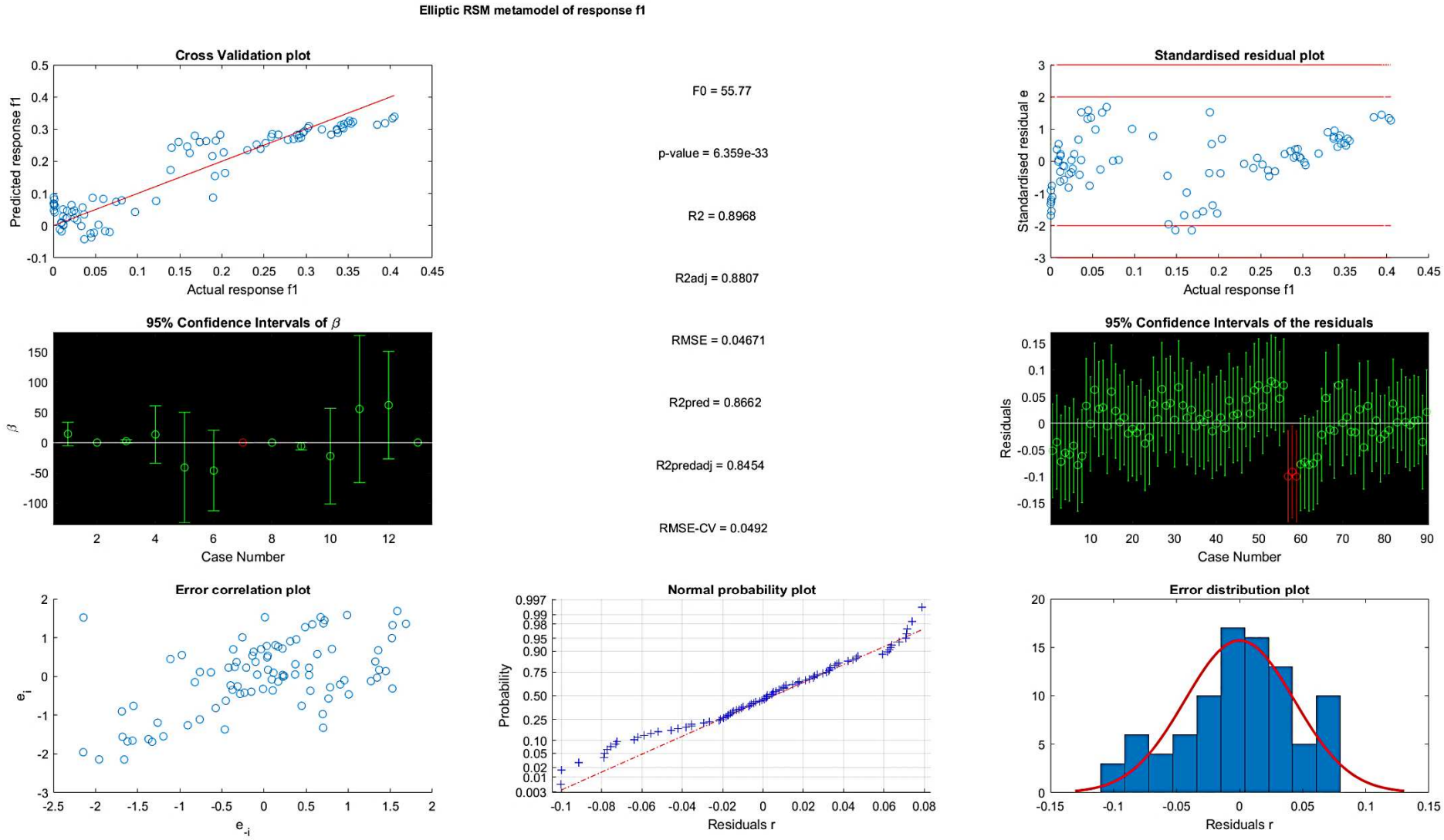
Elliptic RSM metamodel of response f1
Cross Validation plot
Predicted response f1
Actual response f1
F0 = 55.77
p-value = 6.359e-33
R2 = 0.8968
R2adj = 0.8807
RMSE = 0.04671
R2pred = 0.8662
R2predadj = 0.8454
RMSE-CV = 0.0492
Standardised residual plot
Standardised residual e
Actual response f1
95% Confidence Intervals of β
β
Case Number
95% Confidence Intervals of the residuals
Residuals
Case Number
Error correlation plot
e_i
e_-i
Normal probability plot
Probability
Residuals r
Error distribution plot
Residuals r

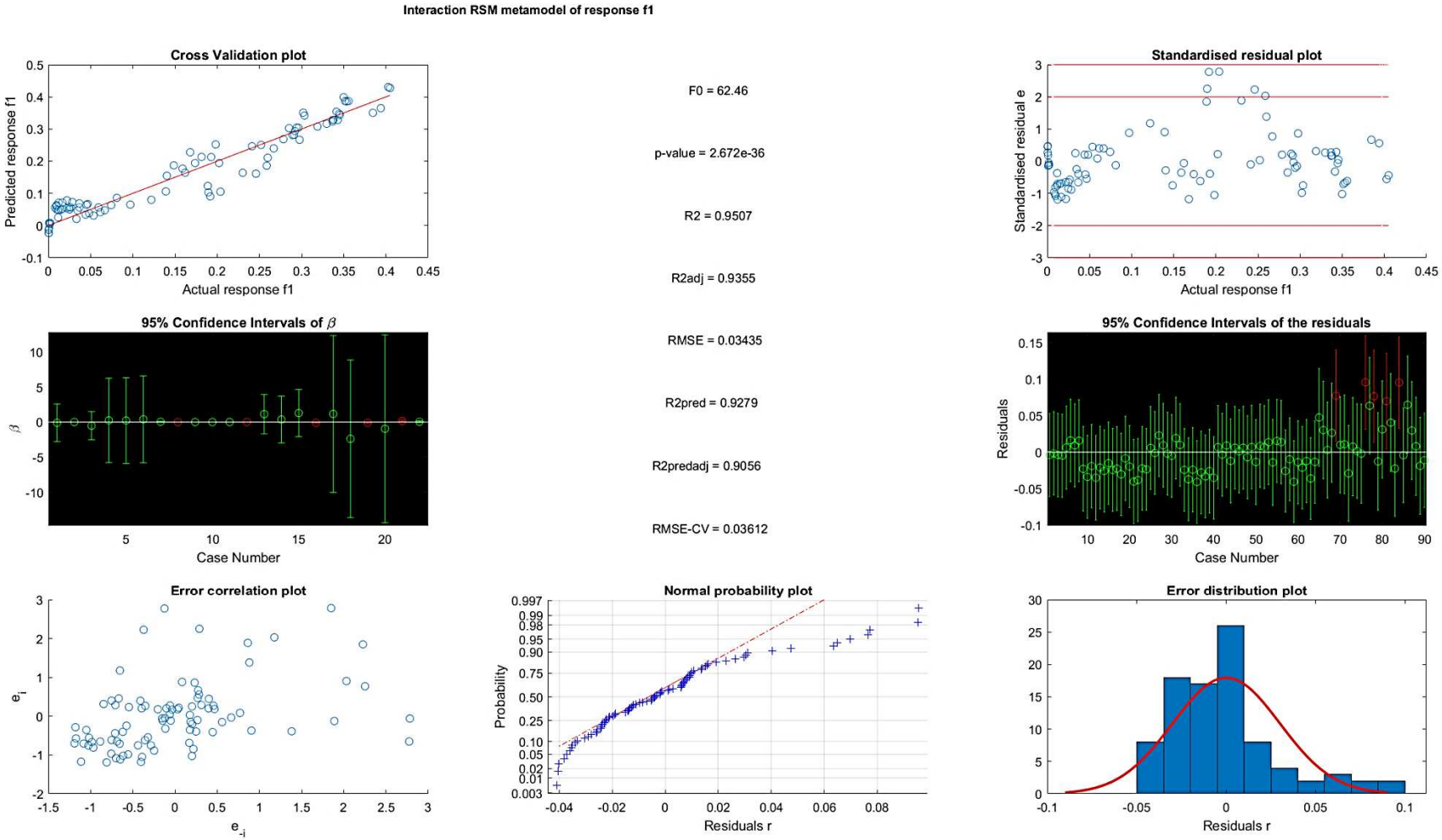
Interaction RSM metamodel of response f1
Cross Validation plot
Predicted response f1
Actual response f1
F0 = 62.46
p-value = 2.672e-36
R2 = 0.9507
R2adj = 0.9355
RMSE = 0.03435
R2pred = 0.9279
R2predadj = 0.9056
RMSE-CV = 0.03612
Standardised residual plot
Standardised residual e
Actual response f1
95% Confidence Intervals of β
β
Case Number
95% Confidence Intervals of the residuals
Residuals
Case Number
Error correlation plot
e_i
e_-i
Normal probability plot
Probability
Residuals r
Error distribution plot
Residuals r

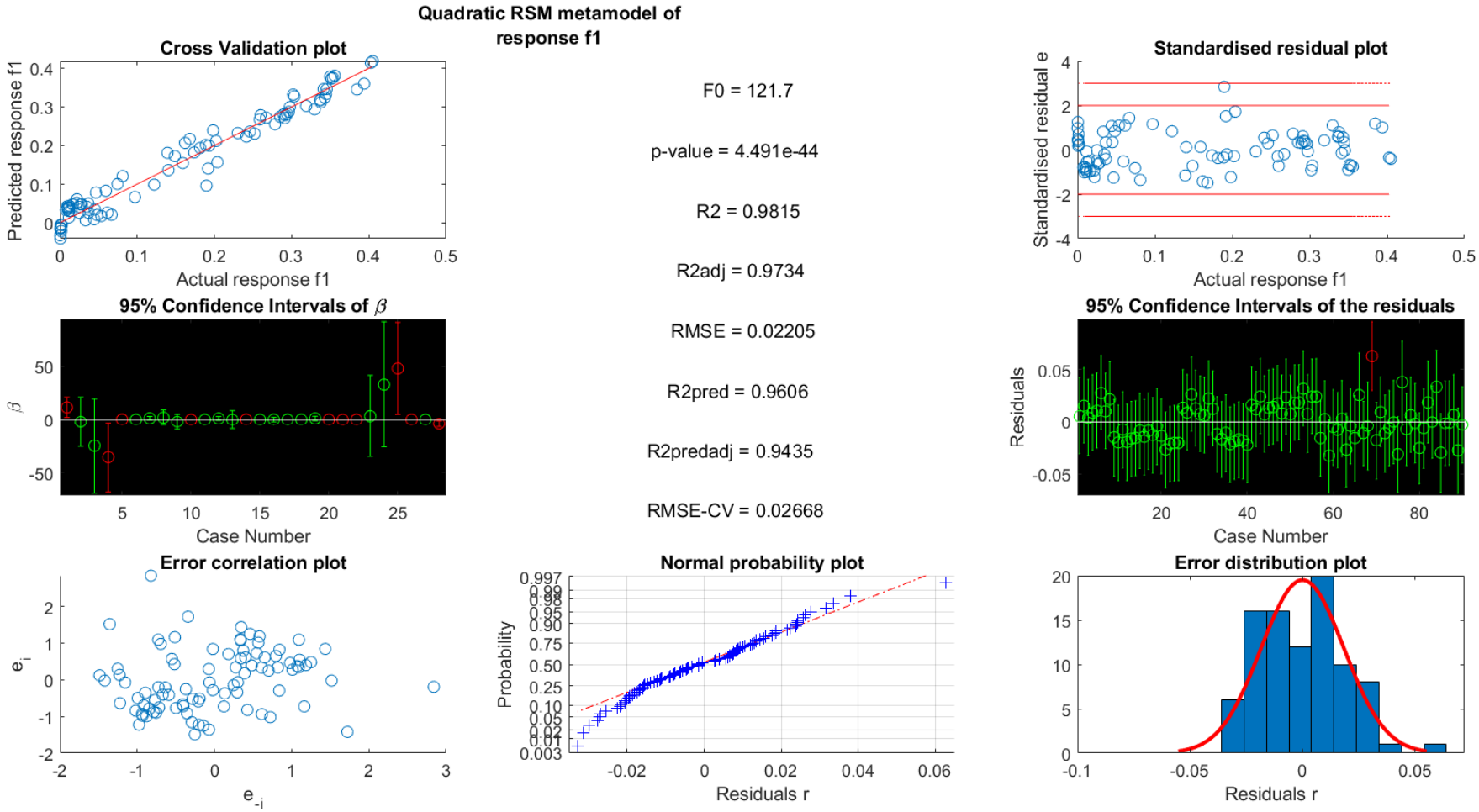

8.4.2 Appendix 4.2- Kriging model

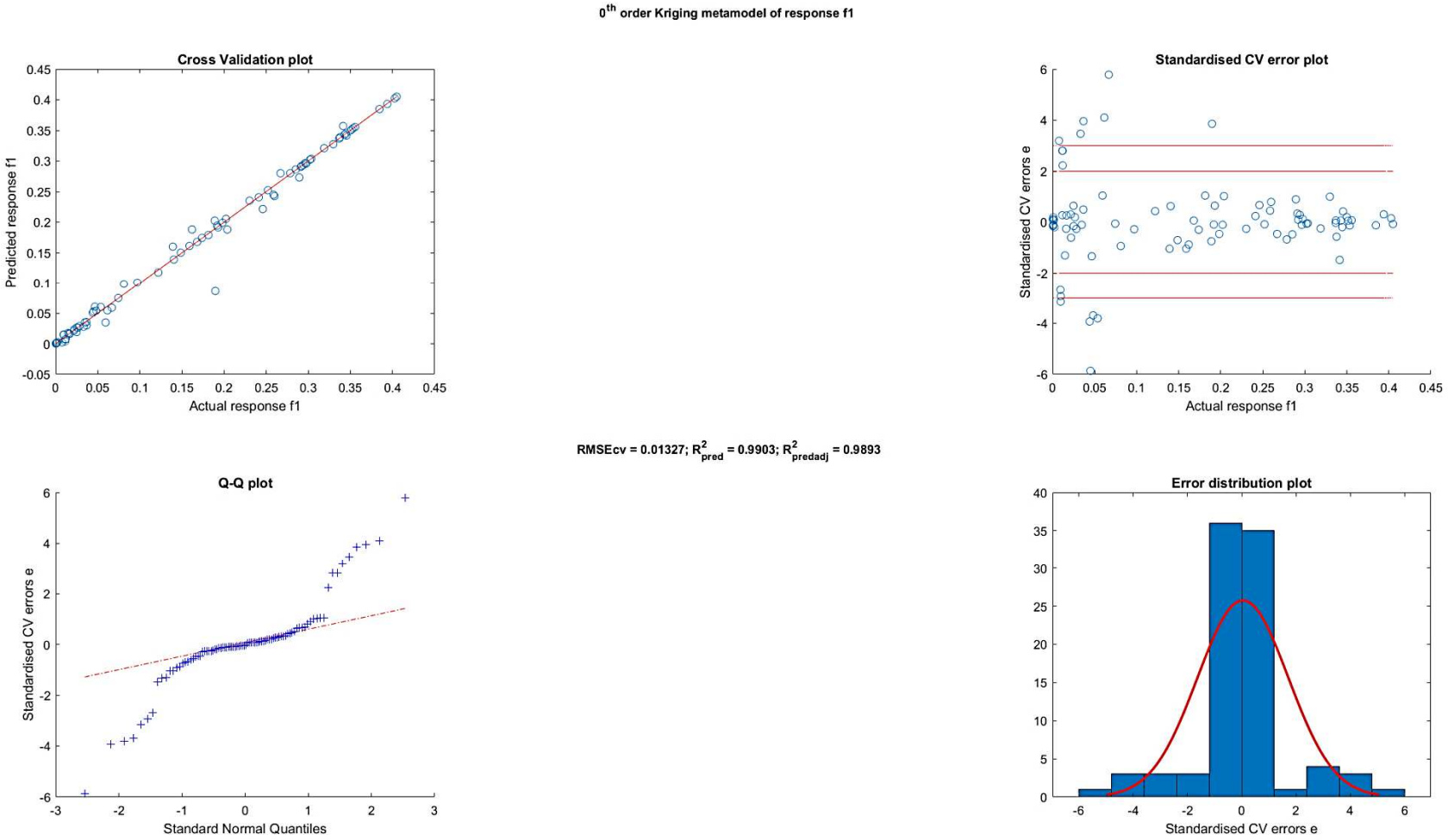
0th order Kriging metamodel of response f1
Cross Validation plot
Predicted response f1
Actual response f1
Standardised CV error plot
Standardised CV errors e
Actual response f1
RMSEcv = 0.01327; R2pred = 0.9903; R2predadj = 0.9893
Q-Q plot
Standardised CV errors e
Standard Normal Quantiles
Error distribution plot
Standardised CV errors e

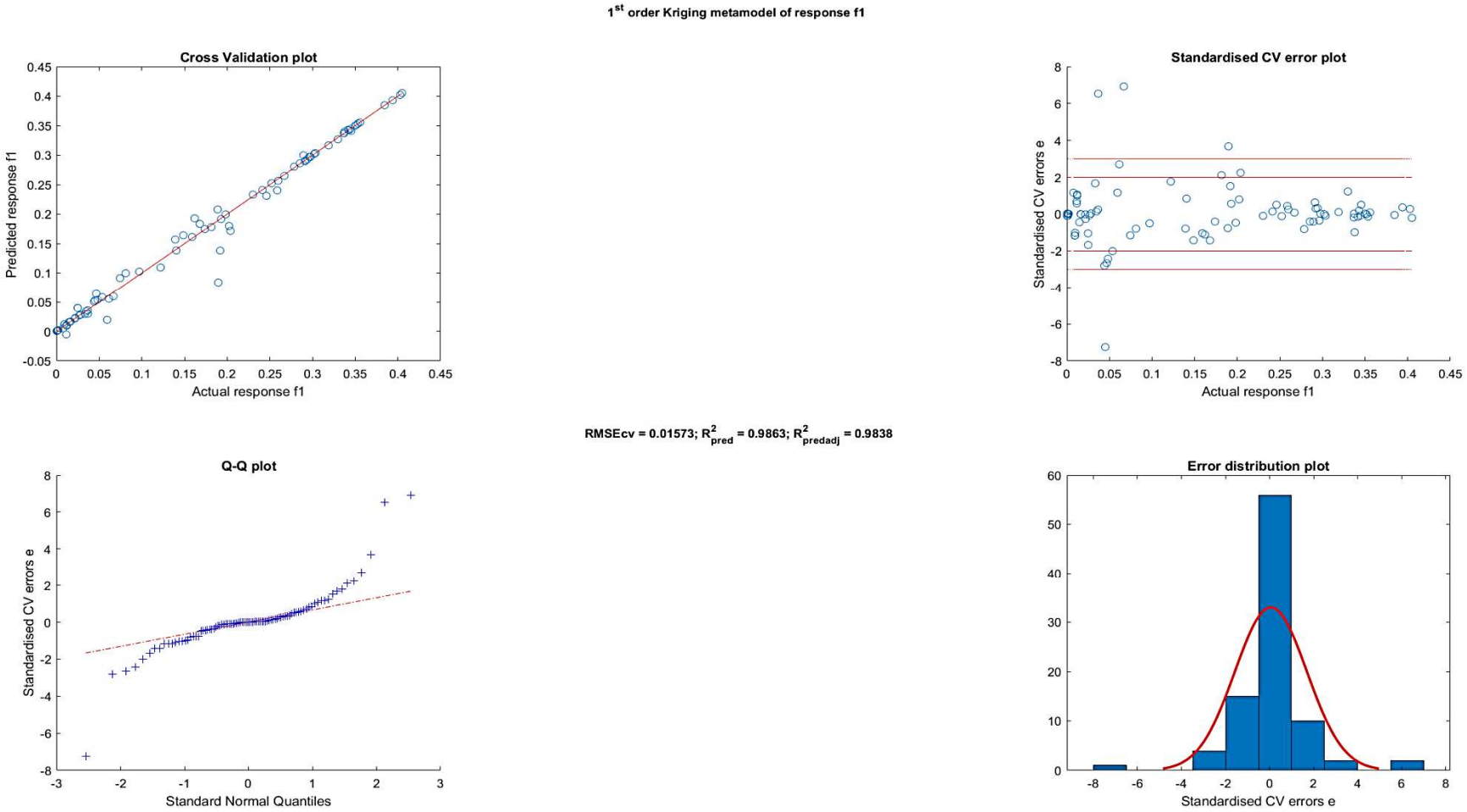
1st order Kriging metamodel of response f1
Cross Validation plot
Predicted response f1
Actual response f1
Standardised CV error plot
Standardised CV errors e
Actual response f1
RMSEcv = 0.01573; R²pred = 0.9863; R²predadj = 0.9838
Q-Q plot
Standardised CV errors e
Standard Normal Quantiles
Error distribution plot
Standardised CV errors e

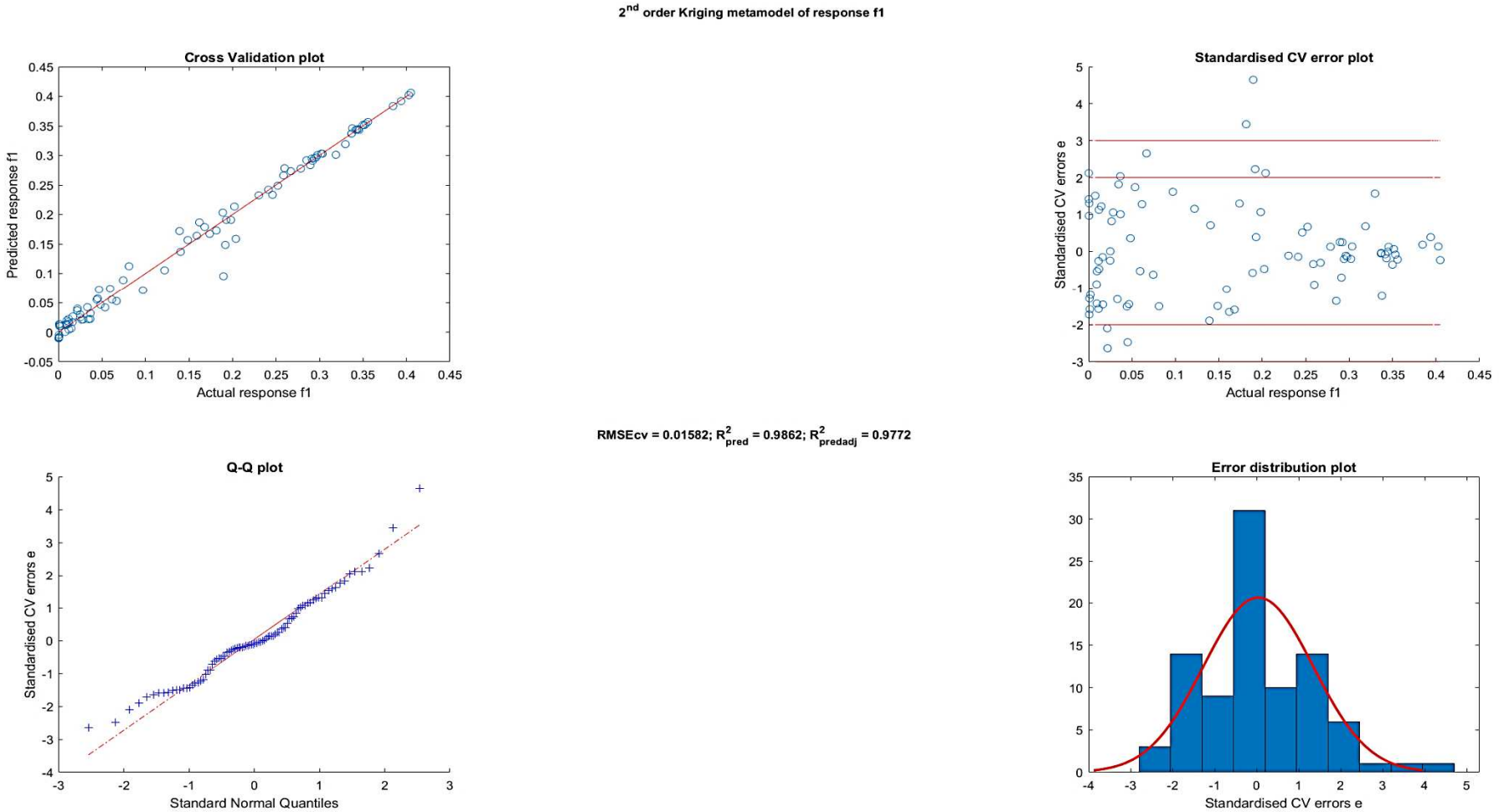
2nd order Kriging metamodel of response f1
Cross Validation plot
Predicted response f1
Actual response f1
Standardised CV error plot
Standardised CV errors e
Actual response f1
RMSEcv = 0.01582; R2pred = 0.9862; R2predadj = 0.9772
Q-Q plot
Standardised CV errors e
Standard Normal Quantiles
Error distribution plot
Standardised CV errors e

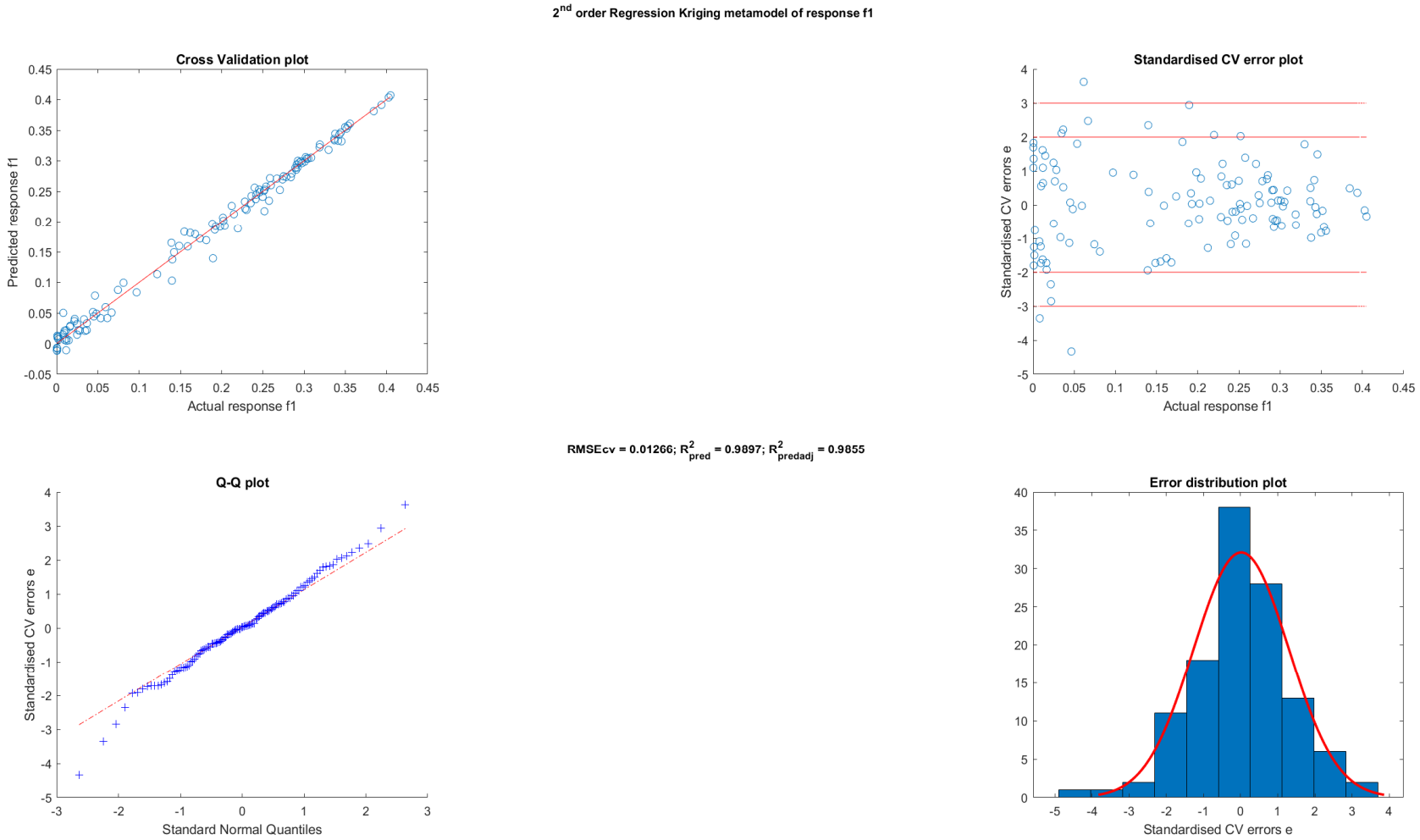
2nd order Regression Kriging metamodel of response f1
Cross Validation plot
Predicted response f1
Actual response f1
Standardised CV error plot
Standardised CV errors e
Actual response f1
RMSEcv = 0.01266; R2pred = 0.9897; R2predadj = 0.9855
Q-Q plot
Standardised CV errors e
Standard Normal Quantiles
Error distribution plot
Standardised CV errors e

8.5 Appendix 5- Metamodels validation for the FFD plus the 32 LHD for the front back angle

8.5.1 Appendix 5.1 -RSM model

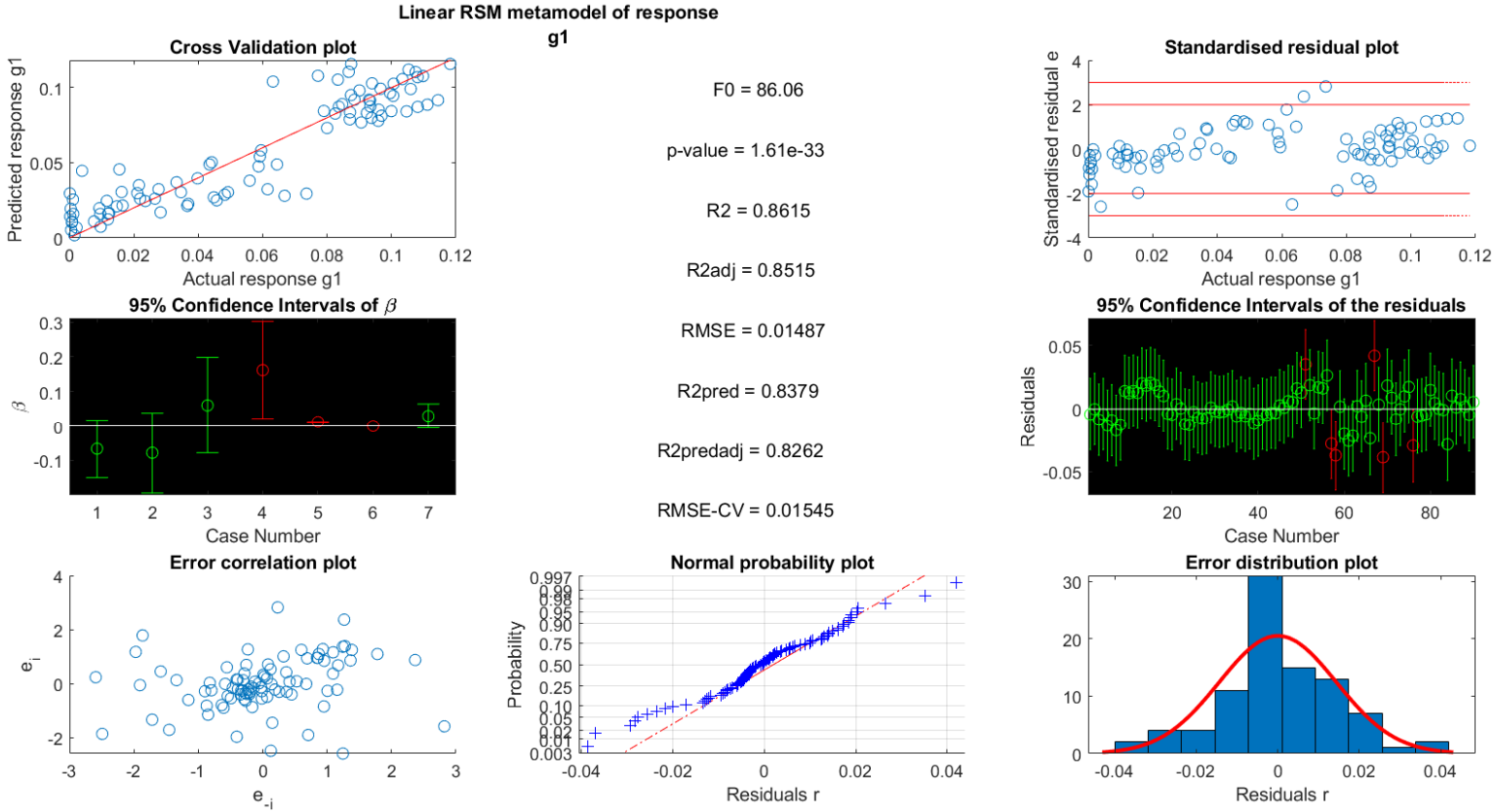

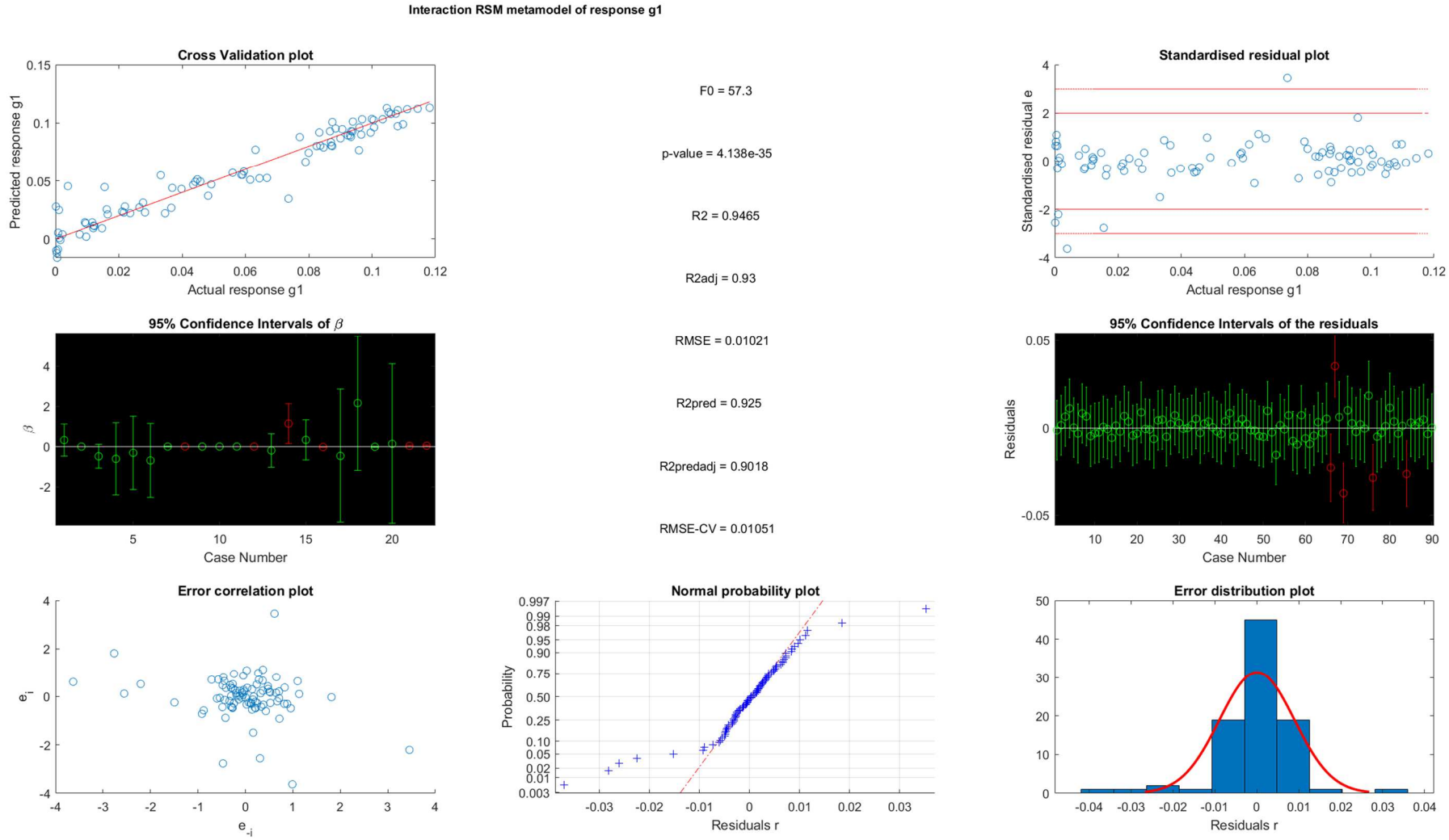
Interaction RSM metamodel of response g1
Cross Validation plot
Predicted response g1
Actual response g1
F0 = 57.3
p-value = 4.138e-35
R2 = 0.9465
R2adj = 0.93
RMSE = 0.01021
R2pred = 0.925
R2predadj = 0.9018
RMSE-CV = 0.01051
Standardised residual plot
Standardised residual e
Actual response g1
95% Confidence Intervals of β
β
Case Number
95% Confidence Intervals of the residuals
Residuals
Case Number
Error correlation plot
e_i
e_-i
Normal probability plot
Probability
Residuals r
Error distribution plot
Residuals r

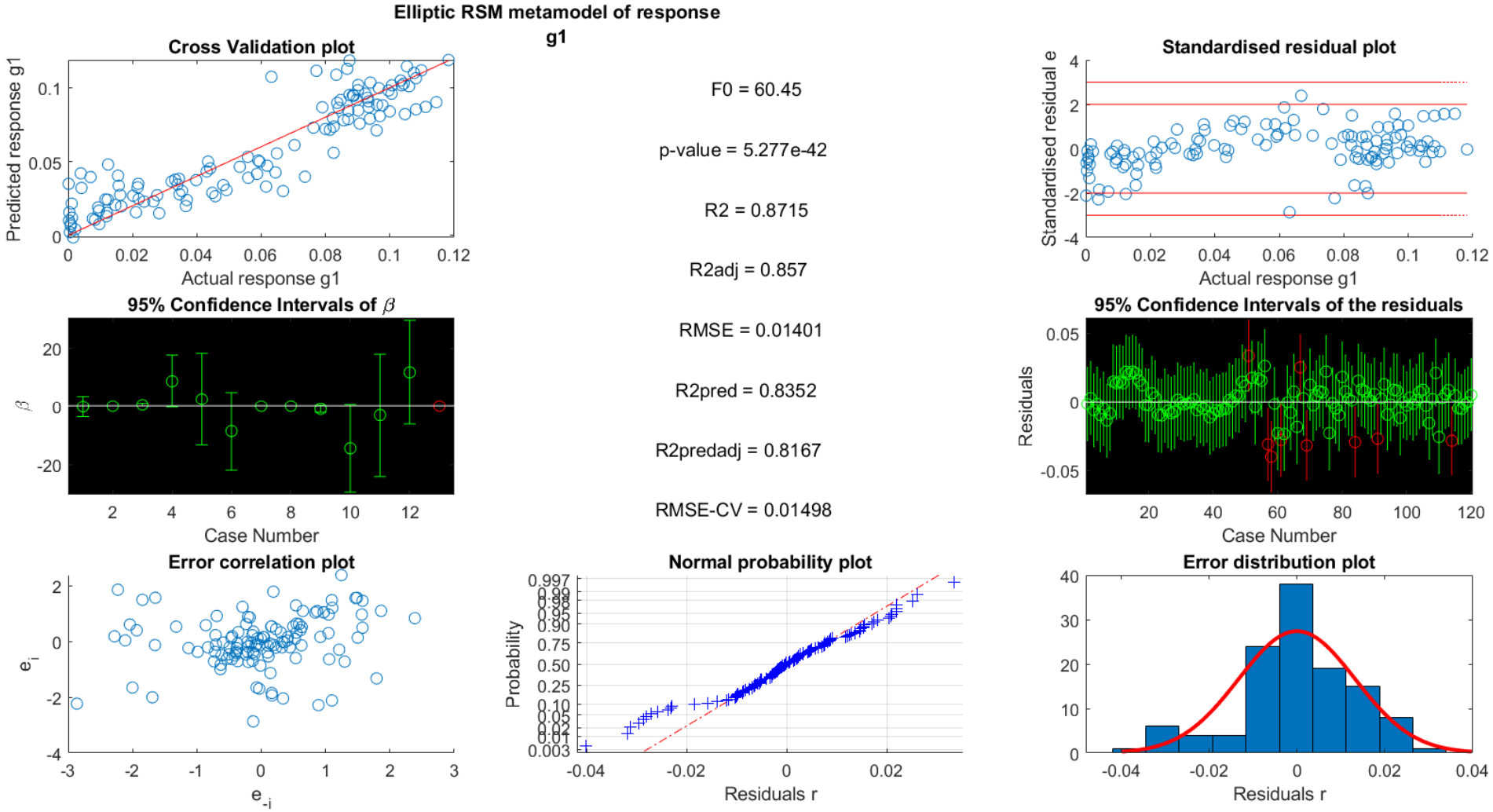
Elliptic RSM metamodel of response
g1
Cross Validation plot
Predicted response g1
Actual response g1
F0 = 60.45
p-value = 5.277e-42
R2 = 0.8715
R2adj = 0.857
RMSE = 0.01401
R2pred = 0.8352
R2predadj = 0.8167
RMSE-CV = 0.01498
Standardised residual plot
Standardised residual e
Actual response g1
95% Confidence Intervals of β
β
Case Number
95% Confidence Intervals of the residuals
Residuals
Case Number
Error correlation plot
e_i
e_-i
Normal probability plot
Probability
Residuals r
Error distribution plot
Residuals r

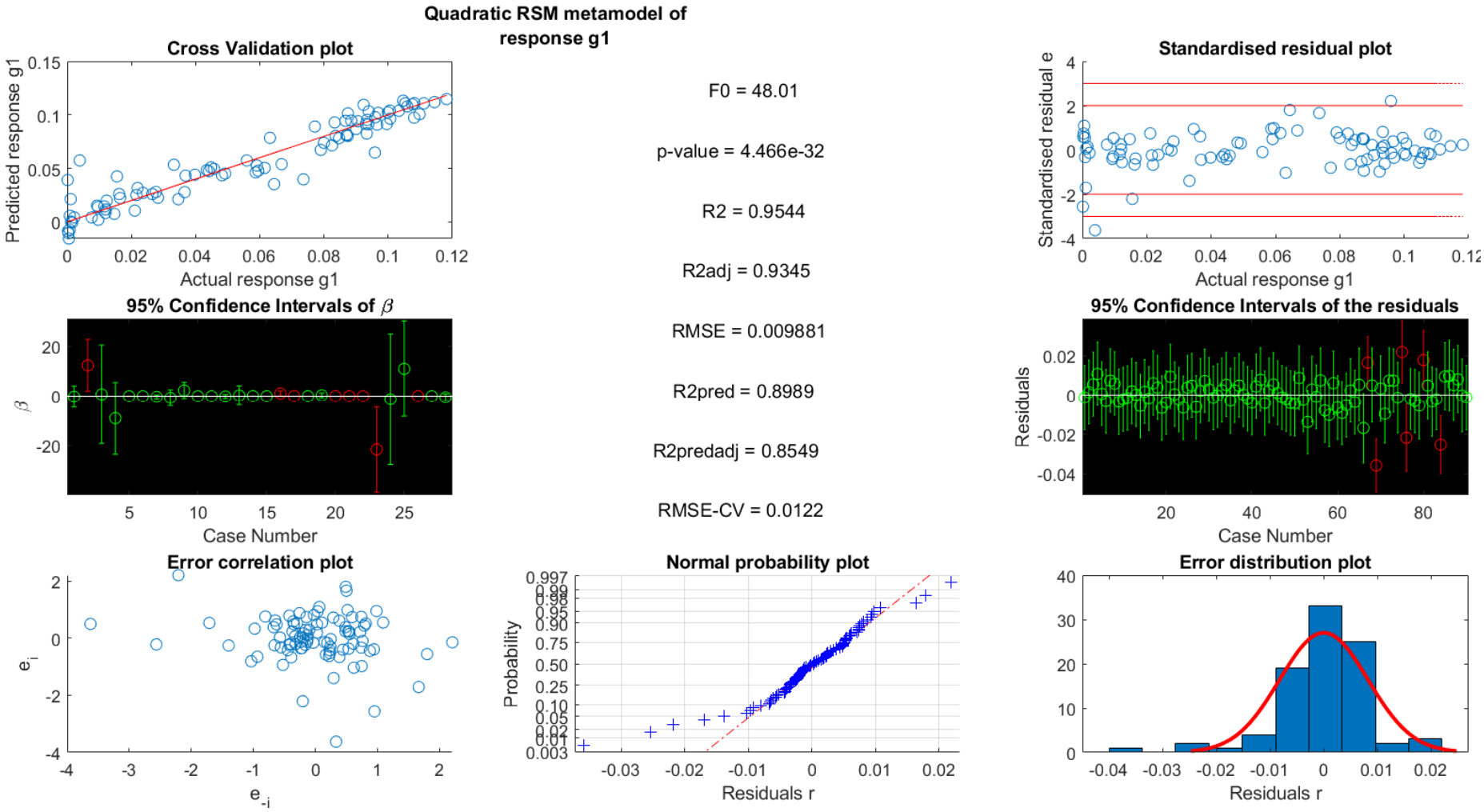
Quadratic RSM metamodel of response g1
Cross Validation plot
Predicted response g1
Actual response g1
F0 = 48.01
p-value = 4.466e-32
R2 = 0.9544
R2adj = 0.9345
RMSE = 0.009881
R2pred = 0.8989
R2predadj = 0.8549
RMSE-CV = 0.0122
Standardised residual plot
Standardised residual e
Actual response g1
95% Confidence Intervals of β
β
Case Number
95% Confidence Intervals of the residuals
Residuals
Case Number
Error correlation plot
e_i
e_-i
Normal probability plot
Probability
Residuals r
Error distribution plot
Residuals r

8.5.2 Appendix 5.2 -Kriging

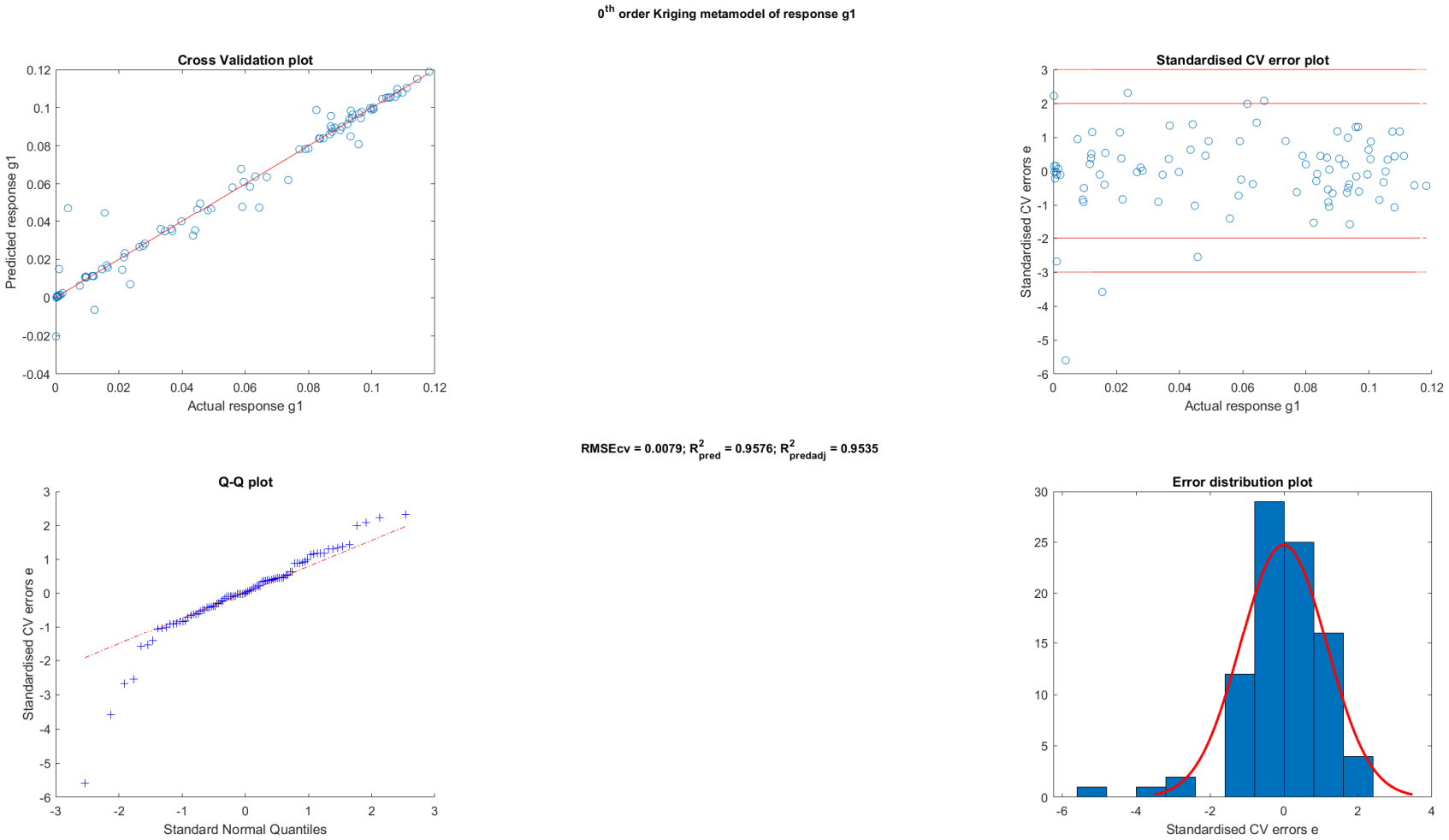

1st order Kriging metamodel of response g1

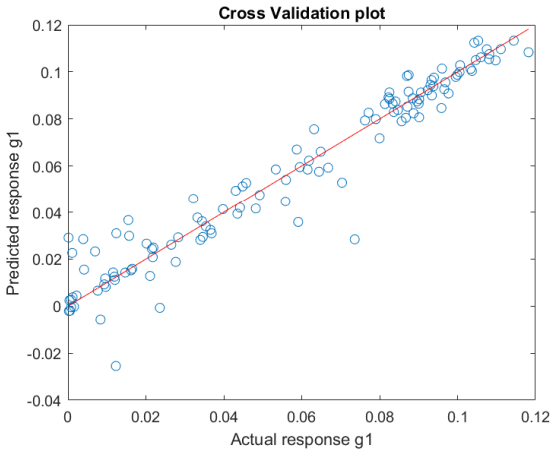

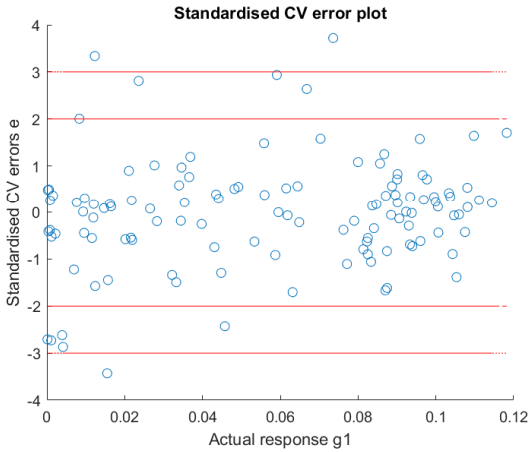

RMSEcv = 0.009596; R^2_{pred} = 0.9323; $R^2_{predadj}$ = 0.9233

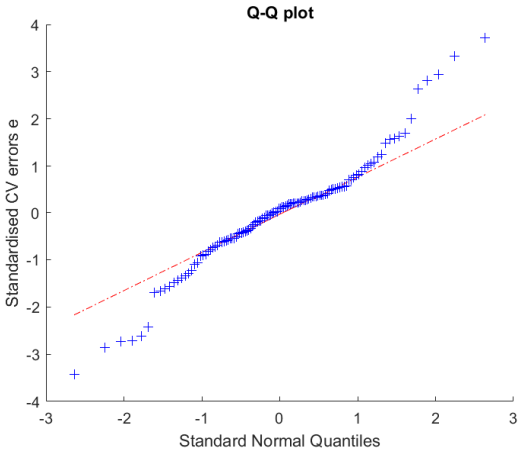

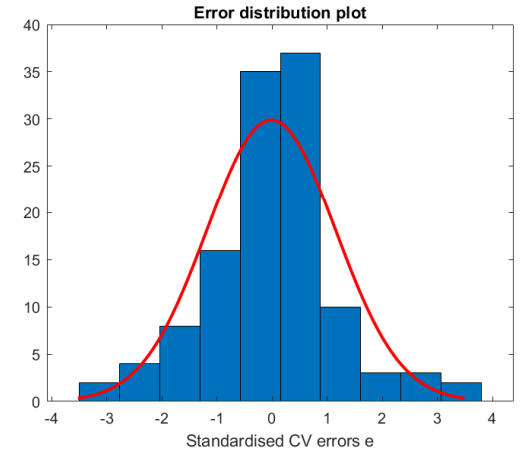

2^{nd} order Kriging metamodel of response g1

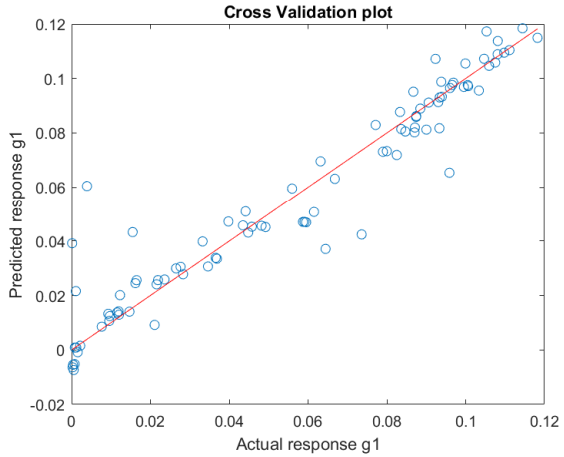

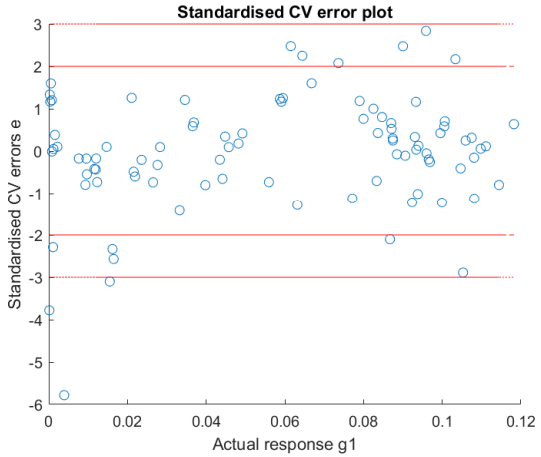

RMSEcv = 0.01117; R^2_{pred} = 0.9153; $R^2_{predadj}$ = 0.8604

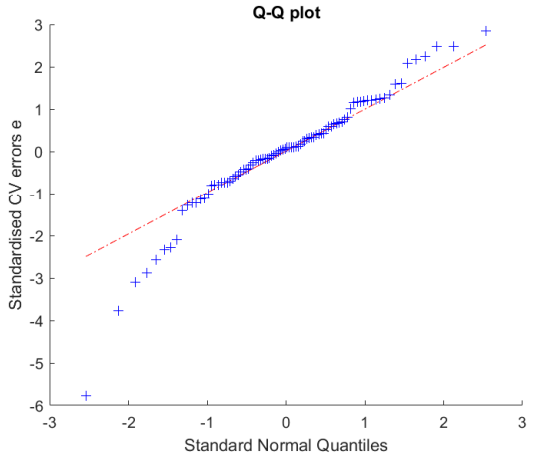

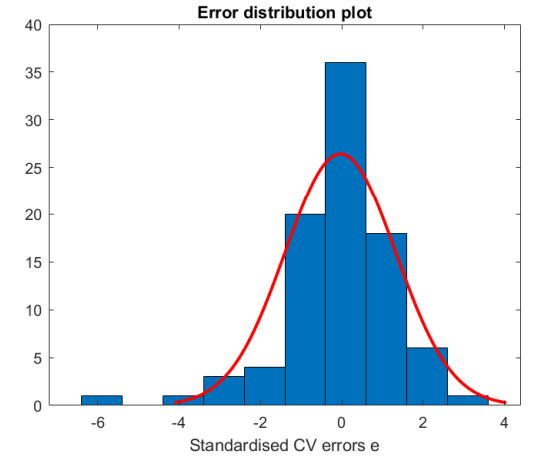

2nd order Regression Kriging metamodel of response g1

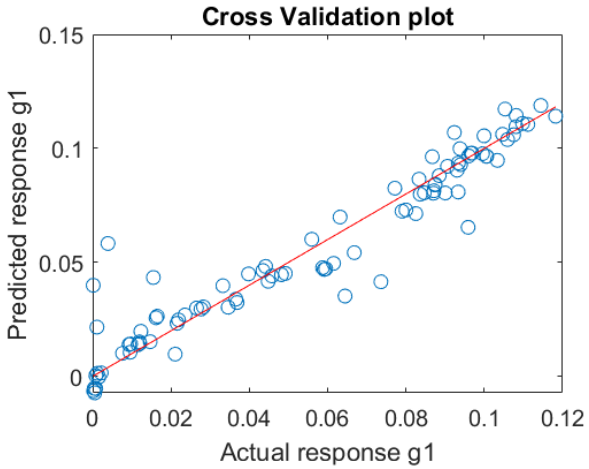

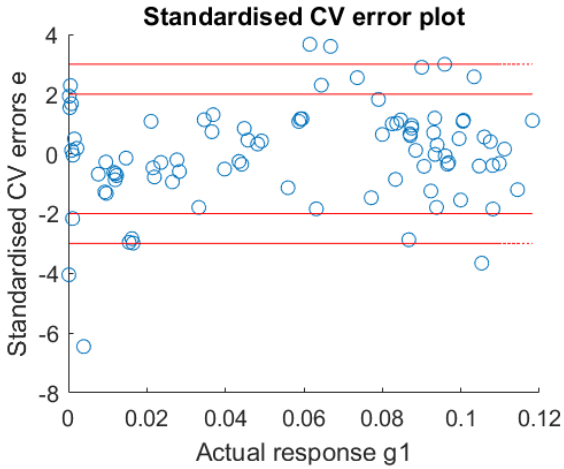

RMSEcv = 0.01133; R^2_{pred} = 0.9129; $R^2_{predadj}$ = 0.8565

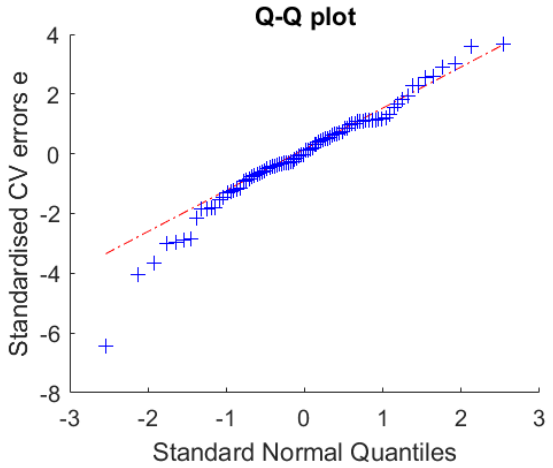

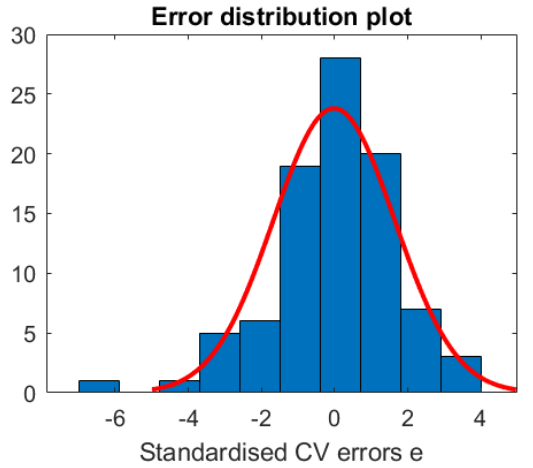

8.6 Appendix 6 - Metamodels validation for the FFD plus the 32 LHD for the thickness

8.6.1 Appendix 6.1 - RSM model

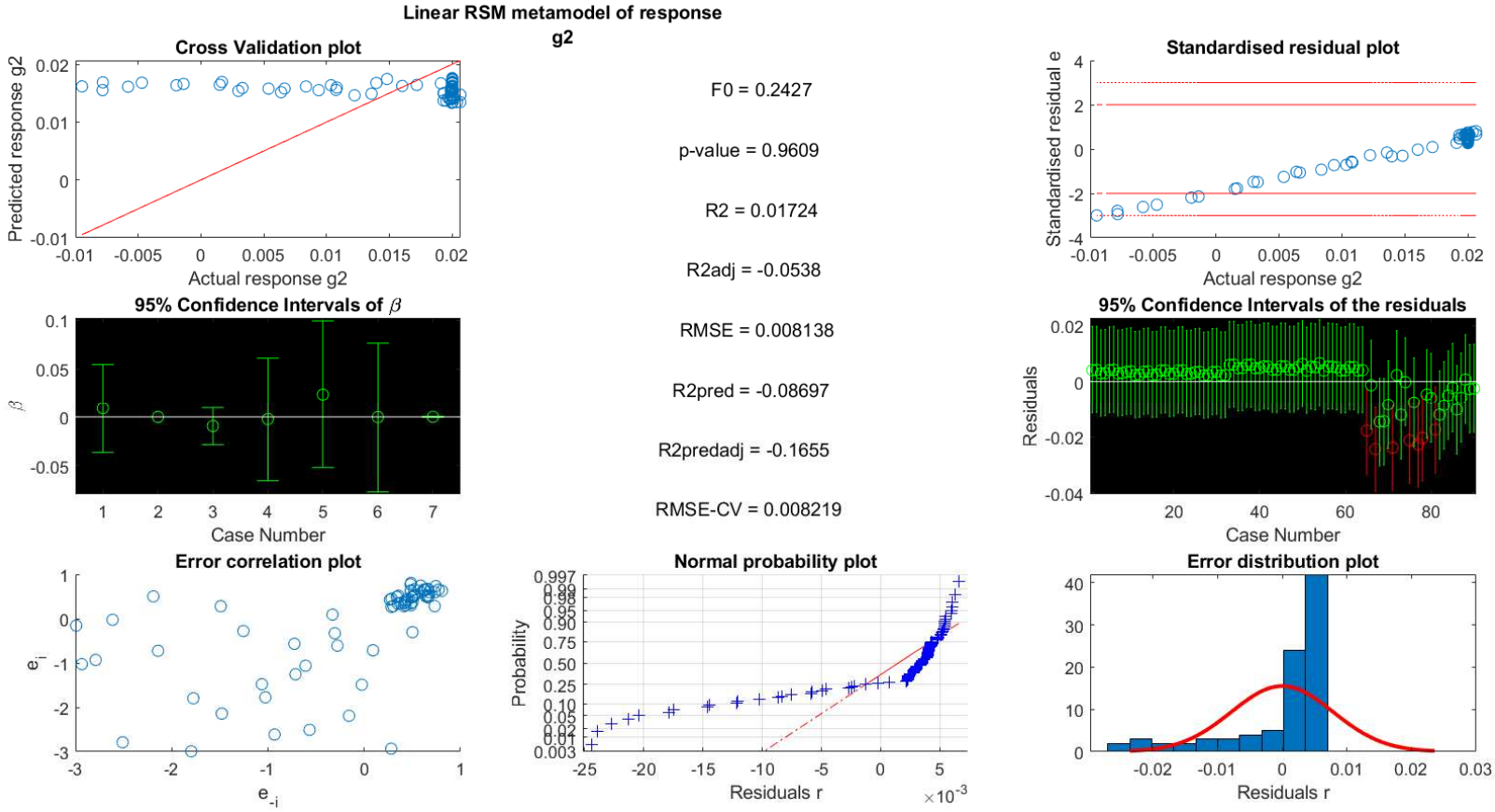

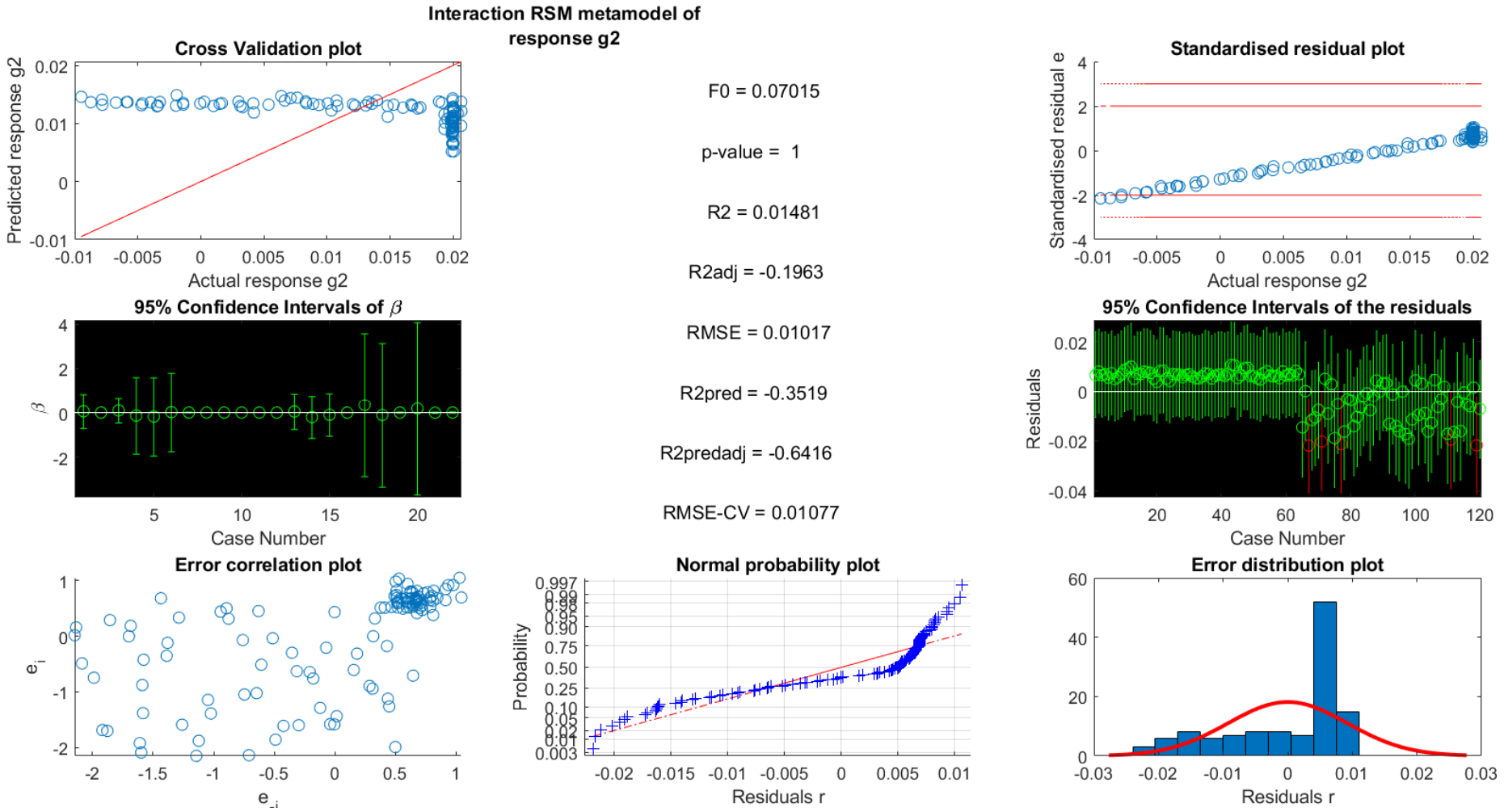
Interaction RSM metamodel of response g2
Cross Validation plot
Predicted response g2
Actual response g2
F0 = 0.07015
p-value = 1
R2 = 0.01481
R2adj = -0.1963
RMSE = 0.01017
R2pred = -0.3519
R2predadj = -0.6416
RMSE-CV = 0.01077
Standardised residual plot
Standardised residual e
Actual response g2
95% Confidence Intervals of β
β
Case Number
95% Confidence Intervals of the residuals
Residuals
Case Number
Error correlation plot
e_i
e_-i
Normal probability plot
Probability
Residuals r
Error distribution plot
Residuals r

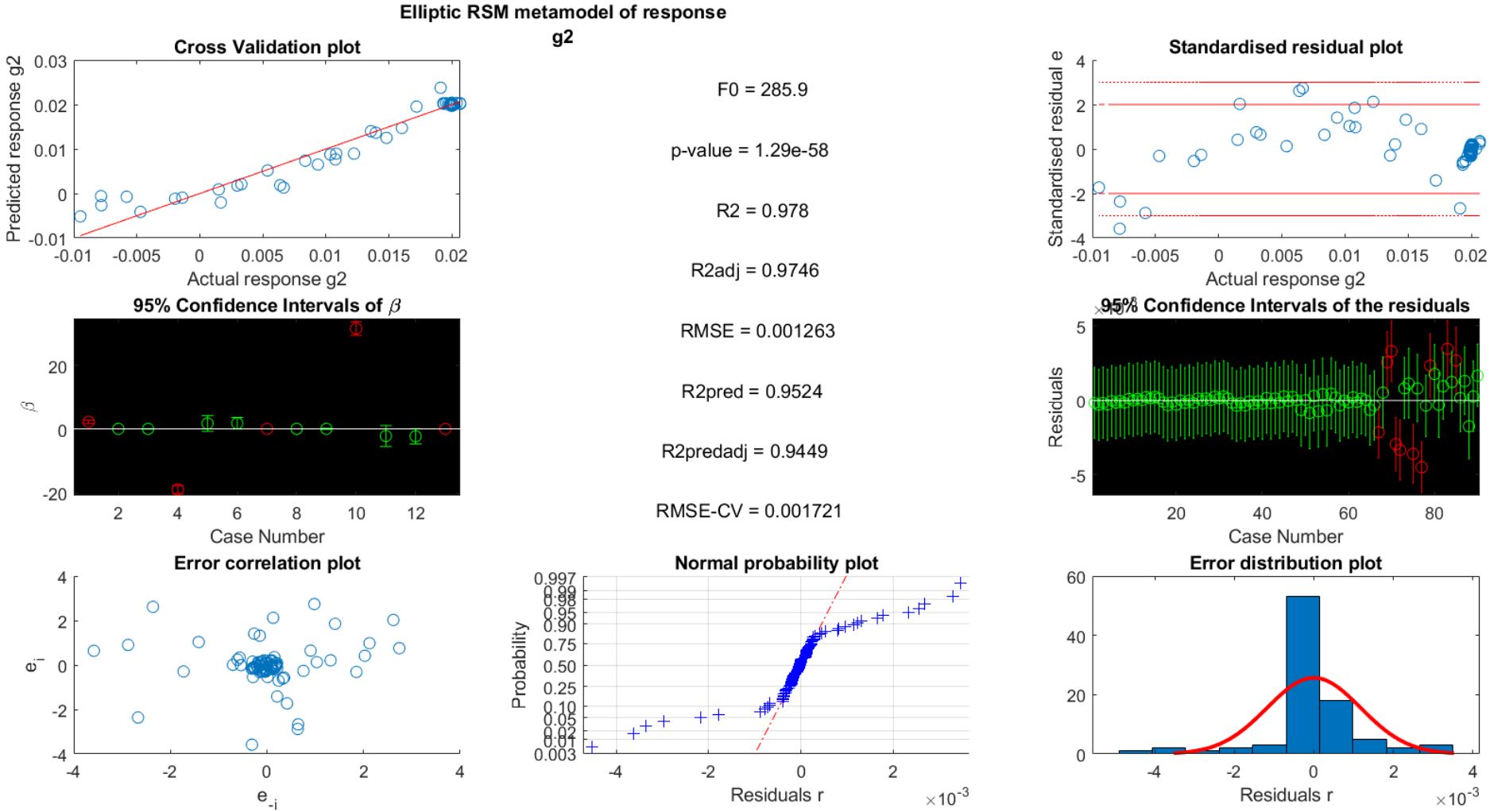
Elliptic RSM metamodel of response
g2
Cross Validation plot
Predicted response g2
Actual response g2
F0 = 285.9
p-value = 1.29e-58
R2 = 0.978
R2adj = 0.9746
RMSE = 0.001263
R2pred = 0.9524
R2predadj = 0.9449
RMSE-CV = 0.001721
Standardised residual plot
Standardised residual e
Actual response g2
95% Confidence Intervals of β
β
Case Number
95% Confidence Intervals of the residuals
Residuals
Case Number
Error correlation plot
e_i
e_-i
Normal probability plot
Probability
Residuals r
Error distribution plot
Residuals r

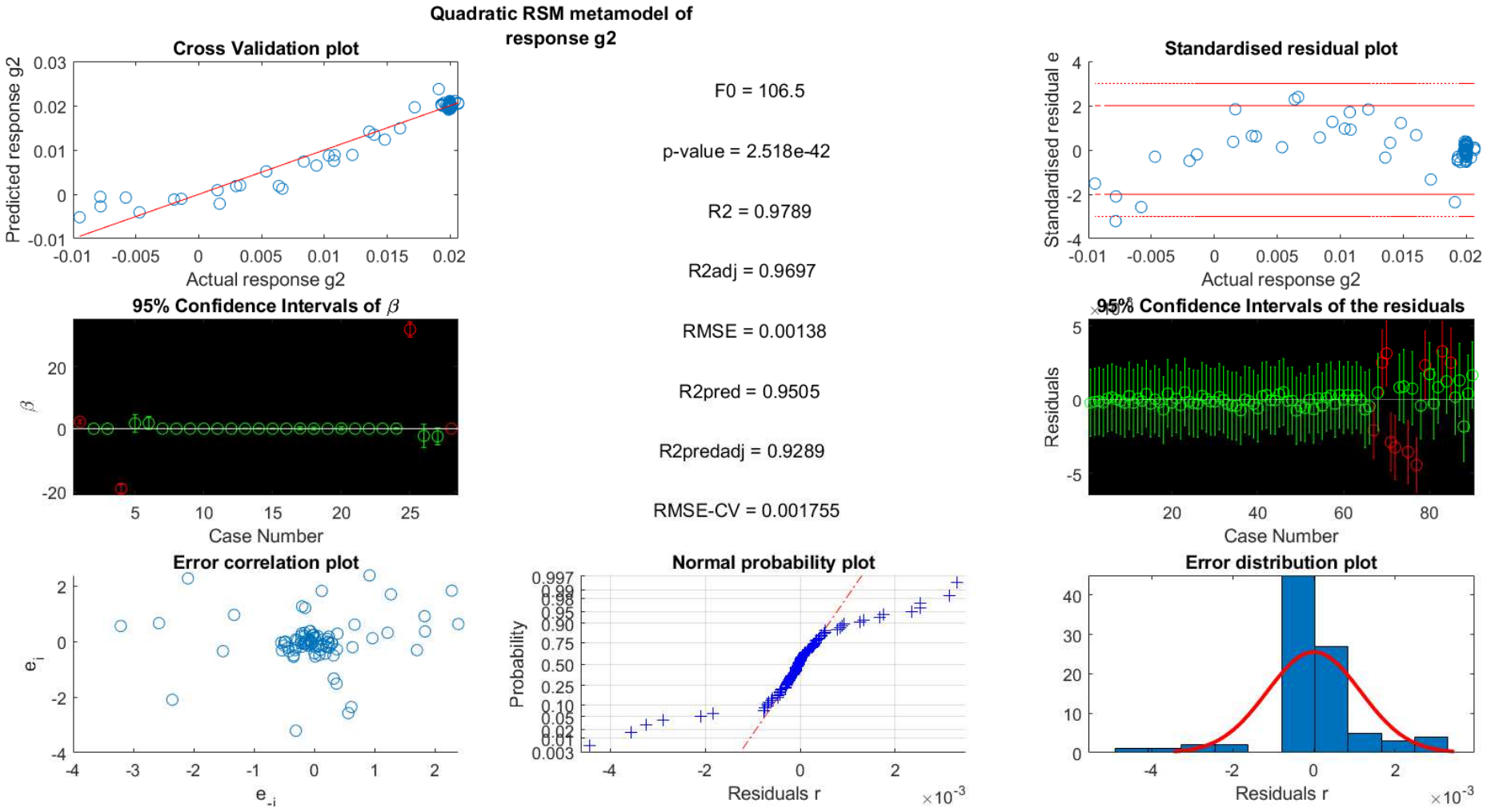
Quadratic RSM metamodel of response g2
Cross Validation plot
Predicted response g2
Actual response g2
F0 = 106.5
p-value = 2.518e-42
R2 = 0.9789
R2adj = 0.9697
RMSE = 0.00138
R2pred = 0.9505
R2predadj = 0.9289
RMSE-CV = 0.001755
Standardised residual plot
Standardised residual e
Actual response g2
95% Confidence Intervals of β
β
Case Number
95% Confidence Intervals of the residuals
Residuals
Case Number
Error correlation plot
e_i
e_-i
Normal probability plot
Probability
Residuals r
×10^-3
Error distribution plot
Residuals r
×10^-3

8.6.2 Appendix 6.2 -Kriging

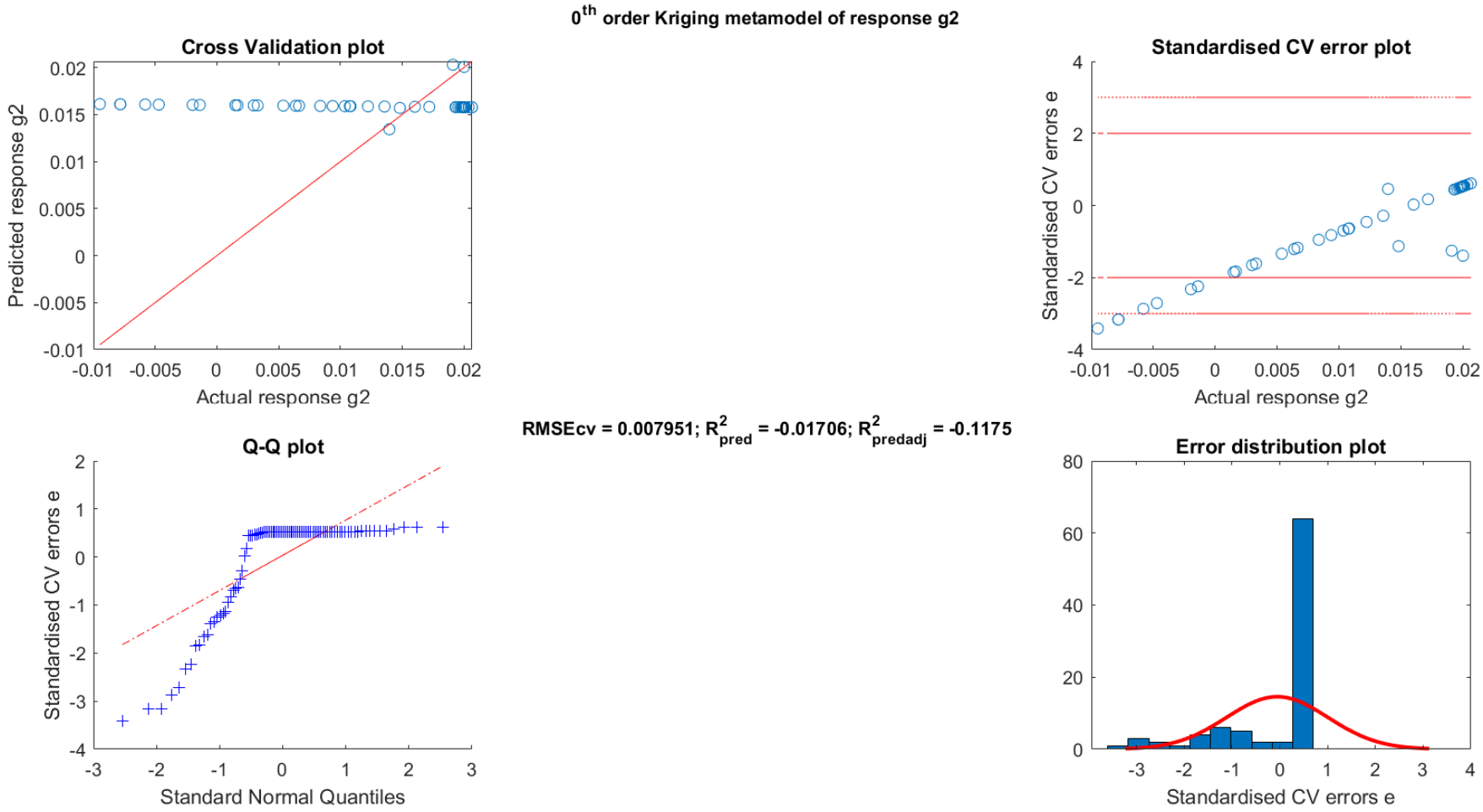

1st order Kriging metamodel of response g2

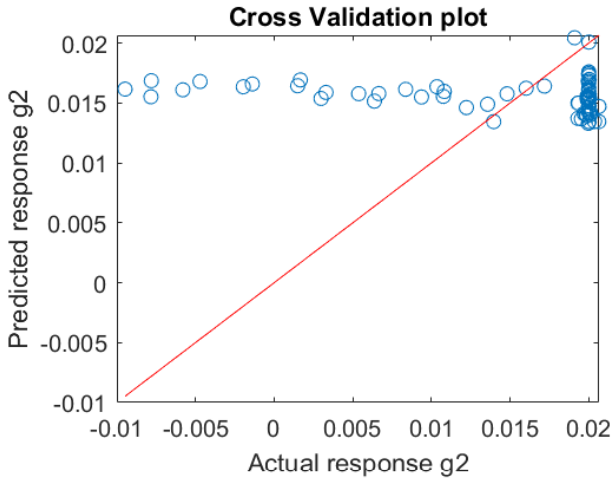

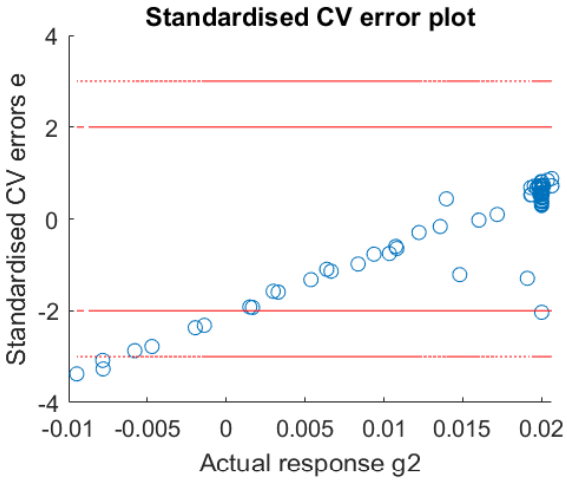

RMSEcv = 0.008203; R^2_{pred} = -0.08253; $R^2_{predadj}$ = -0.2846

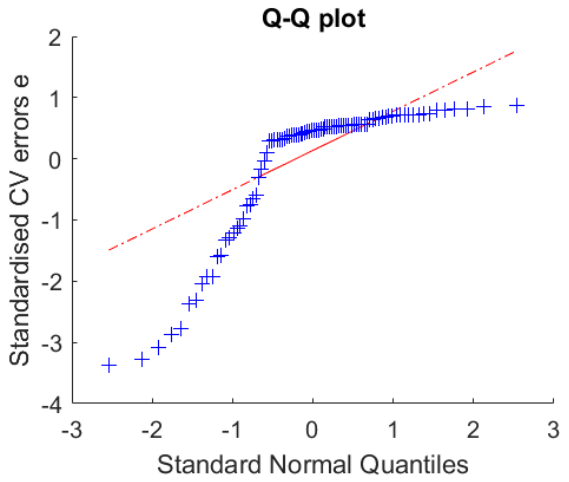

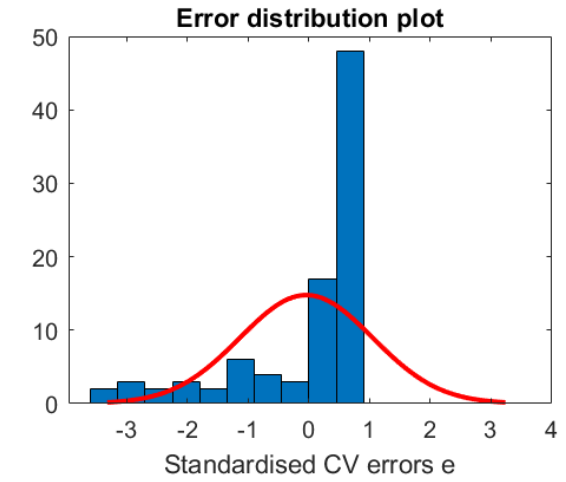

2nd order Kriging metamodel of response g2

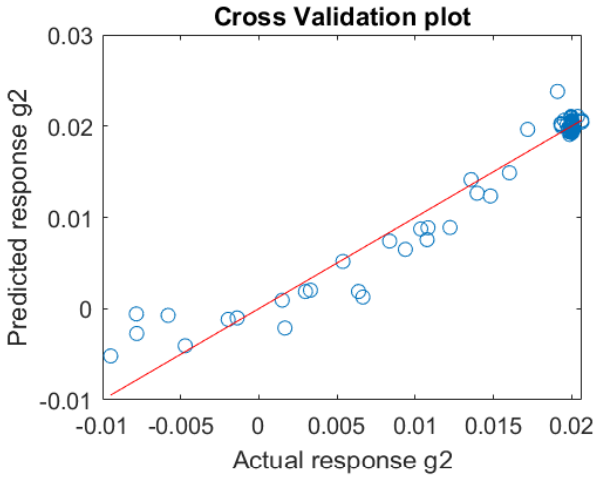

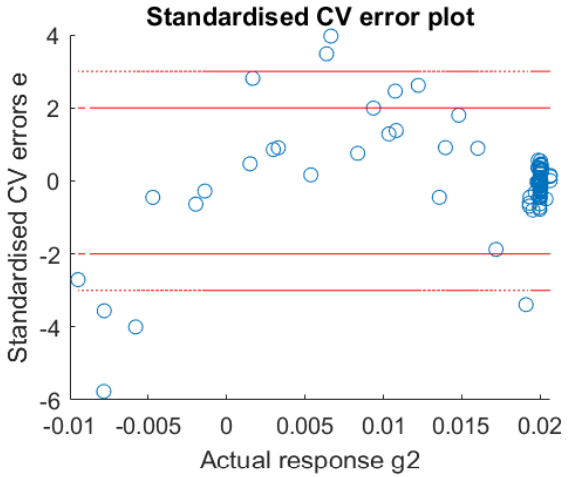

RMSEcv = 0.001761; R^2_{pred} = 0.9501; $R^2_{predadj}$ = 0.9178

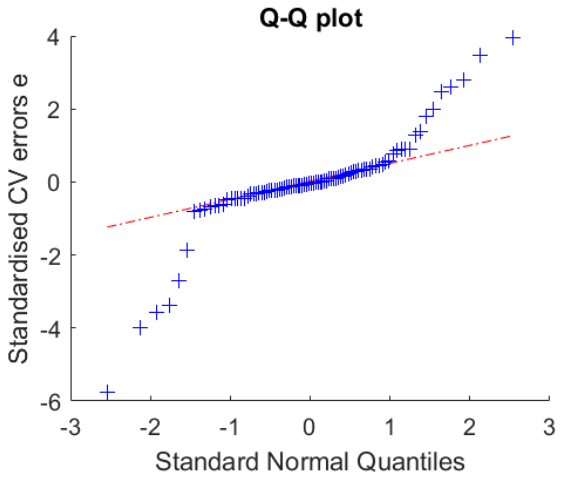

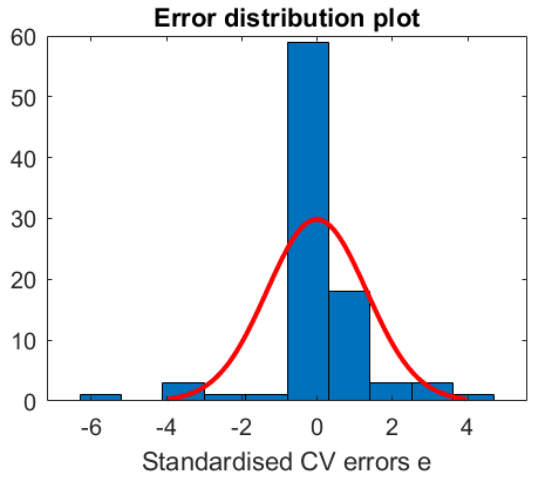

2nd order Regression Kriging metamodel of response g2

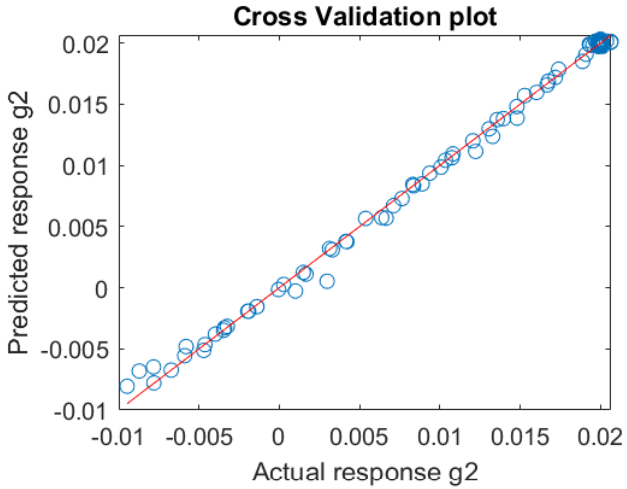

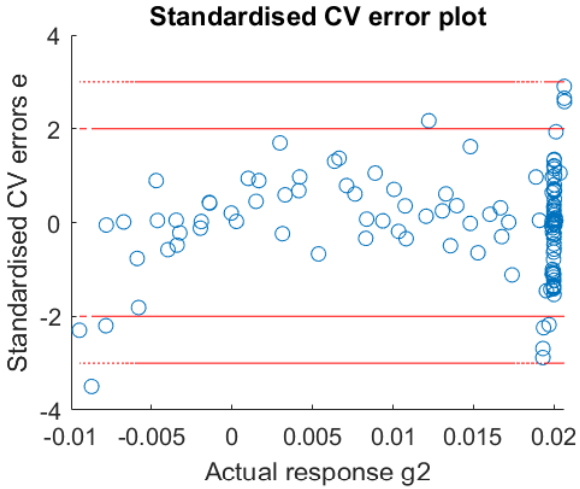

RMSEcv = 0.0004727; R^2_{pred} = 0.9974; $R^2_{predadj}$ = 0.9963

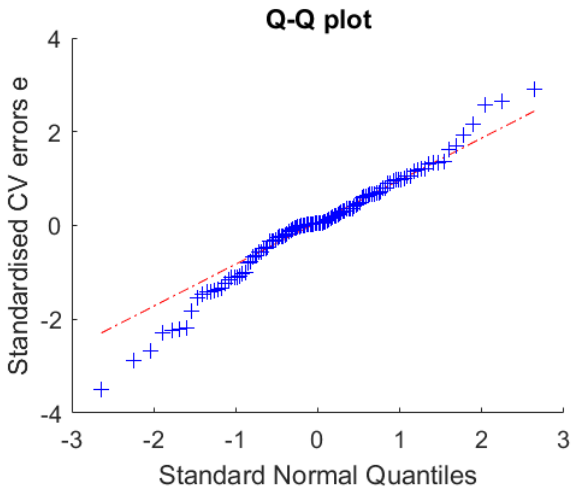

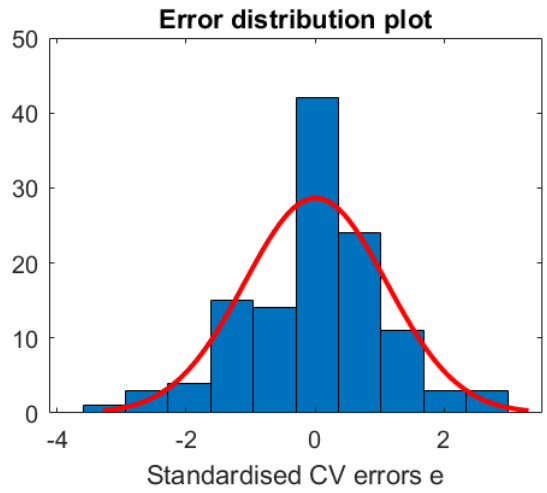

8.7 Appendix 7 -Metamodels validation for the FFD plus the 64 LHD for the left right angle

8.7.1 Appendix 7.1 -RSM model

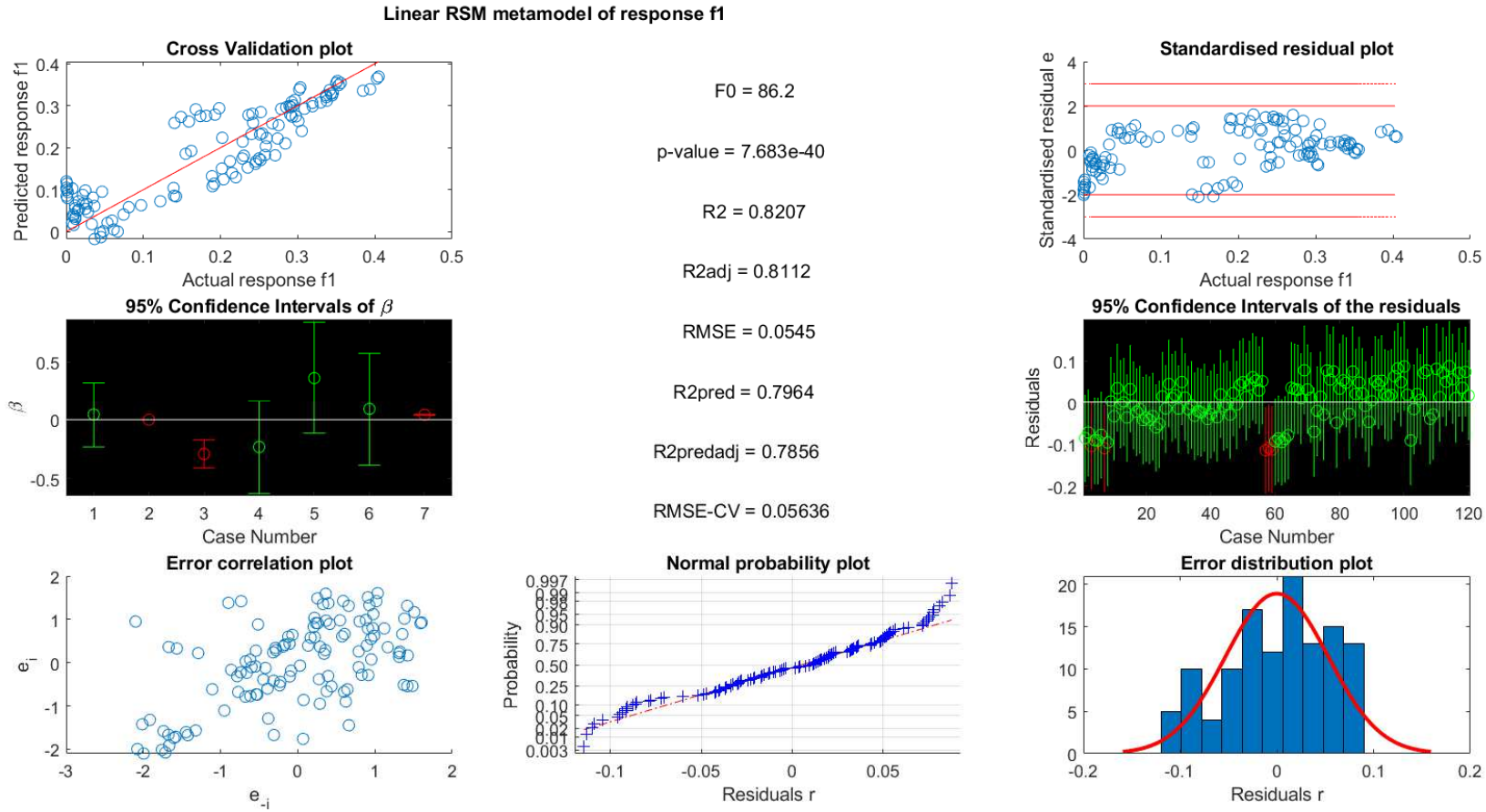

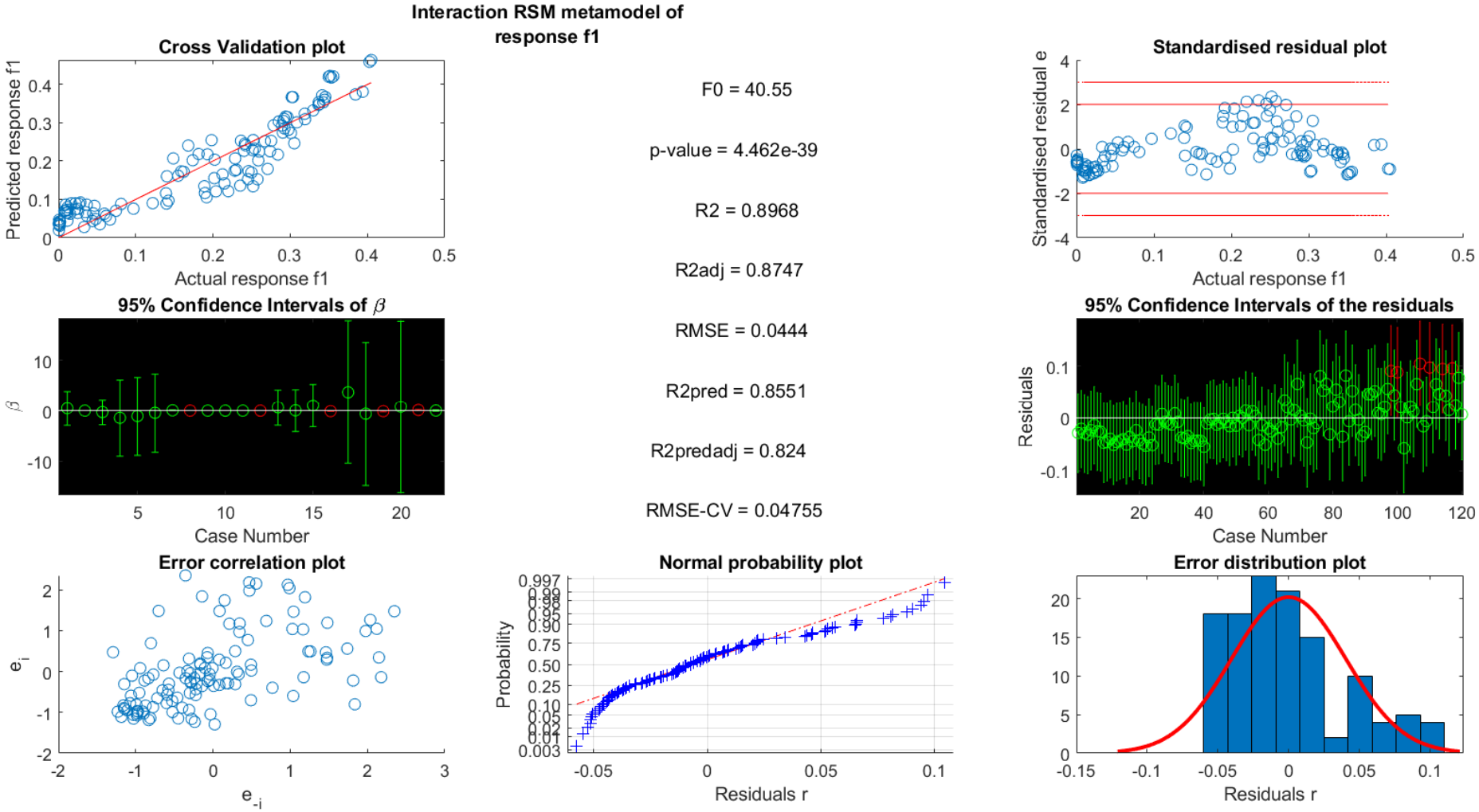
Interaction RSM metamodel of response f1
Cross Validation plot
Predicted response f1
Actual response f1
F0 = 40.55
p-value = 4.462e-39
R2 = 0.8968
R2adj = 0.8747
RMSE = 0.0444
R2pred = 0.8551
R2predadj = 0.824
RMSE-CV = 0.04755
Standardised residual plot
Standardised residual e
Actual response f1
95% Confidence Intervals of β
β
Case Number
95% Confidence Intervals of the residuals
Residuals
Case Number
Error correlation plot
e_i
e_-i
Normal probability plot
Probability
Residuals r
Error distribution plot
Residuals r

Elliptic RSM metamodel of response f1

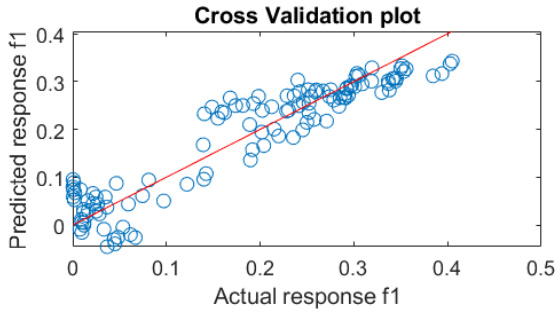

F0 = 74.29

p-value = 3.528e-46

R2 = 0.8928

R2adj = 0.8808

RMSE = 0.0433

R2pred = 0.8678

R2predadj = 0.853

RMSE-CV = 0.04542

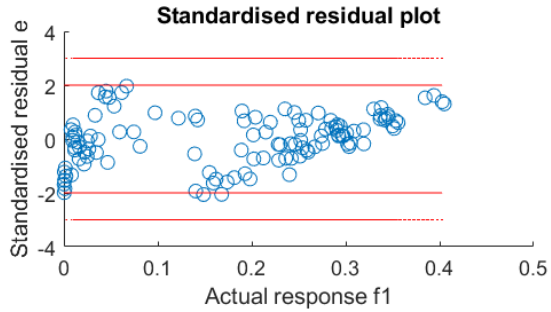

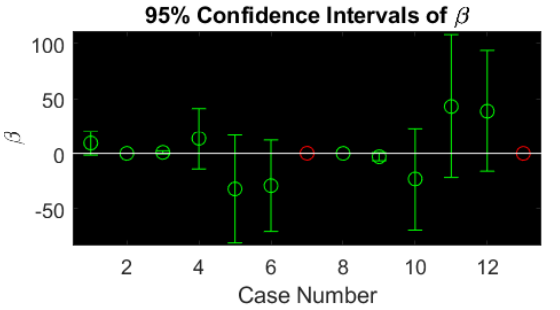

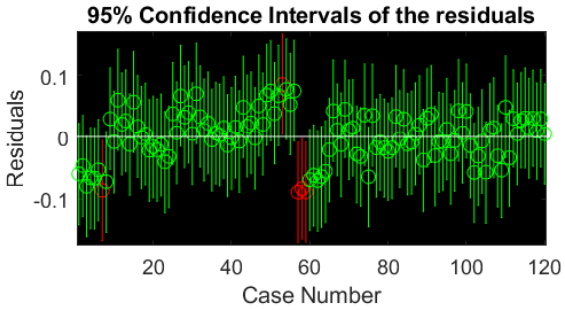

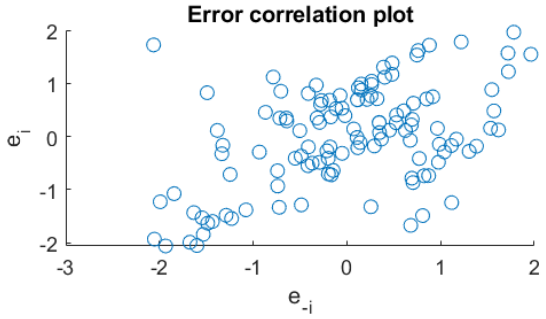

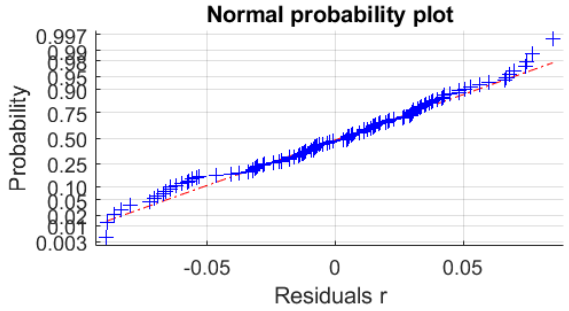

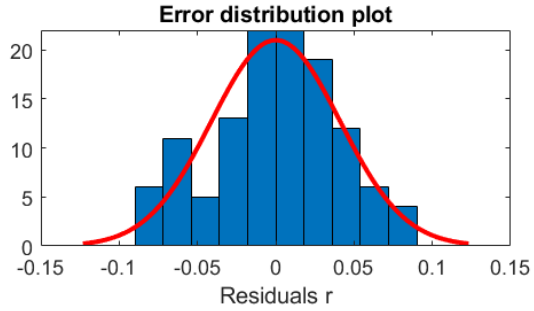

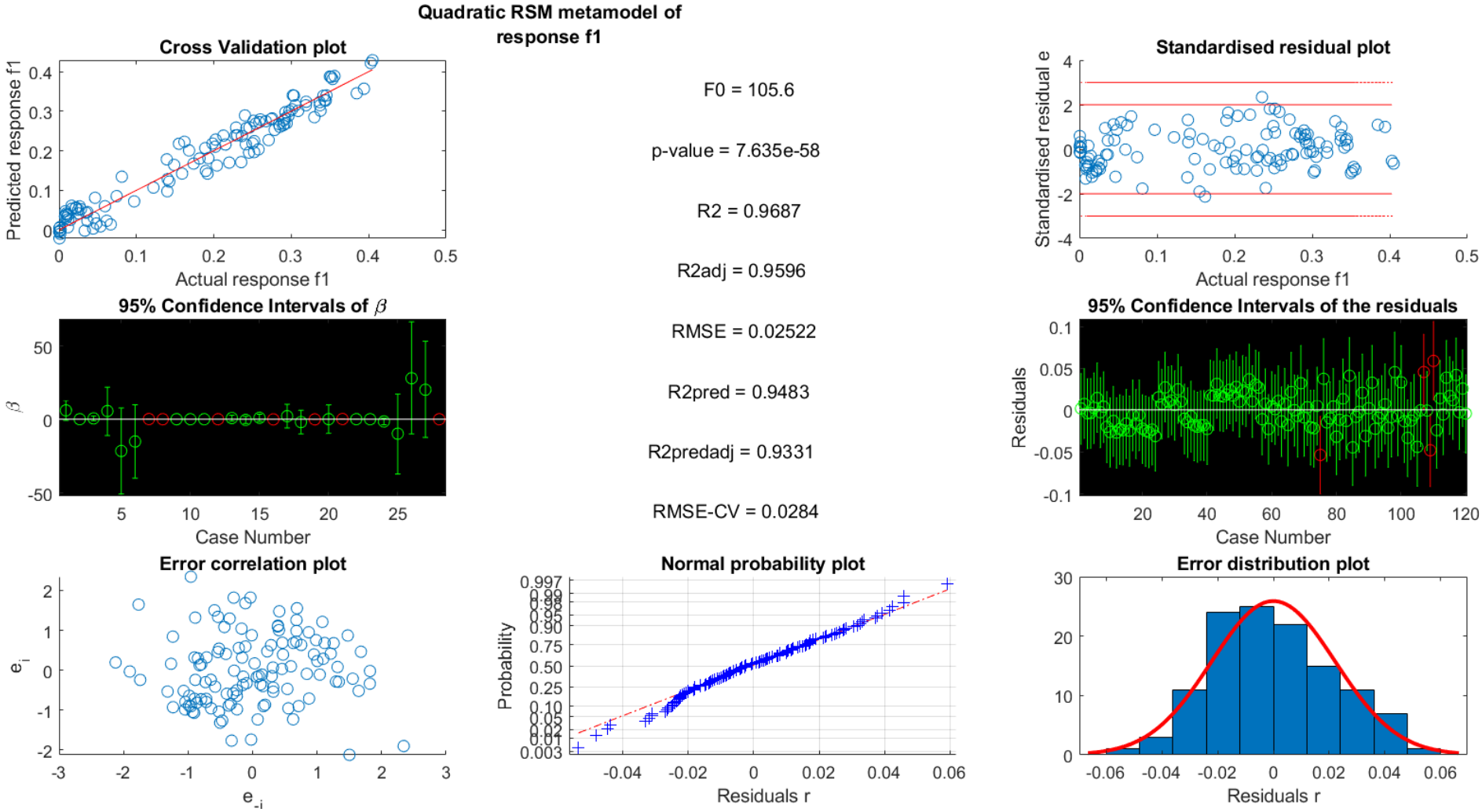

8.7.2 Appendix 7.2 -kriging

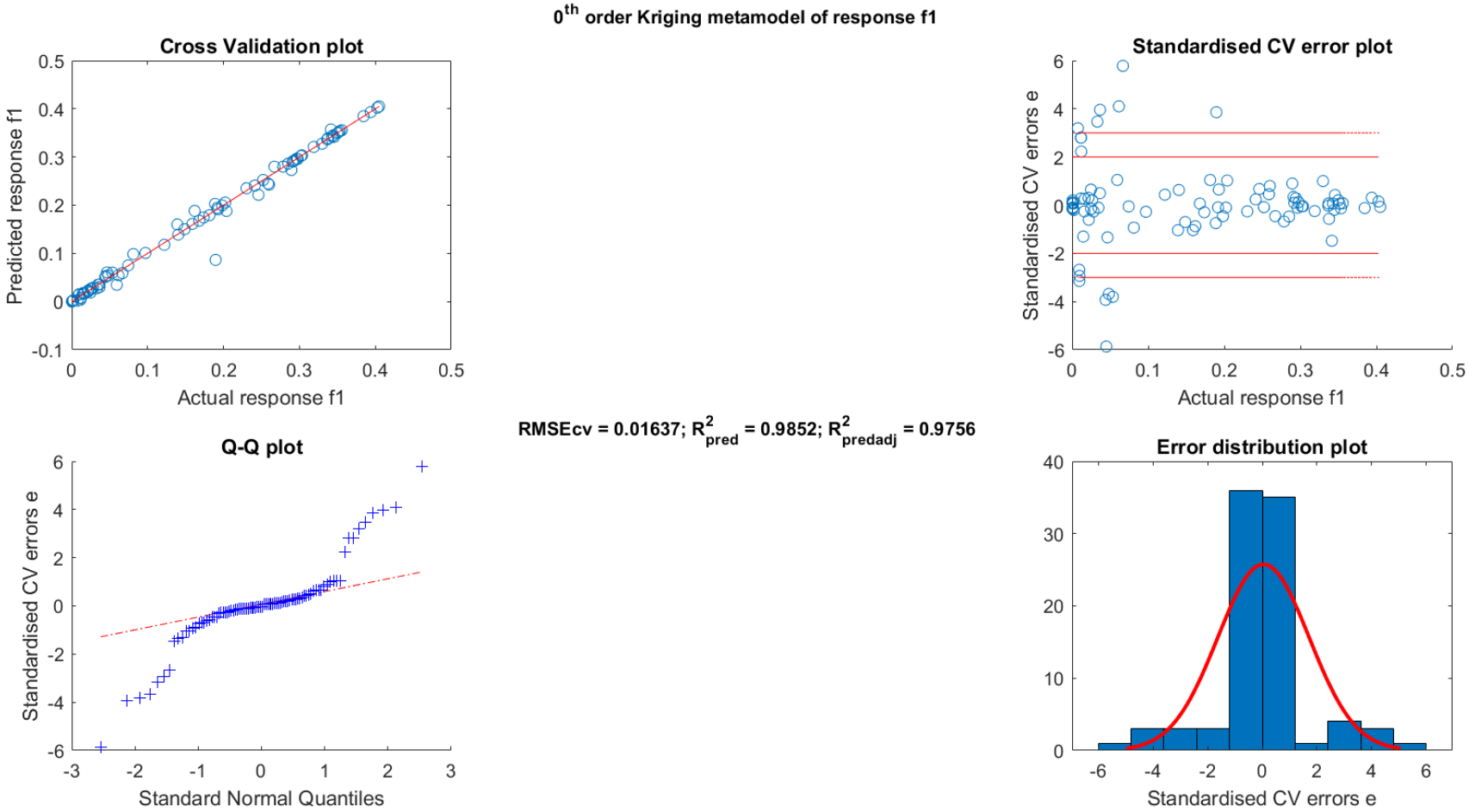
0th order Kriging metamodel of response f1
Cross Validation plot
Predicted response f1
Actual response f1
Standardised CV error plot
Standardised CV errors e
Actual response f1
RMSEcv = 0.01637; R2pred = 0.9852; R2predadj = 0.9756
Q-Q plot
Standardised CV errors e
Standard Normal Quantiles
Error distribution plot
Standardised CV errors e

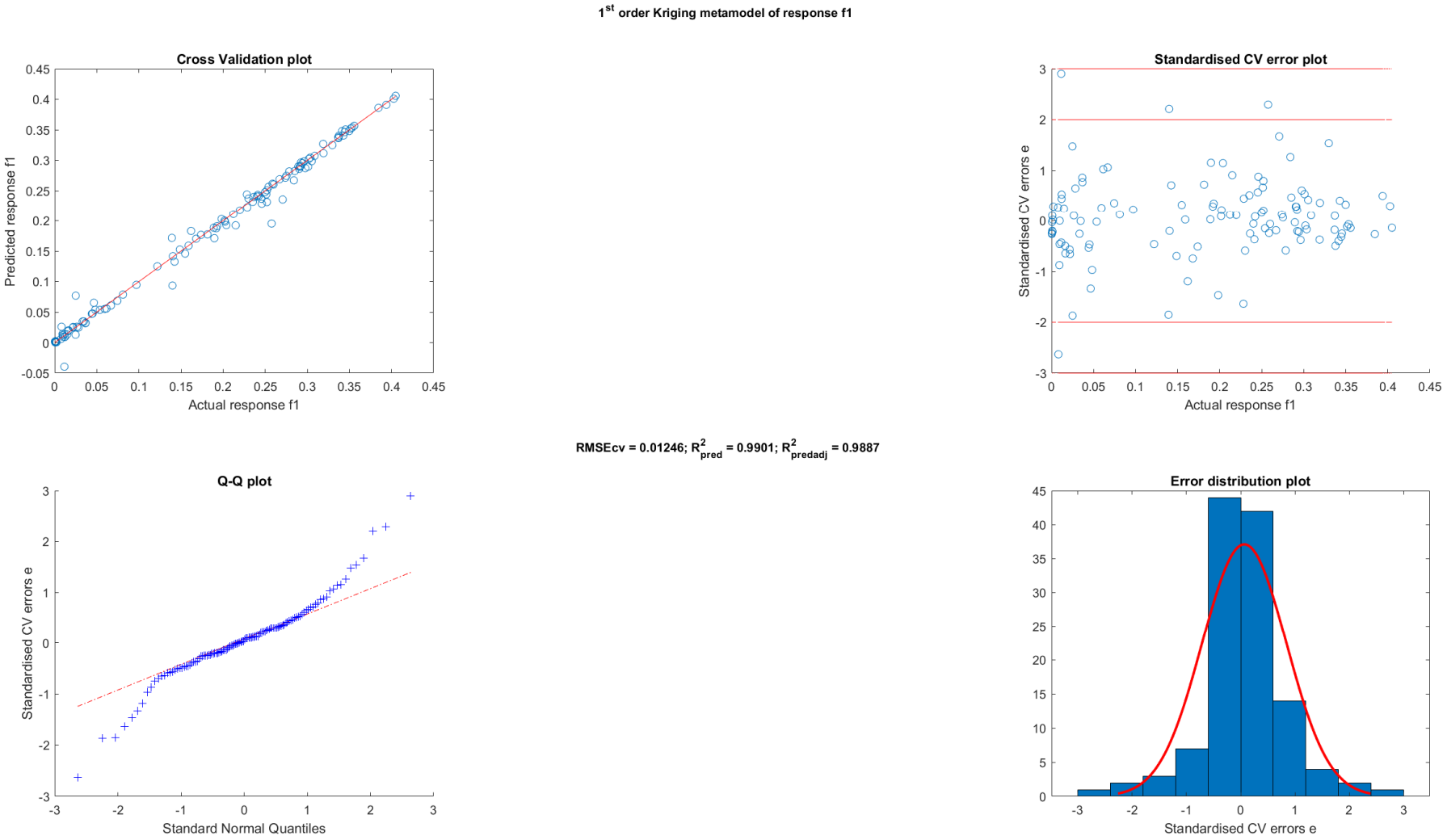
1st order Kriging metamodel of response f1
Cross Validation plot
Predicted response f1
Actual response f1
Standardised CV error plot
Standardised CV errors e
Actual response f1
RMSEcv = 0.01246; R2pred = 0.9901; R2predadj = 0.9887
Q-Q plot
Standardised CV errors e
Standard Normal Quantiles
Error distribution plot
Standardised CV errors e

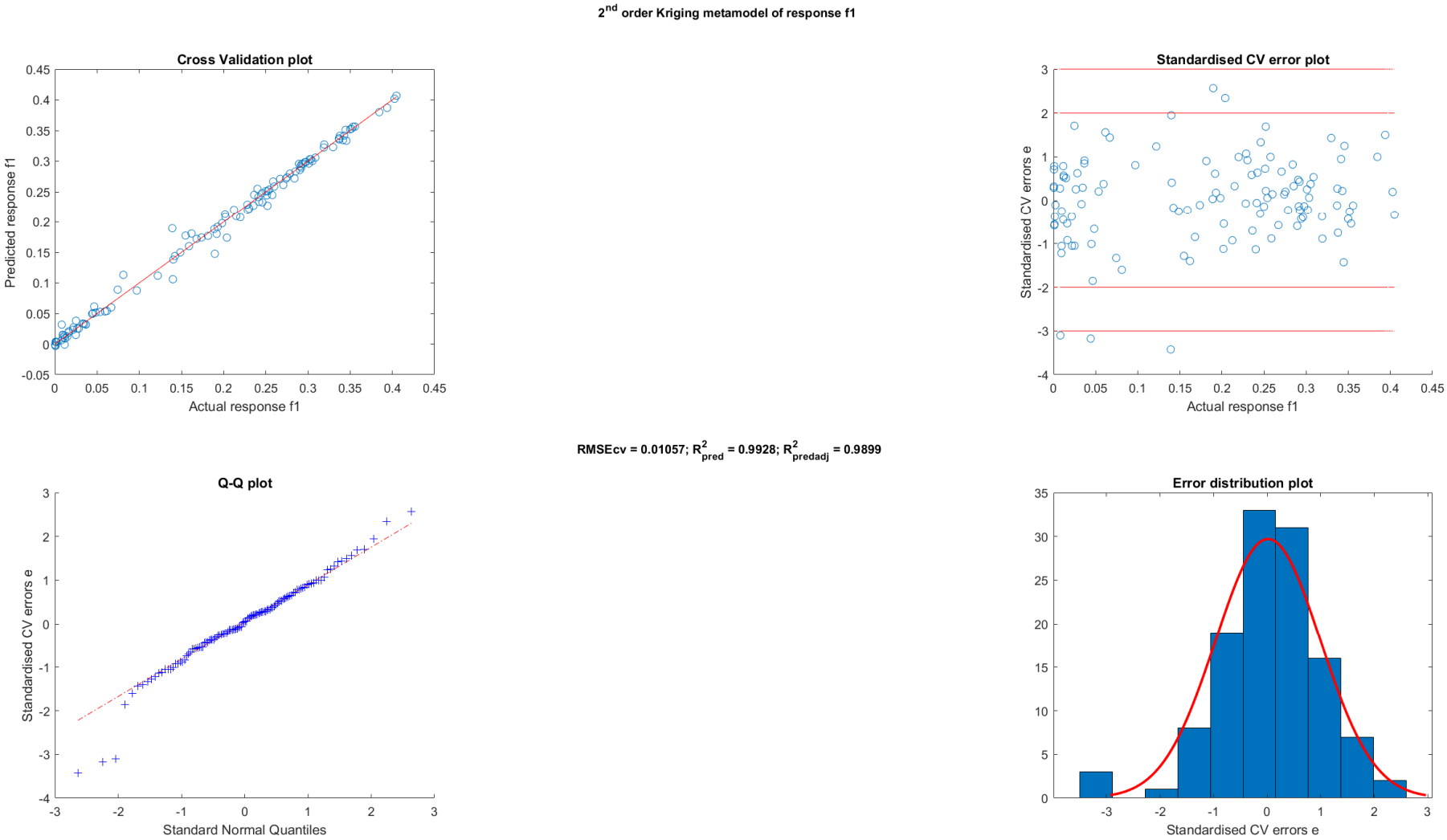
2nd order Kriging metamodel of response f1
Cross Validation plot
Predicted response f1
Actual response f1
Standardised CV error plot
Standardised CV errors e
Actual response f1
RMSEcv = 0.01057; R2pred = 0.9928; R2predadj = 0.9899
Q-Q plot
Standardised CV errors e
Standard Normal Quantiles
Error distribution plot
Standardised CV errors e

2nd order Regression Kriging metamodel of response f1

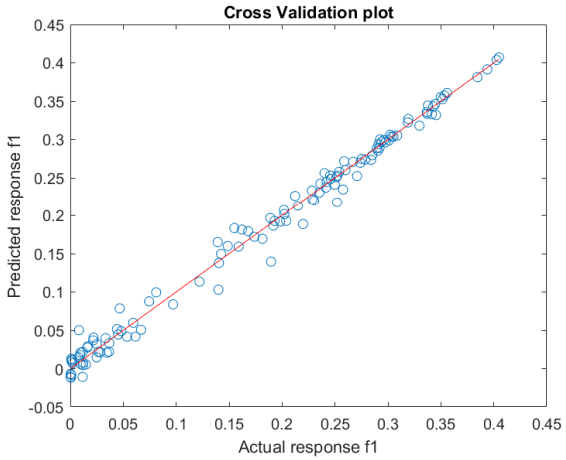

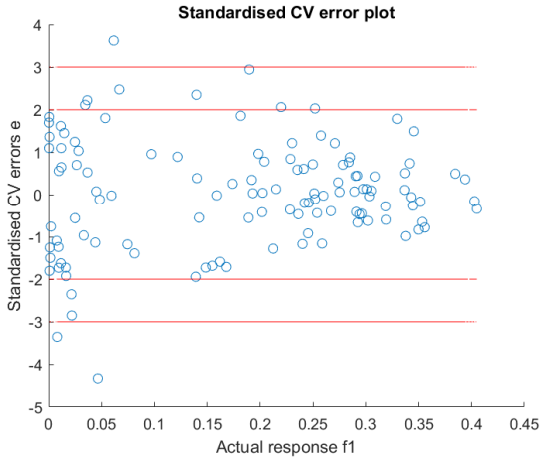

RMSEcv = 0.01266; R^2_{pred} = 0.9897; $R^2_{predadj}$ = 0.9855

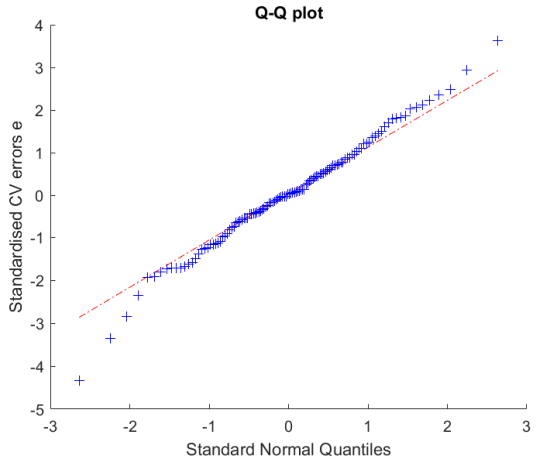

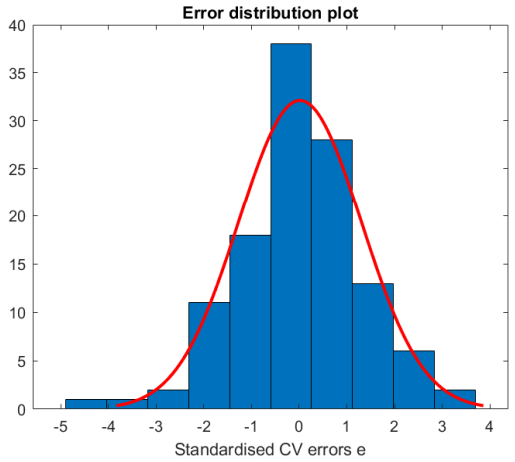

8.8 Appendix 8 -Metamodels validation for the FFD plus the 64 LHD for the front back angle

8.8.1 Appendix 8.1 -RSM model

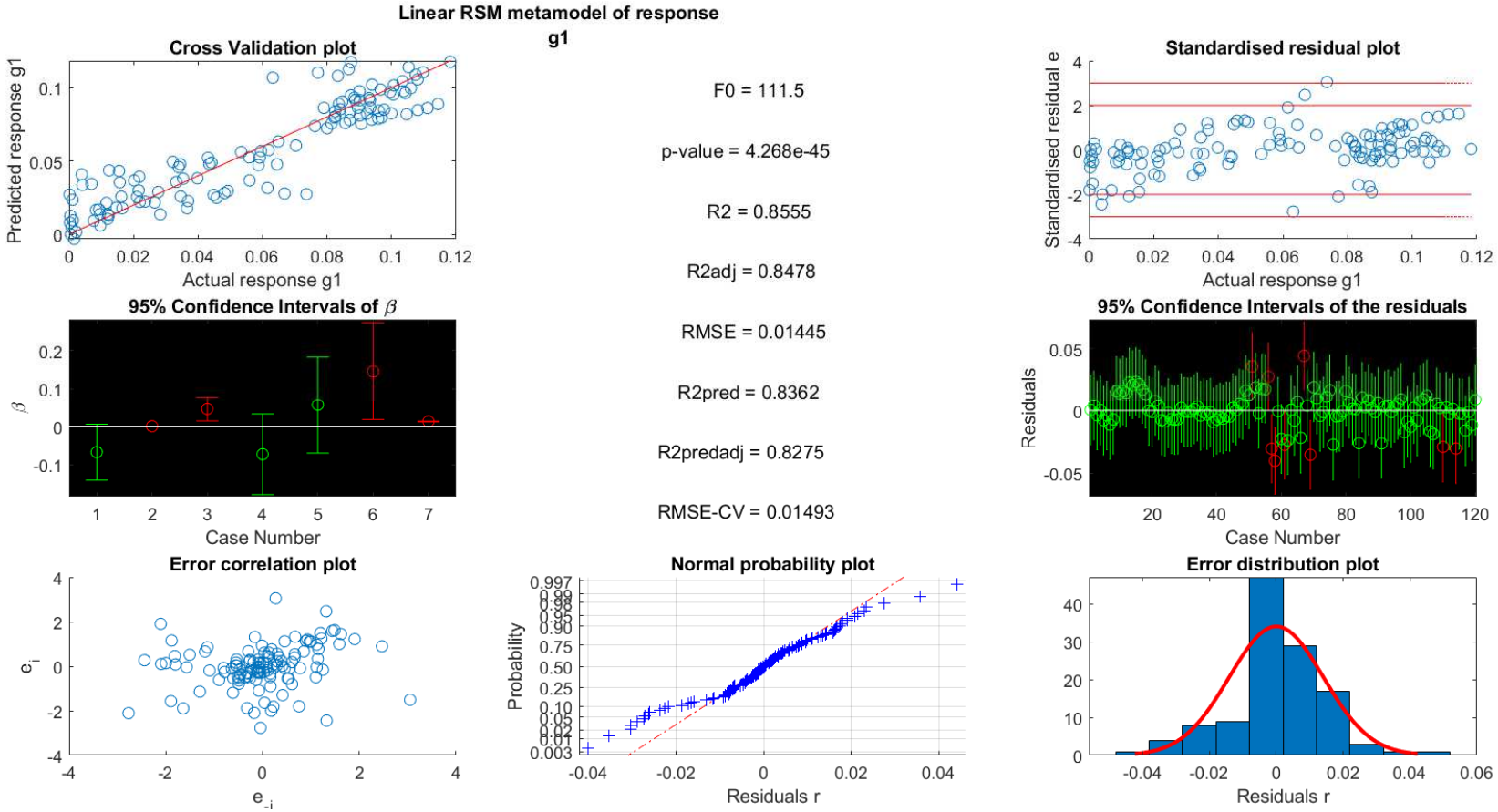

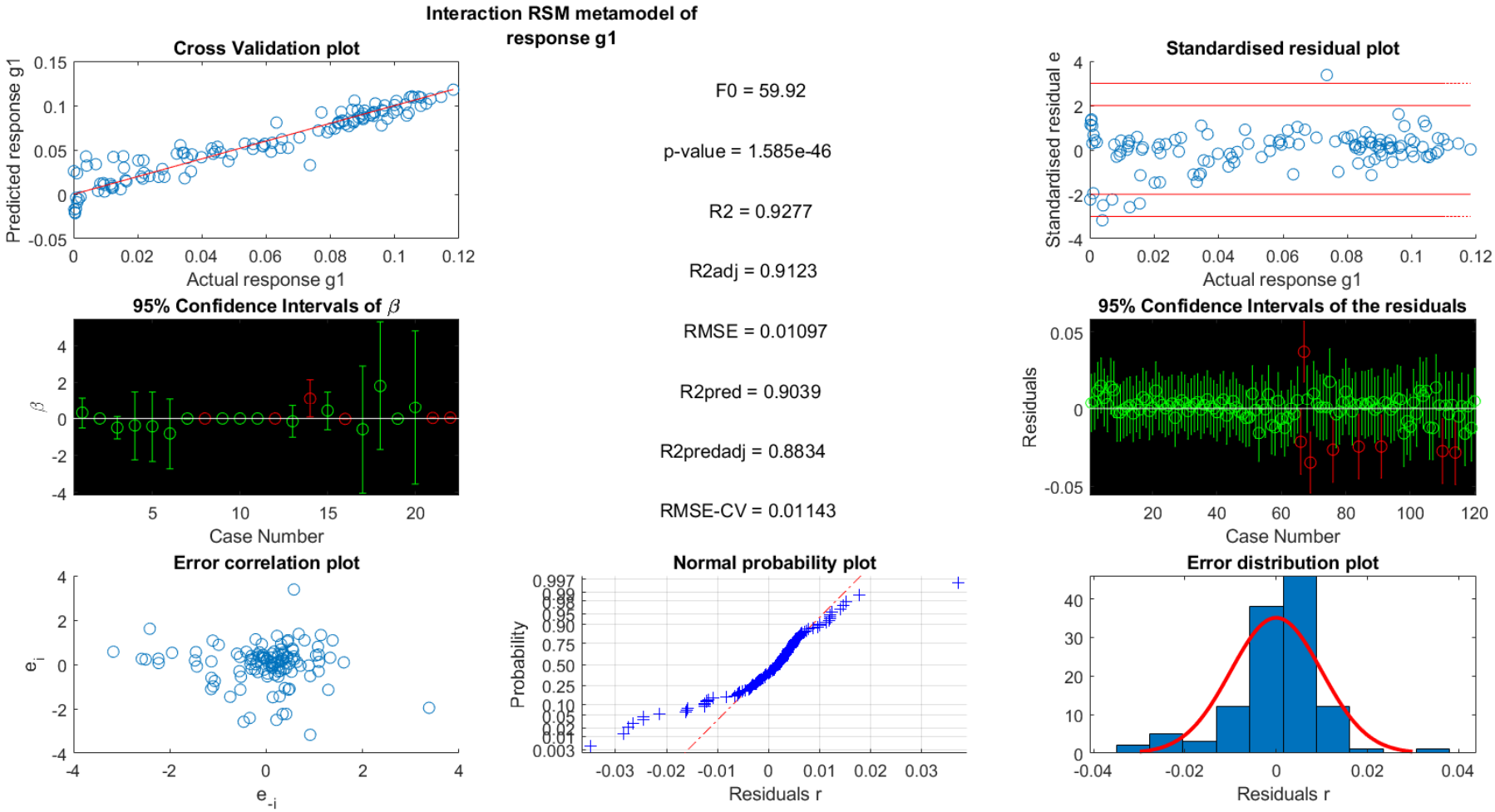
Interaction RSM metamodel of response g1
Cross Validation plot
Predicted response g1
Actual response g1
F0 = 59.92
p-value = 1.585e-46
R2 = 0.9277
R2adj = 0.9123
RMSE = 0.01097
R2pred = 0.9039
R2predadj = 0.8834
RMSE-CV = 0.01143
Standardised residual plot
Standardised residual e
Actual response g1
95% Confidence Intervals of β
β
Case Number
95% Confidence Intervals of the residuals
Residuals
Case Number
Error correlation plot
e_i
e_-i
Normal probability plot
Probability
Residuals r
Error distribution plot
Residuals r

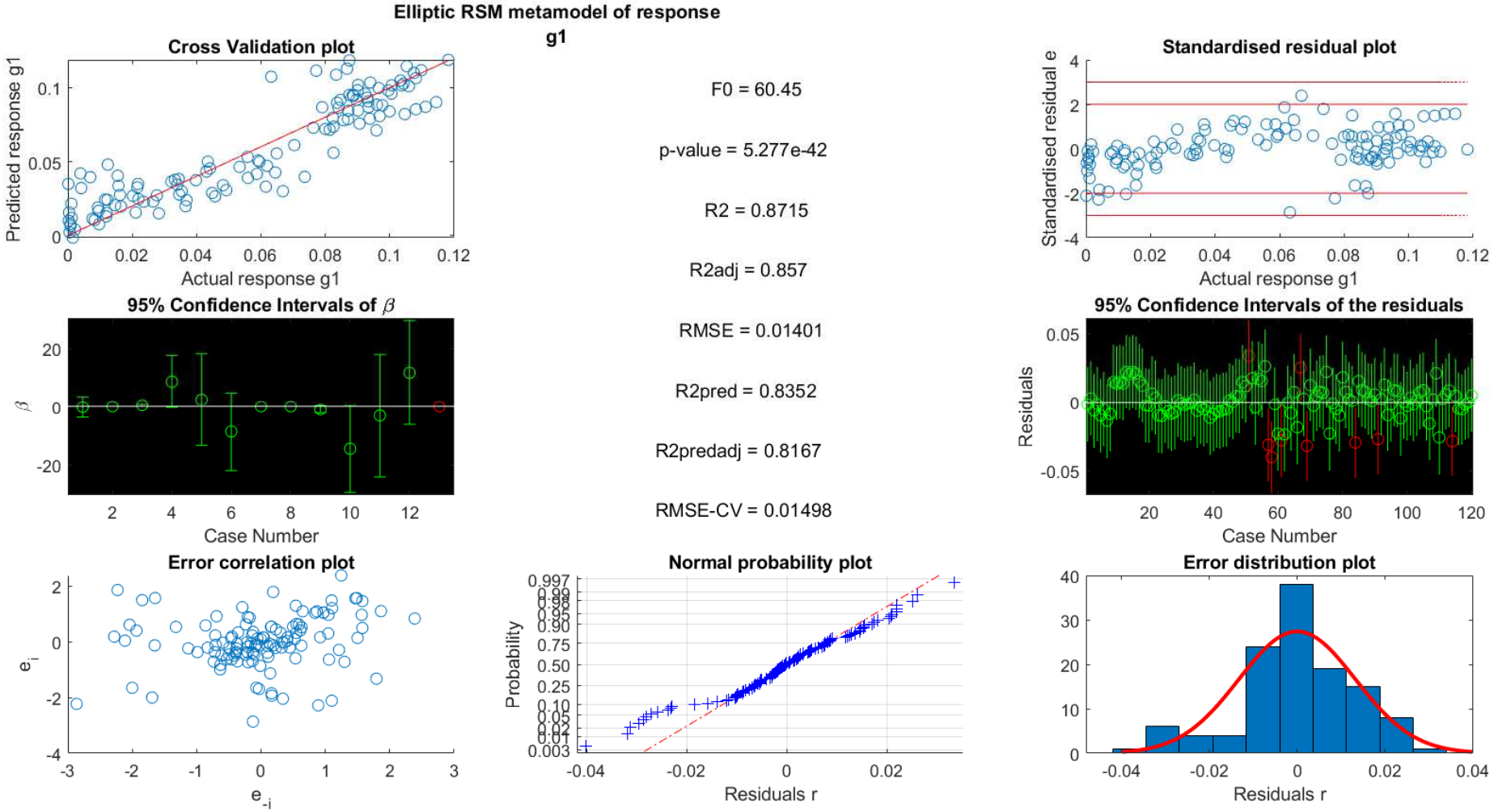
Elliptic RSM metamodel of response
g1
Cross Validation plot
Predicted response g1
Actual response g1
F0 = 60.45
p-value = 5.277e-42
R2 = 0.8715
R2adj = 0.857
RMSE = 0.01401
R2pred = 0.8352
R2predadj = 0.8167
RMSE-CV = 0.01498
Standardised residual plot
Standardised residual e
Actual response g1
95% Confidence Intervals of β
β
Case Number
95% Confidence Intervals of the residuals
Residuals
Case Number
Error correlation plot
e_i
e_-i
Normal probability plot
Probability
Residuals r
Error distribution plot
Residuals r

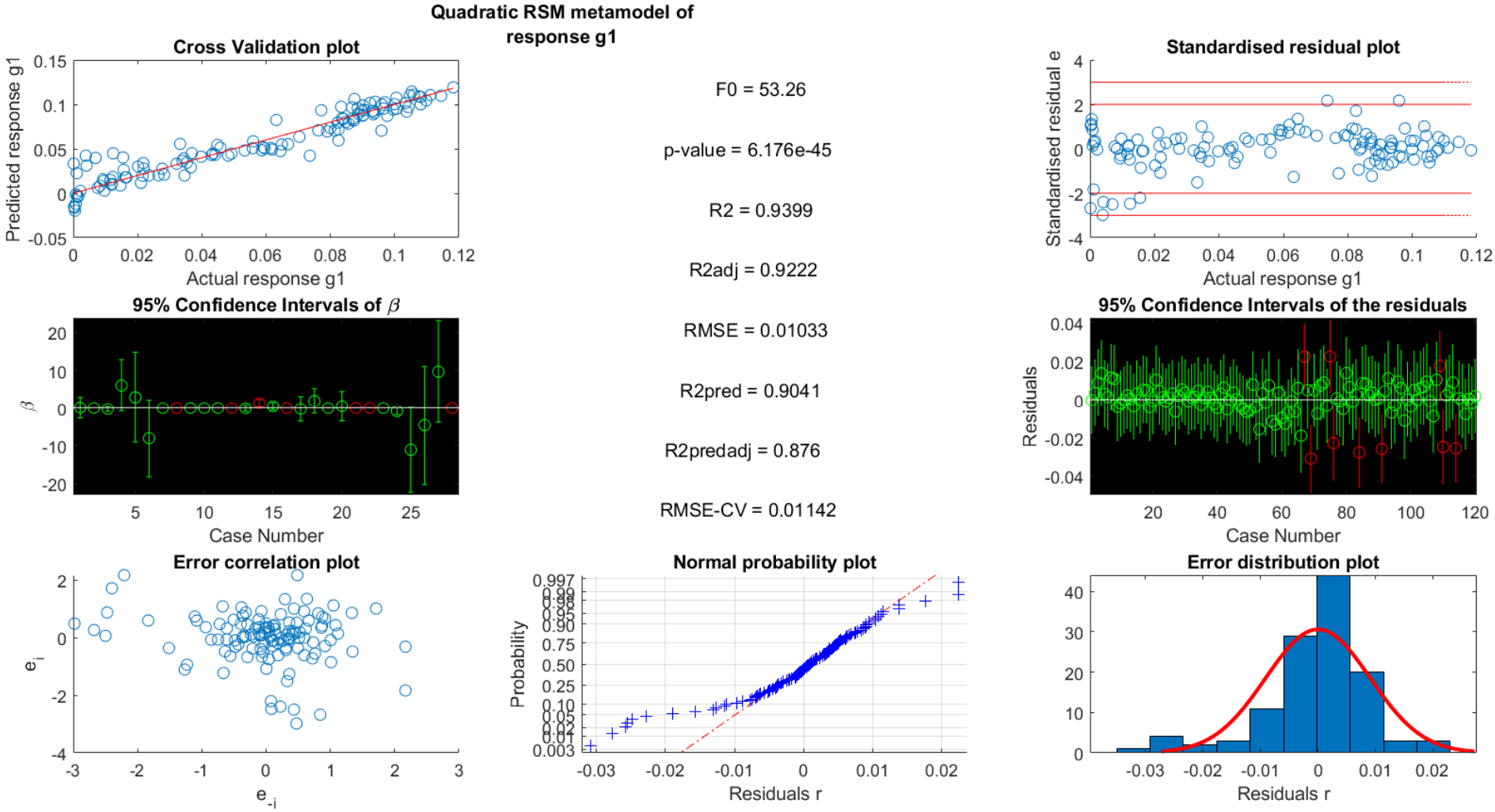

8.8.2 Appendix 8.2 -Kriging

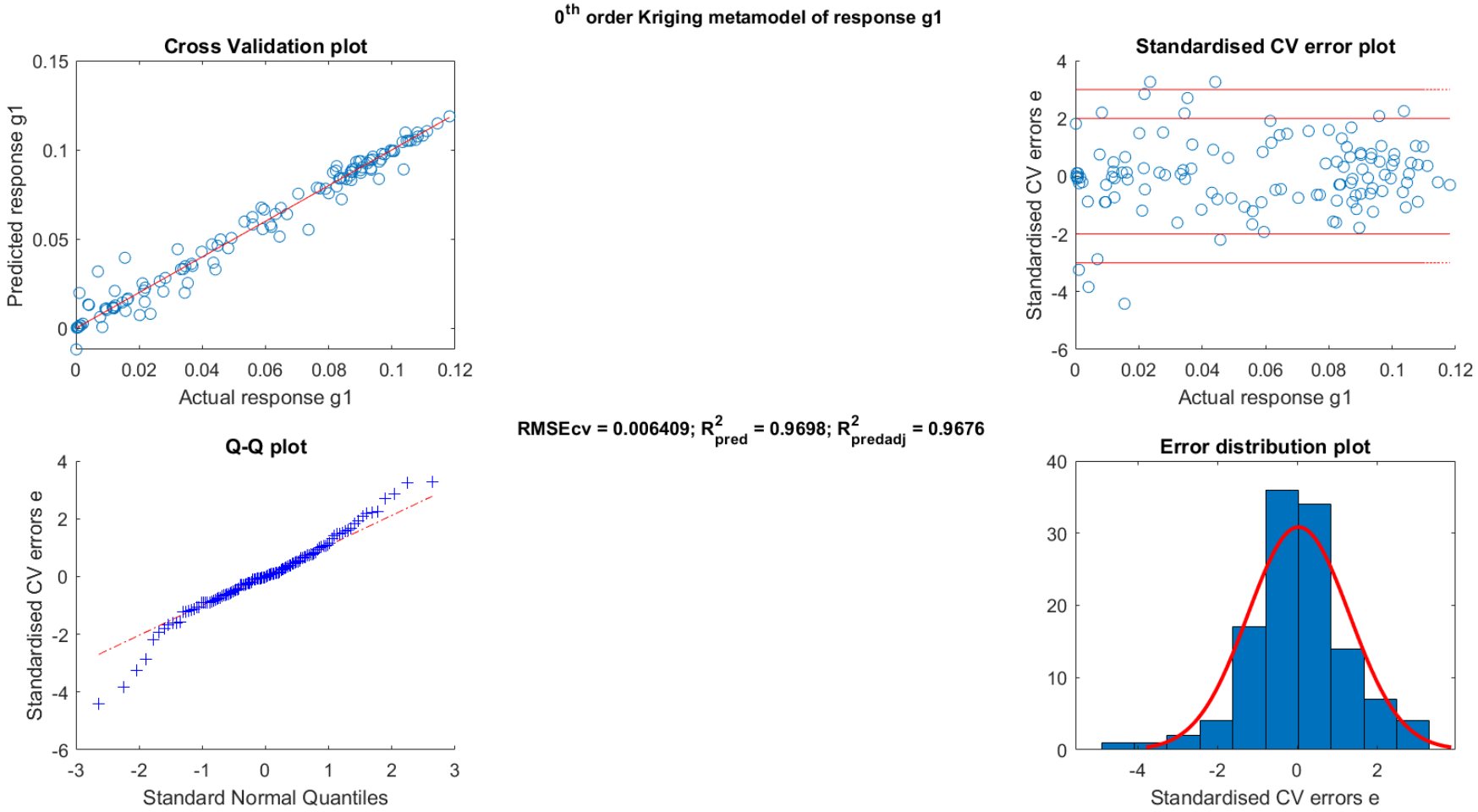
0th order Kriging metamodel of response g1
Cross Validation plot
Predicted response g1
Actual response g1
Standardised CV error plot
Standardised CV errors e
Actual response g1
RMSEcv = 0.006409; R2pred = 0.9698; R2predadj = 0.9676
Q-Q plot
Standardised CV errors e
Standard Normal Quantiles
Error distribution plot
Standardised CV errors e

1st order Kriging metamodel of response g1

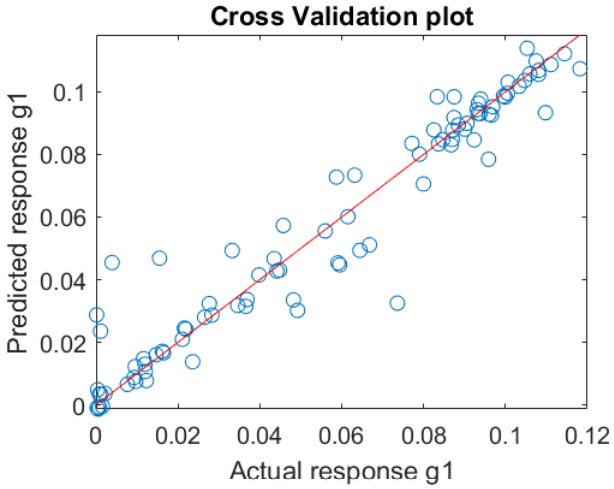

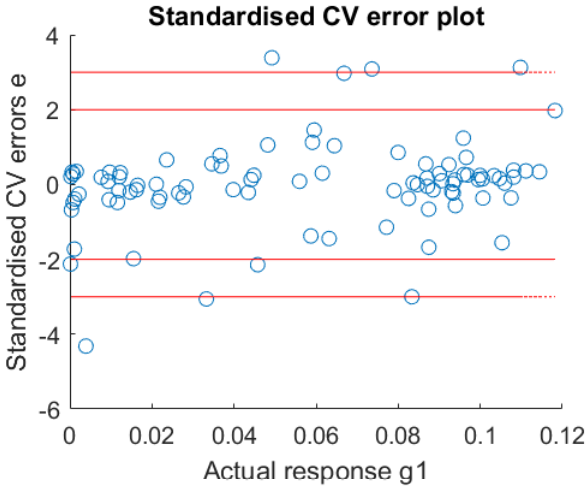

RMSEcv = 0.01133; R^2_{pred} = 0.9129; $R^2_{predadj}$ = 0.8565

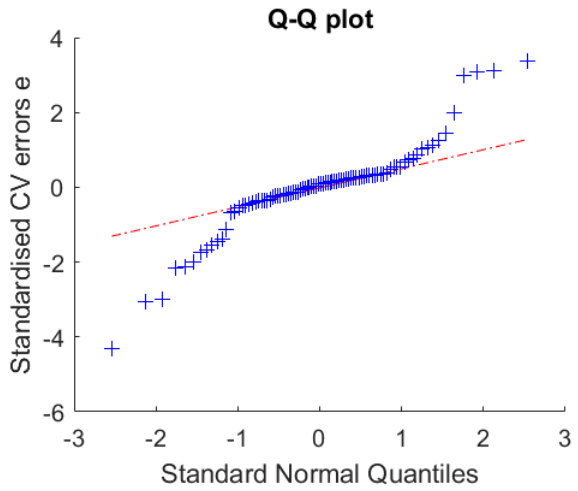

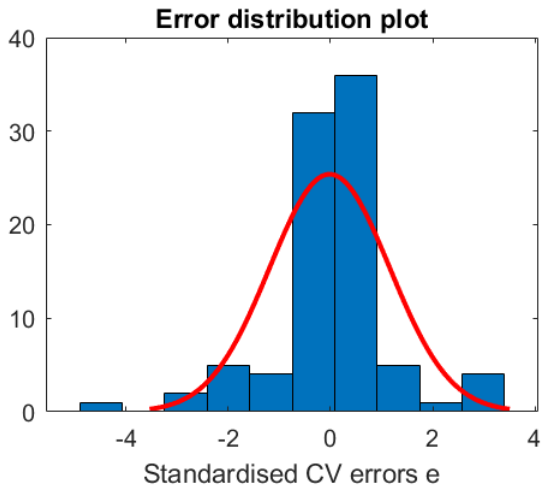

2nd order Kriging metamodel of response g1

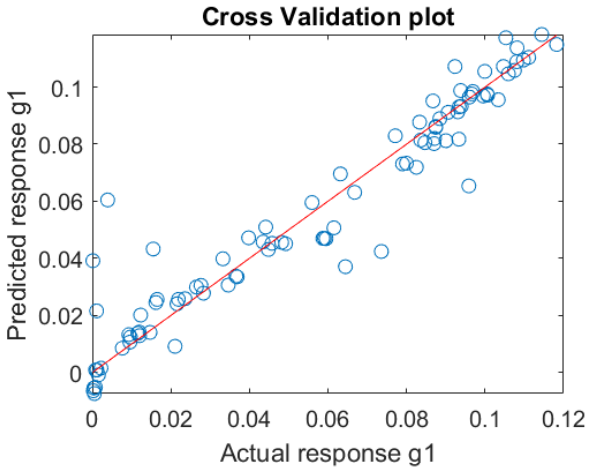

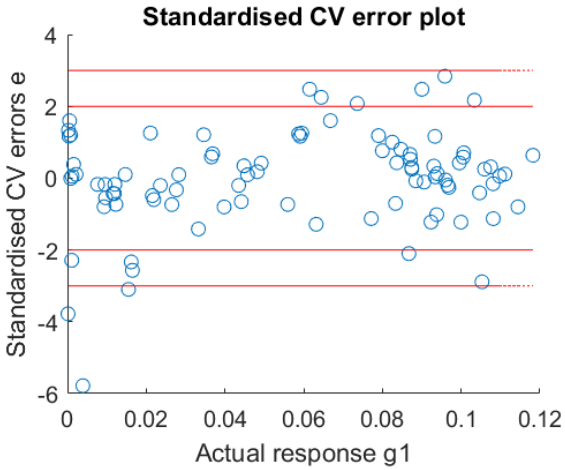

RMSEcv = 0.01133; R^2_{pred} = 0.9129; $R^2_{predadj}$ = 0.8565

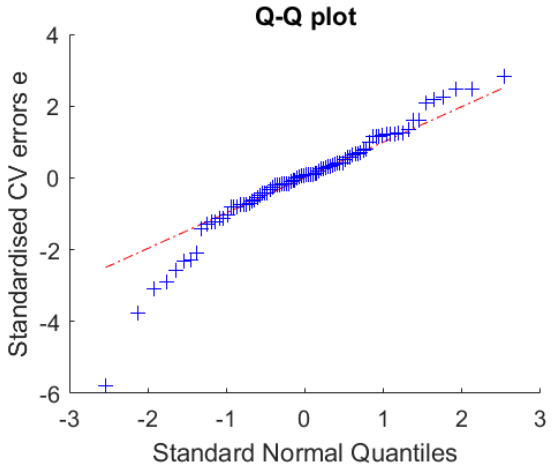

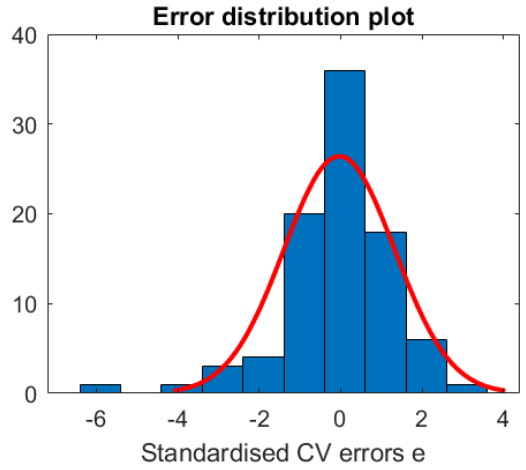

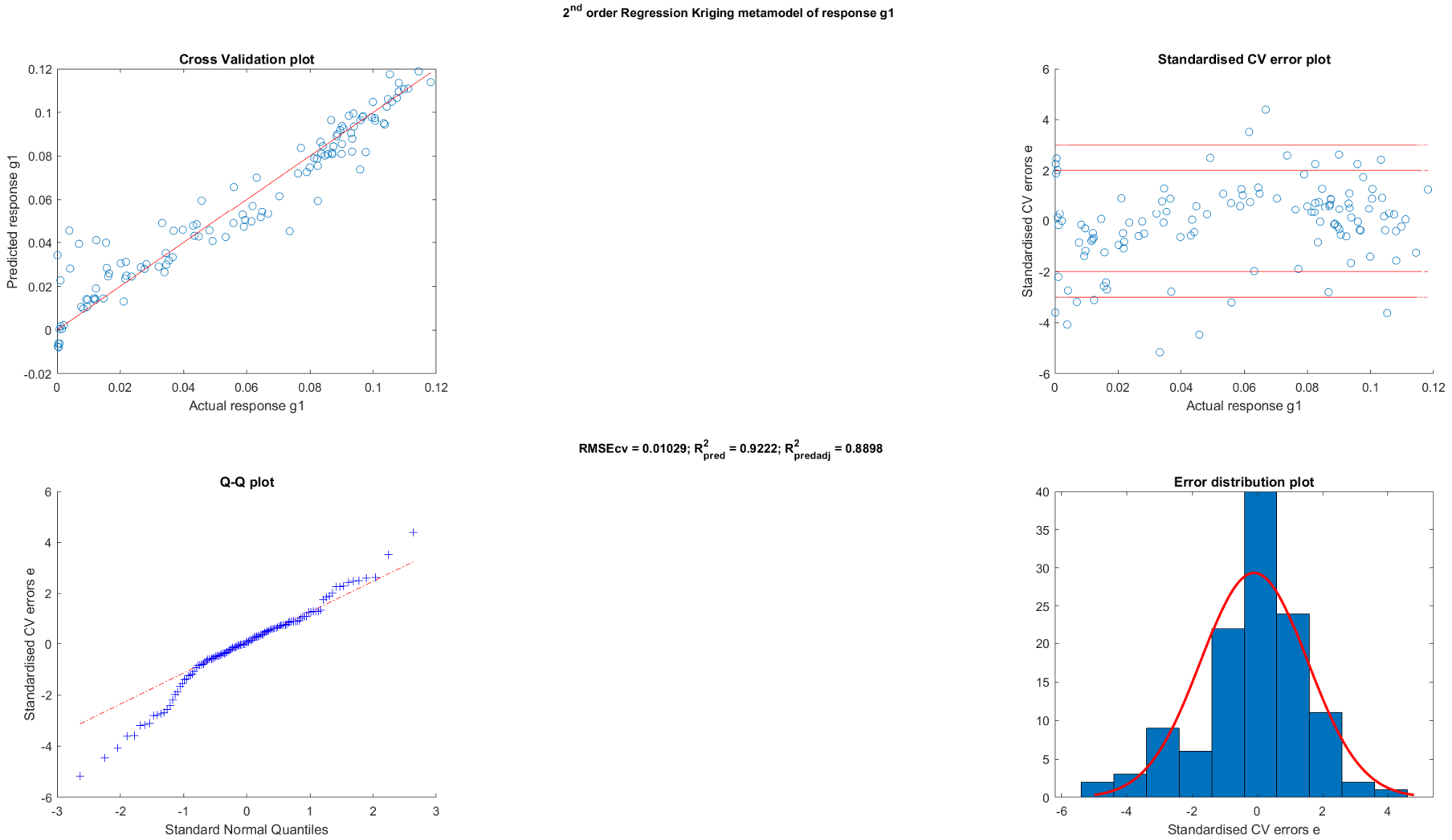

8.9 Appendix 9 -Metamodels validation for the FFD plus the 64 LHD thickness

8.9.1 Appendix 9.1 -RSM model

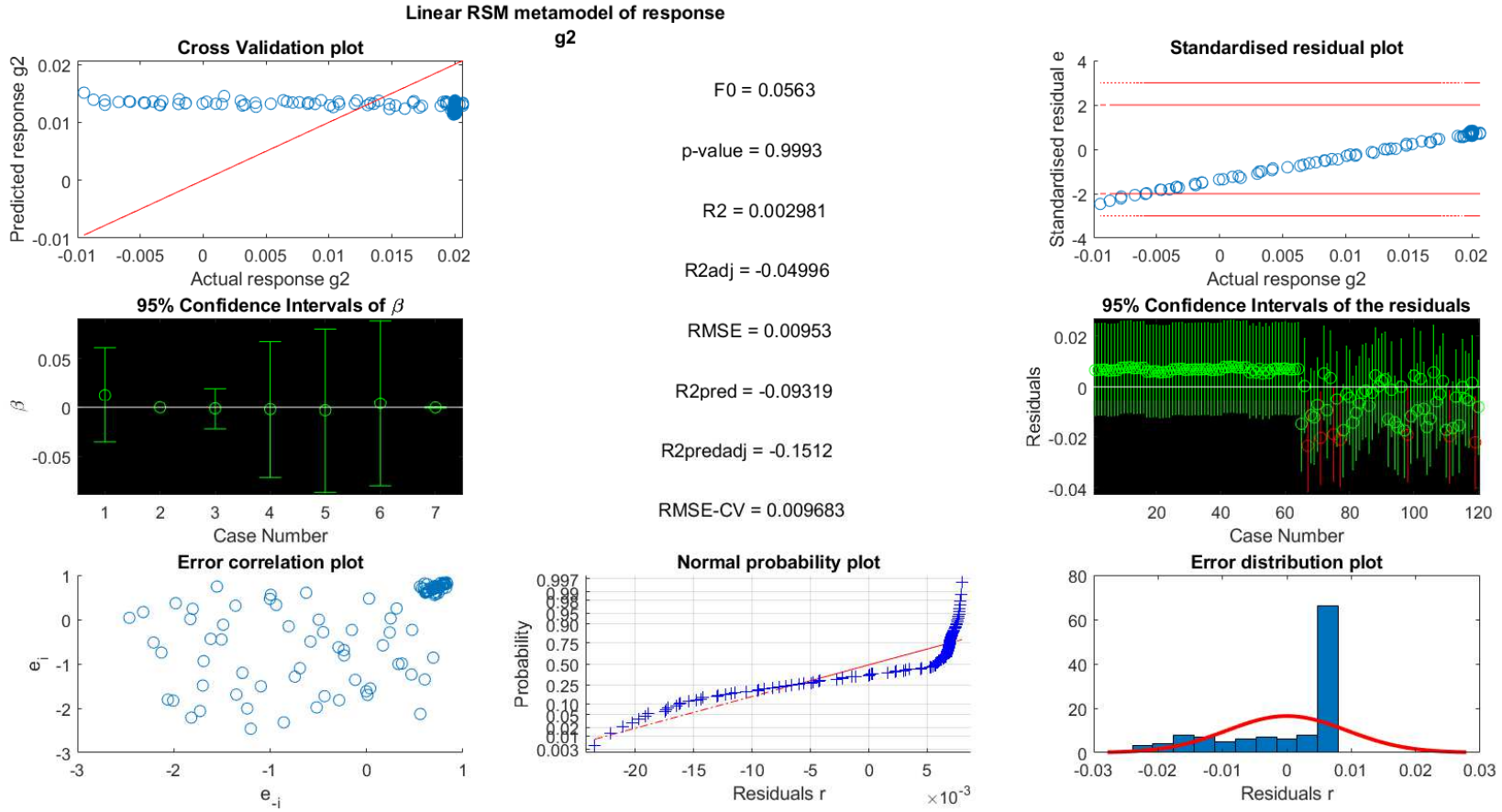

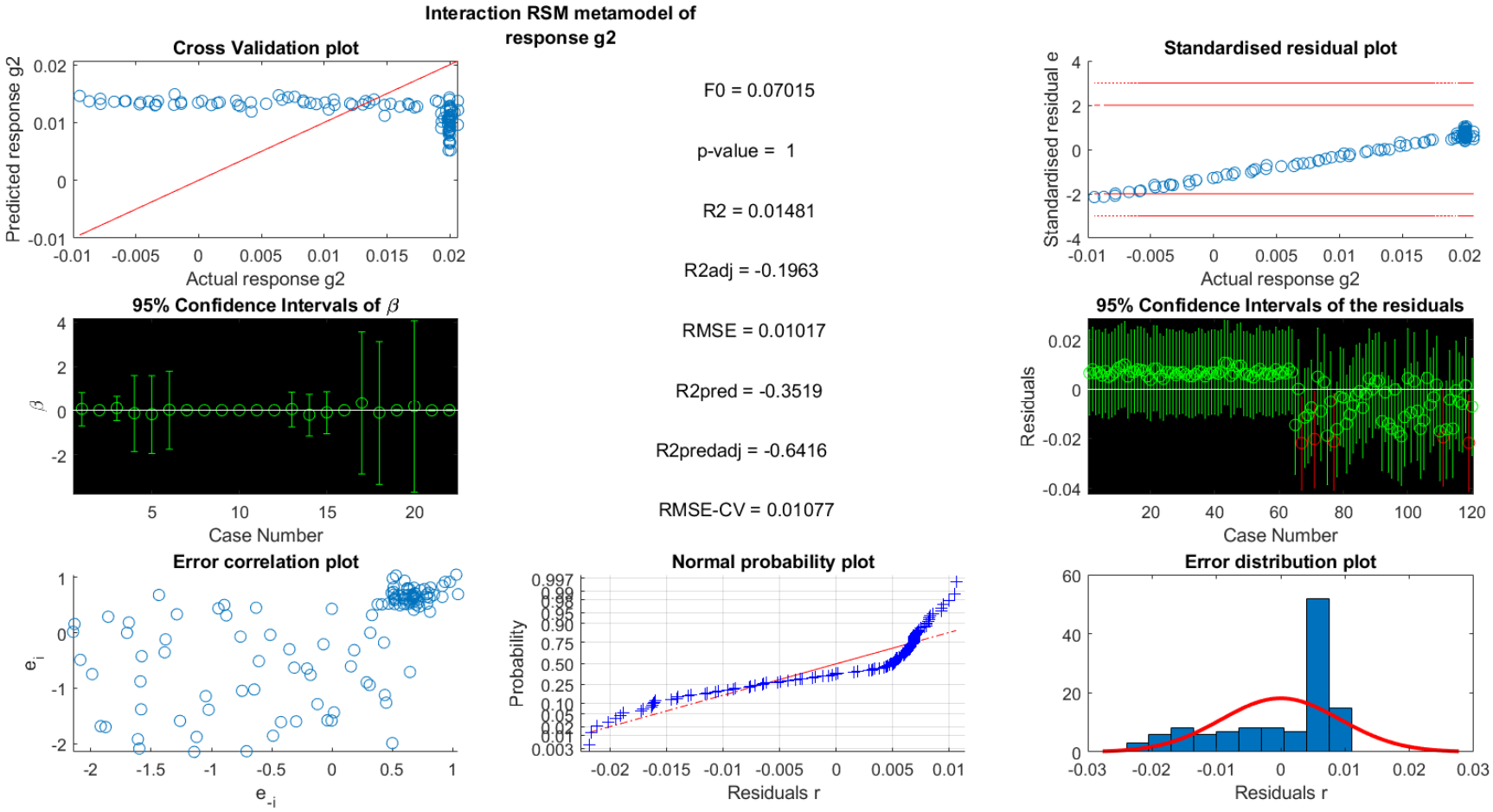
Interaction RSM metamodel of response g2
Cross Validation plot
Predicted response g2
Actual response g2
F0 = 0.07015
p-value = 1
R2 = 0.01481
R2adj = -0.1963
RMSE = 0.01017
R2pred = -0.3519
R2predadj = -0.6416
RMSE-CV = 0.01077
Standardised residual plot
Standardised residual e
Actual response g2
95% Confidence Intervals of β
β
Case Number
95% Confidence Intervals of the residuals
Residuals
Case Number
Error correlation plot
e_i
e_-i
Normal probability plot
Probability
Residuals r
Error distribution plot
Residuals r

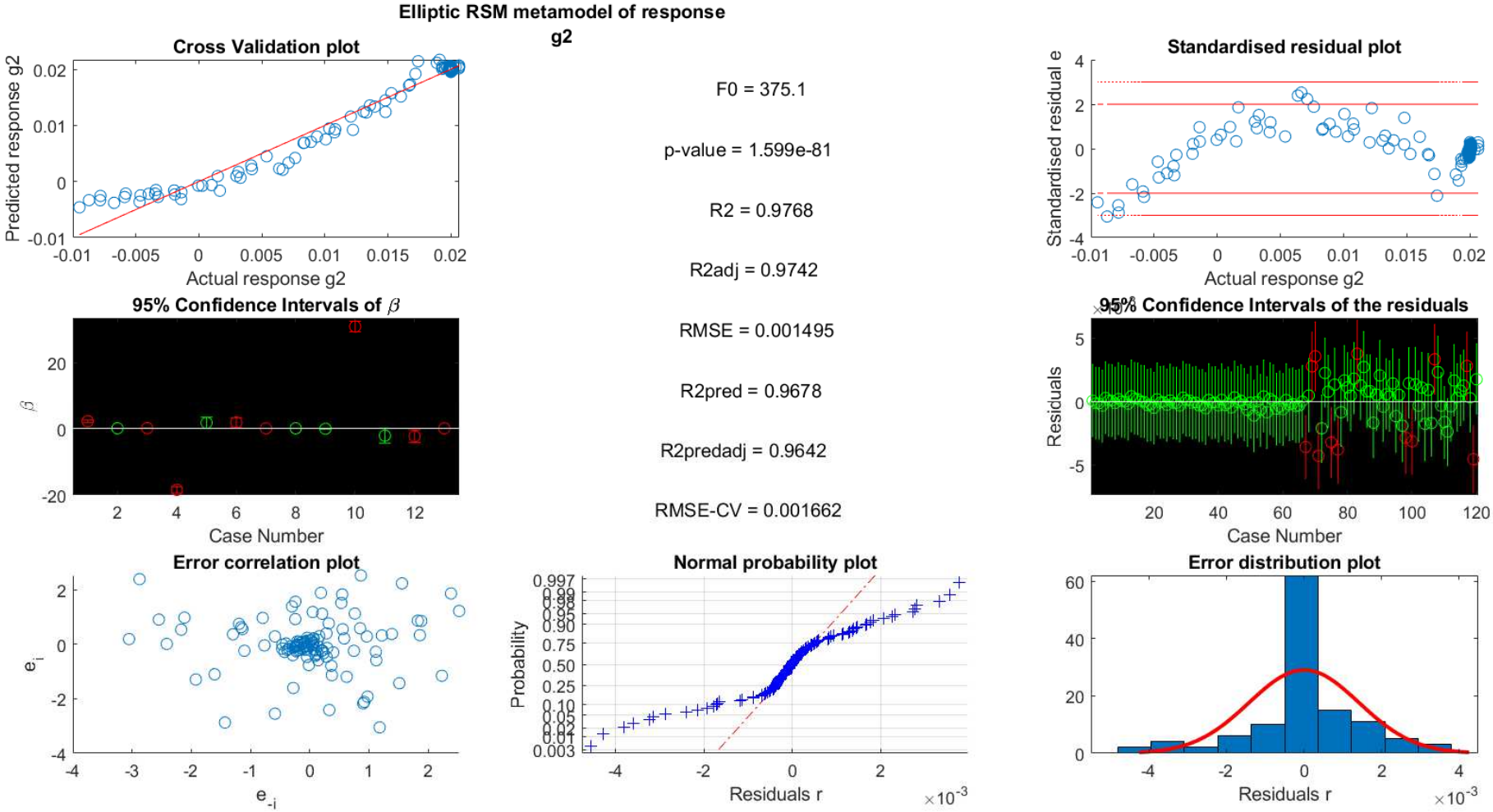
Elliptic RSM metamodel of response
g2
Cross Validation plot
Predicted response g2
Actual response g2
F0 = 375.1
p-value = 1.599e-81
R2 = 0.9768
R2adj = 0.9742
RMSE = 0.001495
R2pred = 0.9678
R2predadj = 0.9642
RMSE-CV = 0.001662
Standardised residual plot
Standardised residual e
Actual response g2
95% Confidence Intervals of β
Case Number
95% Confidence Intervals of the residuals
Residuals
Case Number
Error correlation plot
Normal probability plot
Probability
Residuals r
Error distribution plot
Residuals r

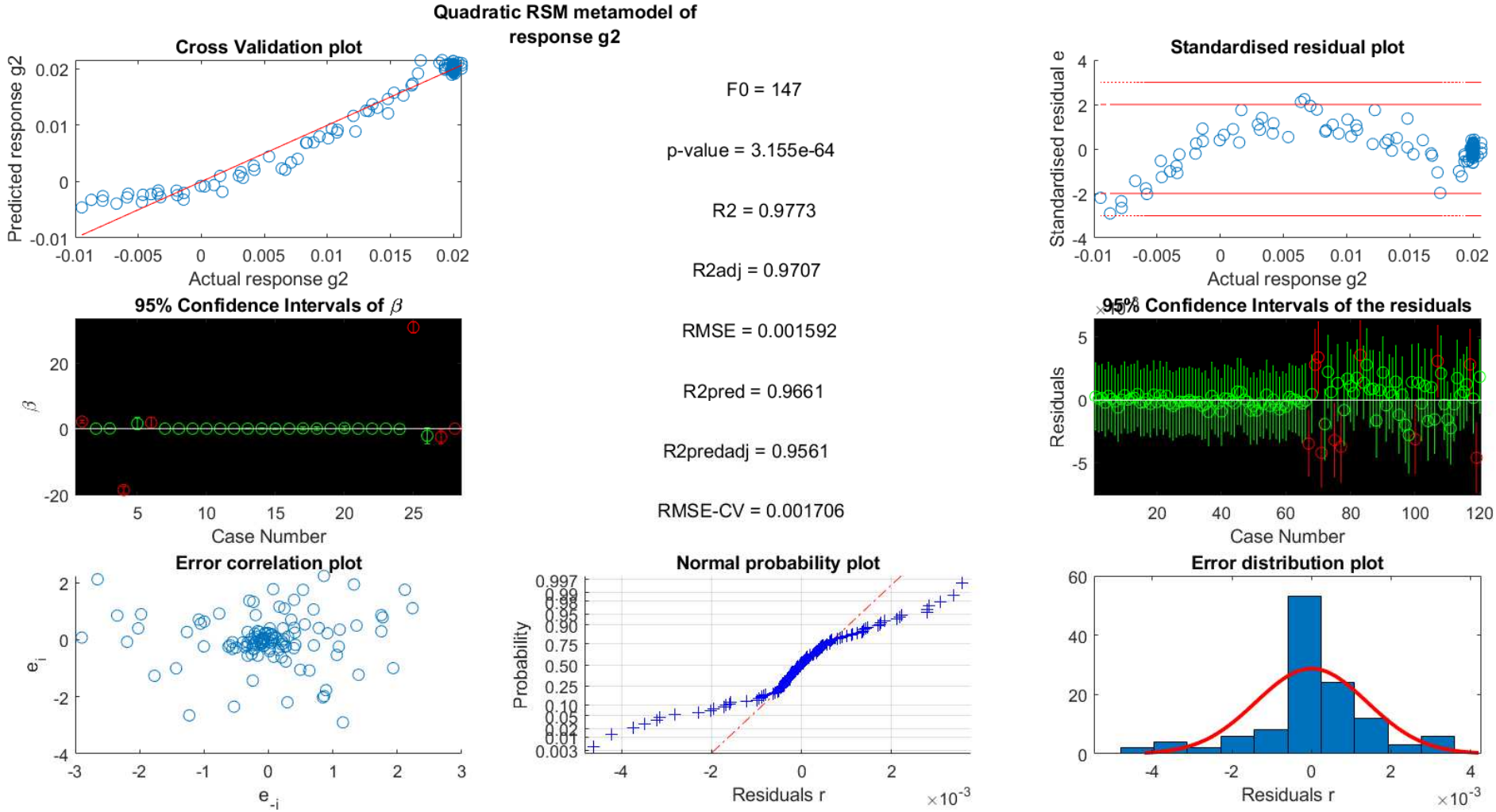

8.9.2 Appendix 9.2 -Kriging

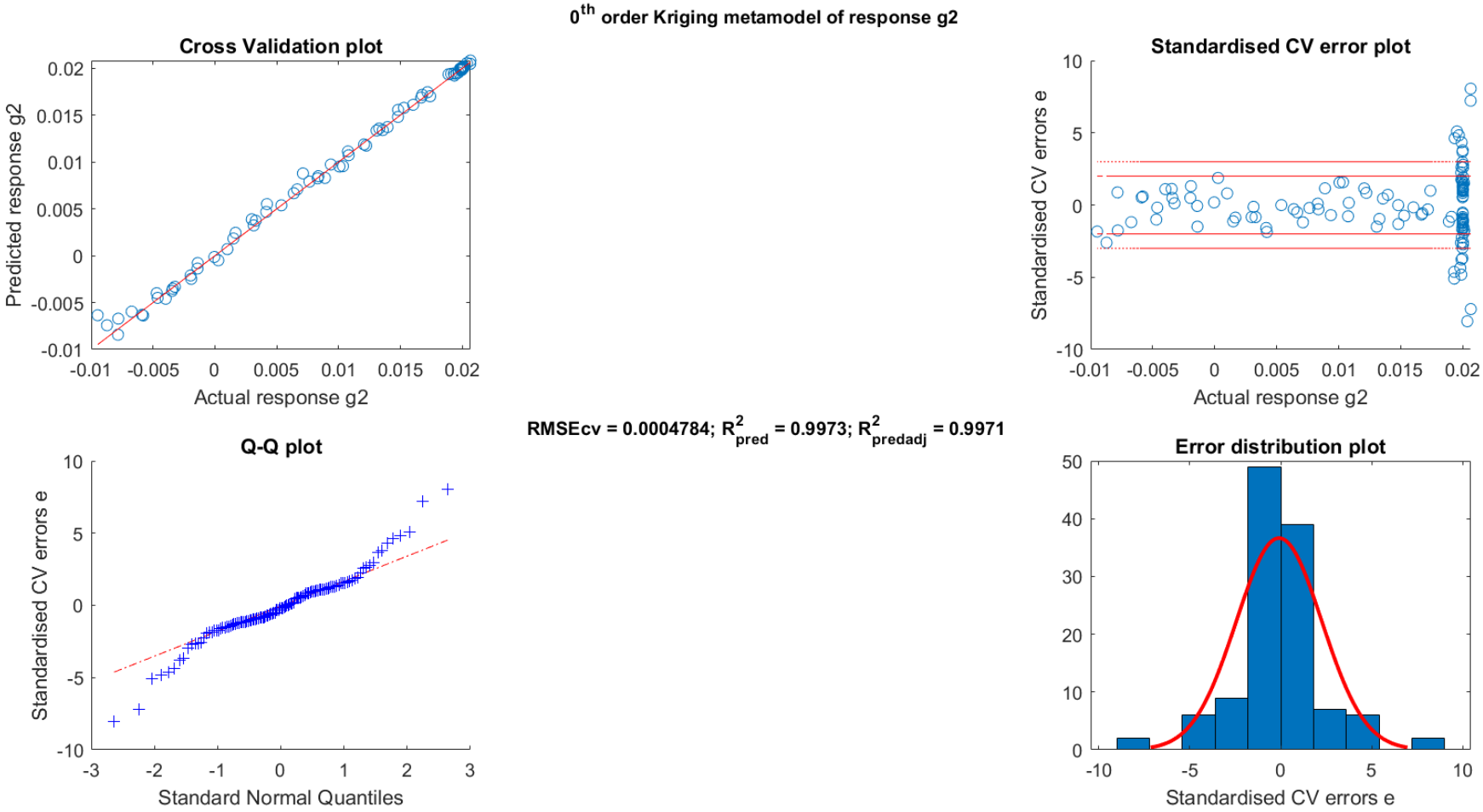
0th order Kriging metamodel of response g2
Cross Validation plot
Predicted response g2
Actual response g2
Standardised CV error plot
Standardised CV errors e
Actual response g2
RMSEcv = 0.0004784; R2pred = 0.9973; R2predadj = 0.9971
Q-Q plot
Standardised CV errors e
Standard Normal Quantiles
Error distribution plot
Standardised CV errors e

1st order Kriging metamodel of response g2

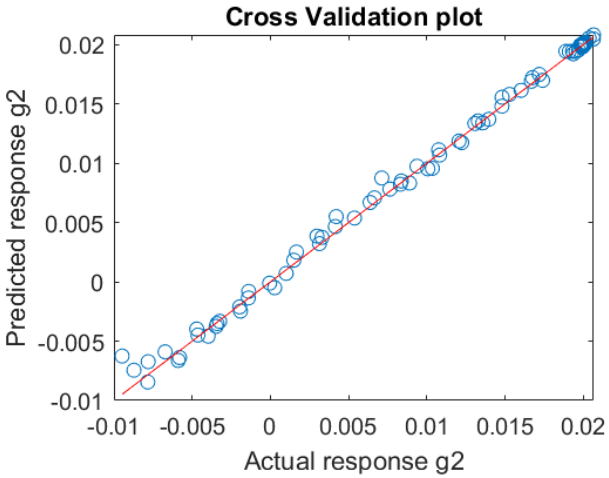

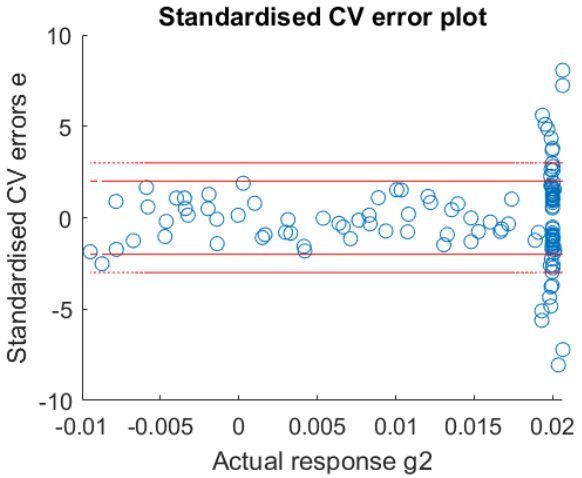

RMSEcv = 0.0004883; R^2_{pred} = 0.9972; $R^2_{predadj}$ = 0.9968

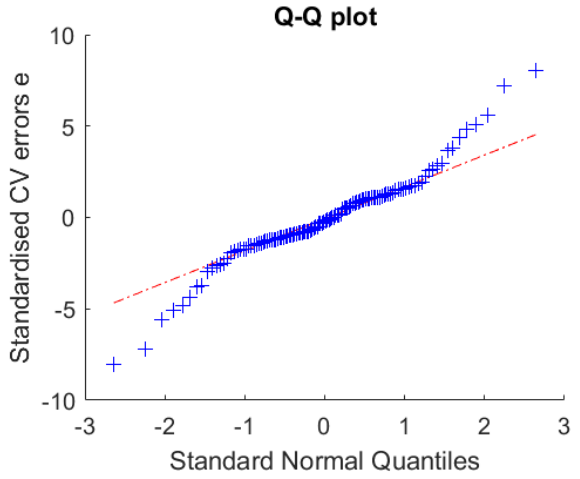

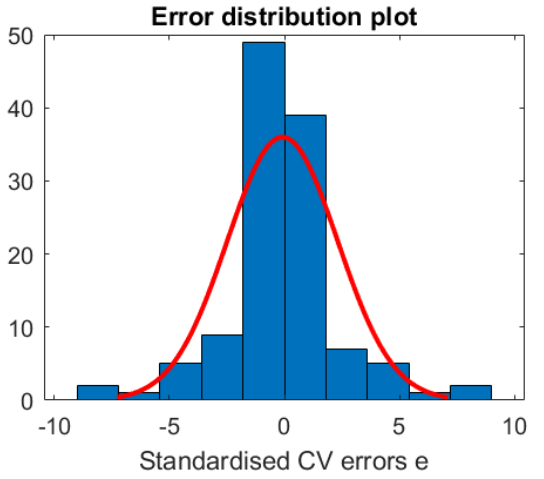

2nd order Kriging metamodel of response g2

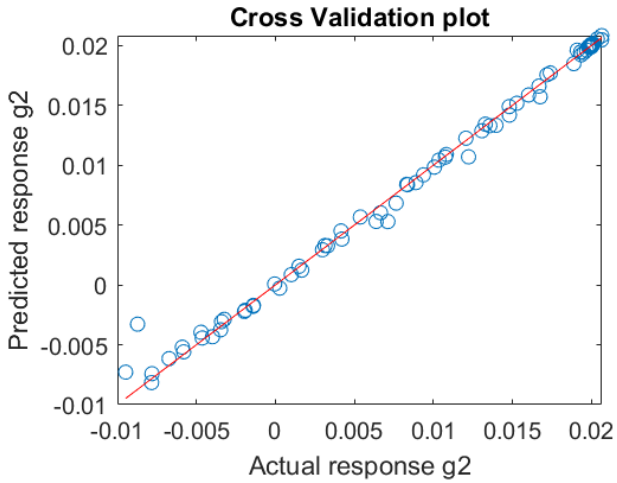

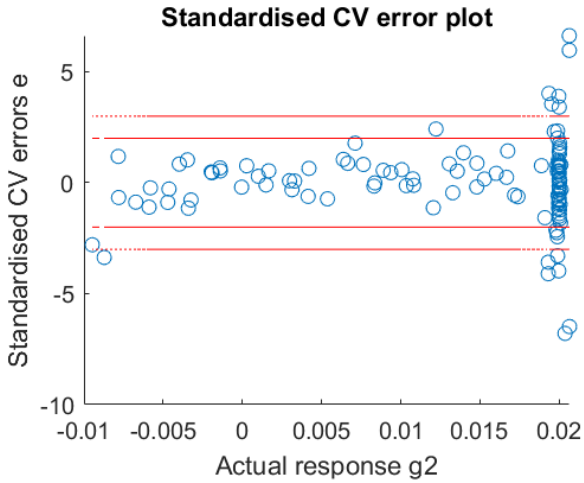

RMSEcv = 0.0006395; R^2_{pred} = 0.9952; $R^2_{predadj}$ = 0.9932

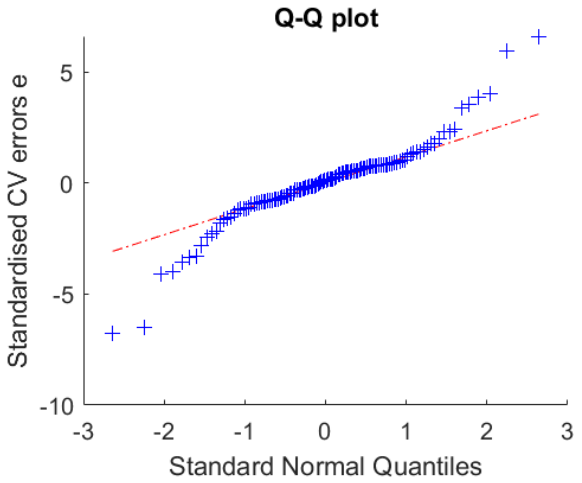

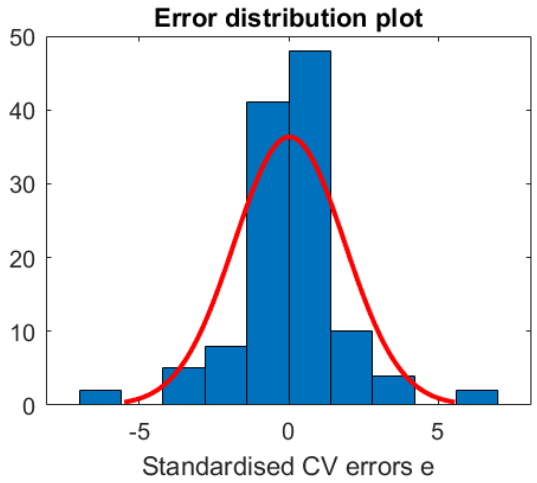

2nd order Regression Kriging metamodel of response g2

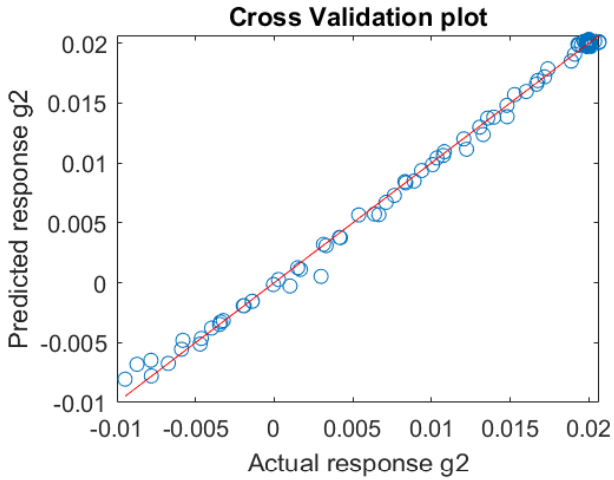

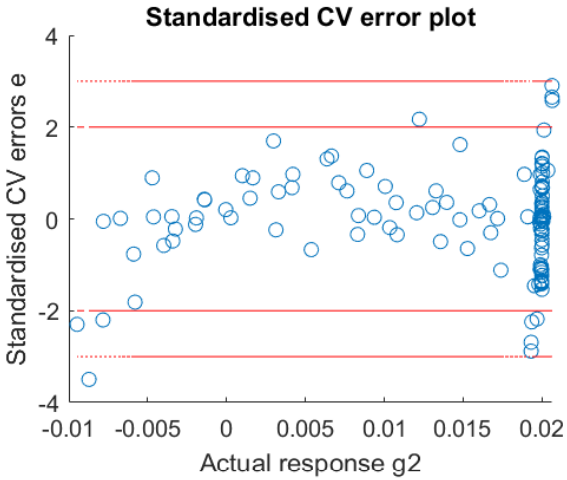

RMSEcv = 0.0004727; R^2_{pred} = 0.9974; $R^2_{predadj}$ = 0.9963

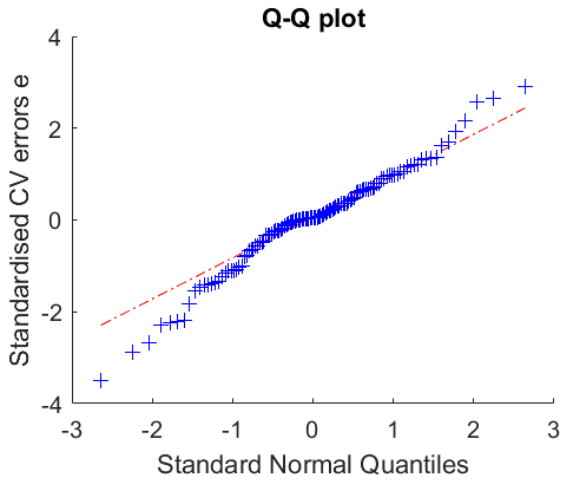

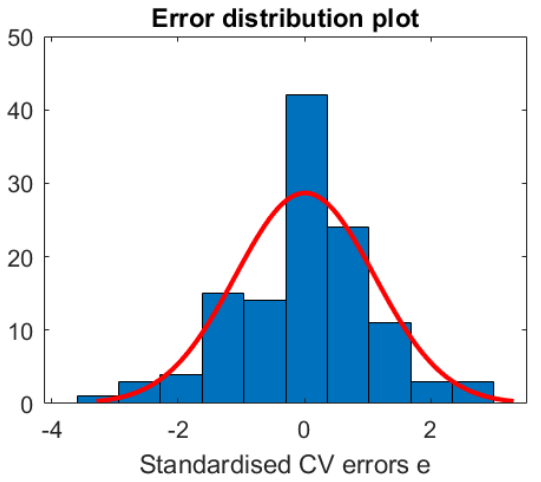

8.10 Appendix 10 -Metamodels validation for the FFD plus the 64 LHD plus 32 LHD taking consideration the optimum for the left right angle

8.10.1 Appendix 10.1 -RSM model

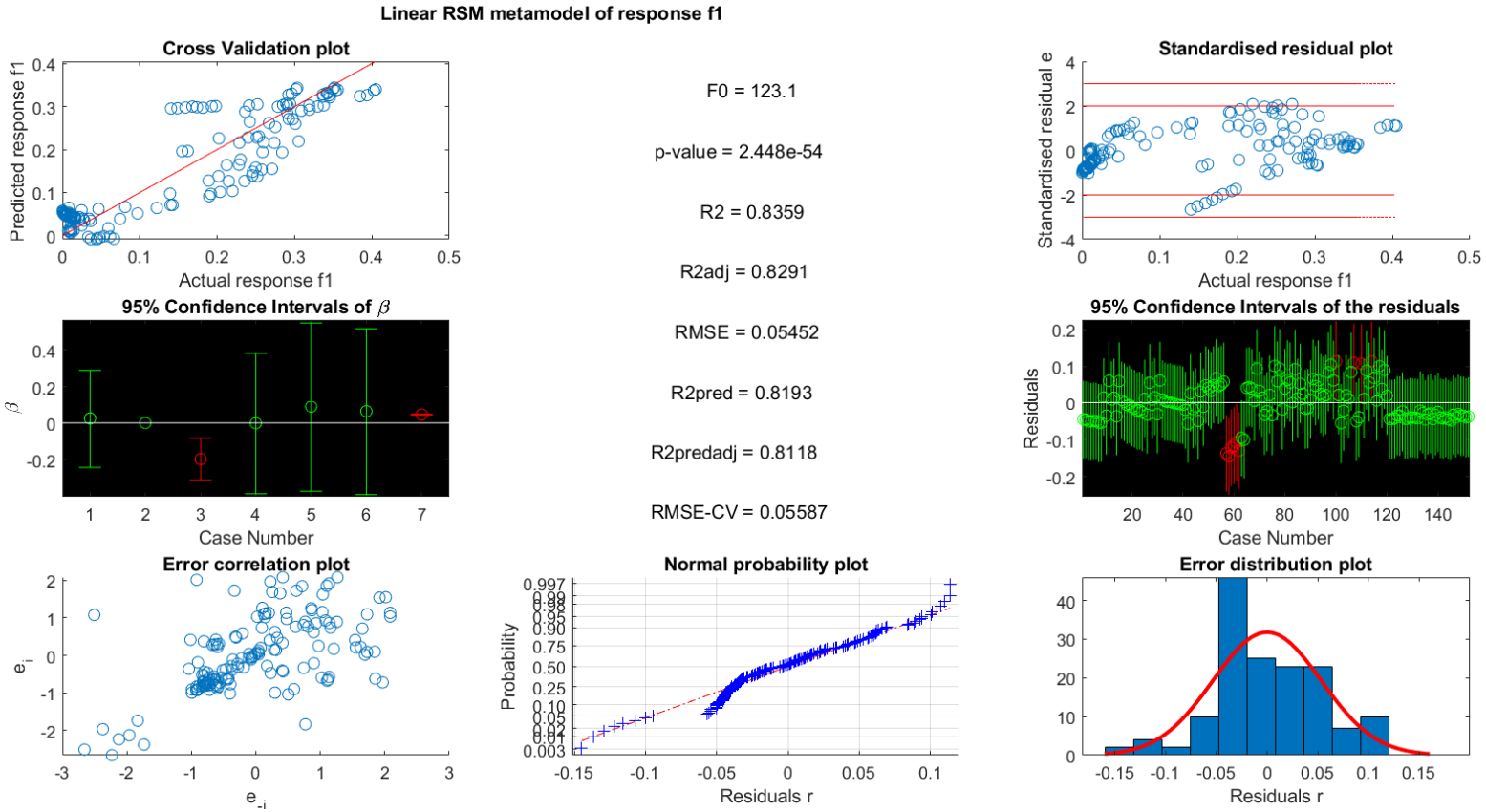

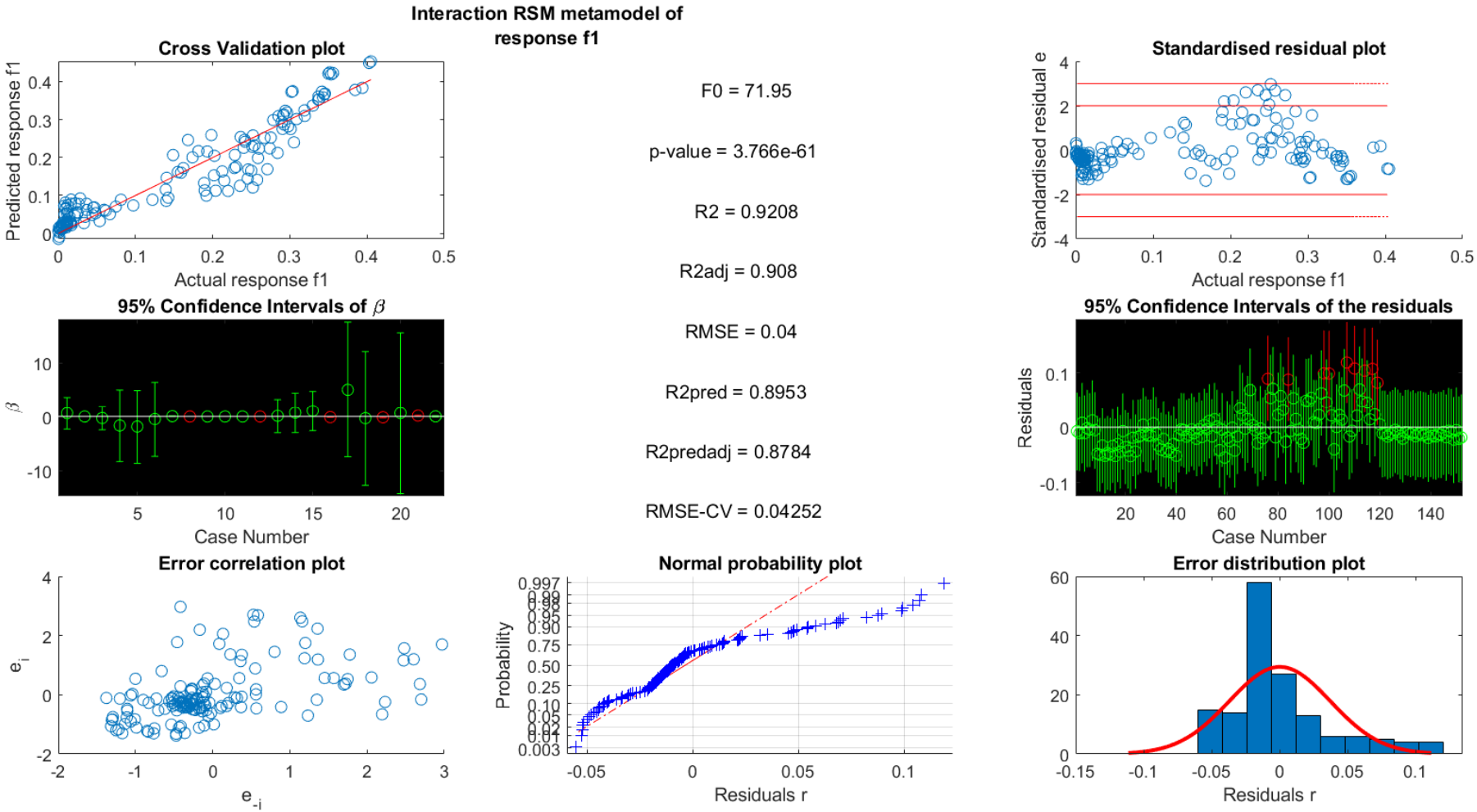
Interaction RSM metamodel of response f1
Cross Validation plot
Predicted response f1
Actual response f1
F0 = 71.95
p-value = 3.766e-61
R2 = 0.9208
R2adj = 0.908
RMSE = 0.04
R2pred = 0.8953
R2predadj = 0.8784
RMSE-CV = 0.04252
Standardised residual plot
Standardised residual e
Actual response f1
95% Confidence Intervals of β
β
Case Number
95% Confidence Intervals of the residuals
Residuals
Case Number
Error correlation plot
e_i
e_-i
Normal probability plot
Probability
Residuals r
Error distribution plot
Residuals r

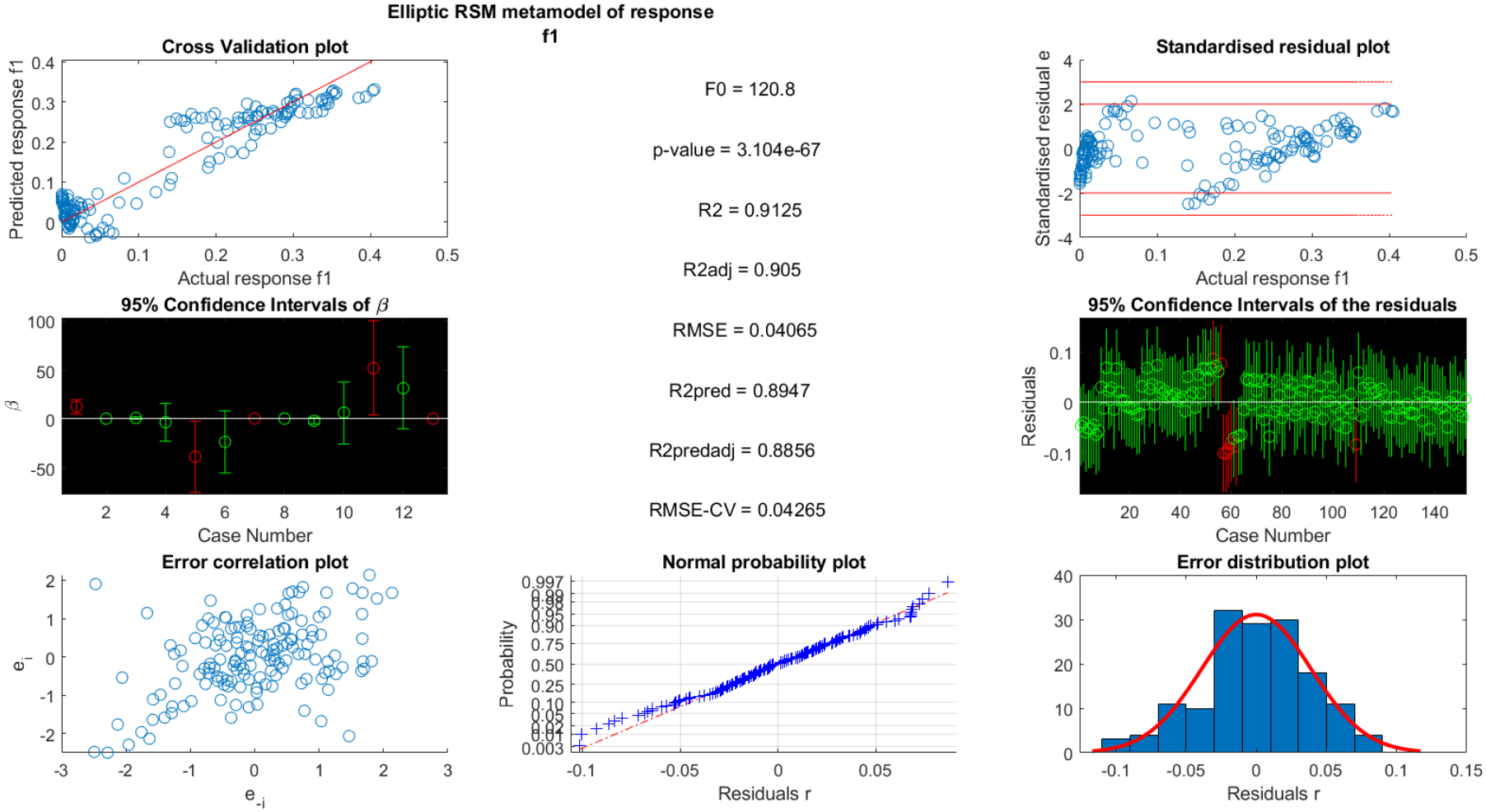
Elliptic RSM metamodel of response
f1
Cross Validation plot
Predicted response f1
Actual response f1
F0 = 120.8
p-value = 3.104e-67
R2 = 0.9125
R2adj = 0.905
RMSE = 0.04065
R2pred = 0.8947
R2predadj = 0.8856
RMSE-CV = 0.04265
Standardised residual plot
Standardised residual e
Actual response f1
95% Confidence Intervals of β
β
Case Number
95% Confidence Intervals of the residuals
Residuals
Case Number
Error correlation plot
e_i
e_-i
Normal probability plot
Probability
Residuals r
Error distribution plot
Residuals r

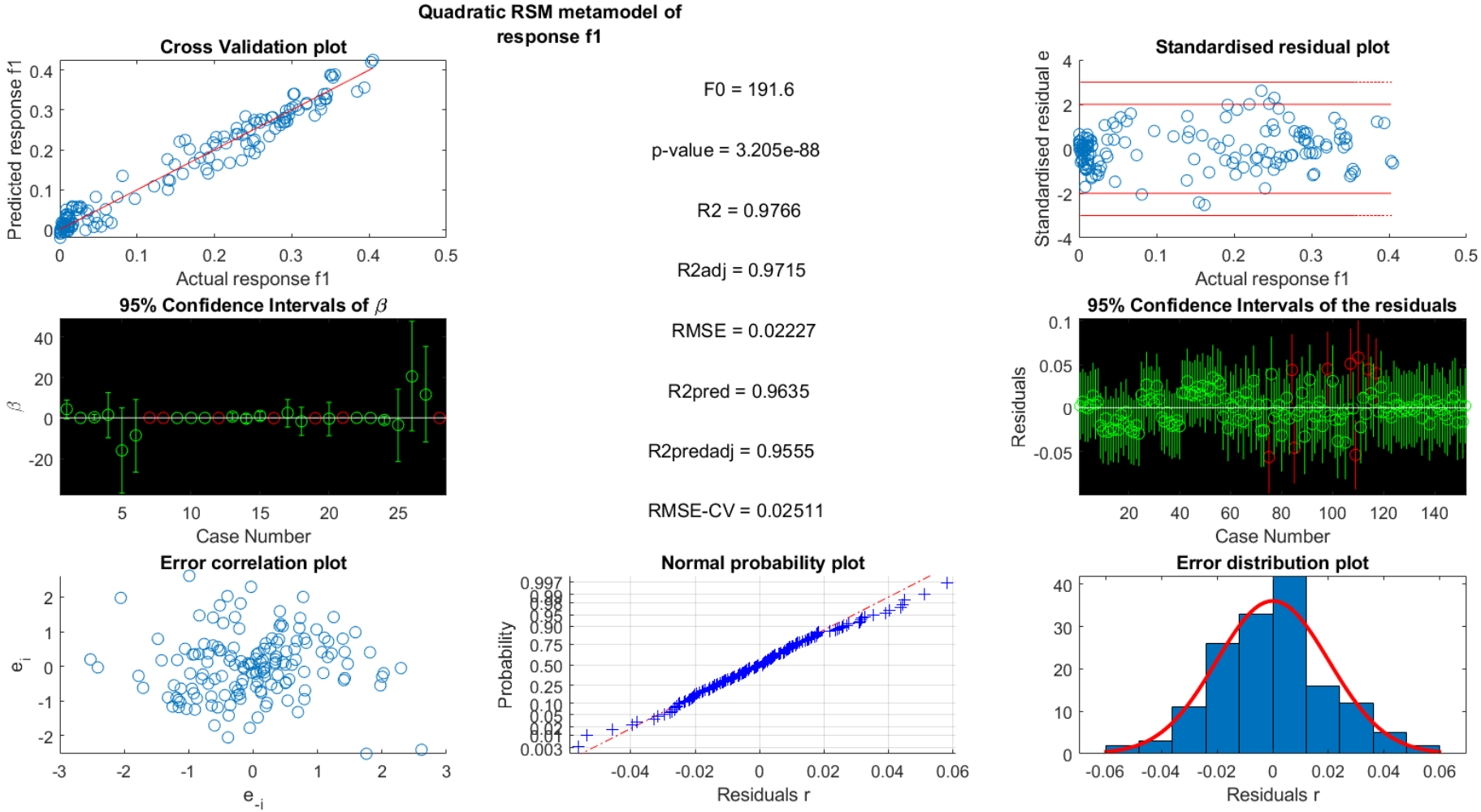
Quadratic RSM metamodel of response f1
Cross Validation plot
Predicted response f1
Actual response f1
F0 = 191.6
p-value = 3.205e-88
R2 = 0.9766
R2adj = 0.9715
RMSE = 0.02227
R2pred = 0.9635
R2predadj = 0.9555
RMSE-CV = 0.02511
Standardised residual plot
Standardised residual e
Actual response f1
95% Confidence Intervals of β
β
Case Number
95% Confidence Intervals of the residuals
Residuals
Case Number
Error correlation plot
e_i
e_-i
Normal probability plot
Probability
Residuals r
Error distribution plot
Residuals r

8.10.2 Appendix 10.2 -RSM model

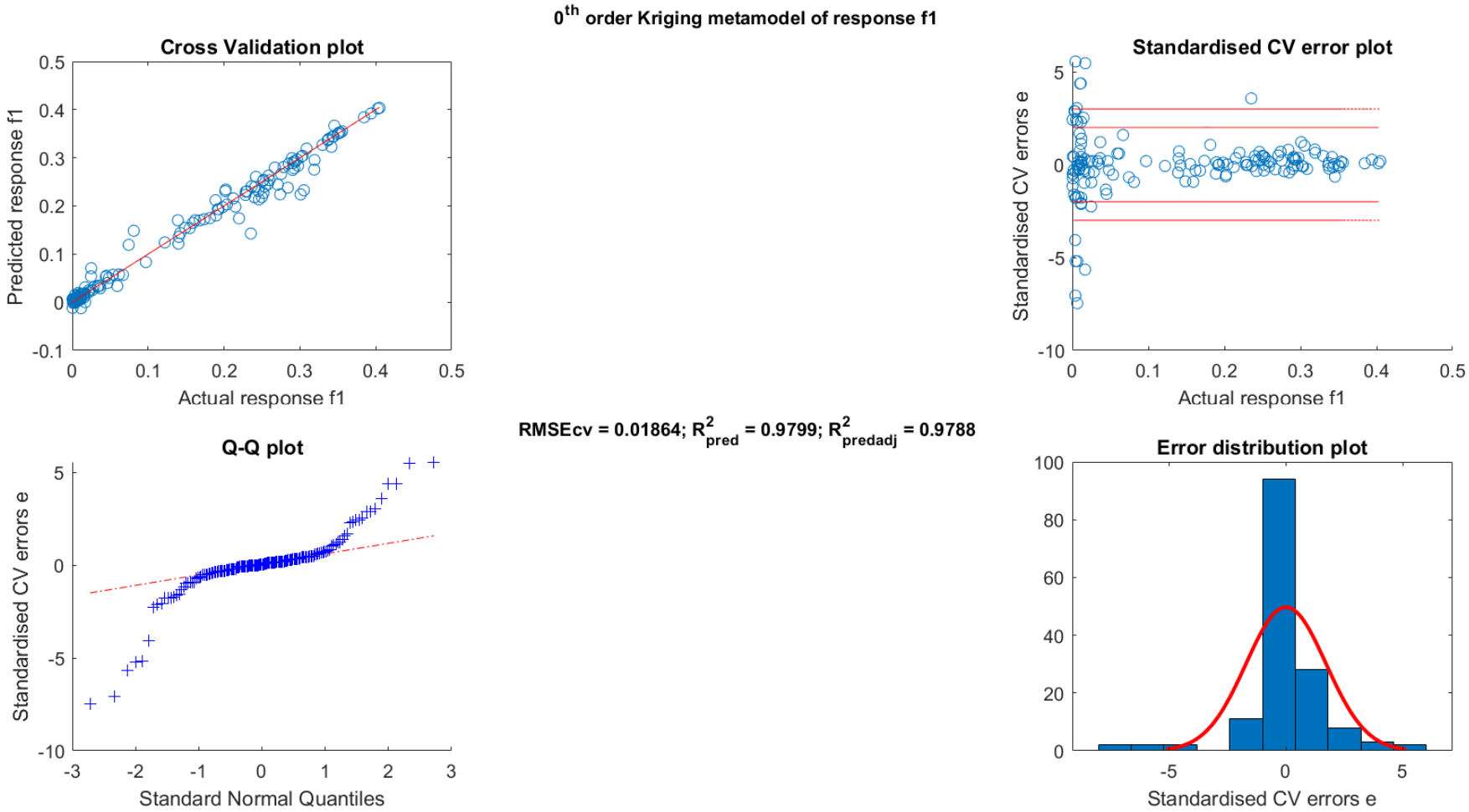

1st order Kriging metamodel of response f1

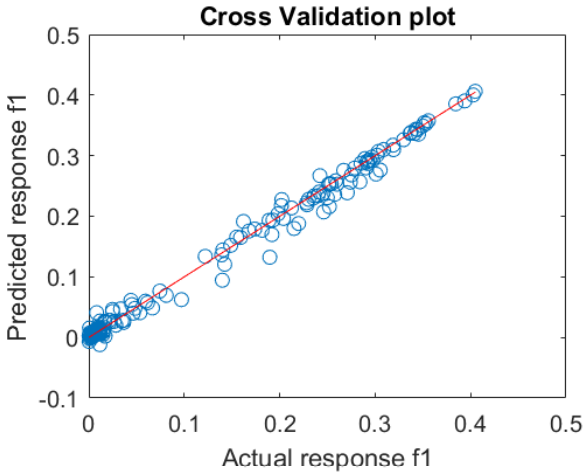

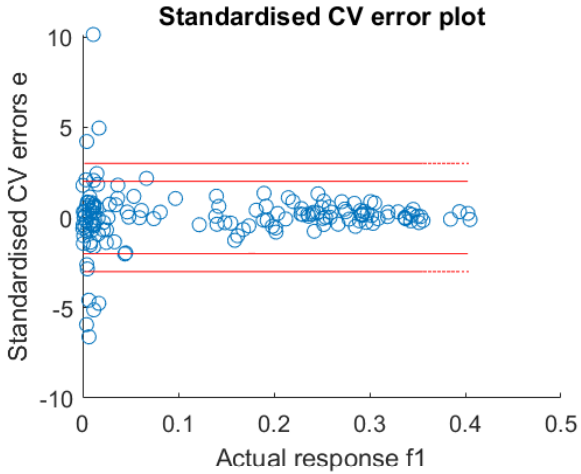

RMSEcv = 0.01326; R^2_{pred} = 0.9898; $R^2_{predadj}$ = 0.9888

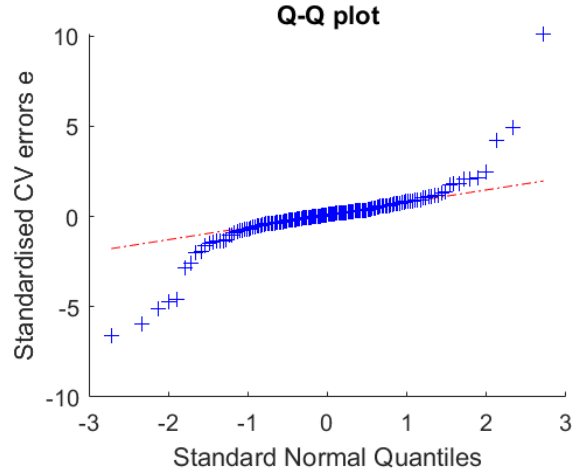

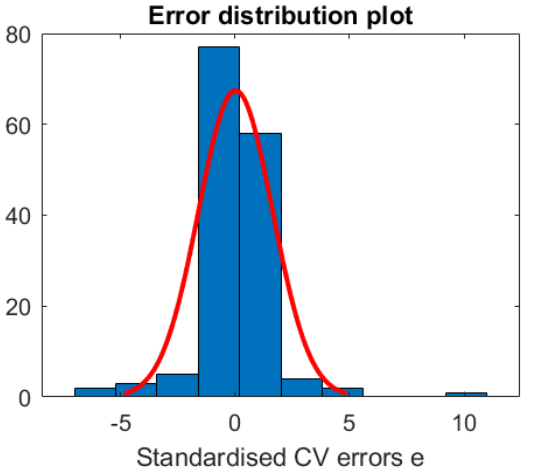

2nd order Kriging metamodel of response f1

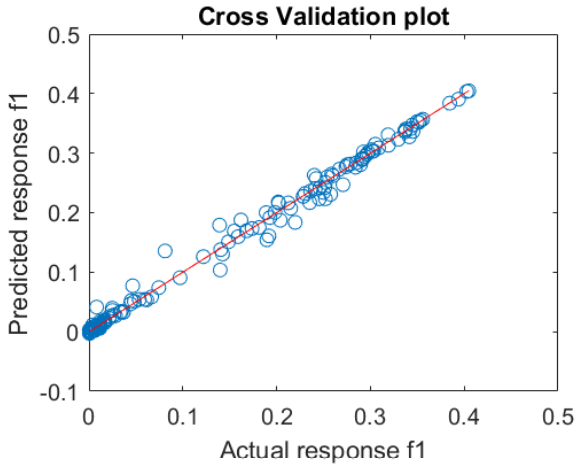

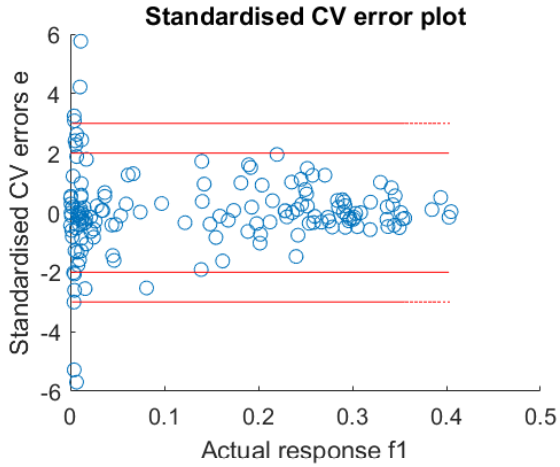

RMSEcv = 0.01135; R^2_{pred} = 0.9925; $R^2_{predadj}$ = 0.9903

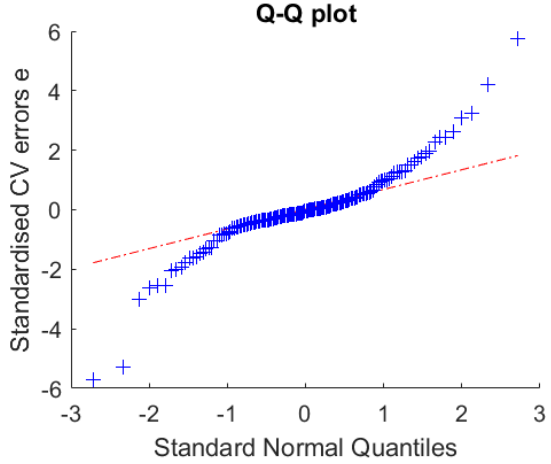

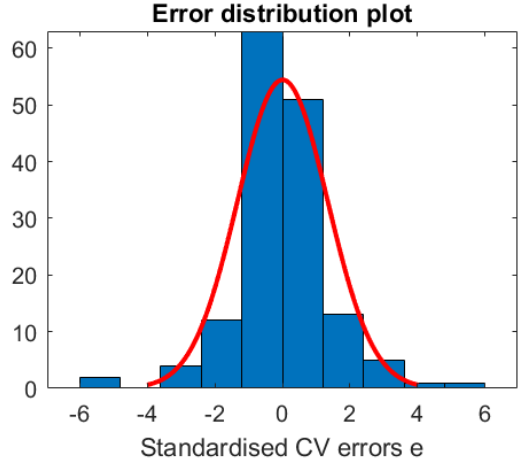

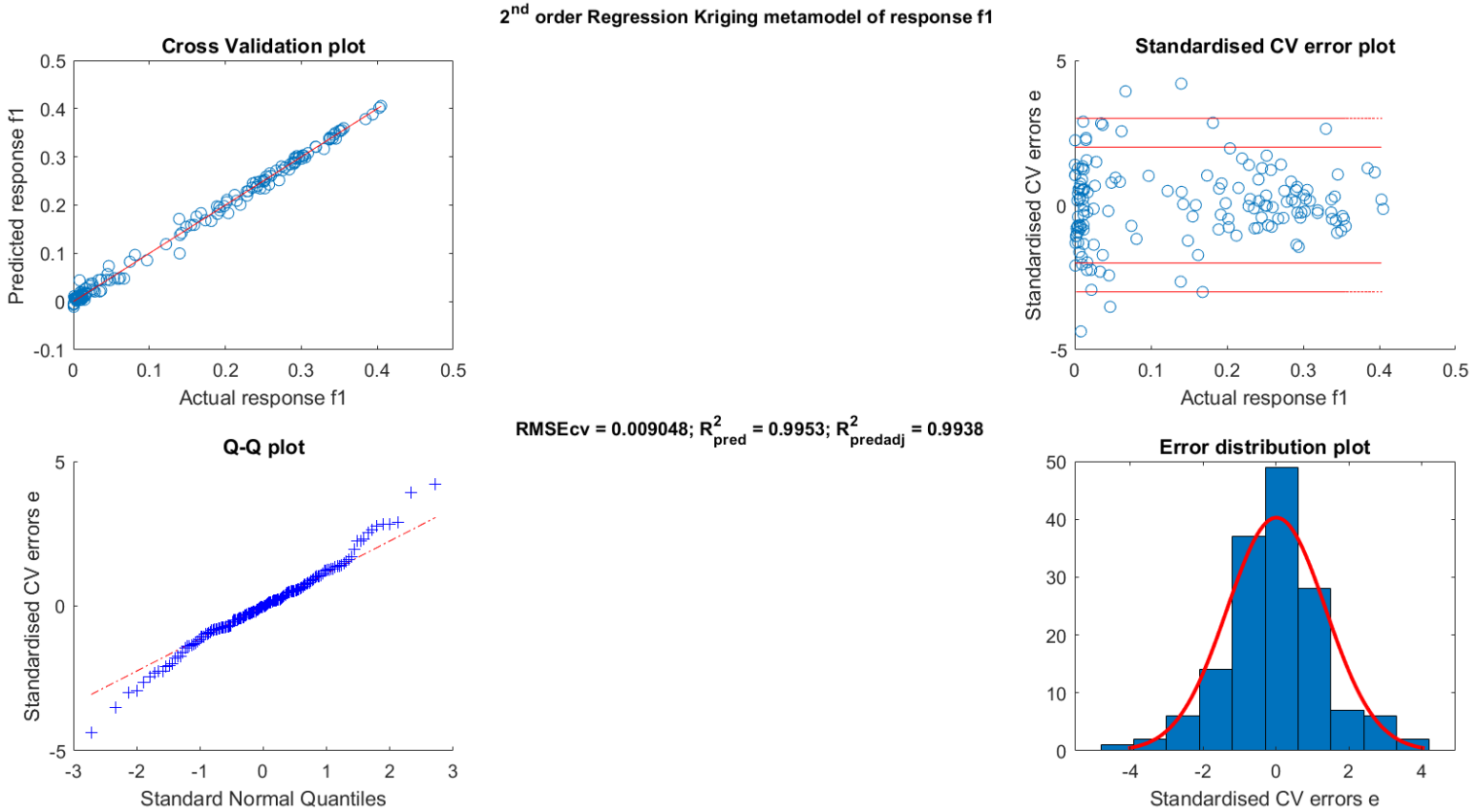
2nd order Regression Kriging metamodel of response f1
Cross Validation plot
Predicted response f1
Actual response f1
Standardised CV error plot
Standardised CV errors e
Actual response f1
RMSEcv = 0.009048; R2pred = 0.9953; R2predadj = 0.9938
Q-Q plot
Standardised CV errors e
Standard Normal Quantiles
Error distribution plot
Standardised CV errors e

8.11 Appendix 11 - Metamodels validation for the FFD plus the 64 LHD plus 32 LHD taking consideration the optimum for the front back angle

8.11.1 Appendix 11.1 -RSM model

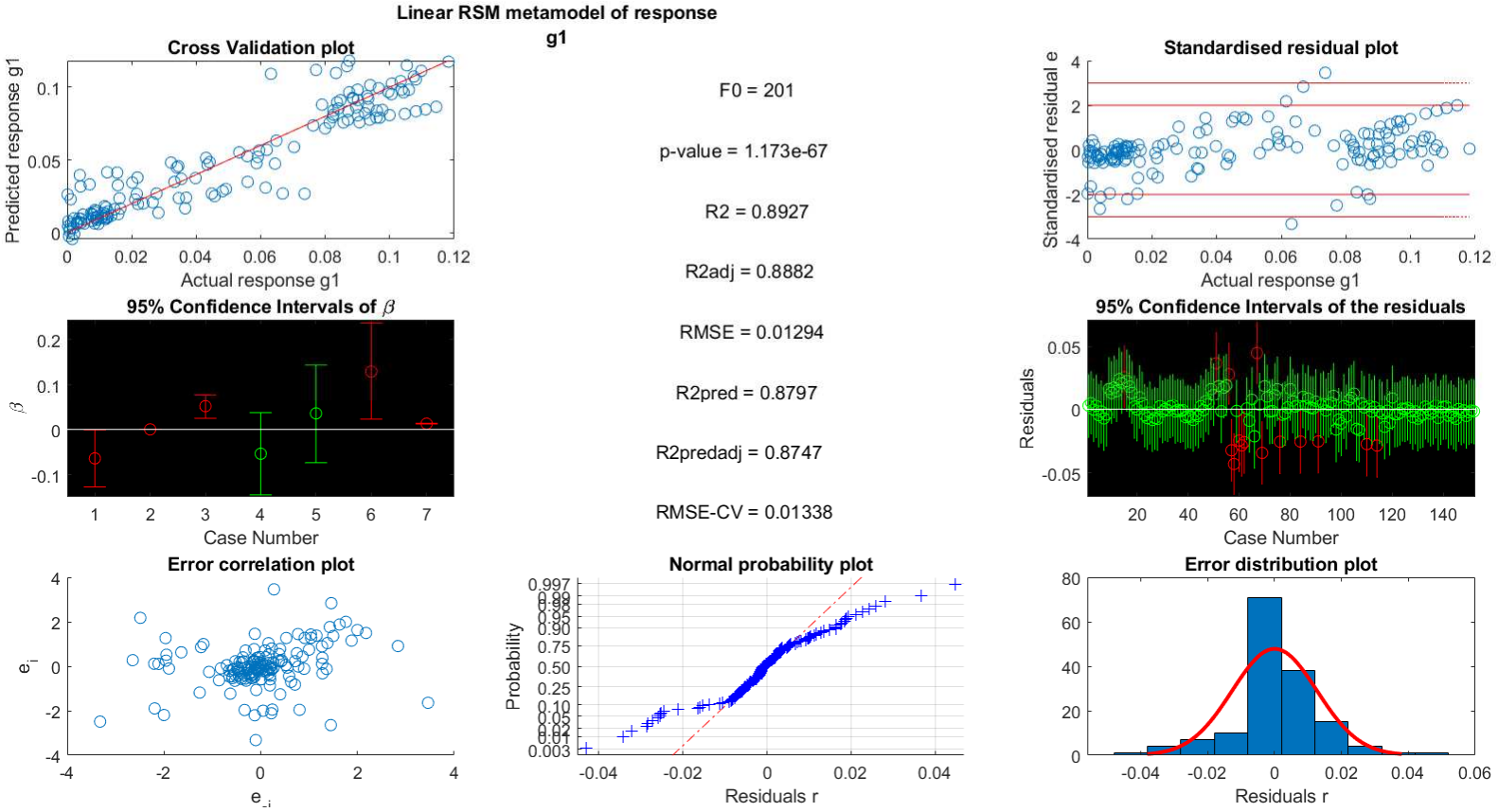

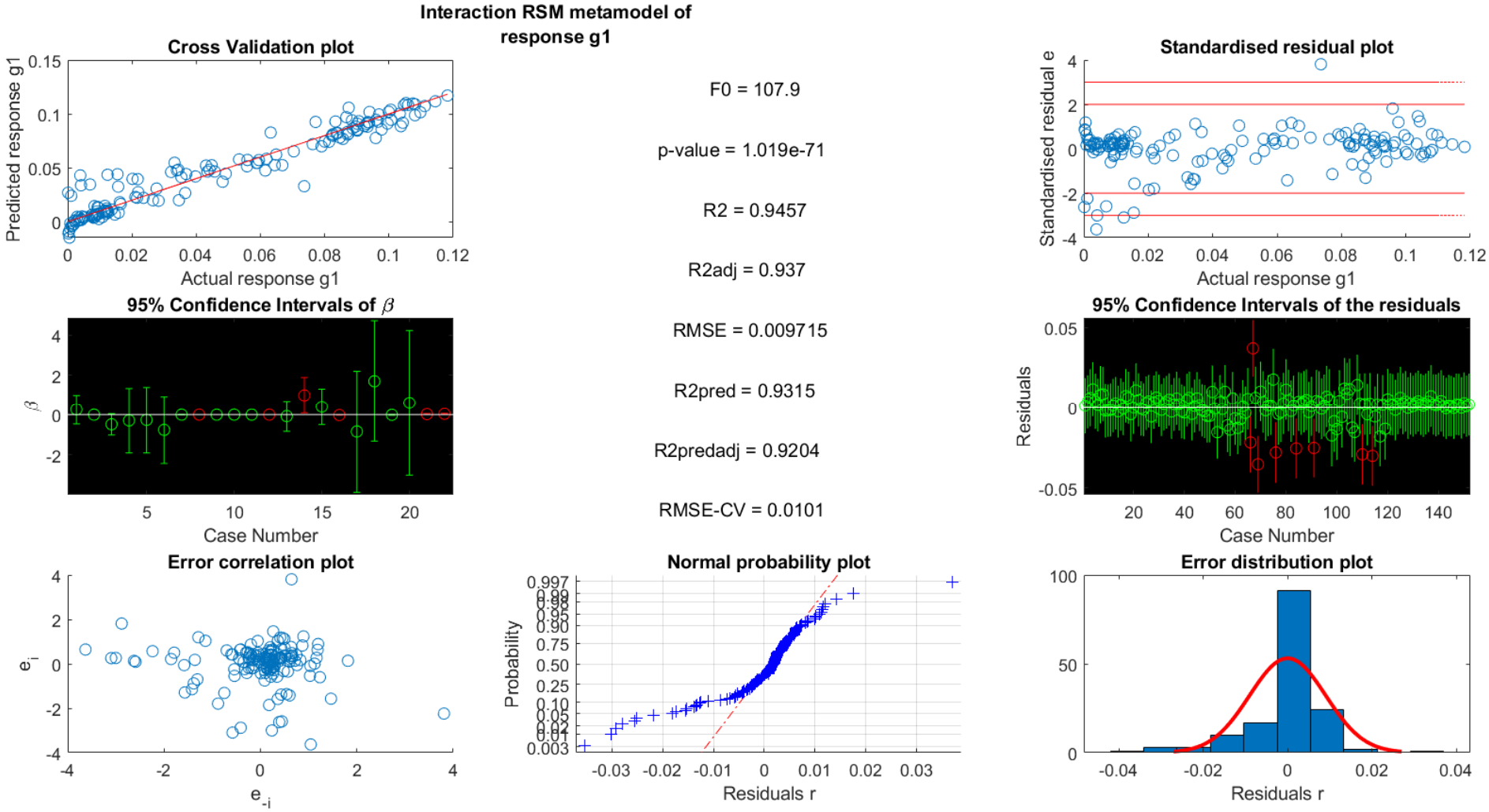
Interaction RSM metamodel of response g1
Cross Validation plot
Predicted response g1
Actual response g1
F0 = 107.9
p-value = 1.019e-71
R2 = 0.9457
R2adj = 0.937
RMSE = 0.009715
R2pred = 0.9315
R2predadj = 0.9204
RMSE-CV = 0.0101
Standardised residual plot
Standardised residual e
Actual response g1
95% Confidence Intervals of β
β
Case Number
95% Confidence Intervals of the residuals
Residuals
Case Number
Error correlation plot
e_i
e_-i
Normal probability plot
Probability
Residuals r
Error distribution plot
Residuals r

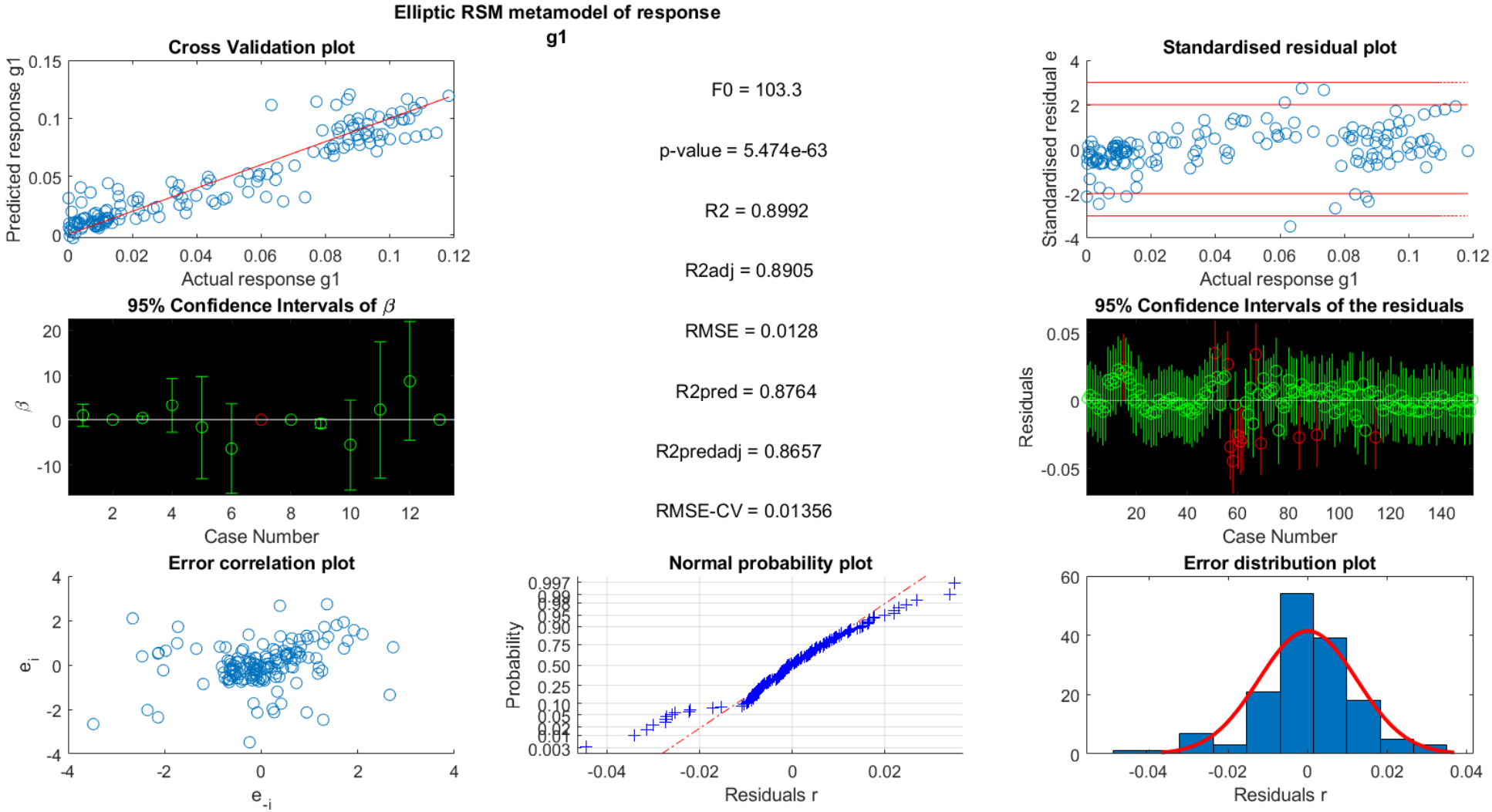
Elliptic RSM metamodel of response
g1
Cross Validation plot
Predicted response g1
Actual response g1
F0 = 103.3
p-value = 5.474e-63
R2 = 0.8992
R2adj = 0.8905
RMSE = 0.0128
R2pred = 0.8764
R2predadj = 0.8657
RMSE-CV = 0.01356
Standardised residual plot
Standardised residual e
Actual response g1
95% Confidence Intervals of β
β
Case Number
95% Confidence Intervals of the residuals
Residuals
Case Number
Error correlation plot
e_i
e_-i
Normal probability plot
Probability
Residuals r
Error distribution plot
Residuals r

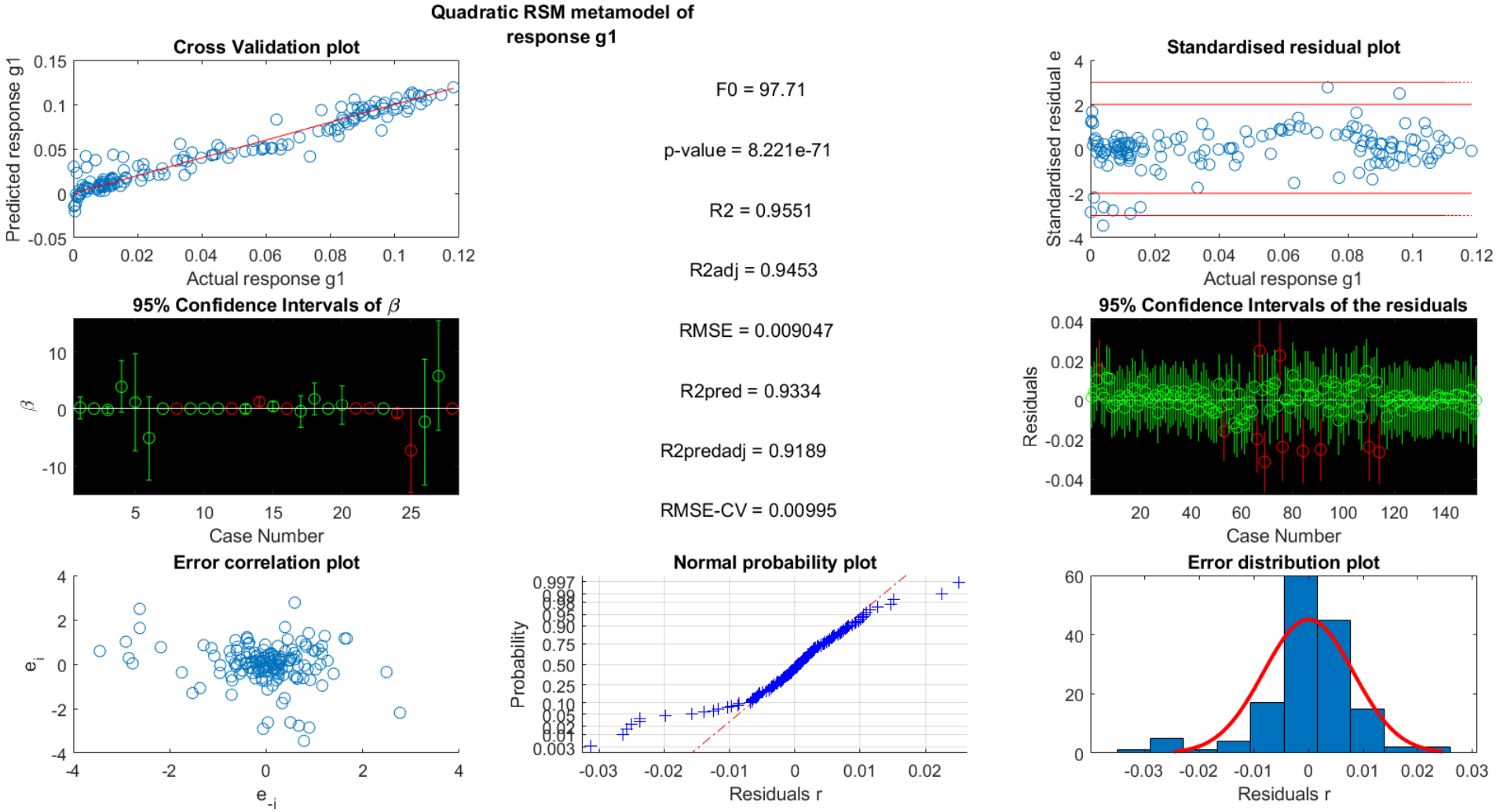

8.11.2 Appendix 11.2 -Kriging

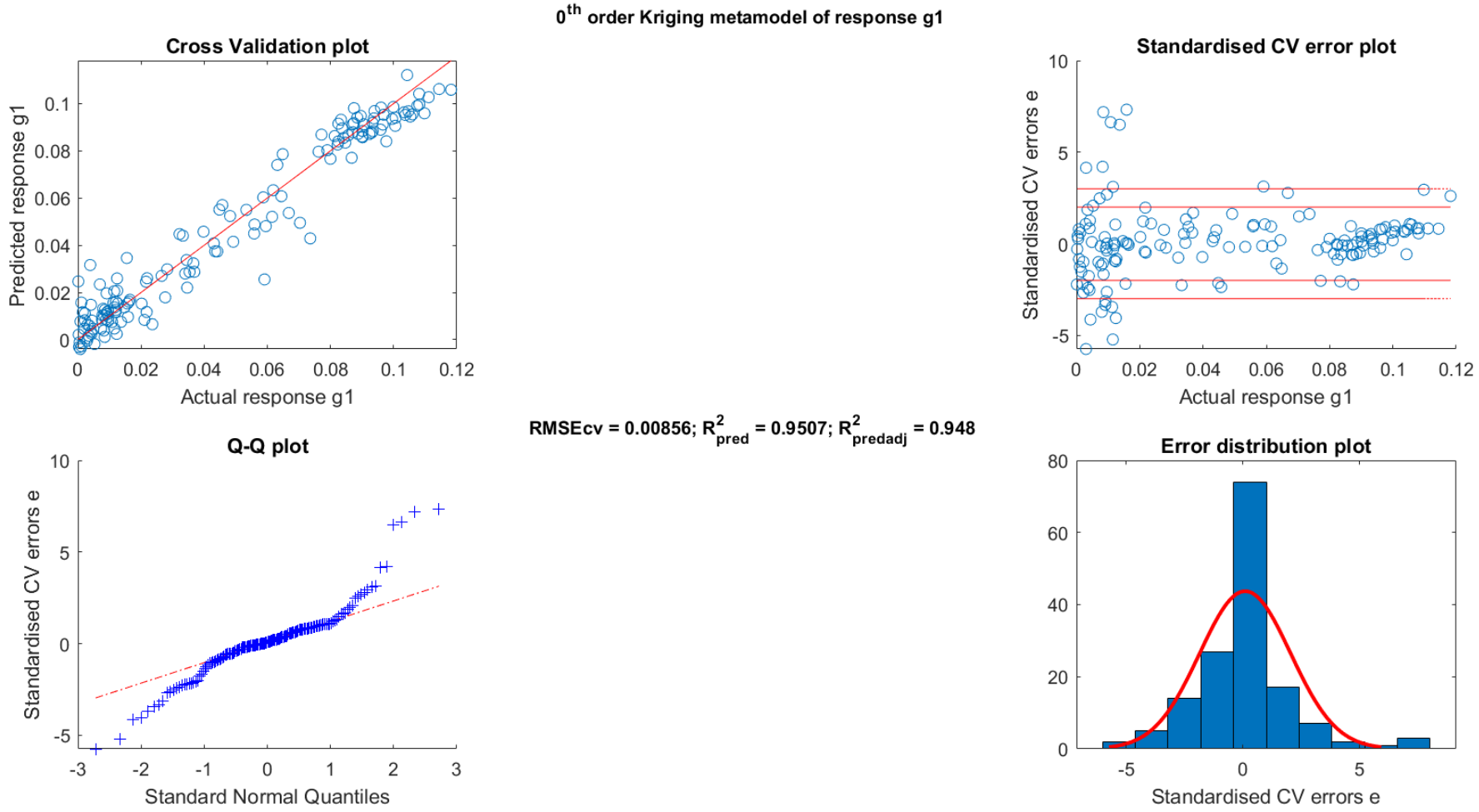
0th order Kriging metamodel of response g1
Cross Validation plot
Predicted response g1
Actual response g1
RMSEcv = 0.00856; R2pred = 0.9507; R2predadj = 0.948
Standardised CV error plot
Standardised CV errors e
Actual response g1
Q-Q plot
Standardised CV errors e
Standard Normal Quantiles
Error distribution plot
Standardised CV errors e

1st order Kriging metamodel of response g1

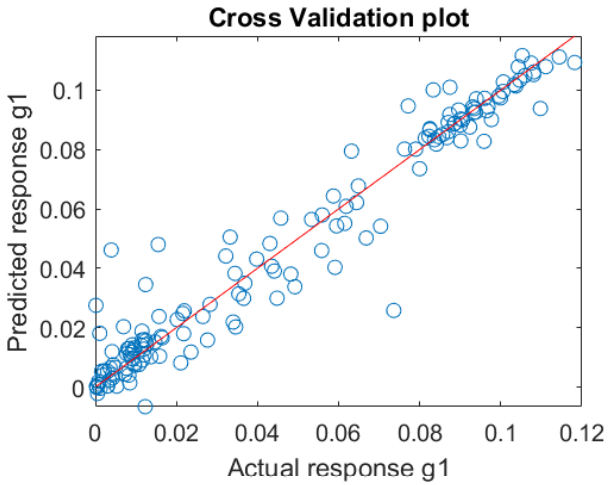

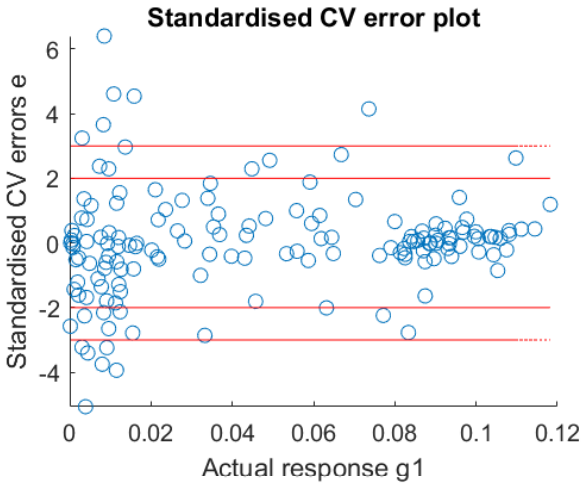

RMSEcv = 0.009261; R^2_{pred} = 0.9423; $R^2_{predadj}$ = 0.9364

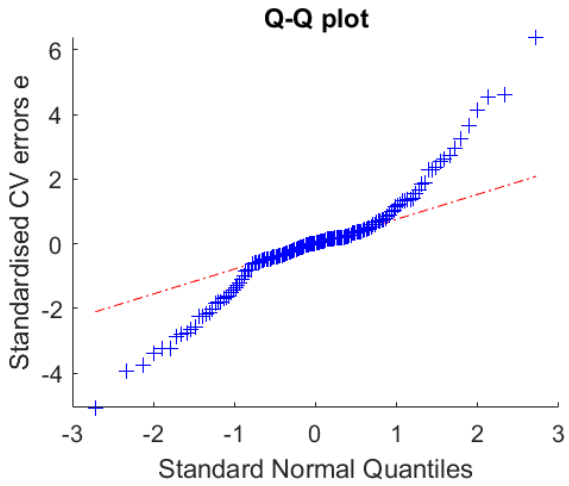

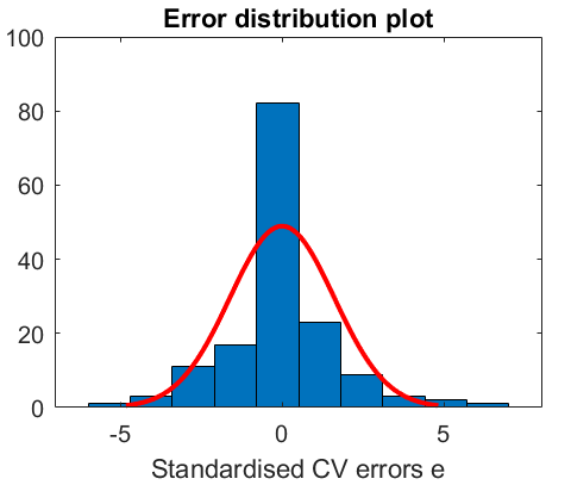

2nd order Kriging metamodel of response g1

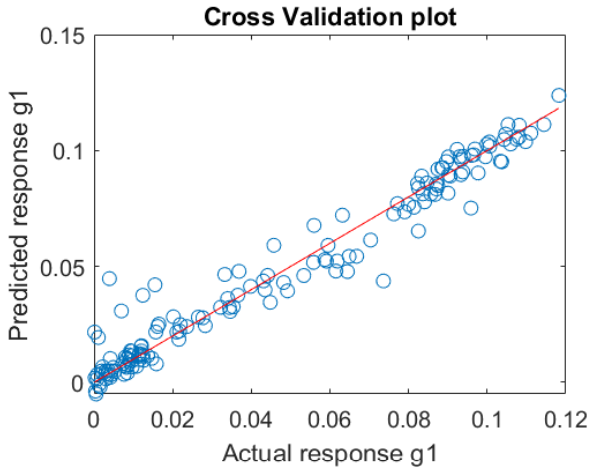

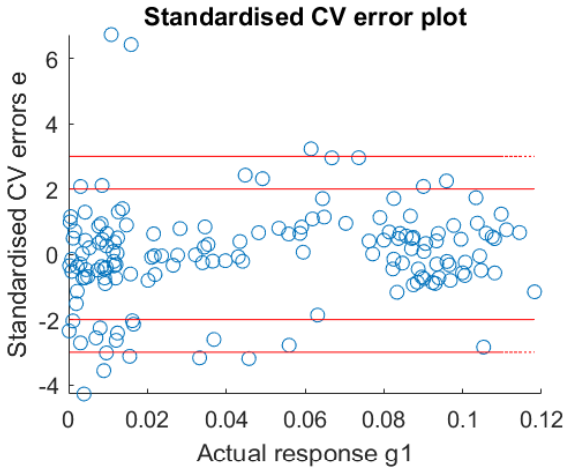

RMSEcv = 0.007985; R^2_{pred} = 0.9571; $R^2_{predadj}$ = 0.9442

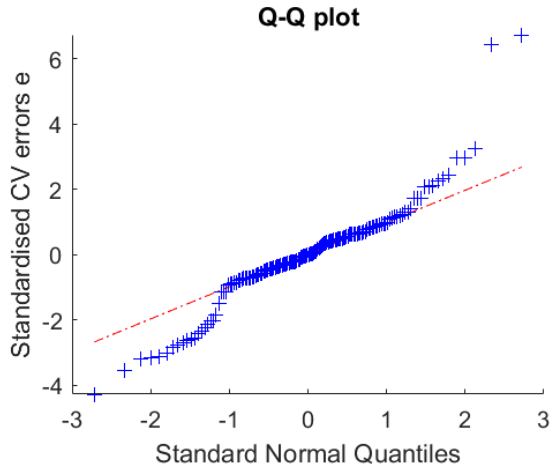

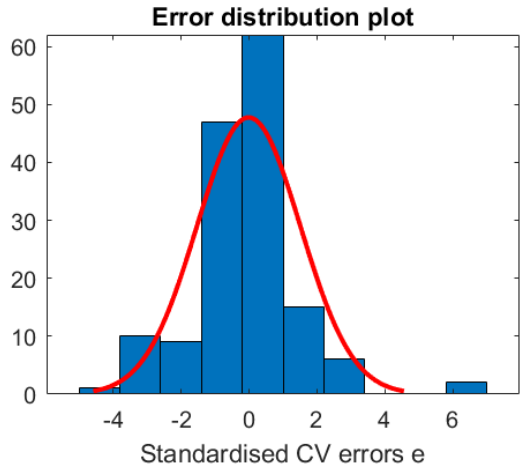

2nd order Regression Kriging metamodel of response g1

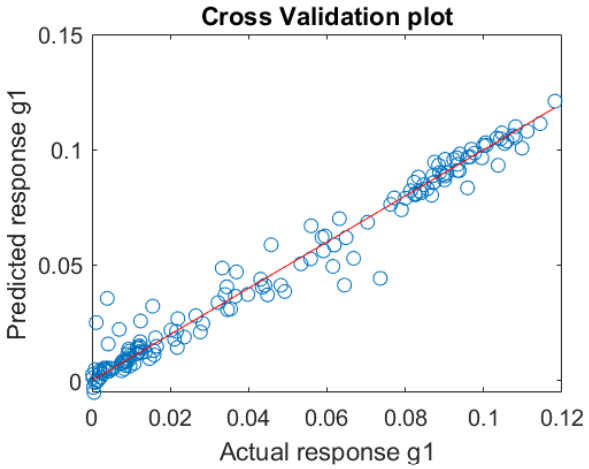

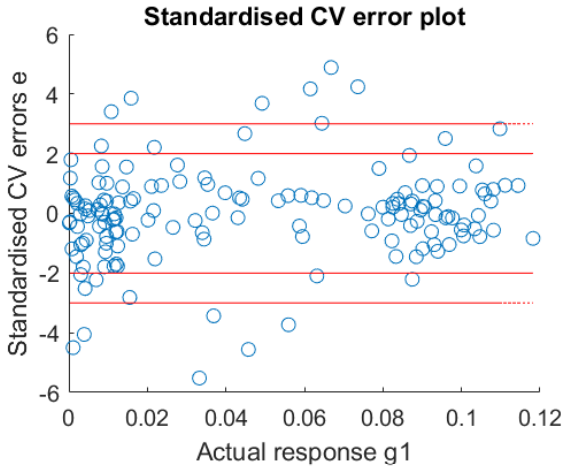

RMSEcv = 0.006511; R^2_{pred} = 0.9715; $R^2_{predadj}$ = 0.9629

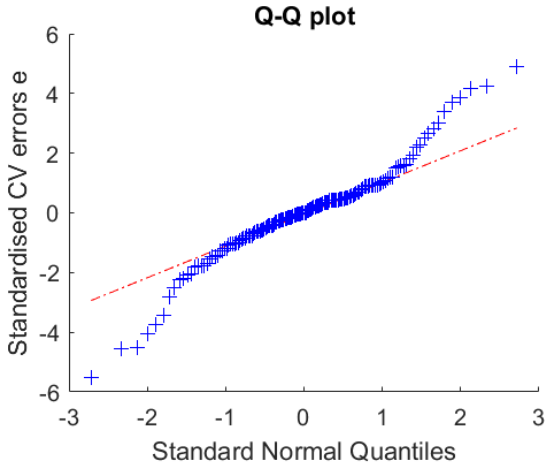

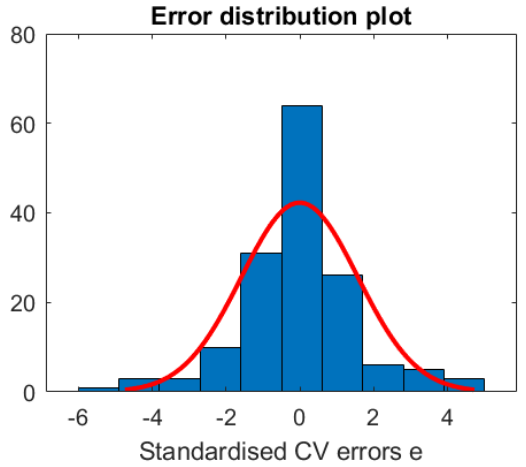

8.12 Appendix 12 - Metamodels validation for the FFD plus the 64 LHD plus 32 LHD taking consideration the optimum for the thickness

8.12.1 Appendix 12.1 - RSM model

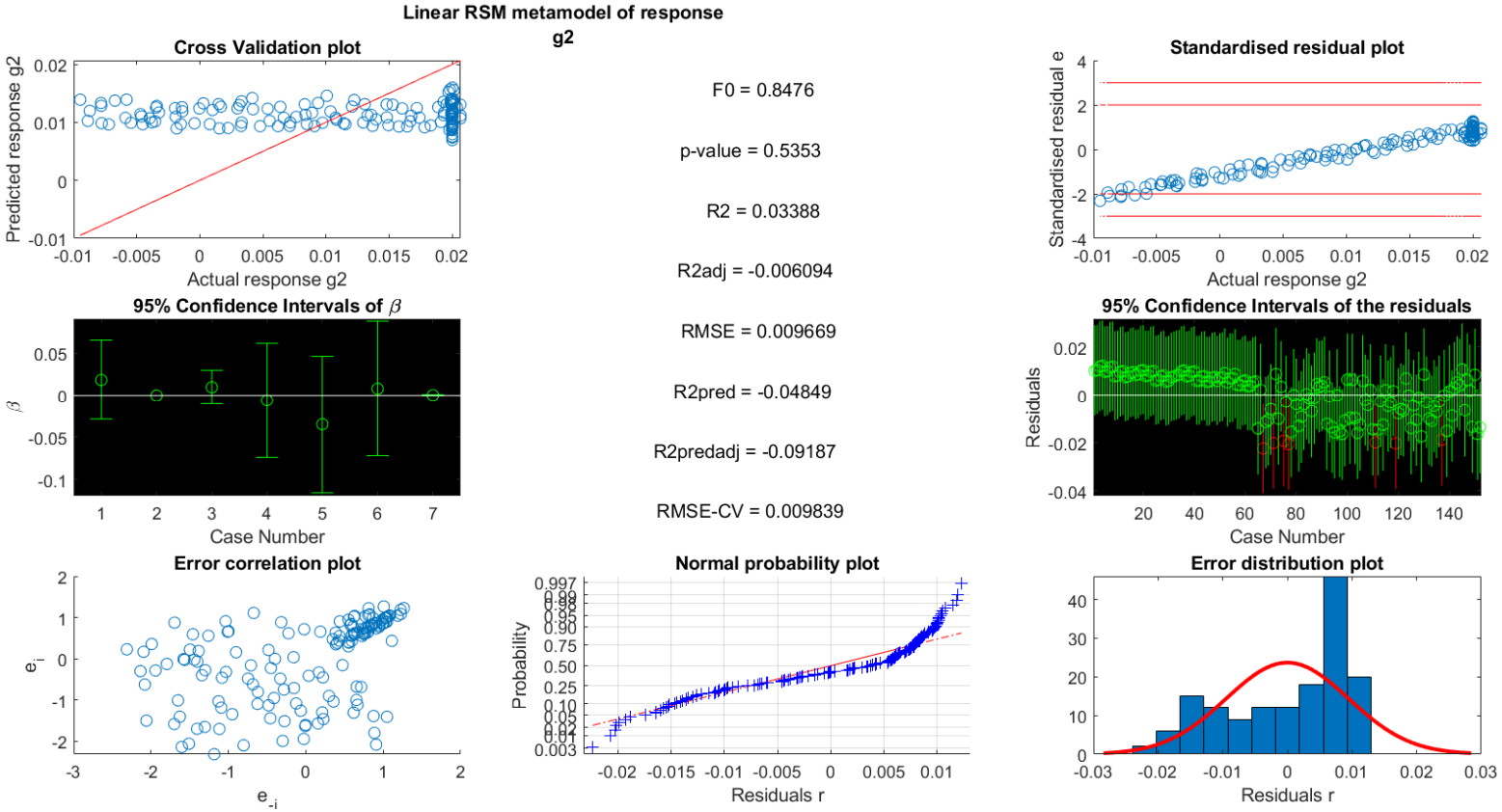

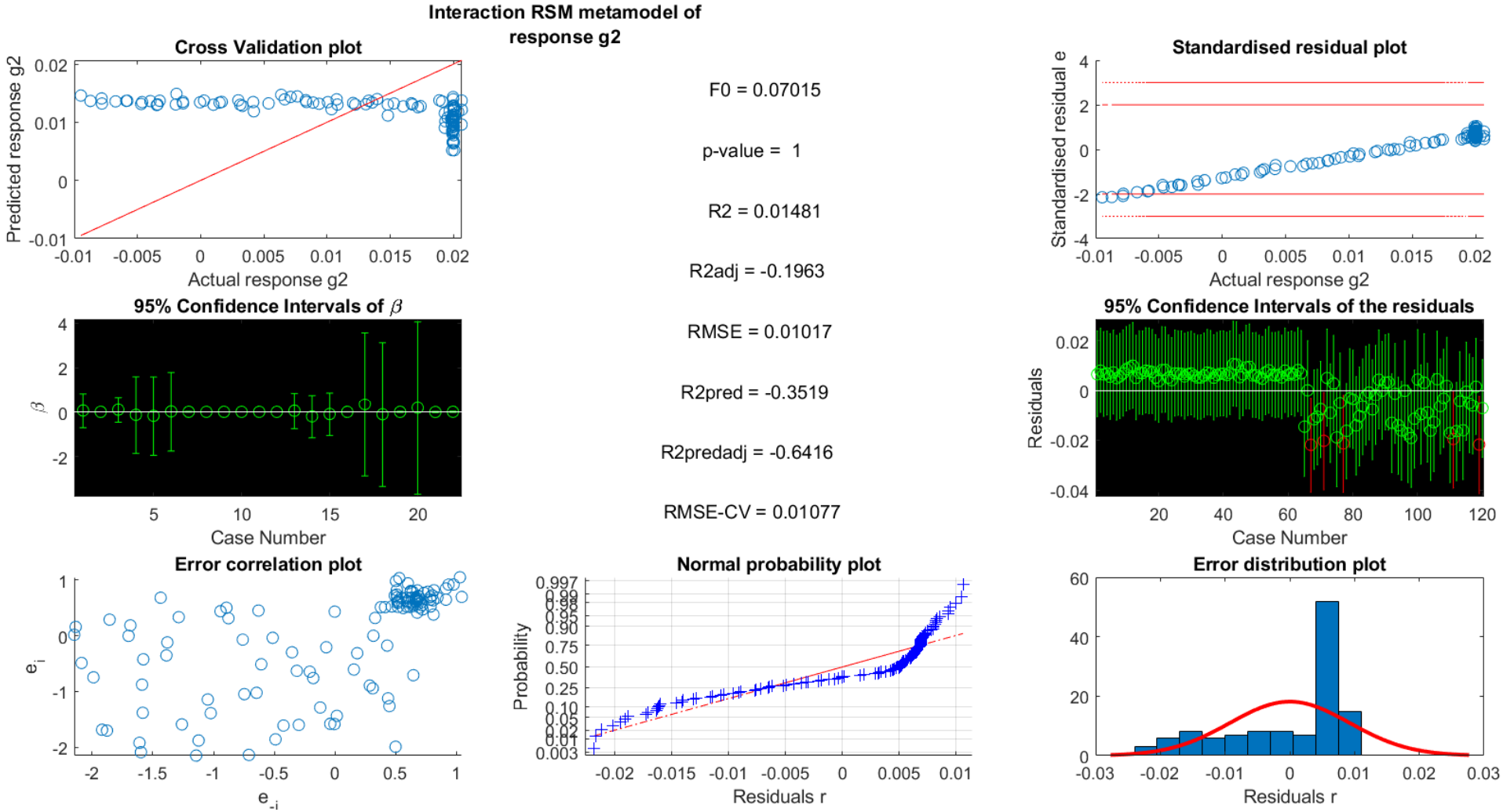
Interaction RSM metamodel of response g2
Cross Validation plot
Predicted response g2
Actual response g2
F0 = 0.07015
p-value = 1
R2 = 0.01481
R2adj = -0.1963
RMSE = 0.01017
R2pred = -0.3519
R2predadj = -0.6416
RMSE-CV = 0.01077
Standardised residual plot
Standardised residual e
Actual response g2
95% Confidence Intervals of β
β
Case Number
95% Confidence Intervals of the residuals
Residuals
Case Number
Error correlation plot
e_i
e_-i
Normal probability plot
Probability
Residuals r
Error distribution plot
Residuals r

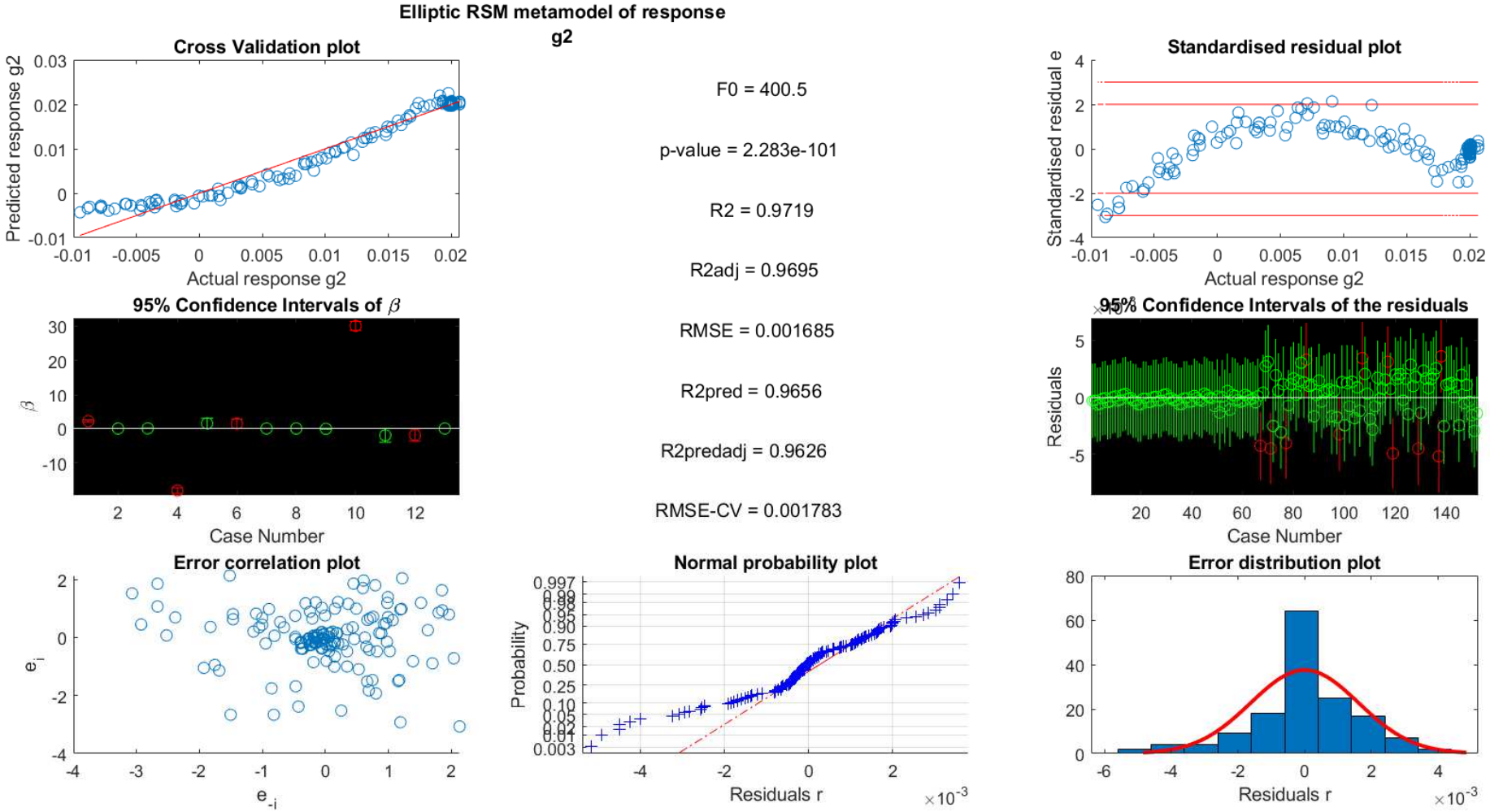
Elliptic RSM metamodel of response
g2
Cross Validation plot
Predicted response g2
Actual response g2
F0 = 400.5
p-value = 2.283e-101
R2 = 0.9719
R2adj = 0.9695
RMSE = 0.001685
R2pred = 0.9656
R2predadj = 0.9626
RMSE-CV = 0.001783
Standardised residual plot
Standardised residual e
Actual response g2
95% Confidence Intervals of β
β
Case Number
95% Confidence Intervals of the residuals
Residuals
Case Number
Error correlation plot
e_i
e_-i
Normal probability plot
Probability
Residuals r
×10^-3
Error distribution plot
Residuals r
×10^-3

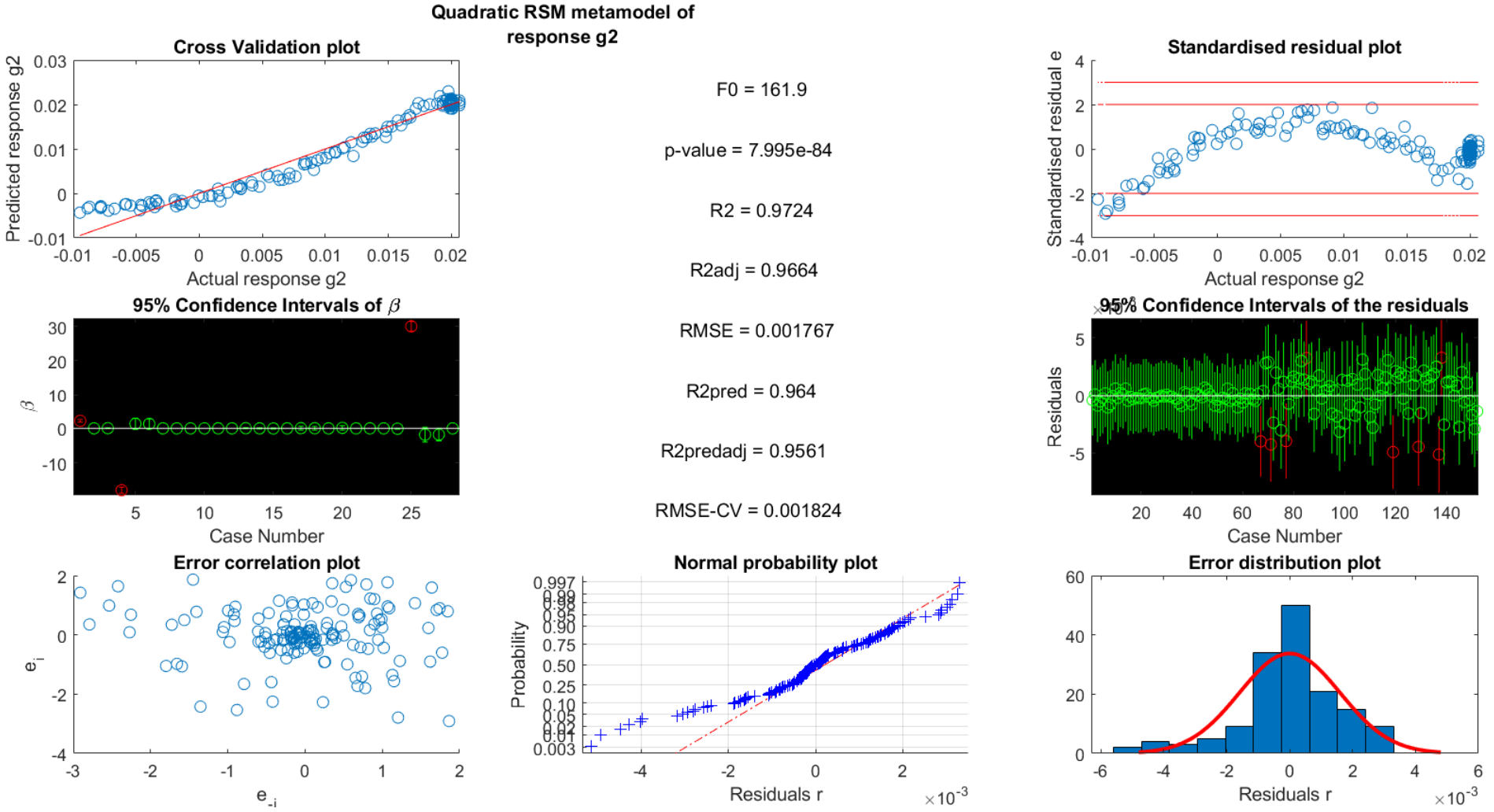

8.12.2 Appendix 12.2 - Kriging

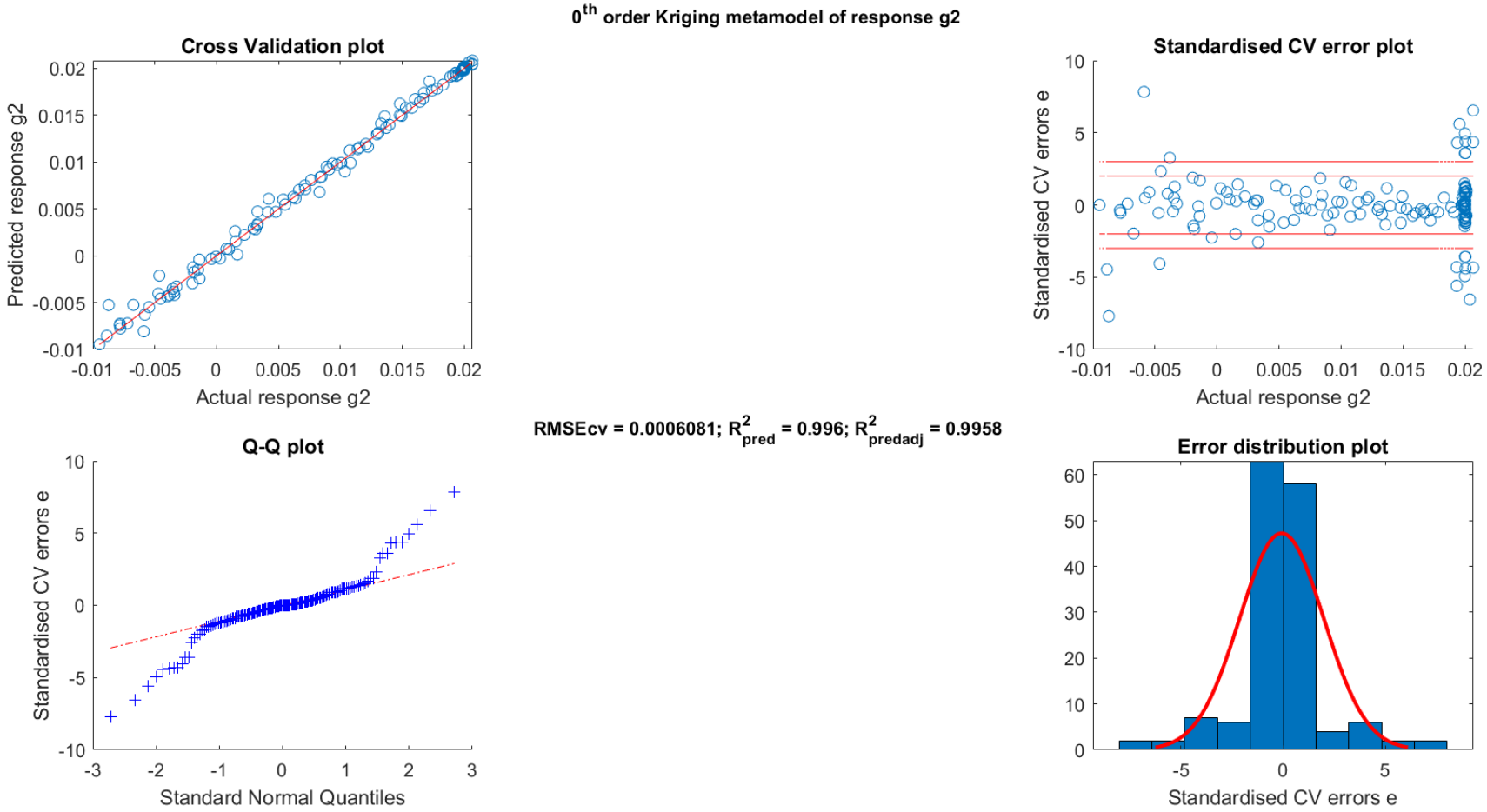
0th order Kriging metamodel of response g2
Cross Validation plot
Predicted response g2
Actual response g2
Standardised CV error plot
Standardised CV errors e
Actual response g2
RMSEcv = 0.0006081; R2pred = 0.996; R2predadj = 0.9958
Q-Q plot
Standardised CV errors e
Standard Normal Quantiles
Error distribution plot
Standardised CV errors e

1st order Kriging metamodel of response g2

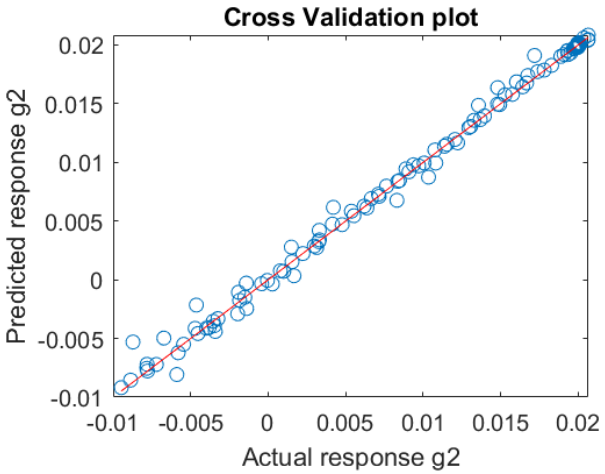

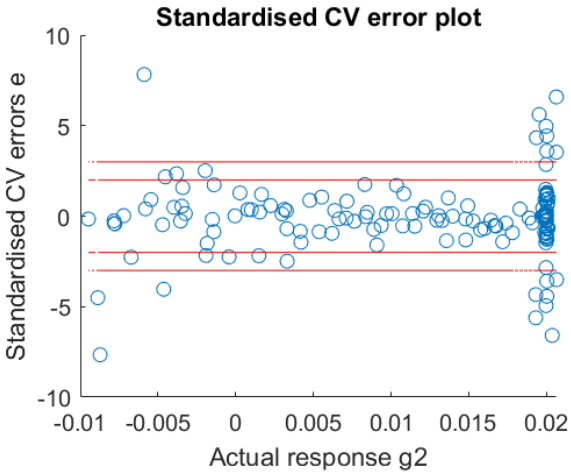

RMSEcv = 0.00062; R^2_{pred} = 0.9958; $R^2_{predadj}$ = 0.9954

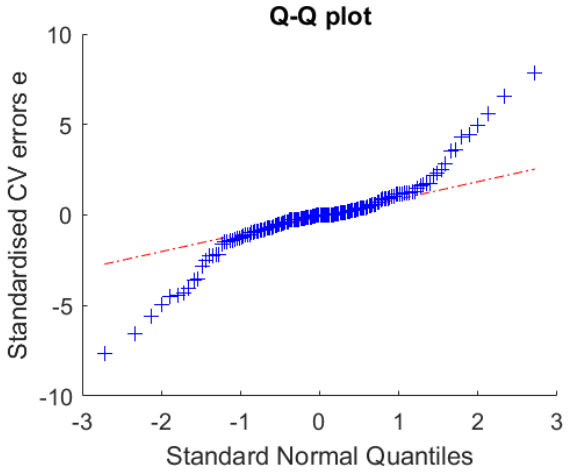

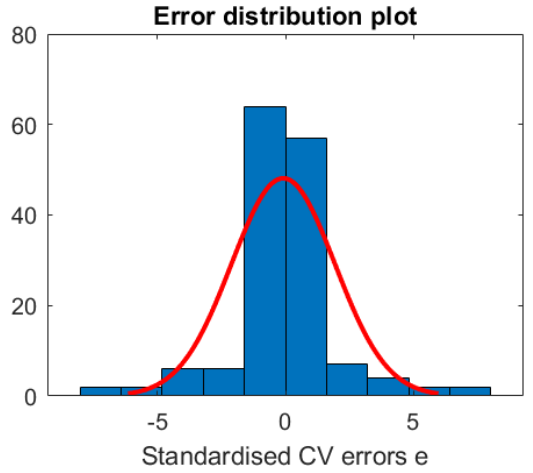

2nd order Kriging metamodel of response g2

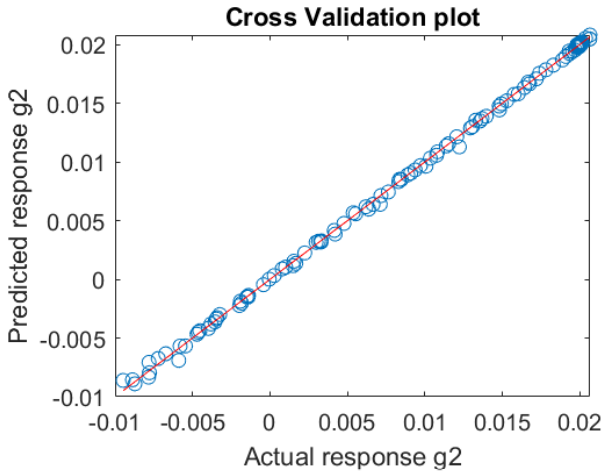

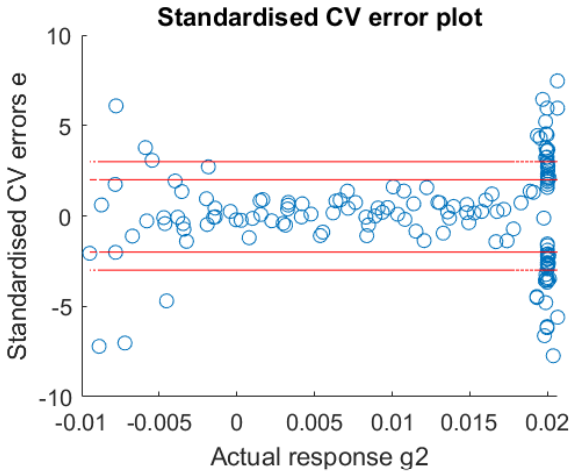

RMSEcv = 0.0002145; R^2_{pred} = 0.9995; $R^2_{predadj}$ = 0.9994

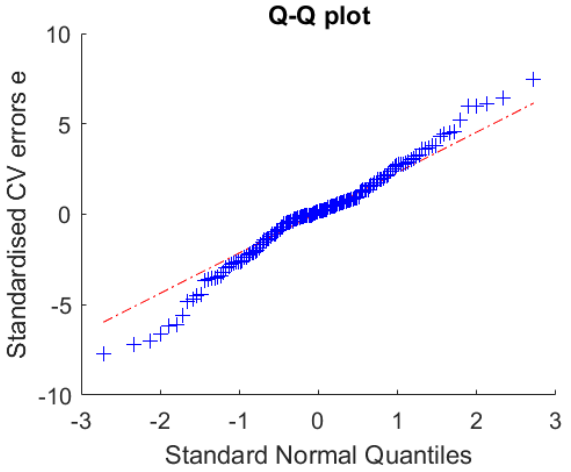

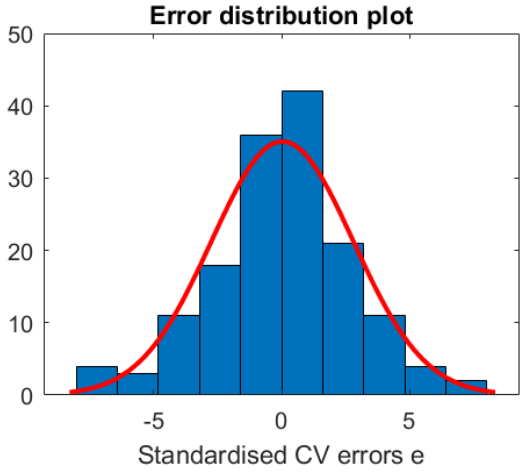

2nd order Regression Kriging metamodel of response g2

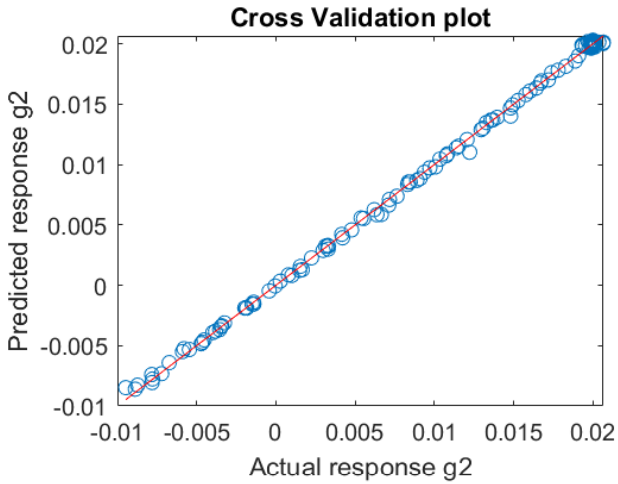

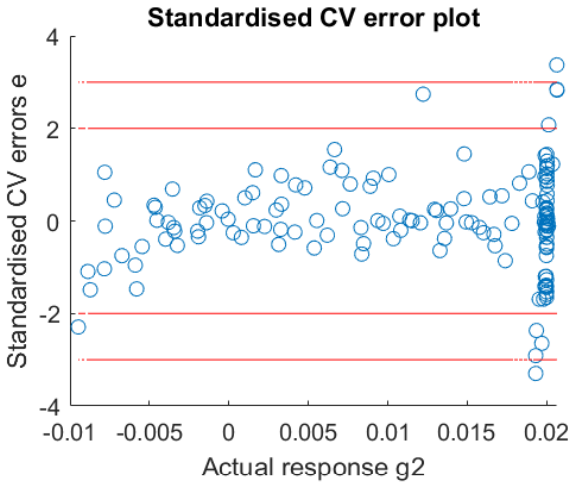

RMSEcv = 0.0002632; R^2_{pred} = 0.9992; $R^2_{predadj}$ = 0.999